



**UNIVERSITAT POLITÈCNICA  
DE CATALUNYA**  
**BARCELONATECH**

Escola Tècnica Superior d'Enginyeria Industrial de Barcelona  
Universitat Politècnica de Catalunya

# **Efficient Operation of photo-Fenton Process for the Treatment of Emerging Contaminants in Water Solutions**

**Evelyn Yamal Turbay**

M.Sc. in Process Engineering

Thesis Presented for the degree of Doctor of Philosophy.  
Directed by Dr. Montserrat Pérez Moya and Dr. Moisès Graells.

Barcelona, September 2013

Copyright © by Evelyn Yamal Turbay

*A mi familia...*



*El tiempo de Dios es perfecto*



## Summary

The growth of population density in some areas of the planet and the increasing fast advances in technology and energy issues, have resulted in a remarkable increment in the necessity for goods and services, with a subsequent over-exploitation and pollution of the environmental resources. Water, a non-renewable resource, does not escape from the harmful effects of human activity and its increasing pollution levels threaten the normal development of ecosystems and life as well.

In the last decades, the occurrence of a new generation of contaminants has been detected in wastewaters, surface and underground waters, and even in drinking water. These substances, called “emerging contaminants” or “emerging pollutants”, are not subject to regulation, but their recalcitrant character and their effects as endocrine disruptors suggest that their bio-accumulation will have severe consequences to the environment. These non-biodegradable compounds cannot be removed in conventional wastewater treatment plants, and there is a need for chemical processes to oxidize them at least to bio-degradable or non-toxic species. Advanced oxidation processes (AOPs) have demonstrated to be particularly useful in degrading and eventually mineralizing emerging contaminants, but the complexity of their mechanisms and the high reagent and energy costs involved, make necessary to develop options to improve their performance.

This thesis specifically addresses the photo-Fenton process, an advanced oxidation process which has been widely applied and has demonstrated to be efficient in the degradation of recalcitrant organic contaminants. The objective of this thesis is to investigate and to propose operating alternatives to improve the performance of photo-Fenton process. For that aim, it was necessary to fulfill some specific objectives: to perform a detailed study of the variables involved in the process, propose its enhancement throughout a systematic dosage of hydrogen peroxide along the treatment span, simulate the process and to investigate opportunities to optimize the process batch recipe.

In the first stage of the investigation, with a clear experimental approach, the variables involved in the process were studied and a novel, flexible and easy-to-implement hydrogen peroxide systematic dosage protocol was proposed, improving the mineralization of three emerging contaminants, reaching almost total mineralization in some of the cases. However, the effectiveness of the protocol is strongly influenced by the crossed effect between the involved parameters.

In a subsequent stage, a computational approach, the process involving the proposed dosage protocol is simulated and the performance of the process was predicted at different operational conditions. The opportunities for improving process performance when the parameters concerning the dosage protocol are conveniently adjusted can be addressed. Finally, taking a step forward, a first attempt to investigate the alternatives for process optimization was investigated, demonstrating that operational costs can be reduced without diminishing the quality of the final product.

As a final remark, this thesis supposes a step forward in the improvement of advanced oxidation processes and it opens the door to continue developing strategies to model, simulate and optimize these complex processes.



## Resumen

El aumento de la densidad poblacional en algunas zonas del planeta y los cada vez más rápidos avances en las áreas tecnológicas y energéticas han traído como consecuencia un crecimiento notable en los requerimientos de bienes y servicios, lo que a su vez ha ocasionado una sobreexplotación y una consecuente contaminación de los recursos ambientales. El agua, un recurso no renovable, no escapa de los efectos nocivos de la actividad humana y los crecientes niveles de contaminación que la afectan amenazan con interferir con el desarrollo normal de los ecosistemas y, eventualmente, de la vida misma.

En las últimas décadas, se ha detectado la presencia de una nueva generación de contaminantes en aguas residuales, superficiales, subterráneas e incluso potables. Estos contaminantes, llamados “contaminantes emergentes”, no son aún objeto de regulación, pero su carácter recalcitrante y sus efectos como disruptores endocrinos sugieren que su bio-acumulación tendrá graves consecuencias. Al no ser biodegradables, no es posible removerlos en las plantas de tratamiento de aguas convencionales, por lo que se requiere de un proceso químico que los oxide al menos a contaminantes más biodegradables y/o no tóxicos. Los procesos de oxidación avanzada han demostrado ser particularmente útiles en la degradación y eventual mineralización de contaminantes emergentes, pero la complejidad de sus mecanismos y los altos costos de reactivos y energía que involucran obligan a investigar opciones para mejorar su desempeño.

El objetivo de esta tesis consiste en investigar y proponer alternativas para mejorar el desempeño del proceso foto-Fenton, un proceso de oxidación avanzada ampliamente utilizado que ha demostrado ser eficiente en la degradación de contaminantes orgánicos recalcitrantes. Para tal fin, se cumplieron los siguientes objetivos específicos: un estudio detallado de las variables involucradas en el proceso, la mejora del proceso a través de una dosificación sistemática del peróxido de hidrógeno, la simulación del proceso bajo las condiciones de adición propuestas y la investigación de una alternativa de optimización para la reducción de costos operativos.

En la primera fase de la investigación, a través del mencionado enfoque experimental, se estudian las variables involucradas en el proceso y se propone un protocolo de adición de peróxido de hidrógeno novedoso, flexible y de fácil implementación que mejora de manera considerable la mineralización de soluciones acuosas de tres contaminantes emergentes, llegando en algunos casos hasta la total eliminación del carbono orgánico total. Sin embargo, la efectividad

del protocolo de adición propuesto se ve fuertemente influenciada por el efecto cruzado entre los parámetros involucrados.

En una etapa posterior, de carácter computacional, se simula el proceso con el protocolo de adición propuesto, de modo que puede predecirse fácilmente la mejora del desempeño del proceso cuando los parámetros del protocolo se ajustan de manera conveniente. En un paso más allá, en la búsqueda de una herramienta que permita identificar la mejor combinación de los parámetros que controlan la adición del peróxido de hidrógeno, se investiga la optimización de la operación batch, demostrándose que es posible reducir los costos del proceso sin desmejora de la calidad del producto.

Para concluir, esta tesis supone un paso hacia adelante en el mejoramiento de los procesos de oxidación avanzada y abre las puertas a continuar investigando propuestas de modelaje, simulación y optimización de estos complejos procesos.

## **Acknowledgements**

I fully appreciate financial support from my alma mater, Universidad de Carabobo. This fantastic professional opportunity would have not been possible other way.

Thanks to CEPIMA for giving me the opportunity to develop this research.

Thanks a lot, Montserrat and Moisés, for accompanying me through this path and for guiding my steps towards success.

To IMRCP, for allowing me to learn so much during my three months research stage, especially to Marie-Thérèse Maurette, Esther Oliveros and André Braun.

To my friends, the old and the new, here and there... Life would be empty (and boring) without you guys...

To the best family anybody may have... You are the reason I keep going on...

And last, but not least, to God... what would I be without You?!



# Table of contents

<b>PART I. OVERVIEW</b>	<b>1</b>
<b>Chapter I. Introduction</b>	<b>1</b>
1.1 Water, world, industry and engineering	3
1.2 Thesis scope	5
1.3 Objectives	5
1.4 Thesis outline	6
1.5 References	7
<b>Chapter II. State-of-the-Art</b>	<b>9</b>
2.1. Water pollution and treatment	11
2.2. Advanced oxidation processes (AOPs)	13
2.2.1. Ozone and related	15
2.2.2. Heterogeneous photocatalysis	16
2.2.3. H <sub>2</sub> O <sub>2</sub> /UV and related	17
2.2.4. VUV photolysis	17
2.3. Fenton and related processes	18
2.3.1. Fenton processes operation	26
2.3.2. Modeling of Fenton processes	28
2.4. References	30
<b>Chapter III. Materials and Methods</b>	<b>47</b>
3.1. Experimental Methods	49
3.1.1. Pilot plant description	49
3.1.2. Analytical methods	52
3.1.2.1. Determination of total organic carbon (TOC)	52
3.1.2.2. Determination of contaminant concentration	53
3.1.2.3. Determination of hydrogen peroxide concentration	54
3.1.2.4. Chemical actinometry	55
Potassium ferrioxalate actinometry	56
3.2. Mathematical Tools	58

3.2.1. Optimization tools	58
<b>3.3. References</b>	<b>59</b>
<b>PART II. EXPERIMENTAL APPROACH</b>	<b>61</b>
<b>Chapter IV. Characterization of Paracetamol Degradation by Fenton and photo-Fenton processes</b>	<b>63</b>
<b>4.1. Introduction</b>	<b>65</b>
<b>4.2. Preliminary Assays</b>	<b>65</b>
4.2.1. Selection of the reagent doses	65
4.2.2. Mixing characterization	66
4.2.3. Blank assays	66
<b>4.3. PCT Degradation and Mineralization Performance</b>	<b>67</b>
<b>4.4. Photonic Efficiency</b>	<b>70</b>
4.4.1. Photonic efficiency of PCT degradation ( $\phi_{app,PCT}$ )	71
4.4.2. Photonic efficiency of mineralization ( $\phi_{app,TOC}$ )	72
<b>4.5. Conclusions</b>	<b>73</b>
<b>4.6. References</b>	<b>74</b>
<b>Chapter V. Systematic Assessment of a Hydrogen Peroxide dosage on Caffeine Degradation by photo-Fenton Process</b>	<b>75</b>
<b>5.1. Introduction</b>	<b>77</b>
<b>5.2. Preliminary assays and reagent load settings</b>	<b>78</b>
5.2.1. Ferrous salt load	78
5.2.2. Blank assays	79
5.2.3. Stepwise dosage	79
<b>5.3. Experimental Design</b>	<b>81</b>
5.3.1. Dosage protocol: model and factors	81
5.3.2. Dosage time interval	82
5.3.3. Performance assessment	83
5.3.4. Design of experiments	84
<b>5.4. Results and Discussion</b>	<b>84</b>
<b>5.5. Conclusions</b>	<b>88</b>
<b>5.6. References</b>	<b>89</b>

<b><i>Chapter VI. Enhanced photo-Fenton Process for Tetracycline Degradation using Efficient Hydrogen Peroxide Dosage Protocol</i></b>	<b>91</b>
<b>6.1. Introduction</b>	<b>93</b>
<b>6.2. Results and Discussion</b>	<b>94</b>
6.2.1. Preliminary assays	94
6.2.1.1. Reagent doses	94
6.2.1.2. Blank assays	95
6.2.2. DOE for dosage characterization	96
<b>6.3. Conclusions</b>	<b>100</b>
<b>6.4. References</b>	<b>101</b>
<b><i>Chapter VII. Degradation of Sulfamethazine by Means of an Improved photo-Fenton Process Involving a Hydrogen Peroxide Systematic Dosage Protocol</i></b>	<b>105</b>
<b>7.1. Introduction</b>	<b>107</b>
<b>7.2. Results and Discussion</b>	<b>107</b>
7.2.1. Fenton reagents	107
7.2.2. Blank assays	108
7.2.3. SMT degradation performance	109
7.2.4. Influence of dosage on process performance	110
<b>7.3. Conclusions</b>	<b>114</b>
<b>7.4. References</b>	<b>115</b>
<b><i>PART III. COMPUTATIONAL APPROACH</i></b>	<b>117</b>
<b><i>Chapter VIII. Simulation and Parameter Adjustment</i></b>	<b>119</b>
<b>8.1. Model statement</b>	<b>121</b>
8.1.1. Simulation of base cases	124
<b>8.2. Dosage protocol model</b>	<b>134</b>
8.2.1. Simulation of the dosage protocol	136
<b>8.3. Simulation code</b>	<b>137</b>
<b>8.4. Parameter adjustment</b>	<b>139</b>
<b>8.5. Conclusions</b>	<b>140</b>
<b>8.6. References</b>	<b>141</b>
<b><i>Chapter IX. Optimization of the Batch Process Recipe</i></b>	<b>143</b>

<b>9.1. Introduction</b>	<b>145</b>
<b>9.2. Problem statement</b>	<b>145</b>
<b>9.3. Optimization model</b>	<b>146</b>
9.3.1. Optimization tools	147
9.3.1.1. Pareto frontier for cost function $\xi$ versus processing time, $t_{\text{end}}$	147
9.3.1.2. Dosage profile qH2O2 optimization for a given time horizon.	149
<b>9.4. Conclusions</b>	<b>151</b>
<b>9.5. References</b>	<b>151</b>
<b><i>Chapter X. General Conclusions and Future Work</i></b>	<b><i>153</i></b>
<b>10.1. Conclusions</b>	<b>155</b>
<b>10.2. Future Work</b>	<b>157</b>
<b><i>APPENDIXES</i></b>	<b><i>159</i></b>
<b><i>Appendix A. Publications</i></b>	<b><i>161</i></b>
<b>A.1. Journal publications</b>	<b>163</b>
<b>A.2. Conference proceeding articles</b>	<b>163</b>
<b>A.3. Participation in Congresses</b>	<b>163</b>
<b><i>Appendix B. Application of Fault Diagnosis and Detection to the photo-Fenton Process</i></b>	<b><i>165</i></b>
<b>B.1. Introduction</b>	<b>167</b>
<b>B.2. Materials and Methods</b>	<b>167</b>
B.2.1. Case study	167
B.2.2. Novelty detection approach	168
<b>B.3. Results and Discussions</b>	<b>169</b>
<b>B.4. Conclusions</b>	<b>170</b>
<b>B.5. References</b>	<b>170</b>
<b><i>Appendix C. Characterization of the photo-Oxidation of Tetracycline</i></b>	<b><i>171</i></b>
<b>C.1. Introduction</b>	<b>173</b>
<b>C.2. TC photo-oxidation and production of singlet oxygen</b>	<b>174</b>
C.2.1. Single oxygen analysis	174
C.2.2. Results and discussion	175



<b>C.3. Degradation of TC by UV and UV/H<sub>2</sub>O<sub>2</sub> processes</b>	<b>177</b>
C.3.1. Laboratory reactor description and analytical methods	177
C.3.2. Results and discussion	178
Intermediates identification by LC/MS	179
<b>C.4. Conclusions</b>	<b>179</b>
<b>C.5. References</b>	<b>180</b>



## List of Figures

Figure 1.1. Freshwater availability in 2007 (Source: <a href="http://www.unep.org/dewa/vitalwater/">http://www.unep.org/dewa/vitalwater/</a> ). .....	4
Figure 1.2. Thesis outline .....	7
Figure 2.1. Possible sources, pathways and effects for the occurrence of pharmaceutical residues in the aquatic environment.....	12
Figure 2.2. Schematic representation of a conventional wastewater treatment plant (Source: <a href="http://www.biosolids.com.au/images/sewage-treatment-process.jpg">http://www.biosolids.com.au/images/sewage-treatment-process.jpg</a> ).....	13
Figure 2.3. Electromagnetic spectrum .....	14
Figure 2.4. Reaction of carbon-centered radicals towards mineralization in the presence of dissolved oxygen.....	15
Figure 3.1. Spectral distribution of irradiation sources.....	50
Figure 3.2. Pilot plant schematic representation.....	50
Figure 3.3. Shimadzu TOC-VCSH/CSN analyzer measurement flow diagram .....	53
Figure 3.4. Calibration curve used to calculate $H_2O_2$ concentration by spectrophotometric technique after reaction with ammonium metavanadate.....	55
Figure 3.5. Example of a plot of absorbance against time for a potassium ferrioxalate actinometry.....	58
Figure 4.1. Evolution of normalized concentrations at different values of recirculation flow. <b>(a)</b> TOC concentration, <b>(b)</b> PCT concentration .....	66
Figure 4.2. Evolution of TOC and PCT concentrations for blank assays. Continuous lines correspond to TOC concentrations.....	67
Figure 4.3. Absorption spectrum of a $40\text{ mg L}^{-1}$ PCT sample .....	67
Figure 4.4. Evolution of TOC concentration for Fenton (void symbols) and photo-Fenton (solid symbols) processes <b>(a)</b> $5\text{ mg L}^{-1}$ Fe(II) <b>(b)</b> $10\text{ mg L}^{-1}$ Fe(II).....	69
Figure 4.5. Evolution of PCT and intermediate concentrations for Fenton (void symbols) and photo-Fenton (solid symbols) processes. <b>(a)</b> $5\text{ mg L}^{-1}$ Fe(II) <b>(b)</b> $10\text{ mg L}^{-1}$ Fe(II) .....	70
Figure 4.6. Photonic efficiency of PCT degradation for Fe(II) = $10\text{ mg L}^{-1}$ and different ratios $H_2O_2:Fe(II)$ .....	72
Figure 4.7. Photonic efficiency for PCT degradation at 1.5 min treatment as a function of $H_2O_2:Fe(II)$ ratio for two Fe(II) initial concentration (Blue: $10\text{ mg L}^{-1}$ . Red: $5\text{ mg L}^{-1}$ ) .....	72
Figure 4.8. Photonic efficiency of mineralization for Fe(II) = $10\text{ mg L}^{-1}$ and different ratios $H_2O_2:Fe(II)$ .....	73

Figure 4.9. Photonic efficiency for mineralization at 15 min treatment as a function of $H_2O_2:Fe(II)$ ratio for two $Fe(II)$ initial concentration (Blue: $10\text{ mg L}^{-1}$ . Red: $5\text{ mg L}^{-1}$ ) .....	73
Figure 5.1. Comparative blank assays of the degradation profile of TOC (solid line) and caffeine (dashed line). Standard sample with $C_{eq,\infty}^{H_2O_2} = 500\text{ mg L}^{-1}$ .....	79
Figure 5.2. Normalized TOC (solid line) and normalized hydrogen peroxide concentration (dashed line) for the standard sample undergoing three stepwise dosage protocols (gray line). $C_{eq,\infty}^{H_2O_2}$ values are specified in the figure.....	80
Figure 5.3. Definition of the addition protocol. The three independent parameters ( $y_0$ , $t_{ini}$ , $\Delta t_{add}$ ) are highlighted.....	82
Figure 5.4. Comparison of the effect of different dosage span values: $\Delta t_{add}$ and kick-off fractions $y_0$ . Solid lines denote TOC concentrations(■,◆,●) while dashed lines indicates $H_2O_2$ concentrations (□,◇,○). $C_{eq,\infty}^{H_2O_2} = 500\text{ mg L}^{-1}$ ; $C_0^{Fe(II)} = 10\text{ mg L}^{-1}$ ; $C_0^{coffee} = 300\text{ mg L}^{-1}$ .....	83
Figure 5.5. TOC and caffeine concentration behavior for the central experiment of the design: $y_0 = 20\%$ ; $t_{ini} = 15\text{ min}$ ; $C_0^{Fe(II)} = 10\text{ mg L}^{-1}$ , $C_{eq,\infty}^{H_2O_2} = 500\text{ mg L}^{-1}$ ; $C_0^{coffee} = 300\text{ mg L}^{-1}$ . (◇=TOC concentration; ◆=caffeine concentration). .....	86
Figure 5.6. TOC and caffeine concentration behavior for different dosage protocols (dashed lines = caffeine concentration). $C_0^{Fe(II)} = 10\text{ mg L}^{-1}$ , $C_{eq,\infty}^{H_2O_2} = 500\text{ mg L}^{-1}$ ; $C_0^{coffee} = 300\text{ mg L}^{-1}$ .....	87
Figure 5.7. TOC and caffeine concentration behavior for different $y_0$ at $t_{ini} = 0\text{ min}$ . (dashed lines = caffeine concentration). $C_0^{Fe(II)} = 10\text{ mg L}^{-1}$ ; $C_{eq,\infty}^{H_2O_2} = 500\text{ mg L}^{-1}$ ; $C_0^{coffee} = 300\text{ mg L}^{-1}$ .....	88
Figure 6.1. (a) $\zeta^{TS}$ obtained for different reagent doses according to the DOE. (b) TOC (continuous lines, ▲,■,◆), TC (-.-Δ,□,◇-.-) and $H_2O_2$ (dashed lines, ▲,■,◆) normalized concentration profiles for blank assays.....	96
Figure 6.2. (a) TOC (◆) and $H_2O_2$ (◇) normalized concentration profiles for central experiment of the design.(b) TOC (solid lines) and TC (dashed lines) normalized concentration profiles for different dosage protocols.....	98
Figure 6.3. Relation between $t^{TC}$ (to be minimized) $\zeta^{TS}$ (to be maximized).....	99
Figure 6.4. TOC (solid lines) and TC (dashed lines) normalized concentration profiles for different $y_0$ when $t_{ini} = 15\text{ min}$ .....	100
Figure 7.1. First order rate constants for TOC degradation ( $k_{TOC}$ ) versus $C_{eq,\infty}^{H_2O_2}$ for a $25\text{ mg L}^{-1}$ SMT concentration and $10\text{ mg L}^{-1}$ iron concentration. ....	108
Figure 7.2. Evolution of SMT degradation during blank assays. $C_0^{SMT} = 25\text{ mg L}^{-1}$ ; $C_0^{Fe(II)} = 10\text{ mg L}^{-1}$ ; $C_0^{H_2O_2} = 200\text{ mg L}^{-1}$ .....	109

Figure 7.3. TOC, SMT and H <sub>2</sub> O <sub>2</sub> normalized concentration profiles for different AOPs. $C_0^{SMT} = 25 \text{ mgL}^{-1}$ ; $C_0^{Fe(II)} = 10 \text{ mgL}^{-1}$ ; $C_0^{H_2O_2} = 200 \text{ mgL}^{-1}$ .....	110
Figure 7.4. TOC, SMT and H <sub>2</sub> O <sub>2</sub> normalized concentration profiles for different dosage protocols compared to reference experiment. $C_0^{SMT} = 25 \text{ mgL}^{-1}$ ; $C_0^{Fe(II)} = 10 \text{ mgL}^{-1}$ ; $C_{eq,\infty}^{H_2O_2} = 200 \text{ mgL}^{-1}$ .....	112
Figure 7.5. Relation between the time necessary to degrade 95% of initial SMT ( $t_{SMT}$ ) and the time necessary to achieve total mineralization ( $t_{TOC}$ ) for all of the DOE and reference assays. Final TOC conversion is indicated in brackets in the case when mineralization (100%) is not achieved (Assay R_100).....	113
Figure 7.6. TOC, SMT and H <sub>2</sub> O <sub>2</sub> normalized concentration profiles for different $y_0$ where $t_{ini} \geq 30 \text{ min}$ . $C_0^{SMT} = 25 \text{ mgL}^{-1}$ ; $C_0^{Fe(II)} = 10 \text{ mgL}^{-1}$ ; $C_{eq,\infty}^{H_2O_2} = 200 \text{ mgL}^{-1}$ .....	114
Figure 8.1. Fenton and photo-Fenton process simulation when no organic matter is present .....	125
Figure 8.2. Fenton and photo-Fenton process simulation for PCT base case 1.....	127
Figure 8.3. Fenton and photo-Fenton process simulation for PCT base case 2.....	128
Figure 8.4. Fenton and photo-Fenton process simulation for PCT base case 3.....	129
Figure 8.5. Fenton and photo-Fenton process simulation for PCT base case 4.....	130
Figure 8.6. Fenton and photo-Fenton process simulation for PCT base case 5.....	131
Figure 8.7. Fenton and photo-Fenton process simulation for SMT base case 1.....	132
Figure 8.8. Fenton and photo-Fenton process simulation for TC base case 1.....	133
Figure 8.9. Simulation of Fenton and photo-Fenton processes when dosage protocol is applied: $y_0 = 0\%$ ; $\Delta t_{add} = 1 \text{ h}$ , $t_{ini} = 15 \text{ min}$ .....	136
Figure 8.10. Simulation of Fenton and photo-Fenton processes when dosage protocol is applied: $y_0 = 20\%$ ; $\Delta t_{add} = 1 \text{ h}$ , $t_{ini} = 15 \text{ min}$ .....	137
Figure 8.11. Parameter adjustment performed with the available experimental data. Continuous lines: simulated variables. Dots: experimental data .....	140
Figure 9.1. Pareto frontier for cost function $\xi$ versus processing time $t_{end}$ (no dosage is considered) for $X_{max}^{TOC} = 0.1$ and $X_{max}^{PCT} = 0.001$ . .....	149
Figure 9.2. Control ( $q_{H_2O_2}$ ) and process (normalized $C_{TOC}$ , $C_{H_2O_2}$ and $C_{PCT}$ ) variable profiles: <b>(a)</b> base case, <b>(b)</b> optimal solution with no dosage, <b>(c)</b> with dosage protocol, <b>(d)</b> with PWC strategy.....	150
Figure C.1. Tetracycline absorption spectrum in deionized water .....	173
Figure C.2. Absorption spectra evolution during TC irradiation at 367 nm (a) $7.5 \times 10^{-5} \text{ mol L}^{-1}$ (b) $1 \times 10^{-4} \text{ mol L}^{-1}$ .....	176
Figure C.3. Evolution of the <sup>1</sup> O <sub>2</sub> signal and the absorption factor during TC irradiation at 367 nm for two different TC initial concentrations: Red lines: $7.5 \times 10^{-5} \text{ mol L}^{-1}$ (Initial absorption = 1.02); blue lines: $1 \times 10^{-4} \text{ mol L}^{-1}$ (Initial absorption = 1.49).....	177
Figure C.4. Evolution of TC normalized concentration during UV-C photodegradation...	178

Figure C.5. Evolution of the apparent reaction rate of TC degradation by UV/H<sub>2</sub>O<sub>2</sub> as a function of the ratio H<sub>2</sub>O<sub>2</sub>/TC ..... 179

Figure C.6. Possible pathway for the hydroxylation of the TC molecule ..... 179

## List of Tables

Table 2.1.	AOPs classification .....	14
Table 2.2.	Peak wavelengths (nm) obtained in dielectric-barrier discharges with mixtures of noble gas (NG) and halogen (X). (IUPAC, 2012).....	18
Table 2.3.	Review of AOPs applied to different types of diverse wastewaters.....	19
Table 2.4.	Treatment technologies used for remediation of sulfamethazine (SMT) .....	22
Table 2.5.	Treatment technologies used for remediation of tetracycline (TC) .....	23
Table 2.6.	Treatment technologies used for remediation of paracetamol (PCT).....	25
Table 2.7.	Treatment technologies used for remediation of coffee/caffeine .....	26
Table 2.8.	Researches involving empirical modeling via experimental design .....	29
Table 2.9.	Researches involving mechanistic modeling.....	30
Table 3.1.	Photo-reactor and configurations available in the pilot plant under study.....	49
Table 3.2.	Units for data acquisition and control in the pilot plant.....	51
Table 3.3.	Chromatographic conditions used for each studied contaminant.....	54
Table 4.1.	Design of experiments for the characterization of PCT degradation.....	68
Table 5.1.	Design of experiment variables levels. The resulting dosing slope is also included.....	84
Table 5.2.	List of assays carried out: reference (R); design (A to K) and additional (L to N). .....	85
Table 6.1.	Average results of the planned assays: earliest sample time at which TC is not detected (tTC) and TC conversion at TS ( $\xi$ TS).....	97
Table 7.1.	Assays carried out according to the DOE. $C_{eq, \infty}^{H_2O_2} = 200$ mg L-1. ....	111
Table 8.1.	Kinetic constants and stoichiometric coefficients reported by Cabrera-Reina et al. (2012) and used for simulating the base cases.....	124
Table 8.2.	Initial concentrations considered for the simulation of the PCT base cases. .	126
Table 8.3.	Kinetic parameters obtained by adjustment with experimental data .....	140
Table 9.1.	Case base definition .....	147
Table 9.2.	Optimum operational cost for different time horizons when no dosage protocol is applied.....	148
Table 9.3.	Key performance indicators (KPIs) in the base case and optimal solutions ...	150
Table B.1.	Plant configurations considered in the pilot plant.....	167
Table B.2.	Variables and parameters values in the photo-Fenton process at NOC .....	168
Table B.3.	Performance of the binary classification stage.....	169
Table B.4.	Performance of the multi-class classification stage.....	169
Table B.5.	ND approach validation on two novel faults. Performance in terms of F1(%) .....	170





## **PART I. OVERVIEW**



# **Chapter I**

## **Introduction**

This chapter presents an overview to introduce the object of study. Environmental issues related to water scarcity and pollution and their relationship with industry and Engineering are first described and then the objectives and scope of this work are outlined.



## 1.1 Water, world, industry and engineering

One of the most difficult challenges Chemical Engineering must face in recent times is to deal with the necessity to respond to constantly changing world, taking into account the needs of the market as well as those of chemical processes. Concepts of globalization and sustainability have forced Chemical Engineering to change, grow and get involved in brand new areas. According to this, Engineering future objectives involve increasing processes productivity and selectivity throughout intelligent operations, designing new equipment based in scientific principles and new production methods as well, extending its methodologies through a product focused Engineering taking into account consumer requirements and implementing process modeling and simulation multiscale applications into real situations, since molecular scale until complex industrial scale (Charpentier, 2004).

Participation of Chemical Engineering into new and wider multidisciplinary areas has been forced for several reasons: the exponential increase of new products and substances, the rate at which information generates and the need for more strict controls in processes for economic and environmental aspects. These factors are responsible for a more often necessity to relate Chemical Engineering with computer technologies which permit higher response velocity and consequently a higher quantity of information in a less time, increasing R+D+I productivity.

That same increment in knowledge and necessities (and products and services to satisfy those necessities) has caused important damages to the environment: global warming, climate change, drinking water scarcity, soil pollution, among others worldwide issues are a consequence of human activities and population growth. The development of sustainable activities and technologies is another great challenge Chemical Engineering has to deal with (Committee on Challenges for the Chemical Sciences in the 21st Century, National Research Council, 2003), and its knowledge is required for improving and maintaining environmental conditions and supporting the generation of clean technologies and products at the same time, so it will be possible to maintain and even increase society life quality with the least environmental damage.

Among environmental problems, water-related ones are the most important to deal with because of the serious threats they represent for humankind: according to UN Water, water scarcity affects almost one-fifth of the world's population and almost one quarter of them face economic water shortage. Among the reasons of water scarcity, pollution, waste and wrong management of this resource are mentioned. Figure 1.1 shows the water availability for 2007 (UNEP, 2008).

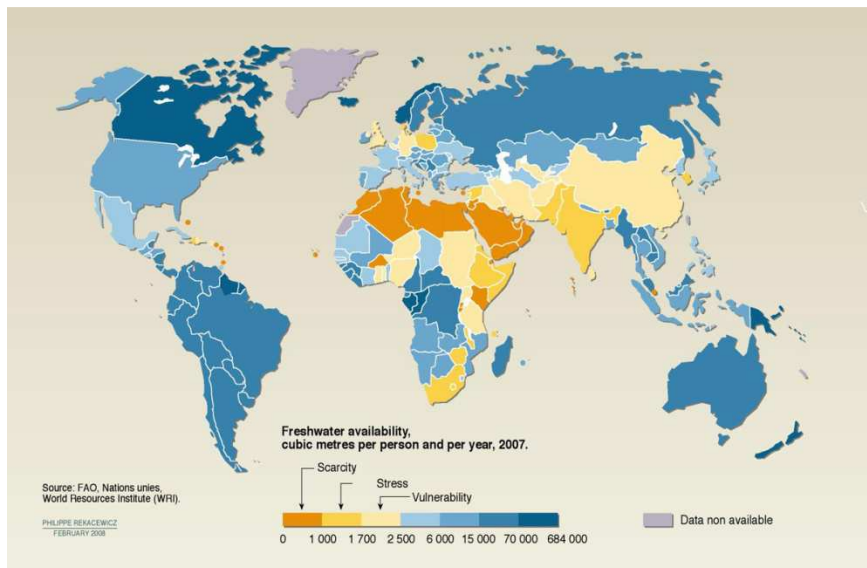


Figure 1.1. Freshwater availability in 2007 (Source: <http://www.unep.org/dewa/vitalwater/>).

Most of the UN Millennium Development Goals (MDG) refer to this problem and call for wastewater management and treatment to contribute to reduce pressure on freshwater resources. They also stand for international cooperation for the creation of technologies which lead to enhance water productivity and financing opportunities.

Regarding the enhancement of water availability and productivity, beyond the obvious need to reduce the sources and frequency of pollution, the treatment of wastewater to be reused has been a well-received option, as it minimizes clean water consumption and is framed into clean or sustainable technologies. The nature of such treatment (or combination of them) will depend on the nature of the pollutants as well as the further use to be given to the treated water (Rosal et al., 2010; Oller et al., 2011).

A lot of research has been devoted to develop and improve wastewater treatment technologies. Pollution is not a new issue, but its causes and contaminants are somehow new as they had not been detected before, which requires new technologies for its treatment and control.

Among these “new” contaminants, those called emerging contaminants (ECs) or emerging pollutants (EPs) are of special interest because of their high risk of bioaccumulation and impact on ecosystems. Pharmaceuticals and personal care products (PPCPs) have been cataloged as ECs and have become a matter of serious concern over the last decades due to their persistence, toxicity and consequent effects on human and animal health.

Most of this PPCPs (antibiotics, anti-inflammatories, antiepileptics, lipid regulators, hormones, cosmetics, fragrances, etc.) are of particular concern because they can act as endocrine disruptors, promote the formation of antibiotic-resistant bacteria and are able to inactivate microorganisms used in conventional water treatment plants (Oller et al., 2011; Becerril, 2009). Many of these organic compounds have been found in surface water, groundwater and even in drinking water at concentrations in the order of  $\text{ng L}^{-1}$ - $\mu\text{g L}^{-1}$  (Broséus et al., 2009).

As these contaminants are not biodegradable and can risk the effectiveness of conventional treatment plants, their remediation from wastewaters requires non-conventional water treatment technologies. Advanced Oxidation Processes (AOPs) which uses strong chemical oxidants and/or the presence of an irradiation source have been studied for that aim, with promising results over the years.

Among AOPs, Fenton and related processes have demonstrated to be effective in remediating non-biodegradable and recalcitrant organic matter, and have been widely studied, even when their mechanisms and degradation pathways are not completely understood. In a general way, these processes consist in the production of highly oxidant hydroxyl radical by the reaction of an iron salt with hydrogen peroxide. According to Malato et al. (2009), Fenton and photo-Fenton processes are the most used AOPs and have been proved to treat a wide range of pollutants at a wide range of organic loads.

The most important handicaps of AOPs are the cost of reagents (and irradiation, when it applies) and their complexity, which difficult their complete understanding and modeling. New strategies have been underlined in order to minimize operation time and reagents consumption, but scarce research has been done to obtain models which lead to a better understanding. To improve the efficiency and reduce cost of these processes are objectives of great interest for scientists and engineers all over the world.

## **1.2 Thesis scope**

This thesis aims to improve Fenton and photo-Fenton processes operation through strategies leading to achieve more efficiency in the remediation of emerging contaminants in water solutions.

## **1.3 Objectives**

The work involves the knowledge, definition and improvement of photo-Fenton process at laboratory and pilot plant scales. Additionally, an effort to explore its modeling and optimization is performed, which initiates a further research line to be developed.

The degradation and mineralization of several emerging contaminants is tested at laboratory and pilot scale, proving the effectiveness of photo-Fenton

process for that aim. As an improvement, a reagent dosage protocol is proposed and tested on the studied contaminants.

Then, a kinetic model from the literature is selected and adapted for photo-Fenton process and finally a reagent dosage protocol and an optimization strategy are proposed.

According to the previous statements, the objectives of this work can be outlined as follows:

- To identify the best operational conditions for the remediation of emerging contaminants in wastewater by means of photo-Fenton process.
- To improve photo-Fenton process through a systematic dosage protocol strategy.
- To model and simulate the operation of the improved photo-Fenton process.
- To investigate opportunities for the optimization of the batch process recipe for the degradation of emerging contaminants by photo-Fenton process.

### **1.4 Thesis outline**

This work is divided into three parts, which are presented in Figure 1.2: a general overview, the description of the experimental approach and the results obtained, and the exploration of the computational approach and its potential outcomes. The first one comprises chapters from I to III, the second part includes chapters from IV to VII and the latter chapters VIII and IX.

This first chapter is dedicated to provide a general introduction to the problem and to underline the objectives and scope of the study, while Chapter II contains a State-of-the-Art review. In Chapter III, a description of reagent and materials as well as experimental and computational methods is presented.

Chapters IV to VII, included in Part II, present the results of the experimental work done initially to identify operational conditions and process variables using paracetamol as a model pollutant (Chapter IV) and to propose the systematic reagent dosage protocol and its application to the remediation of caffeine, tetracycline antibiotic and sulfamethazine antibiotic, (Chapters V, VI and VII, respectively).

Later, within Part III, the formulation and resolution of the operational model is presented in Chapter VIII, while the optimization strategies are considered in Chapter IX.

Finally, the general conclusions of the study and the formulation of the further work to be explored are presented.



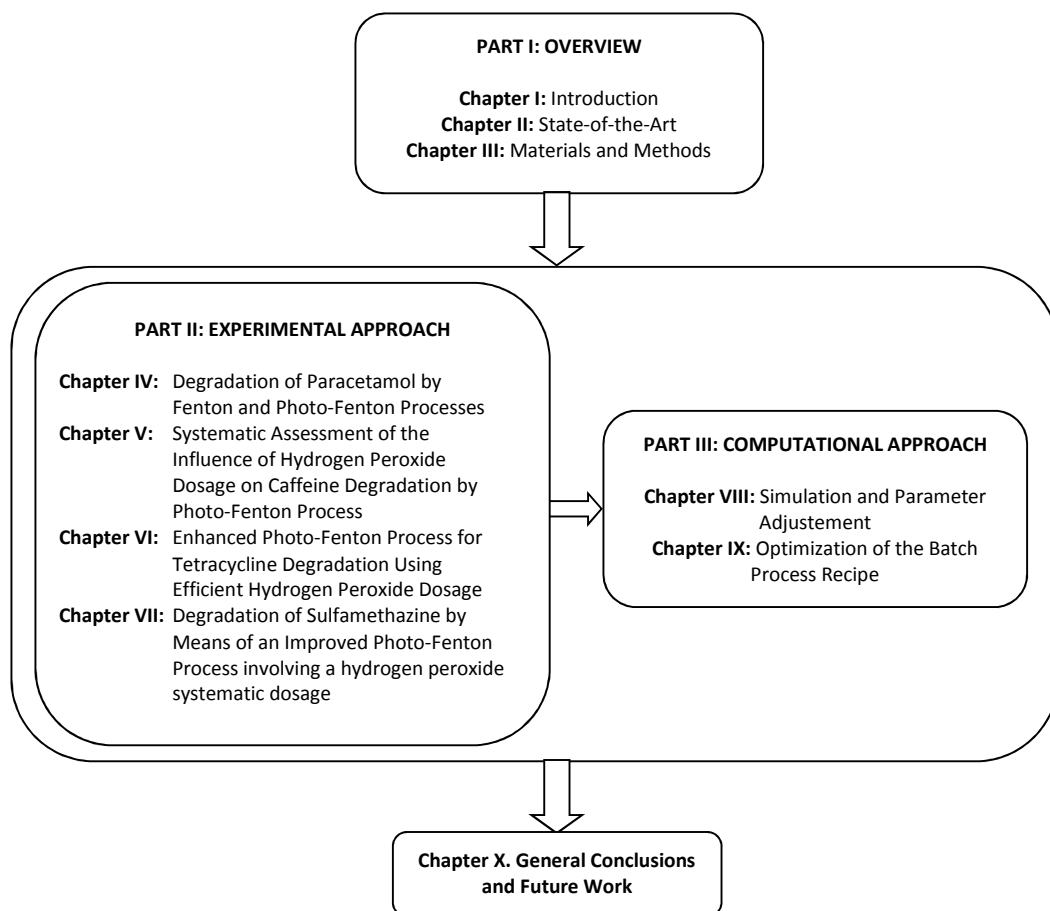


Figure 1.2. Thesis outline

## 1.5 References

Becerril, K. 2009. Contaminantes emergentes en el agua. Digital Journal 10, 8. [URL: <http://www.revista.unam.mx/vol.10/num8/art54/art54.pdf>].

Broséus, R.; Vincent, S.; Aboufadi, K.; Daneshvar, A.; Sauvé, S.; Barbeau, B.; Prévost, M. 2009. Ozone oxidation of pharmaceuticals, endocrine disruptors and pesticides during drinking water treatment. *Water Res.* 43, 4707-4717

Charpentier, J. 2004. The triplet “molecular processes–product–process” engineering: the future of chemical engineering? *Chemical Engineering Science* 57, 4667-4690.

Committee on Challenges for the Chemical Sciences in the 21st Century, National Research Council. 2003. Beyond the molecular frontier: Challenges for the XXI century. The National Academy Press. Washington, D.C., U.S.A.

Malato, S., Fernández-Ibáñez, P., Maldonado, M.I., Blanco, J., Gernjak, W. 2009. Decontamination and disinfection of water by solar photocatalysis: Recent overview and trends. *Catal. Today* 147, 1–59.

Oller, I.; Malato, S.; Sánchez-Pérez, J.A. 2011. Combination of Advanced Oxidation Processes and biological treatments for wastewater decontamination—A review. *Sci. Total. Environ.* 409, 4141-4166.

Rosal, R.; Rodríguez, A.; Perdigón-Melón, A.; Petrea, A.; García-Calvo, E.; Gómez, M.J.; Agüera, A.; Fernández-Alba, A. 2010. Occurrence of emerging pollutants in urban wastewater and their removal through biological treatment followed by ozonation. *Water Research* 44, 578-588.

UNEP. Vital Water Graphics. 2008. An Overview of the State of the World's Fresh and Marine Waters - 2nd Edition. URL: <http://www.unep.org/dewa/vitalwater/>. Consulted: June 2013

## **Chapter II**

### **State-of-the-Art**

The following section is dedicated to review the application of advanced oxidation process to wastewater treatment during the last decades. A brief explanation of “new generation” pollutants, namely emerging contaminants, and new treatment possibilities is presented, as well as the evolution of the operation, control and modeling of advanced oxidation processes.



## 2.1. Water pollution and treatment

Water pollution refers to the presence of chemical, physical or biological species which change the quality of water and are able to produce harmful effects on ecosystems. It affects surface water, groundwater and even drinking water with serious consequences to human health.

Polluted drinking water is usually present in less-developed countries and in time of war and it is a threat to public health because of the transmission of bacterial waterborne disease. Surface water pollution is harmful to aquatic organisms and causes public health problems, while groundwater pollution is a source of serious health risks. (Peirce et al., 1998)

There are several types of pollutants and all of them affect ecosystems and human health in different ways. Biological pollutants, such as bacteria, viruses, parasitic worms or protozoa are direct disease-causing agents, especially in countries lacking both water and sanitary conditions. Physical pollutants, i.e. sediments, suspended solids or changes in temperature can cause eutrophication and may affect ecosystems natural processes. Chemical pollutants from industrial discharges, agricultural sources or municipal wastewater usually have toxic effects on life. Oxygen demanding substances (from milk processing plants, breweries or paper mills, among other sources) are one of the most important kinds of pollutants as depleting the oxygen dissolved in water when decomposing, and creating anaerobic conditions.

In the last decade, a new group of pollutants, namely emerging contaminants (ECs), have been detected in surface water, ground waters and even in drinking water (because an incomplete removal in conventional wastewater treatment plants) (Broséus et al., 2009) and it has been proved that they interfere with the normal functioning of endocrine systems. ECs are mostly unregulated compounds that may be subject to future regulations depending on their potential effects on health (Petrovic et al., 2003).

ECs have been found in concentrations around  $\mu\text{g L}^{-1}$ ; despite their low concentrations, their high toxicity and pseudo persistent characteristics will become an environmental problem and their consequences over human and animal health can be serious. Actually, in most of the cases effects over human cells physiology and morphology have been demonstrated. Among these contaminants, the following can be mentioned: pharmaceuticals and personal care products (PPCPs, including antibiotics, anti-inflammatories, antiepileptics, lipid regulators, hormones, cosmetics, fragrances, etc.), illicit drugs, perfluorinated compounds, surfactants, fire retardants and disinfection sub products and they are of particular concern because of their endocrine-disrupting properties (Oller et al., 2011; Becerril et al., 2009).

Even when the effects of ECs have been evaluated to determine the consequences of their accumulation, bigger efforts have been made to identify

their sources and ecotoxicology. Regarding PPCPs, they may have toxic effects over most of the biological organisms; in addition to toxic effects, some pharmaceuticals like antibiotics may cause resistant micro-organisms even at low concentrations and their presence in water alters natural ecosystems and inactivate or destroy bacteria used in biological wastewater treatment (Klavarioti et al., 2009).

As it was mentioned before, a lot of these synthetic organic compounds are endocrine disruptors, defined by the US Environmental Protection Agency (US EPA) as exogenous agents that interfere with the synthesis, secretion, transport, bond, action and elimination of natural hormones, which are responsible for homeostasis maintenance, reproduction, development and behavior. Endocrine disruption of living organisms due to synthetic organic compounds has been receiving growing interest in recent years because of the detection of a great number of them in the environment (Gültekin et al, 2007).

Several studies (Heberer, 2002; Petrovic et al., 2003; Esplugas et al., 2007; Ziylan and Ince, 2011; Stuart et al., 2012) report different sources and possible pathways and environmental effects of the occurrence of pharmaceutical contaminants into the aquatic environment, as Figure 2.1 shows. Most of the pharmaceuticals present in the environment are due to their incomplete assimilation in human and animal bodies, being excreted only slightly transformed and even unchanged. After their discharge, they go to the sewage systems and they are hardly eliminated in conventional wastewater treatment plants or in the environment.

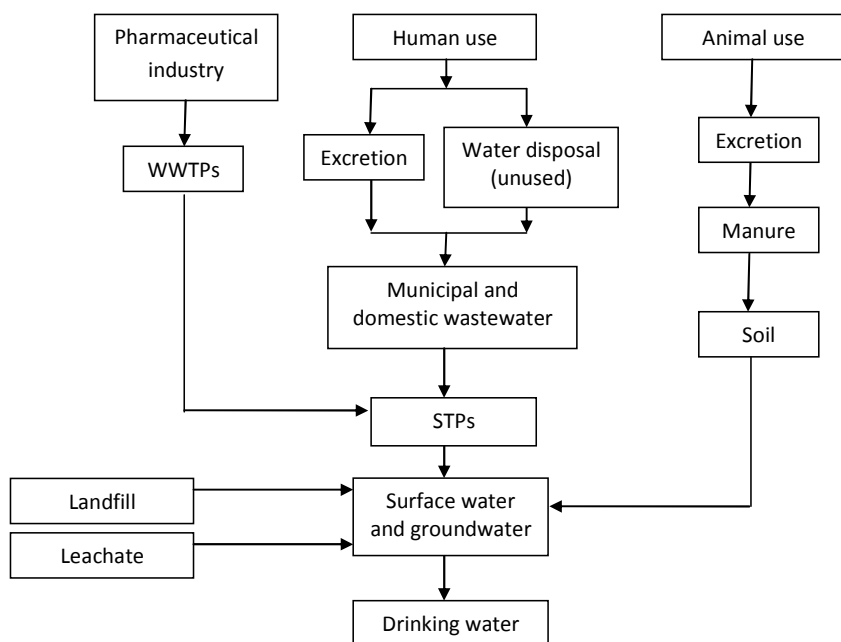


Figure 2.1. Possible sources, pathways and effects for the occurrence of pharmaceutical residues in the aquatic environment

Taking into account the variety of pollutants present in every source of water, the technologies applied to treat a water stream will depend specifically on both the kind of pollutant and the ultimate use such water will have. For instance, drinking water treatment comprises a group of physical treatments to remove suspended solids, color and odor (filtration, settling and flocculation) and a chemical treatment for disinfection (chlorination, UV irradiation, among others). Sewage water requires additional treatments, including biological processes to eliminate oxygen demanding organic matter and/or advanced chemical treatments to remove recalcitrant organic substances.

Generally, every water treatment process starts with a physical treatment (primary treatment) for separating suspended solids, color and other. Then a biological process (secondary treatment) is applied for degrading biodegradable organic matter by means of controlled use of aerobic or anaerobic bacteria. Figure 2.2 presents a schematic representation of a conventional wastewater treatment plant.

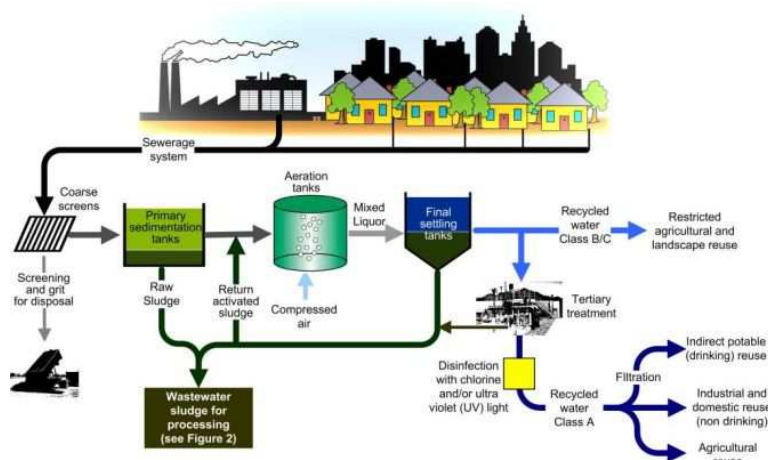


Figure 2.2. Schematic representation of a conventional wastewater treatment plant (Source: <http://www.biosolids.com.au/images/sewage-treatment-process.jpg>)

When reusable water needs to be free of toxic or non-biodegradable substances, a chemical process (tertiary treatment) can be used for refining the waste and eliminate recalcitrant organic matter that cannot be eliminated by biological treatment. In the late times chemical treatments have been used before biological process for avoiding recalcitrant contaminants to inactivate bacteria. These chemical processes are usually advanced oxidation processes (AOPs).

## 2.2. Advanced oxidation processes (AOPs)

AOPs are abiotic degradation processes based on in situ generation of highly oxidant species, such as hydroxyl radicals ( $\text{HO}^\bullet$ ,  $E^0 = 2.73 \text{ V}$ ) among others, capable to degrade organic compounds into  $\text{CO}_2$ ,  $\text{H}_2\text{O}$  and inorganic acids. These processes

have shown to be highly efficient in removing refractory contaminants from wastewaters (Klamerth et al., 2010; Pignatello et al., 2006).

AOPs can be employed before or after conventional treatment; on one hand, when they are used as a pre-treatment stage, they can convert recalcitrant compounds to be more readily biodegradable intermediates and, on the other hand, they can be used as an affine post-treatment after conventional plant to improve effluent quality before its disposal (Klavarioti et al., 2009).

One of the most conventional classifications groups AOPs into photochemical and non-photochemical processes. Photochemical processes are characterized by the use of an irradiation source (normally UV irradiation, see electromagnetic spectrum in Figure 2.3) while the others do not use any kind of irradiation. Table 2.1 presents a classification of AOPs between two categories depending whether the use or not of photo-irradiation; it is important to mention that the absence of photo-irradiation does not imply the absence of an energy source (e.g. electricity).

Table 2.1. AOPs classification

Non-photochemical	Photochemical
Radiolysis $\gamma$	Subcritical and supercritical water oxidation
Electrochemical oxidation	Photolysis ( $\lambda=254\text{nm}$ )
Non thermal plasma	Water photolysis in vacuum ultraviolet (VUV)
Ozonation with hydrogen peroxide	UV / hydrogen peroxide
Ozonation	UV / ozonation
Fenton and related	Photo-Fenton and related
Electro-hydraulic discharge - ultrasound	Heterogeneous photocatalysis

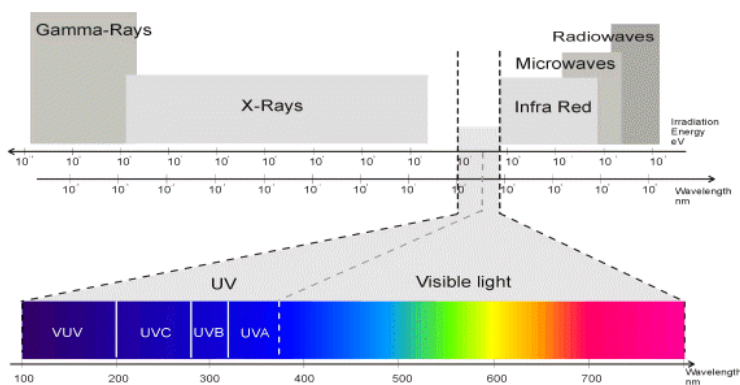


Figure 2.3. Electromagnetic spectrum

Hydroxyl radicals generated are able to degrade organic matter throughout several mechanisms, producing carbon-centered radicals,  $R^\bullet$  (Legrini et al., 1993; Pignatello et al., 2006):

Hydrogen Abstraction:

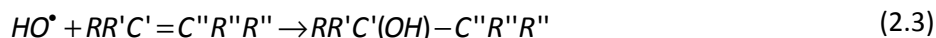




Electron transfer:



Double bonds addition:



According to Pignatello et al., (2006), when oxygen is present in the solution, carbon-centered radicals react to give organic intermediates which may further react with  $HO^\bullet$  or  $O_2$ , leading to an eventual mineralization to  $CO_2$ , water and inorganic acids (if the contaminant contains heteroatoms):

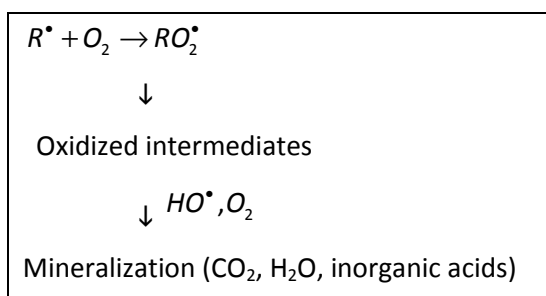
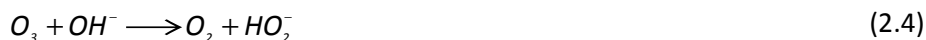


Figure 2.4. Reaction of carbon-centered radicals towards mineralization in the presence of dissolved oxygen

Different AOPs are briefly explained in this section, providing enhanced information on those which are object of this study:

### 2.2.1. Ozone and related

Ozone is a strong oxidant ( $E^0 = 2.07 \text{ V}$ ) and may react directly with nucleophilic molecules (Homem and Santos, 2011). As this direct oxidation does not involve production of hydroxyl radicals, it is not considered an AOP. But when ozone is present in alkaline media, formation of  $HO^\bullet$  is initiated through the decomposition of ozone in water, according to the following mechanism:



The principal limitation of this treatment lies in the low solubility of ozone in water, but the performance of the process can be improved by combining ozone with UV irradiation. The photolysis of the ozone dissolved in water when it is irradiated in the UV-C range, leads to the production of  $H_2O_2$ , which also absorbs irradiation in the same range and dissociates into hydroxyl radicals. Production of  $HO^\bullet$  is described by the following reaction sequence (Homem and Santos, 2011):



The combination of ozone with hydrogen peroxide (perozonation) has also been used and it has proved to be useful for contaminant degradation.

### 2.2.2. Heterogeneous photocatalysis

Heterogeneous photocatalysis is based in direct or indirect absorption or radiant energy by a semiconductor which acts as a sensitizer for light-induced RedOx processes due to their electronic structure, characterized by a filled valence band and an empty conduction band (Malato et al., 2009). Degradation occurs on the interface between the excited solid and the solution without chemical changes in catalyst. Such an excitation can be achieved by two ways:

- Direct excitation of the semiconductor, which absorbs used photons
- Initial excitation of molecules adsorbed on the surface and later charge injection to the semiconductor

Several solids are used as catalysts:  $TiO_2$ ,  $ZnO$ ,  $Fe_2O_3$ ,  $CdS$  and  $ZnS$ , but  $TiO_2$  has demonstrated to be the most active photocatalyst. It absorbs at wavelengths below 388nm and it is widely used because of its high chemical stability and non-toxicity. Oliveros et al. (1993) propose the following mechanism for hydroxyl radical production:



### 2.2.3. H<sub>2</sub>O<sub>2</sub>/UV and related

The homolytic cleavage of hydrogen peroxide by irradiation at wavelengths below 300 nm is presented in Eq. 2.14 and it is safer and more economical way to generate hydroxyl radicals when compared with ozonation. Besides, H<sub>2</sub>O<sub>2</sub> can be mixed with water in any proportion (García et al., 2002).

It must be taken into account that the molar absorption coefficient of H<sub>2</sub>O<sub>2</sub> at 254 nm ( $\xi_{254nm}$ ) is only 18.7 L mol<sup>-1</sup> cm<sup>-1</sup> (Bolton et al., 1994). For that reason, the absorption of incident radiation by the contaminant and other species present in the media competes with absorption by H<sub>2</sub>O<sub>2</sub>. The production of HO<sup>•</sup> will depend on the absorbance spectrum and molar absorption coefficient of the contaminant, the quantum yield of the photolysis, the concentrations of H<sub>2</sub>O<sub>2</sub> and contaminant and the water matrix (López et al., 2000).

As H<sub>2</sub>O<sub>2</sub> absorbs irradiation below 300 nm, low pressure mercury lamps (emitting mostly at 254nm) are used as source of irradiation in hydrogen peroxide/UV processes.

### 2.2.4. VUV photolysis

Water absorbs a great quantity of energy at low wavelengths and its molecules break generating hydroxyl radicals with quantum efficiency depending on used wavelength:



According to Imoberdorf et al. (2012), radiation needed for this aim can be generated by excimer lamps and ozone-generating low-pressure Hg lamps (VUV-Hg lamps); low pressure mercury lamps in Suprasil<sup>®</sup> holders are also useful for this process. Excimer is the name given to “an electronically excited dimer, 'non-bonding' in the ground state. For example, a complex formed by the interaction of an excited molecular entity with a ground state partner of the same structure” (IUPAC, 2012).

The operation of the excimer lamps relies on the radiative decomposition of excimers or exciplexes created by various types of discharges. Using a noble gas, halogen or noble gas/halogen mixtures with fill pressure around 30 kPa, the radiative decomposition of the excimer or the exciplex produces nearly monochromatic radiation. Some particular excimer or exciplexes are commercially available, for example, Ar<sub>2</sub> (126 nm), Xe<sub>2</sub> (192 nm), KrCl (222 nm), among others. Table 2.2 shows the different peak wavelengths (nm) obtained in dielectric-barrier discharges with mixtures of noble gas (NG) and halogen (X<sub>2</sub>).

Table 2.2. Peak wavelengths (nm) obtained in dielectric-barrier discharges with mixtures of noble gas (NG) and halogen (X). (IUPAC, 2012)

	X <sub>2</sub>	Ne	Ar	Kr	Xe
NG <sub>2</sub>			126	146	172
F	157	108	193	249	354
Cl	259		175	222	308
Br	291		165	207	283
I	341			190	253

### 2.3. Fenton and related processes

Fenton process is one of the most studied AOPs in the last three decades; but it was in the 90's when its use in wastewater treatment started to develop. It was first described by Henry John Hornstman Fenton (1894), and it consists in the in situ generation of hydroxyl radicals by the reaction of hydrogen peroxide in presence of a ferrous salt (Haber and Weiss, 1934). This physical-chemical process is capable to change chemical structure of contaminants as hydroxyl radical oxidizes organic matter in a non-selective way. A total mineralization leading to CO<sub>2</sub>, water and organic acids can be finally achieved with adequate process conditions (Chacón et al., 2006).

When, additionally, reaction mixture is irradiated with UV light, hydroxyl radical production is remarkably increased and this process is known as photo-Fenton or photo enhanced Fenton process (Pignatello, 1992). These processes are widely recognized as potentially convenient and economical for treating wastewater containing recalcitrant contaminants because of the harmless, non-expensive, easy handling and environmental friendly characteristics of both, hydrogen peroxide and ferrous salts as (Pignatello et al., 2006; Ríos-Enriquez et al., 2004).

First stage in photo-Fenton process consists in the reaction between ferrous salt and hydrogen peroxide, generating hydroxyl radicals and oxidizing Fe(II) to Fe(III), as the following reaction shows (Chacón et al., 2006; Tokumura et al., 2006):



In other words, hydroxyl radicals generation is due to hydrogen peroxide decomposition catalyzed by ferrous ion; this reaction presents a kinetic constant between 53 and 76 L/mol<sup>-1</sup>s<sup>-1</sup>. The ferric ion formed may react again with hydrogen peroxide, regenerating ferrous ion but at a very low rate  $k = (1-2) \times 10^{-2}$  L/(mol<sup>-1</sup> s<sup>-1</sup>):



However, ferrous ion can go to an excited state when it is irradiated at wavelengths between 300 and 650 nm, regenerating in a faster rate; which increases reaction rate throughout new hydroxyl radical production:



The sequential occurrence of these two oxide-reduction reactions permits organic contaminants mineralization to CO<sub>2</sub> and water (Tokumura et al., 2008).

Most recent studies report the use of heterogeneous Fenton catalysts like Fe-exchanged zeolites, ZSM5 type (Vilhunen et al., 2010), clays and goethite or ion-exchanged clays (Catrinescu et al., 2012). Electro-Fenton and Sono-Fenton technologies involve the combination of Fenton reagent with electricity and/or ultrasound and it has been applied to generate hydroxyl radicals with Fenton reagent at neutral pH.

Table 2.3 presents a brief review of the application of AOPs to the treatment of different types of diverse wastewaters and, more specifically, Tables 2.4 to 2.7 offer a review of the use of AOPs for the remediation of the different contaminants which are object of this study.

Table 2.3. Review of AOPs applied to different types of diverse wastewaters

AOP	Type of WW	References	Relevant results	
Ozone and related	Textile or dyeing	Wang et al. (2003) Babuna et al. (2009) Ledakowicz and Gonera (1999) Lidia et al. (2001) Stanislaw et al. (2001) Cisneros et al. (2002) Baban et al. (2003)	Treatment increases toxicity  Dyes and synthetic textile wastewater are effectively decolorize, but COD removed is not complete	
	Paper mill	Amat et al. (2003b)	COD decrease was dependent on the fatty acids/phenols ratio.	
	Olive mill	Beltrán-Heredia et al. (2001)	Not capable of completely treating highly concentrated olive mill effluents. COD removal not surpasses 20–30%	
	Landfill leachate	Wu et al. (2004) Poznyak et al. (2008) Kurniawan et al. (2006)	Biodegradability increased from a BOD <sub>5</sub> /COD ratio of 0.06 to 0.5 with 1.2 g/L of O <sub>3</sub> . Decomposing toxic compounds after 15 min of ozonation. Treated raw leachate did not comply with the 200 mg/L of COD limit.	
	Tannery	Preethi et al. (2009)	Biodegradability ratio increased from 0.18 to 0.49	
	Pharmaceutical		Sánchez-Polo et al. (2008)	Degradations higher than 90% and 10-20% of TOC removal. Ozonation generates highly toxic oxidation by-products.
			Lin et al. (2009)	H <sub>2</sub> O <sub>2</sub> accelerated the degradation (optimum molar ratio H <sub>2</sub> O <sub>2</sub> /O <sub>3</sub> of 5). 97% removal after 10 min and complete degradation in 20 min for all the compounds.
		Ternes et al. (2003)	Degradation below quantification limit for each compound within 18 min	

Table 2.3. Review of AOPs applied to different types of diverse wastewaters (cont.)

AOP	Type of WW	References	Relevant results
Heterogeneous photocatalysis	Textile or dyeing	Liu and Chiou (2005) Reddy and Kotaiah (2005)	High removal efficiency for reactive dyes
	Paper mill	Pérez et al. (2001) Pérez et al. (2002c)	50% mineralization. Total decolorization and phenols removal from a cellulose ECF effluent High efficiency removal of TOC and COD of a Kraft pulp mill bleaching effluent
	Landfill leachate	Cho et al. (2002)	Study of the relationship between TiO <sub>2</sub> dose and reaction rate
	Winery	Vilar et al. (2009)	Determine the optimal energy dose to reduce real cork boiling wastewater toxicity
	Petrochemical industry	Saien and Nejati (2007) Kuburovic et al. (2007)	More than 90% reduction in COD. Achieved 91% degradation of methyl tertiary butyl ether and the biodegradability improvement was verified with <i>Pseudomonas</i> strain CY
	Olive processing	Chatzisyneon et al. (2008)	Degradation completed with aerobic non-acclimated activated sludge
	Pharmaceutical	Rajkumar and Palanivelu (2004)	95% DOC removal at 44 Ah/L charge with first-order kinetics. Energy consumption = 17 kWh/kg COD
UV/H <sub>2</sub> O <sub>2</sub> and related	Olive mill	Drouiche et al. (2004)	Efficient to finish the treatment of the permeate
	Pharmaceutical	Hofl et al. (1997)	Quantitative AOX removal in 240 min.
	Dyeing	Shu and Hsieh (2006)	Effective decolouration and mineralization of dye effluent
	Distillery	Mohajerani et al. (2011)	Optimal H <sub>2</sub> O <sub>2</sub> concentration = 400 mg L <sup>-1</sup>
VUV photolysis	Textile	Al-Momani et al. (2002)	VUV photolysis enhances biodegradability and could be used as a pre-treatment for conventional biological wastewater treatment.
	Pharmaceutical	Martignac et al. (2013)	The predominant reaction pathway is a photo-Fries rearrangement of paracetamol
	Dyeing	Huang et al. (2013)	VUV photolysis enhances TiO <sub>2</sub> photocatalysis efficiency
Fenton and related	Textile or dyeing	Pérez et al. (2002a) Torrades et al. (2004) Amat et al. (2004) Liu et al. (2007) Ay et al. (2009)	Successful treatment of textile dyes and commercial surfactants
	Paper mill	Pérez et al. (2002b) Torrades et al. (2003)	Successful degradation of the organic content of a Kraft pulp mill bleaching effluent
	Olive mill	Ahmadi et al. (2005) Rizzo et al. (2008a) Lucas and Peres (2009) Dogruel et al. (2009)	Successfully used for removing organic pollutants
		Gernjak et al. (2003, 2004)	Solar photo-Fenton is a promising, cost-effective method for treating olive mill effluents
	Landfill leachate	Lopez et al. (2004) Kang and Hwang (2000) Surmacz-Gorska (2001) Gotvajn et al. (2009)	COD removal efficiency from 60% to 86% for mature, heavily polluted tannery landfill leachate and biologically pre-treated leachate
	Winery	Guedes et al. (2003) Beltrán et al. (2004)	79% and 87% COD removal. Biodegradability ratio increased from 0.27 to 0.63
	Petrochemical industry	Millioli et al. (2003)	Removal and oxidation of oil spilled onto the beach in Guanabara Bay in Rio de Janeiro

Table 2.3. Review of AOPs applied to different types of diverse wastewaters (cont.)

AOP	Type of WW	References	Relevant results
Fenton and related (cont)	Pharmaceutical	Zhang et al. (2006)	Fenton improves degradation of organic compounds before the two-stage reverse osmosis system (TOC removal of 38%). TOC removal efficiency can be up to 99.7%.
		Yang et al. (2009)	Optimal conditions: microwave power 300 W, radiation time 6 min, initial pH 4.42, H <sub>2</sub> O <sub>2</sub> dosage 1300 mg/L and Fe <sub>2</sub> (SO <sub>4</sub> ) <sub>3</sub> 4900 mg/L. COD removal was 57.53%, TOC removal >40%, 55.06% degradation. Microwave enhanced Fenton-like reaction had superior treatment efficiency
		San Sebastián Martínez et al. (2003)	55% COD removal after 10 min at 3 M H <sub>2</sub> O <sub>2</sub> , 0.3 M Fe(II), 40°C
	Biologically pre-treated pharmaceutical	Xing et al. (2006)	94% color and 73% removal after 30 min at pH=3. H <sub>2</sub> O <sub>2</sub> :Fe(II) ratio 3:1, COD:H <sub>2</sub> O <sub>2</sub> ratio 1:0.27 and coagulation at pH=5
	Hospital	Kajitvichyanukul and Suntronvipart (2006)	Increase of aerobic biodegradability and decrease of ecotoxicity at COD:H <sub>2</sub> O <sub>2</sub> :Fe(II) ratio 1:4:0.1 and pH=3
	Textile or dyeing	Pérez et al. (2002a) Torrades et al. (2004) Amat et al. (2004) Liu et al. (2007) Ay et al. (2009)	Successful treatment of textile dyes and commercial surfactants
	Paper mill	Pérez et al. (2002b) Torrades et al. (2003)	Successful degradation of the organic content of a Kraft pulp mill bleaching effluent
	Olive mill	Ahmadi et al. (2005) Rizzo et al. (2008a) Lucas and Peres (2009) Dogruel et al. (2009)	Successfully used for removing organic pollutants
		Gernjak et al. (2003, 2004)	Solar photo-Fenton is a promising, cost-effective method for treating olive mill effluents
	Landfill leachate	Lopez et al. (2004) Kang and Hwang (2000) Surmacz-Gorska (2001) Gotvajn et al. (2009)	COD removal efficiency from 60% to 86% for mature, heavily polluted tannery landfill leachate and biologically pre-treated leachate
	Winery	Guedes et al. (2003) Beltrán et al. (2004)	79% and 87% COD removal. Biodegradability ratio increased from 0.27 to 0.63
	Petrochemical industry	Millioli et al. (2003)	Removal and oxidation of oil spilled onto the beach in Guanabara Bay in Rio de Janeiro
	Pharmaceutical	Zhang et al. (2006)	Fenton improves degradation of organic compounds before the two-stage reverse osmosis system. After the combined treatment the overall TOC removal efficiency was 99.7%.
		Yang et al. (2009)	Microwave enhanced Fenton-like reaction had superior treatment efficiency
		San Sebastián Martínez et al. (2003)	55% COD removal after 10 min at 3 M H <sub>2</sub> O <sub>2</sub> , 0.3 M Fe(II), 40°C
	Biologically pre-treated pharmaceutical	Xing et al. (2006)	94% color and 73% removal after 30 min at pH=3. H <sub>2</sub> O <sub>2</sub> :Fe(II) ratio 3:1, COD:H <sub>2</sub> O <sub>2</sub> ratio 1:0.27 and coagulation at pH=5
Hospital	Kajitvichyanukul and Suntronvipart (2006)	Increase of aerobic biodegradability and decrease of ecotoxicity at COD:H <sub>2</sub> O <sub>2</sub> :Fe(II) ratio 1:4:0.1 and pH=3	

Table 2.3. Review of AOPs applied to different types of diverse wastewaters (cont.)

AOP	Type of WW	References	Relevant results
Electro-Fenton	Dyeing	El-Desoky et al. (2010) Wang et al. (2010)	Successful treatment of textile effluents and real dyeing wastewater
	Landfill leachate	Atmaca (2009) Mohajer et al. (2010) Deng and Englehardt (2007)	Study of the effect of treatment time, DC current, initial pH, initial H <sub>2</sub> O <sub>2</sub> concentration, H <sub>2</sub> O <sub>2</sub> /Fe(II) molar ratio and distance between electrodes
	Tannery	Kurt et al. (2007)	Recovery and reuse of tannery wastewater.

Table 2.4. Treatment technologies used for remediation of sulfamethazine (SMT)

Authors	SMT initial conc.	Applied treatment	Matrix	Relevant results
Adams et al. (2002)	50 µg/L	Coagulation/ flocculation/ sedimentation...	Deionized water, river water, surface water	The process is ineffective to degrade SMT
Kaniou et al. (2005)	10-70 mg/L	Photocatalysis	Deionized water	Pseudo first order kinetics. H <sub>2</sub> O <sub>2</sub> increases remediation rate. TiO <sub>2</sub> improves remediation over ZnO but mineralization is slower.
Chamberlain, E. and Adams, C. (2006)	0.5–1 mg/L	Chlorination	Laboratory and surface water	An initial concentration of 1 mg/L of free chlorine removed an average of 88% of the antibiotics over a pH range of 6.1–9.1.
Košutić et al. (2007)	10 µg/L	Reverse osmosis/ nanofiltration	Pharmaceutical wastewater	Remotion over 0.989
Koyuncu et al. (2008)	10 µg/L	Nanofiltration	Deionized water	
Lin et al. (2009)	40 mg/L	Ozonization	Deionized water/ pharmaceutical wastewater	Presence of H <sub>2</sub> O <sub>2</sub> increases remediation rate. Complete degradation is achieved
Pérez-Moya et al. (2010)	50 mg/L	Photo-Fenton	Deionized water	Doses: 600 mg/L H <sub>2</sub> O <sub>2</sub> , 50 mg/L Fe(II). Total degradation achieved in 2 min. Toxicity increases
Baeza, C. and Knappe, D.R.U. (2011)	4 (±1) µM	Photolysis and UV/H <sub>2</sub> O <sub>2</sub>	Ultra-pure water, lake water, WWTP effluent	pH affected photolysis rates but had little effect on the *OH oxidation rate.
Gao et al. (2012)	0.02 mM	Ultraviolet (UV) light-activated persulfate oxidation	Ultra-pure water	Efficient process to degrade SMT. A reaction pathway is proposed.
Choi et al. (2012)	10 µg/L	Ion exchange	Deionized water	Ion exchange is ineffective to remediate SMT
García-Galán et al. (2012)	40 mg/L	UV	WWTP effluent and ultra-pure water	30 h would be required to fully degrade the analytes at 40 mg/L. 7 different products were identified



Table 2.5. Treatment technologies used for remediation of tetracycline (TC)

Authors	TC initial conc.	Applied treatment	Matrix	Relevant results
Davis et al. (1979)	NE	Photolysis	Deionized water	A red product is formed when TC solution is irradiated at $\lambda < 290$ nm.
Hassan et al. (1985)	NE	Photolysis	$\text{CCl}_4$	AnhydroTC is a major product of TC photolysis
Drexel et al. (1990)	NE	Photolysis	Deionized water	A new photoproduct ("lumiTC", LTC), formed by the irradiation of the phototoxic antibiotic tetracycline (TC) in organic or aqueous media, has been isolated in good yield
Morrison et al. (1991)	1 and 0.5 mM	Photolysis	Deionized water	Photoproducts of TC degradation are lumiTC, anhydroTC, quinine and (dimethylamino)TC. They depend on pH, solvent and presence/absence of oxygen.
Morrison et al. (1991)	0.5 mM	Photolysis	NE	The formation of lumiTC structures is general to the TC family
Miskoski et al. (1998)	100 $\mu\text{M}$	Photolysis	Deionized water and deuterated water	Extremely poor $\phi_{\Delta}$ values. Photoproduct formed through irradiation, efficiently generates $^1\text{O}_2$ with $\phi_{\Delta}=0.24$ . First direct evidence of Type II sensitization by TC photoproducts.
Addamo et al. (2005)	10-50 mg/L	Photocatalysis	Deionized water	Pseudo first order kinetics. 70% remediation in 5 h (photolysis). 98% degradation in 2 h with $\text{TiO}_2$ . Total mineralization is possible.
Reyes et al. (2006)	40 mg/L	Photocatalysis	Deionized water	Pseudo first order kinetics. 100% removal
Bautitz and Nogueira. (2007)	24 mg/L	Photo-Fenton	Deionized water, surface water, STP water	100% remediation in 1 min.
Koyuncu et al. (2008)	10 $\mu\text{g/L}$	Nanofiltration	Deionized water	Degradation around 50-90% achieved in 90 min.
Choi et al. (2008)	10 $\mu\text{g/L}$	Coagulation/ granular activated carbon filtration	Synthetic wastewater and river water	Remotion around 68%
Jiao et al. (2008)	10-40 mg/L	UV	Ultra-pure water	First order kinetics. 15% reduction TOC in 5 h and 73% reduction TC. Toxicity increases
Chen et al. (2008)	1 $\mu\text{M}$	Photolysis	Natural water	$^1\text{O}_2$ and $\text{H}_2\text{O}_2$ were generated in the TC solution under simulated sunlight irradiation over the natural pH range. Photolysis and photoproduction of ROS are dependent on TC speciation.
Palominos et al. (2009)	20 mg/L	Photocatalysis	Deionized water	Dose: 15 g/L $\text{TiO}_2$ , pH=8.7. 80% degradation in 15 min.
Kim et al. (2009)	10 mg/L. PPCPs mixture	Photolysis and UV/ $\text{H}_2\text{O}_2$	Pure water	Average k for all PPCPs increased by 1.3 by $\text{H}_2\text{O}_2$ addition. More than 1 h will be necessary for 90% degradation of 18 PPCPs including TC
Chen et al. (2010)	20-110 $\mu\text{M}$	Adsorption	Deionized water	43% adsorption
López-Peñalver et al. (2010)	10, 20, 40, 60 and 100 mg/L	Photolysis and UV/ $\text{H}_2\text{O}_2$		The mineralization percentage was higher at concentrations of 40–100 $\text{mg L}^{-1}$ concentrations, showing a mean of 47.2%.
Rodríguez-Gil et al. (2010)	>58.8 ng/L	Heterog. photo-Fenton	River waters	Mineralization up to 70%. Nicotine and salicylic acid still remained in low concentrations after treatment

Table 2.5. Treatment technologies used for remediation of tetracycline (TC) (cont.)

Authors	TC initial conc.	Applied treatment	Matrix	Relevant results
Kleinman et al. (2010)	0.8 and 71 $\mu$ M	Photolysis	NE	Evidence of singlet oxygen production
Chen et al. (2011)	20 $\mu$ M	Photolysis	Deionized water	The self-sensitized degradation of TC and OTC occurred in the aqueous solutions under simulated sunlight.
Wang et al. (2011)	5 $\mu$ M	Chlorine dioxide	Surface water and wastewater	TCs react rapidly with ClO <sub>2</sub> . The reaction kinetics of TCs with ClO <sub>2</sub> and FAC depend on the deprotonation of TCs' dimethylamino and phenolic-diketone groups
Yuan et al. (2011)	50 $\mu$ M	Photolysis and UV/H <sub>2</sub> O <sub>2</sub>	Ultra-pure water, surface water, treated water from local WTP and wastewater	Efficiency of UV/H <sub>2</sub> O <sub>2</sub> process was affected by water quality. Detoxification was easier than mineralization
Wang et al. (2011)	2.08 mM	Ozone	Deionized water	Pseudo-first order kinetic model. TC degradation rate increased with pH, gaseous ozone concentration and gas flow rate. Simple degradation pathway of tetracycline was proposed. COD removal = 35% after 90 min.
Wammer et al. (2011)	100 $\mu$ M	Photolysis	Natural waters	45 min to total degradation. Nothing clear about antibacterial activity: further studies suggested
Maroga Mboula et al. (2012)	67 mg/L	Photocatalysis	NE	90 min is not sufficient to generate biodegradable by-products.
Wu et al. (2012)	100-300 mg/L	Electrochemical process using carbon-felt cathode and DSA (Ti/RuO <sub>2</sub> -IrO <sub>2</sub> ) anode	Deionized water	TC efficiently degraded by the electrochemical process. The acute toxicity increased, and the electrochemical process could reduce the acute toxicity of the intermediates to some extent.
Gómez-Pacheco et al. (2012)	10, 20, 40, 60 and 100 mg/L	UV	Ultra-pure water, surface water, groundwater and wastewater	Medium pressure Hg lamp is effective for photooxidation of TCs, favored at pH=10. H <sub>2</sub> O <sub>2</sub> increases TC degradation rate and reduces time required to degrade 100% TC.
Choi et al. (2012)	10 $\mu$ g/L	Ion exchange	Deionized water/STP	Self-decomposition slow. Ion exchange achieves over 80% degradation
Chen et al. (2012)	200 $\mu$ M - 24.1 mM	UV	Surface water	Kinetics, toxicity and products

Table 2.6. Treatment technologies used for remediation of paracetamol (PCT)

Authors	PCT initial conc.	Applied treatment	Matrix	Relevant results
Andreozzi et al. (2003)	$5 \times 10^{-6}$ , $10^{-5}$ , $1.5 \times 10^{-5}$ , $2 \times 10^{-5}$ , 1 M	O <sub>3</sub> , H <sub>2</sub> O <sub>2</sub> /UV	Deionized water	Mineralization degrees up to 30% and 40%.
Szabó et al. (2003)	$10^{-6}$ - $10^{-4}$ mM	Radiolysis	NE	Air saturated solution PCT was easily degraded by irradiation.
Trovó et al. (2008)	0.1 mM	Photo-Fenton	Deionized water and STP effluent	Degradation is favored in the presence of potassium ferrioxalate Fe(NO <sub>3</sub> ) <sub>3</sub> , under solar irradiation, the oxidation of PCT is faster than under black-light irradiation.
Yang et al. (2008)	2 mM	Photocatalysis	Ultra-pure water	UVA radiation does not degrade PCT but UVC does with marginal changes in TOC. In the presence of TiO <sub>2</sub> , faster degradation and mineralization occurred
Kim et al. (2009)	10 mg/L. PPCPs mixture	Photolysis and UV/H <sub>2</sub> O <sub>2</sub>	Pure water	Average k for all PPCPs increased by 1.3 by H <sub>2</sub> O <sub>2</sub> addition during UV treatment
Klamerth et al. (2010)	15 EC, each at 100 µg/L	Photo-Fenton	Simulated and real effluent of MWTP	ECs at low concentrations can be degraded to negligible concentrations with solar photo-Fenton at low iron concentrations (5 mg/L) and low initial H <sub>2</sub> O <sub>2</sub> (50 mg/L) concentrations without adjusting the pH.
Santos-Juanes et al. (2011b)	4 mM	Photo-Fenton	Ultra-pure water	Continuous dosing of H <sub>2</sub> O <sub>2</sub> as function of oxygen concentration is proposed. DO is a key parameter in monitoring process
Santos-Juanes et al. (2011a)	1 mM	Photo-Fenton	Deionized water	Mineralization level and reaction time: the keys for increasing plant efficiency
Durán et al. (2011)	10 mg/L	Photo-Fenton	Synthetic MWTP effluent	The reaction takes place mainly through a radical and single oxygen mechanism (96.7%).
Cabrera Reina et al. (2012)	4 and 25 mM of TOC	Photo-Fenton	Ultra-pure water	A semiempirical model has been developed to predict TOC mineralization, H <sub>2</sub> O <sub>2</sub> consumption and DO concentration
Bernabeu et al. (2012)	10 µg/L, 5, 10 and 50 mg/L, in a mixture of 6 EC	Mild solar photo-Fenton	Ultra-pure water	At high concentrations, acidic photo-Fenton was able to achieve a fast removal of the ECs. Complete mineralization was not reached. At neutral media the process was two orders of magnitude less efficient than at acidic pH
De Luna et al. (2012)	8 mM	Electro Fenton	Wastewater	The electro-Fenton process was proven to be more efficient in the treatment of PCT containing wastewater than the photoelectro-Fenton method. A degradation pathway is proposed
De la Cruz et al. (2012)	32 EC: TOC=15.9 mg/L, Micropol=29.5 mg/L	Photolysis, Fenton and neutral photo-Fenton	Wastewater	Potential use of the photo-Fenton process at neutral pH. Photo-Fenton, employing UV <sub>254</sub>
Li et al. (2012)	1 µg/L of each PPCP	Fenton	WWTP effluent	All examined PPCPs except atrazine and iopromide could be completely removed by Fenton at 20 mg/L Fe(II) dose and 2.5 H <sub>2</sub> O <sub>2</sub> /Fe(II) molar ratio. Fenton caused an up to 30% DOC removal
Martignac et al. (2013)	$2.65 \times 10^{-4}$ M	UV/ VUV, UV/H <sub>2</sub> O <sub>2</sub>	Ultra-pure water	The predominant reaction pathway is a photo-Fries rearrangement

Table 2.7. Treatment technologies used for remediation of coffee/caffeine

Authors	Coffee/Caffeine initial conc.	Treatment	Matrix	Relevant results
Tokumura et al. (2006)	0 – 446 mg/L	Photo-Fenton	NE	UV/Fe(II)/H <sub>2</sub> O <sub>2</sub> system is efficient for the treatment of coffee effluents. 93% mineralization of 250mg/L model coffee effluent was achieved after 250 min
Tokumura et al. (2008)	300 mg/L	Solar photo-Fenton	NE	With increasing Fe dosage the rate of the decolorization increased but the enhancement was not pronounced beyond 10 mg/L. Addition of H <sub>2</sub> O <sub>2</sub> increased the decolorization rate up to around 1000 mg/L of H <sub>2</sub> O <sub>2</sub>
Rosal et al. (2009)	50 mg/L	Ozone	Pure water	Ozonation of caffeine was rapid during the initial 15 s reaction period. Second order kinetic constants increased from 0.25 to 1.05 M/s for increasing pH in the 3–10 range.
Broséus et al. (2009)	2074 ng/L	Ozone	Ultra-pure and natural waters	Caffeine removal at bench-scale was similar to removal observed in full-scale DWTPs. Caffeine could be used as an indicator compound to predict full scale removal of ozonation processes for the oxidation of a wide range of EDCs and pharmaceuticals
Yamal-Turbay et al. (2012)	300 mg/L	Photo-Fenton	Natural water	H <sub>2</sub> O <sub>2</sub> systematic dosage protocol increases process efficiency with 70% TOC removal instead of 60% when no dosage protocol is applied. Doses: 500 mg/L H <sub>2</sub> O <sub>2</sub> and 10 mg/L Fe(II) and a low pressure Hg lamp
Trovó et al. (2013)	5 - 50 mg/L	Photo-Fenton	STP and surface water	Photo-Fenton process can be successfully applied in the degradation of caffeine, even when present in complex samples such as SW and STP effluents
Li et al. (2012)	1 µg/L of each PPCP	Fenton	WWTP effluent	Examined PPCPs except atrazine and iopromide were completely removed by Fenton oxidation at a 20 mg/L Fe(II) dose and a 2.5 H <sub>2</sub> O <sub>2</sub> /Fe(II) molar ratio. Treatment caused up to 30% TOC removal

### 2.3.1. Fenton processes operation

Many authors have demonstrated that Fenton processes performance is strongly affected by variables such as pH, temperature, H<sub>2</sub>O<sub>2</sub>/contaminant and H<sub>2</sub>O<sub>2</sub>/Fe(II) ratios, irradiation source, matrix and reagent dosage, among others. (Kuo, 1992; Pignatello et al., 2006; Gulkaya et al., 2006; Burbano et al., 2008; Gernjak et al., 2006)

Initial efforts were devoted to identify the best operation conditions and more recently other energy and irradiation sources and strategies for reagent dosage have been investigated. Some other improvements, such as solid reusable catalysts and nanotechnology have been recently under study.

The most suitable pH has been determined to be slightly below 3.0 because of the dependence of the speciation of Fe(III) with pH; actually, a range between 2.5 and 4.0 is frequently reported as optimal for Fenton processes. At pH>4.0, the formation of ferric hydroxo complexes reduces the generation rate of HO<sup>•</sup> and at pH<2.0, the reaction rate is slower because of the formation of complex species

$[\text{Fe}(\text{H}_2\text{O})_6]^{2+}$  and additionally, high concentrations of  $\text{H}^+$  ions lead to solvate hydrogen peroxide (Kuo, 1992; Pignatello et al., 2006; Gulkaya et al., 2006).

Temperature has been found to be an important parameter in Fenton process, as higher temperatures lead to an improvement in process performance. On the other hand, photo-Fenton process is less susceptible to the influence of temperature as the Fe(III) photo-activation is the most important step.

According to Gulkaya et al. (2006),  $\text{H}_2\text{O}_2/\text{Fe}(\text{II})$  ratio is a critical parameter in Fenton process and keeping such variable within an optimal range makes possible to decrease Fenton's reagents concentrations while maintaining a good COD removal efficiency. However, these authors observe a wide difference among ratios used by different research groups, depending mostly on the types of organics and their loads. As an example of that, the following studies can be mentioned: Herney et al. (2005) reported ratios ranging between 5:1 and 20:1, while other authors present values from 10:1 to 200:1 (Gernjak et al., 2006) and even from 100:1 to 1000:1 (Pignatello et al., 2006).

Actually, several studies confirm that inadequate reagent ratios or doses promote the scavenging of the  $\text{HO}^\bullet$  produced in the first stages of the process (Eq. 2.6 to 2.8). According to Legrini et al., (1993), at high concentrations, hydroxyl radicals may dimerize to  $\text{H}_2\text{O}_2$  (Eq. 2.9) and an excess of  $\text{H}_2\text{O}_2$  may promote the production of hydroperoxyl radicals (Eq. 2.10), which are much less reactive with organic matter. By the other hand, the presence of an excess of Fe(II) is also capable to scavenge  $\text{HO}^\bullet$  (Huston and Pignatello, 1999)



Matrix is another important factor to take into account in contaminants degradation via Fenton processes. Most of the reported researches consist of works using deionized water and even ultra-pure water, but organic load present in natural waters of STP effluents interferes with the efficiency of the process; other species such as humic acids have been reported both to be beneficial for pharmaceuticals degradation and also to inhibit the degradation through competition for  $\text{HO}^\bullet$ . The presence of carbonates also decreases efficiency by scavenging produced  $\text{HO}^\bullet$  (Bautitz and Nogueira, 2007). Presence of quinones, which are by-products of aromatic compounds degradation, has been reported to improve photo-Fenton process by catalyzing the hydroxylation of aromatic rings and favoring the Fe(III) to Fe(II) cycling (Pignatello et al., 2006).

Despite the low cost of used reagents, the main drawback of photochemical AOPs lays in their high energy cost, especially when long process time is required to achieve final product specifications. Consequently, the use of solar energy has been a widely studied alternative to artificial irradiation and it has provided good

results in contaminants degradations and mineralization (Rosetti et al., 2004; Gernjak et al., 2006; Farías et al., 2007). Solar photo-Fenton has been used to treat a wide variety of organic compounds: textile effluents, bleaching effluents, chlorinated solvents, dyes, pesticides, pharmaceuticals, among others (Malato et al., 2009; Farías et al., 2010).

More recently, researchers have been focused in identifying operation conditions which lend to improve process efficiency and the most promising approach involves a continuous reagent dosage during the process span. A sequential addition of reagent favors an efficient usage of HO• produced, minimizing scavenging reactions and therefore increasing process efficiency (Chu et al., 2007; Zazo et al., 2009; Monteagudo et al., 2009; Yamal-Turbay et al., 2012).

Regarding process monitoring, it has been usually undertaken by sampling at regular intervals and measuring parameters such as TOC, contaminant and/or reagents concentrations along the process span. This traditional sampling/measuring system is time-demanding and might involve high costs in reagents and materials, besides providing an important delay in decision making.

The present trend for monitoring process suggests the use of on-line variables such as oxidation reduction potential (ORP) and dissolved oxygen concentration (DO) as they show important variations during the process evolution, as it has been stated by Santos-Juanes et al., (2010), Prieto-Rodríguez et al. (2011) and Tokumura et al., (2011). These investigations suggest that these variables might be useful for process control purposes, but further research is still necessary to reach a more complete understanding of these parameters and to develop rigorous models.

### **2.3.2. Modeling of Fenton processes**

A lot of efforts have been devoted to understand and predict Fenton treatments behavior, but the complex character of the process implies that there is much work ahead in order to completely identify pathways and mechanisms. Even when the most important reaction steps have been elucidated so far (Walling and Goose, 1973; Buxton et al., 1988; Pignatello, 1992; Sun and Pignatello, 1993; de Laat and Gallard, 1999; Pignatello et al., 2006) the determination of the degradation mechanisms and subproducts involved is a very difficult task.

Several approaches have been undertaken in the literature in order to model Fenton and photo-Fenton processes. Empirical and semi-empirical approaches based on design of experiment (DOE) methodology (e.g. Pérez-Moya et al., 2010), artificial neural networks (ANN, e.g. Durán et al., 2006) and/or surface response methodology (SRM, e.g. Gernjak et al., 2006) have been used for researches. Even when these models do not allow generalizations or do not fulfill scaling needs, they are useful for particular cases when the mechanism is not well understood. The pseudo-first-order model is the kinetic model most commonly used to represent photo-Fenton process, especially for explaining TOC degradation.

More rigorous phenomenological models based on mass and energy balances, despite being extremely complex and requiring a full understanding of the process, have been studied during the last decades and a lot of kinetic constants are available in the bibliography. The main difficulty of this kind of approach lays in the complexity of the irradiation model, especially when solar irradiation is involved (Rosetti et al., 2002 and 2004; Fariás et al., 2009 and 2010).

Tables 2.8 and 2.9 summarize some of the researches devoted to model Fenton and photo-Fenton process according to the different approaches presented.

Table 2.8. Researches involving empirical modeling via experimental design

Author(s)	Contaminant	Process	Observation
Oliveros et al., 1997	Industrial WW	Photo-Fenton	RSM
Martínez and López, 2001	Industrial WW	Fenton	ANN
Chan and Chu, 2003	Atrazine	Fenton	$\frac{C_t}{C_0} = 100 - \frac{100t}{\rho + \sigma t}$ (%),
Teixeira et al., 2004	Silicones	Photo-Fenton	ANN
Henry Ramírez et al., 2005	Orange II	Fenton	RSM
Durán et al., 2006	Reactive Blue 4	Photo-Fenton	ANN
Gernjak et al., 2006	Alachlor	Photo-Fenton	RSM
Tokumura et al., 2006	Orange II	Photo-Fenton	Pseudo 1 <sup>st</sup> order
Trovó et al., 2006	4-clorophenol	Photo-Fenton	RSM
Pérez-Moya et al., 2007	2-clorophenol	Fenton and photo-Fenton	RSM
Pérez-Moya et al., 2008	4-clorophenol	Photo-Fenton	2 <sup>nd</sup> order polynomial, potential and Hoerl equation
Pérez-Moya et al., 2008	4-clorophenol	Fenton and photo-Fenton	RSM
Torrades et al., 2008	Dyes	Fenton and photo-Fenton	Pseudo 1 <sup>st</sup> order kinetics
Wang, 2008	C.I. Acid Black 1	Fenton and photo-Fenton	1 <sup>st</sup> order, 2 <sup>nd</sup> order and combined order
Chan and Chu, 2009	Alachlor	Photo-Fenton	Pseudo 1st order
Galehdar et al., 2009	MDF effluent	Photo-Fenton	RSM-Optimization
Lucas and Peres, 2009	Olive mill WW	Fenton	Pseudo 1 <sup>st</sup> order
Monteagudo et al., 2009	Orange II	Photo-Fenton	RSM
Zazo et al., 2009	Phenol	Fenton	2 <sup>nd</sup> order
Arslan-Alaton et al., 2010	H-acid	Photo-Fenton	RSM
Elmolla et al., 2010	Antibiotics	Fenton	ANN
Homem et al., 2010	Amoxicilin	Fenton	RSM
Monteagudo et al., 2010	Protocatechuic acid	Photo-Fenton	ANN
Nichela et al., 2010	Benzoic acid	Fenton-like and Photo-Fenton	$f = \frac{1 - a \times t - d}{1 + (t/b)^c} + d$
Pérez-Moya et al., 2010	Sulfamethazine	Photo-Fenton	RSM
Rozas et al., 2010	Ampicillin	Fenton and photo-Fenton	RSM
Dopar et al., 2011	Simulated WW	Photo-Fenton	RSM
Durán et al., 2011	Paracetamol	Photo-Fenton	ANN
Pérez-Moya et al., 2011	Sulfamethazine	Photo-Fenton	Pseudo 1 <sup>st</sup> order
Pontes and Pinto, 2011	Phenol	Fenton	ANN
Popuri et al., 2011	ABS	Fenton	Pseudo 1 <sup>st</sup> order
Trovó et al., 2012	Caffeine	Photo-Fenton	RSM
De Luna et al., 2013	Paracetamol	Fenton	2 <sup>nd</sup> order

Table 2.9. Researches involving mechanistic modeling

Author(s)	Contaminant	Process
Andreozzi et al., 2000	Benxothiazole	Fenton
Kang et al, 2002	Phenol	Fenton
Rosetti et al., 2002	Formic acid	Photo-Fenton
Rosetti et al., 2004	Formic acid	Photo-Fenton
Duesterberg et al., 2005	Formic acid	Fenton
Duesterberg and Waite, 2006	Formic acid	Fenton
Kusic et al., 2006	Phenol	Photo-Fenton
Farías et al., 2009	Formic acid	Photo-Fenton
Kusic et al., 2010	Dyes	Photo-Fenton
Farías et al., 2010	Formic acid	Photo-Fenton
Ortiz de la Plata et al., 2010	2-clorophenol	Fenton and photo-Fenton
Pontes et al., 2010	Phenol	Fenton
Simunovic et al., 2011	Simulated industrial WW	Photo-Fenton
Conte et al., 2012	2,4-dichlorophenoxyacetic acid	Photo-Fenton
Cabrera Reina et al., 2012	Paracetamol	Photo-Fenton

It is worth mentioning that most of the available models are adapted to a batch operation, with the reagents totally dosed at the beginning of the process, despite it has been demonstrated that this strategy may lead to a waste of  $H_2O_2$  as well as to the scavenging of produced  $HO^\bullet$ . Only a few of the most recent studies (Chu et al., 2007; Zazo et al., 2009; Yamal-Turbay et al., 2012 and Yamal-Turbay et al., 2013) have intended to apply and model different reagent dosage schemes, with satisfactory results.

Hence, this work aims to investigate new strategies to improve Fenton and photo-Fenton process towards a more efficient operation. Next chapter introduces the experimental and mathematical tools which were used for accomplishing such objectives.

## 2.4. References

- Adams, C., Asce, M., Wang, Y., Loftin, K., Meyer, M. 2002. Removal of antibiotics from surface and distilled water in conventional water treatment processes. *J. Environ. Eng.* 128, 253.
- Addamo, M., Augugliaro, V., Di Paola, A., García-López, E., Loddo, V., Marci, G., Palmisano, L. 2005. Removal of drugs in aqueous systems by photoassisted degradation. *J. Appl. Electrochem.* 35, 765.
- Ahmadi, M., Vahabzadeh, F., Bonakdarpour, B., Mofarrah, E., Mehranian, M. 2005. Application of the central composite design and response surface methodology to the advanced treatment of olive oil processing wastewater using Fenton's peroxidation. *J. Hazard. Mater.* 123 (1–3), 187.
- Al-Momani, F., Touraud, E., Degorce-Dumas, J.R., Roussy, J. and Thomas, O. 2002. Biodegradability enhancement of textile dyes and textile wastewater by VUV photolysis. *J. Photochem. Photobio A.* 153(1-3), 191-197.



- Amat, A.M., Arqués, A., Beneyto, H., García, A., Miranda, M.A., Seguí S. 2003. Ozonisation coupled with biological degradation for treatment of phenolic pollutants: a mechanistically based study. *Chemosphere* 53, 79.
- Amat, A.M., Arqués, A., Miranda, M.A., Seguí, S. 2004. Photo-Fenton reaction for the abatement of commercial surfactants in a solar pilot plant. *Sol. Energy*. 77, 559.
- Andreozzi, R., D'Apuzzo, A., Marotta, R. 2000. A kinetic model for the degradation of benzothiazole by Fe<sup>3+</sup>-photo-assisted Fenton process in a completely mixed batch reactor. *J. Hazard. Mater.* 80, 241.
- Andreozzi, R.; Caprio, V.; Marotta, R.; Vogna, D. 2003. Paracetamol oxidation from aqueous solutions by means of ozonation and H<sub>2</sub>O<sub>2</sub>/UV system. *Water Res.* 37, 993.
- Arslan-Alaton, I., Ayten, N., Olmez-Hanci, T. 2010. Photo-Fenton-like treatment of the commercially important H-acid: Process optimization by factorial design and effects of photocatalytic treatment on activated sludge inhibition. *Appl. Catal. B.* 96, 208.
- Atmaca, E. 2009. Treatment of landfill leachate by using electro-Fenton method. *J. Hazard. Mater.* 163, 109.
- Ay, F., Catalkaya, E.C., Kargi, F. 2009. A statistical experiment design approach for advanced oxidation of direct Red azo-dye by photo-Fenton treatment. *J. Hazard. Mater.* 162, 230.
- Baban, A., Yediler, A., Lienert, D., Kemerdere, N., Kettrup, A. 2003. Ozonation of high strength segregated effluents from a woollen textile dyeing and finishing plant. *Dyes. Pigm.* 58(2), 93.
- Bautitz, I.R., Nogueira, R.F.P. 2007. Degradation of tetracycline by photo-Fenton process e solar irradiation and matrix effect. *J Photochem. Photobiol. A.* 187, 33.
- Becerril, K. 2009. Contaminantes emergentes en el agua. *Digital Journal*, 10, 8. [URL: <http://www.revista.unam.mx/vol.10/num8/art54/art54.pdf>]
- Beltrán-Heredía, J., Torregrosa, J., García, J., Domínguez, J.R., Tierno, J.C. 2001. Degradation of olive mill wastewater by the combination of Fenton's reagent and ozonation processes with an aerobic biological treatment. *Water. Sci. Technol.* 44, 103.
- Beltrán-Heredía, J., Domínguez, J.R., López, R. 2004. Advanced oxidation of cork-processing wastewater using Fenton's reagent: kinetics and stoichiometry. *J. Chem. Technol. Biotechnol.* 79, 407.
- Bernabeu, A.; Palacios, S.; Vicente, R.; Vercher, R.F.; Malato, S.; Arques, A.; Amat, A.M. 2012. Solar photo-Fenton at mild conditions to treat a mixture of six emerging pollutants. *Chem. Eng. J.* 198–199, 65.

Bolton, J.R., Cater, S.R. in: Helz, G.R., Zepp, R.G., Crosby, D. G. (Eds.). 1994. Aquatic and Surface Photochemistry, Lewis Publishers, Boca Raton, FL, USA. pp. 467–490.

Braun, A.M., Oliveros, E., Maurette, M-T. Photochemical technology. 1991. John Wiley & Sons Ltd. England.

Broséus, R.; Vincent, S.; Aboufadi, K.; Daneshvar, A.; Sauvé, S.; Barbeau, B.; Prévost, M. 2009. Ozone oxidation of pharmaceuticals, endocrine disruptors and pesticides during drinking water treatment. *Water Res.* 43, 4707.

Burbano, A.A., Dionysiou, D.D., Suidan, M.T. 2008. Effect of oxidant-to-substrate ratios on the degradation of MTBE with Fenton reagent. *Water Res.* 42, 3225.

Buxton, G.V.; Grenstock, C.L.; Helman, W.P.; Ross, A.B. 1988. Critical Review of Rate Constants for Reactions of Hydrated Electrons, Hydrogen Atoms and Hydroxyl Radicals ( $\bullet\text{OH}/\bullet\text{O}$ ) in Aqueous Solution. *J. Phys. Chem. Ref. Data* 17:2, 513.

Cabrera Reina, A., Santos-Juanes, L., García, J.L., Casas, J.L., Sánchez, J.S. 2012. Modelling photo-Fenton process for organic matter mineralization, hydrogen peroxide consumption and dissolved oxygen evolution, *Appl. Catal. B.* 119-120, 132.

Catrinescu, C.; Arsene, D.; Apopei, P.; Teodosiu, C. 2012. Degradation of 4-chlorophenol from wastewater through heterogeneous Fenton and photo-Fenton process, catalyzed by Al-Fe PILC. *Appl. Clay. Sci.* 58, 96.

Chacón, J.M., Leal, M.T., Sánchez, M. y Bandala, E. 2006. Solar photocatalytic degradation of azo-dyes by photo-Fenton process. *Dyes. Pigm.* 69, 144.

Chamberlain, E. and Adams, C. 2006. Oxidation of sulfonamides, macrolides, and carbadox with free chlorine and monochloramine. *Water Res.* 40, 2517.

Chan, K.H. and Chu, W. 2003. The system design of atrazine oxidation by catalytic oxidation process through a kinetic approach. *Water Res.* 37, 3997.

Chan, K.H. and Chu, W. 2009. Reactor model development: The removal performance of ferrous-catalysed photo-oxidation process by examining the reaction parameters. *J. Hazard. Mater.* 167, 199.

Chen, Y., Hu, C., Qu, J., Yang, M. 2008. Photodegradation of tetracycline and formation of reactive oxygen species in aqueous tetracycline solution under simulated sunlight irradiation. *J. Photochem. Photobio. A.* 197, 81.

Chen, W.-R., Huang, C.-H. 2010. Adsorption and transformation of tetracycline antibiotics with aluminium oxide. *Chemosphere* 79, 779.

Chen, Y., Li, H., Wang, Z., Tao, T., Hu, C. 2011. Photoproducts of tetracycline and oxytetracycline involving self-sensitized oxidation in aqueous solutions: Effects of  $\text{Ca}^{2+}$  and  $\text{Mg}^{2+}$ . *Environ. Sci.* 23:10, 1634.

- Chen, Y., Li, H., Wang, Z., Tao, T., Wei, D., Hu, C. 2012. Photolysis of Chlortetracycline in aqueous solution: Kinetics, toxicity and products. *J. Environ. Sci.* 24:2, 254.
- Cheremisinoff, N. *Handbook of Water and Wastewater Treatment Technologies*. Butterworth-Heinemann, USA. 2002. Chapter 1
- Choi, K.-J., Kim, S.-G., Kim, S.-H. 2008. Removal of antibiotics by coagulation and granular activated carbon filtration. *J. Hazard. Mater.* 151, 38.
- Choi, K.-J.; Son, H.-J.; Kim, S.-H. 2012. Ionic treatment for removal of sulfonamide and tetracycline classes of antibiotic. *Sci. Total. Environ.* 387, 247.
- Chu, W.; Chan, K. H.; Kwan, C. Y.; Choi, K. Y. 2007. Degradation of atrazine by modified stepwise-Fenton's processes. *Chemosphere* 67, 755.
- Cisneros, R.L., Espinoza, A.G., Litter, M.I. 2002. Photodegradation of an azo dye of the textile industry. *Chemosphere* 48, 393.
- Conte, L.O., Farías, J., Albizzati, E.D., Alfano, O.M. 2012. Photo-Fenton Degradation of the Herbicide 2,4-Dichlorophenoxyacetic Acid in Laboratory and Solar Pilot-Plant Reactors. *Ind. Eng. Chem. Res.* 51, 4181.
- Costa, C.R., Olivi, P. 2009. Effect of chloride concentration on the electrochemical treatment of a synthetic tannery wastewater. *Electrochim. Acta.* 54, 2046.
- Davies, A.K., McKellar, J.F., Phillips, G.O., Reid, A.G. 1979. Photochemical oxidation of tetracycline in aqueous solution. *J. Chem. Soc., Perkin. Trans. 2*, 369.
- De la Cruz, N., Giménez, J., Esplugas, S., Grandjean, D., de Alencastro, L.F., Pulgarín, C. 2012. Degradation of 32 emergent contaminants by UV and neutral photo-fenton in domestic wastewater effluent previously treated by activated sludge. *Water Res.* 46, 1947.
- De Laat, J. and Gallard, A. 1999. Catalytic Decomposition of Hydrogen Peroxide by Fe(III) in Homogeneous Aqueous Solution: Mechanism and Kinetic Modeling. *Environ. Sci. Technol.* 33, 2726.
- De Luna, M.D.G., Veciana, M.L., Su, C.-C., Lu, M.-C. 2012. Acetaminophen degradation by electro-Fenton and photoelectro-Fenton using a double cathode electrochemical cell. *J. Hazard. Mater.* 217-218, 200.
- De Luna, M.D.G., Briones, R.M., Su, Ch-Ch., Lu, M-Ch. 2013. Kinetics of acetaminophen degradation by Fenton oxidation in a fluidized-bed reactor. *Chemosphere* 90, 1444.
- Deng, Y., Englehardt, J.D. 2007. Electrochemical oxidation for landfill leachate treatment. *Waste Manage.* 27, 380.
- Dogruel, S., Olmez-Hanci, T., Kartal, Z., Arslan-Alaton, I., Orhon, D. 2009. Effect of Fenton's oxidation on the particle size distribution of organic carbon in olive mill wastewater. *Water Res.* 43, 3974.

Dopar, M., Kusic, H., Koprivanac, N. 2011. Treatment of simulated industrial wastewater by photo-Fenton process. Part I: The optimization of process parameters using design of experiments (DOE). *Chem. Eng. J.* 173, 267.

Drexel, R.E., Olack, G. Jones, C., Chmurny, G.N., Santini, R., Morrison, H. 1990. Lumitetracycline: A Novel New Tetracycline Photoproduct. *J. Org. Chem.* 55, 2471.

Duesterberg, C.K., Cooper, W.J., Waite, T.D. 2005. Fenton-Mediated Oxidation in the Presence and Absence of Oxygen. *Environ. Sci. Technol.* 39, 5052.

Duesterberg, C.K. and Waite, D. 2006. Process Optimization of Fenton Oxidation Using Kinetic Modeling. *Environ. Sci. Technol.* 40, 4189.

Durán, A.; Monteagudo, J.M.; Mohedano, M. 2006. Neural networks simulation of photo-Fenton degradation of Reactive Blue 4. *Appl. Catal. B.* 65, 127.

Durán, A., Monteagudo, J.M., Carnicer, A., Ruiz-Murillo, M. 2011. Photo-Fenton mineralization of synthetic municipal wastewater effluent containing acetaminophen in a pilot plant. *Desalination* 270, 124.

El-Desoky, H.S., Choneim, M.M., El-Sheikh, R., Zidan, N.M. 2010. Oxidation of Levafix CA reactive azo-dyes in industrial wastewater of textile dyeing by electro-generated Fenton's reagent. *J. Hazard. Mater.* 175, 858.

Elmolla, E.S., Chaudhuria, M., Meselhy Eltoukhy, M. 2010. The use of artificial neural network (ANN) for modeling of COD removal from antibiotic aqueous solution by the Fenton process. *J. Hazard. Mater.* 179, 127.

Esplugas, S., Bila, D.M., Krause, L.G.T., Dezotti, M. 2007. Ozonation and advanced oxidation technologies to remove endocrine disrupting chemicals (EDCs) and pharmaceuticals and personal care products (PPCPs) in water effluents. *J. Hazard. Mater.* 149, 631.

Farias, J., Rossetti, G.H., Albizzati, E.D., Alfano, O.M. 2007. Solar Degradation of Formic Acid: Temperature Effects on the Photo-Fenton Reaction. *Ind. Eng. Chem. Res.* 46, 7580.

Farias, J., Albizzati, E.D., Alfano, O.M. 2009. Kinetic study of the photo-Fenton degradation of formic acid. Combined effects of temperature and iron concentration. *Catal. Today* 144, 117.

Farias, J., Albizzati, E.D., Alfano, O.M. 2010. New Pilot-Plant Photo-Fenton Solar Reactor for Water Decontamination. *Ind. Eng. Chem. Res.* 49, 1265.

Fatta-Kassinos, D., Vasquez, M.I., Kümmerer, K. 2011. Transformation products of pharmaceuticals in surface waters and wastewater formed during photolysis and advanced oxidation processes – Degradation, elucidation of byproducts and assessment of their biological potency. *Chemosphere* 85, 693.

Fenton, H.J.H. 1894. Oxidation of tartaric acid in presence of iron, *J. Chem. Soc.* 65, 899–910.

- Galehdar, M., Younesi, H., Hadavifar, M., Zinatizadeh, A.A. 2009. Optimization of a Photo-assisted Fenton Oxidation Process: A Statistical Model for MDF Effluent Treatment. *Clean* 37:8, 629.
- Gao, Y., Gao, N. Deng, Y., Yang, Y., Ma, Y. 2012. Ultraviolet (UV) light-activated persulfate oxidation of sulfamethazine in water. *Chem. Eng. J.* 195-196, 248.
- García E.,F.S., Lopez, J., Carlos, L, Capparelli, A.L. 2002. Evaluation of the efficiency of photodegradation of nitroaromatics applying the UV/H<sub>2</sub>O<sub>2</sub> technique. *Environ. Sci. Technol.* 36, 3936-3944.
- García-Galán, M.J., Díaz-Cruz, M.S., Barceló, D. 2012. Kinetic studies and characterization of photolytic products of sulfamethazine, sulfapyridine and their acetylated metabolites in water under simulated solar irradiation. *Water Res.* 46, 711.
- Germirli Babuna, F., Camur, S., Arslan-Alaton, I., Okay, O., Iskender, G. 2009. The application of ozonation for the detoxification and biodegradability improvement of a textile auxiliary: naphthalene sulphonic acid. *Desalination* 249, 682.
- Gernjak, W., Krutzler, T., Glaser, A., Malato, S., Cáceres, J., Bauer, R. 2003. Photo-Fenton treatment of water containing natural phenolic pollutants. *Chemosphere* 50, 71.
- Gernjak, W., Maldonado, M.I., Malato, S., Cáceres, J., Krutzler, T., Glaser, A. 2004. Pilot-plant treatment of olive mill wastewater (OMW) by solar TiO<sub>2</sub> photocatalysis and solar photo-Fenton. *Sol. Energy.* 77, 567.
- Gernjak, W., Fuerhacher, M. Fernández-Ibañez, P., Blanco, J. Malato, S. 2006. Solar photo-Fenton treatment—Process parameters and process control. *Appl. Catal. B* 64, 121
- Gómez-Pacheco, C.V., Sánchez-Polo, M., Rivera-Utrilla, J., López-Peñalver, J.J. Tetracycline degradation in aqueous phase by ultraviolet radiation. *Chem. Eng. J.* 187 (2012) 89-95
- Gotvajn, A.Z., Tisler, T., Zagorc-Koncan, J. 2009. Comparison of different treatment strategies for industrial landfill leachate. *J. Hazard. Mater.* 162, 1446.
- Guedes, A.M.F.M., Madeira, L.M.P., Boaventura, R.A.R., Costa, C.A.V. 2003. Fenton oxidation of cork cooking wastewater—overall kinetic analysis. *Water Res.* 37, 3061.
- Gulkaya, I.; Surucu, A.; Dilek, F. 2006. Importance of H<sub>2</sub>O<sub>2</sub>/Fe<sup>+2</sup> ratio in Fenton's treatment of a carpet dyeing wastewater. *J. Hazard. Mater.* 136, 763.
- Gültekin, I.; Ince, N. 2007. Synthetic endocrine disruptors in the environment and water remediation by advanced oxidation processes. *J. Environ. Manag.* 85, 816.
- Haber, F.; Weiss, J. 1934. The catalytic decomposition of hydrogen peroxide by 100

iron salts. *Proc. Roy. Soc. A.* 134, 332

Hasan, T., Allen, M., Cooperman, B.S. 1985. Anhydrotetracycline is a Major Product of Tetracycline Photolysis. *J. Org. Chem.* 50, 1755.

Heberer, T. 2002. Occurrence, fate, and removal of pharmaceutical residues in the aquatic environment: a review of recent research data. *Toxicol. Lett.* 131, 5.

Herney Ramirez, J., Costa, C.A., Madeira, L.M. 2005. Experimental design to optimize the degradation of the synthetic dye Orange II using Fenton's reagent. *Catal. Today* 107–108, 68.

Homem, V. and Santos, L. 2011. Degradation and removal methods of antibiotics from aqueous matrices - A review. *J. Environ. Manage.* 92, 2304.

Homem, V., Alves, A., Santos, L. 2010. Amoxicillin degradation at ppb levels by Fenton's oxidation using design of experiments. *Sci. Total Environ.* 408, 6272.

Huang, H.B., Leung, D.Y.C., Kwong, P.C.W., Xiong, J., Zhang, L. 2013. Enhanced photocatalytic degradation of methylene blue under vacuum ultraviolet irradiation, *Catal. Today* 201, 189-194.

Huston P.L. and Pignatello, J.J. 1999. Degradation of selected pesticide active ingredients and commercial formulations in water by the photo-assisted Fenton reaction. *Water Res* 33(5), 1238-1246.

Imoberdorf, G.; Mohseni, M. Kinetic study and modeling of the vacuum-UV photoinduced degradation of 2,4-D. *Chem. Eng. J.* 187 (2012) 114-122

IUPAC. 2012. Compendium of Chemical Technology. Gold Book. Version 2.3.2. 2012-08-19. URL: <http://goldbook.iupac.org/PDF/goldbook.pdf>. Consulted: May 2013.

Jiao, S., Zheng, S., Yin, D., Wang, L., Chen, L. 2008. Aqueous photolysis of tetracycline and toxicity of photocatalytic products to luminescent bacteria. *Chemosphere* 73, 377.

Kajitvichyanukul, P., Suntronvipart, N. 2006. Evaluation of biodegradability and oxidation degree of hospital wastewater using photo-Fenton process as the pretreatment method. *J. Hazard. Mater.* 138, 384.

Kang, M., Lee, D.S., Yoon, J. 2002. Kinetic modeling of Fenton oxidation of phenol and monochlorophenols. *Chemosphere* 47, 915.

Kang, Y.H., Hwang, K-Y. 2000. Effects of reaction conditions on the oxidation efficiency in the Fenton process. *Water Res.* 34, 2786.

Kaniou, S., Pitarakis, K., Barlagianni, I., Poullos, I. 2005. Photocatalytic oxidation of sulfamethazine. *Chemosphere* 60, 372.

Kim, I., Tanaka, H. 2009. Photodegradation characteristics of PPCPs in water with UV treatment, *Environ. Int.* 35, 793.

- Kim, I., Yamashita, N., Tanaka, H. 2009. Photodegradation of pharmaceuticals and personal care products during UV and UV/H<sub>2</sub>O<sub>2</sub> treatments. *Chemosphere* 77, 518.
- Klamerth, N.; Rizzo, L.; Malato, S.; Maldonado, M.I.; Agüera, A.; Fernández-Alba, A.R. 2010. Degradation of fifteen emerging contaminants at mg L<sup>-1</sup> initial concentrations by mild solar photo-Fenton in MWTP effluents. *Water Res.* 44, 545.
- Klavarioti, M., Mantzavinos, D., Kassinos, D. 2009. Removal of residual pharmaceuticals from aqueous systems by advanced oxidation processes. *Environ. Int.* 35, 402.
- Kleinman, M.H., Smith, M.D., Kurali, E., Kleinpeter, S., Jiang, K., Zhang, Y., Kennedy-Gabb, S.A., Lynch, A.M., Geddes, C.D. 2010. An evaluation of chemical photoreactivity and the relationship to phototoxicity. *Reg. Toxicol. Pharmacol.*, 58, 224.
- Košutić, K., Dolar, D., Ašperger, D., Kunst, B. 2007. Removal of antibiotic from model wastewater by RO/NF membrane. *Sep. Purif. Technol.* 53, 244.
- Koyuncu, I., Arıkan, O.A., Wiesner, M.R., Rice, C. 2008. Removal of hormones and antibiotics by nanofiltration membranes. *J. Membr. Sci.* 309, 94.
- Kuo, W.G. 1992. Decolorizing dye wastewater with Fenton's reagent. *Water Res.* 26:7, 881.
- Kusic, H., Koprivanac, N., Bozic, A.L., Selanec, I. 2006. Photo-assisted Fenton type processes for the degradation of phenol: A kinetic study. *J. Hazard. Mater.* 136, 632.
- Kusic, H., Koprivanac, N., Horvat, S., Bakija, S., Bozic, A.L. 2009. Modeling dye degradation kinetic using dark- and photo-Fenton type processes. *Chem. Eng. J.* 155, 144.
- Kurt, U., Apaydin, O., Gonullu, M.T. 2007. Reduction of COD in wastewater from an organized tannery industrial region by Electro-Fenton process. *J. Hazard. Mater.* 143, 33.
- Ledakowicz, S., Gonera, M. 1999. Optimisation of oxidants dose for combined chemical and biological treatment of textile wastewater. *Water Res.* 33, 2511.
- Legrini, O., Oliveros, E., Braun, A.M. 1993. Photochemical processes for water treatment. *Chem. Rev.* 93, 671.
- Li, W., Nanaboina, V., Zhou, Q., Korshin, G.V. 2012. Effects of Fenton treatment on the properties of effluent organic matter and their relationships with the degradation of pharmaceuticals and personal care products. *Water Res.* 46, 403.
- Lin, A.Y.-C., Lin, C.-F., Chiou, J.-M.P., Hong. 2009. O<sub>3</sub> and O<sub>3</sub>/H<sub>2</sub>O<sub>2</sub> treatment of sulphonamide and macrolide antibiotics in wastewater. *J. Hazard. Mater.* 171, 452.

Liu, R., Chiu, H.M., Shiao, C-S., Yeh, RY-L., Hung, Y-T. 2007. Degradation and sludge production of textile dyes by Fenton and photo-Fenton processes. *Dyes. Pigm.* 73, 1.

Lopez, A., Pagano, M., Volpe, A., Di Pinto, A.C. 2004. Fenton's pre-treatment of mature landfill leachate. *Chemosphere* 54, 1005.

López, J.L., García Einschlag, F.S., González, M.C., Capparelli, A.L., Oliveros, E., Mashem, T.M., Braun, A.M. 2000. Hydroxyl radical initiated photodegradation of 4-chloro-3,5-dinitrobenzoic acid in aqueous solution. *J Photochem Photobio A* 137, 177–184.

López-Peñalver, J.J.; Sánchez-Polo, M. ; Gómez-Pacheco, C.V.; Rivera-Utrilla, J. 2010. Photodegradation of tetracyclines in aqueous solution by using UV and UV/H<sub>2</sub>O<sub>2</sub> oxidation processes, *J. Chem. Technol. Biotechnol.* DOI 10.1002/jctb.2435

Lucas, M.S., Peres, J.A. 2009. Removal of COD from olive mill wastewater by Fenton's reagent: kinetic study. *J. Hazard. Mater.* 168, 1253.

Malato, S.; Fernández-Ibáñez, P.; Maldonado, M.I.; Blanco, J.; Gernjak, W. 2009. Decontamination and disinfection of water by solar photocatalysis: Recent overview and trends. *Cat. Today.* 147, 1.

Maroga Mboula, V., Héqueta, V., Gru, Y., Colin, R., Andrès, Y. 2012. Assessment of the efficiency of photocatalysis on tetracycline biodegradation, *J. Hazard. Mater.* 209-210, 355.

Martignac, M., Oliveros, E., Maurette, M-T., Claparols, C., Benoit-Marquié, F., 2013. Mechanistic pathways of the photolysis of paracetamol in aqueous solution: an example of photo-Fries rearrangement. *Photochem. Photobiol. Sci.* 12, 527

Martínez, E.C., Lopez, G.D. Adaptive optimal operation of the Fenton's batch process for industrial wastewater treatment. *European Symposium on Computer Aided Process Engineering* 11, 237.

Millioli, V.S., Freire, D.D.C., Cammarota, M.C. 2003. Petroleum oxidation using Fenton's reagent over beach sand following a spill. *J. Hazard. Mater.* 103, 79.

Miskoski, S., Sánchez, E., Garavano, M., López, M., Soltermann, A.T., Garcia, N.A. 1998. Singlet molecular oxygen-mediated photo-oxidation of tetracyclines: kinetics, mechanism and microbiological implications. *J. Photoch. Photobio. B* 43, 163.

Mohajerani, M., Mehrvar, M., Ein-Mozaffari, F. 2011. Photoreactor design and CFD modeling of a UV/H<sub>2</sub>O<sub>2</sub> process for distillery wastewater treatment. *The Canadian Journal of Chemical Engineering* 9999, 1-11.

Mohajerian, S., Aziza, H.A., Isa, M.H., Zahed, M.A., Adlan, M.N. 2010. Statistical optimization of process parameters for landfill leachate treatment using electro-Fenton technique. *J. Hazard. Mater.* 176, 749.



- Monteagudo, J.M., Durán, A., San Martín, I., Aguirre, M. 2009. Effect of continuous addition of H<sub>2</sub>O<sub>2</sub> and air injection on ferrioxalate-assisted solar photo-Fenton degradation of Orange II. *Appl. Catal. B.* 89, 510.
- Monteagudo, J.M., Durán, A., San Martín, I., Aguirre M. 2010. Effect of light source on the catalytic degradation of protocatechuic acid in a ferrioxalate-assisted photo-Fenton process. *Appl. Catal. B.* 96, 486
- Moraes, P.B., Bertazzoli, R. 2005. Electrodegradation of landfill leachate in a flow electrochemical reactor. *Chemosphere* 58, 41.
- Morrison, H. and Olack, G. 1991. Formation and Characterization of Lumitetracycline-Type Photoproducts from Members of the Tetracycline Family. *J. Org. Chem.* 56, 4963.
- Morrison, H., Olack, G., Xiao, C. 1991. Photochemical and photophysical studies of tetracycline. *J. Am. Chem. Soc.* 113, 8110.
- Nichela, D., Haddou, M., Benoit-Marquié, F., Maurette, M-T., Oliveros, E., García Einschlag, F.S. 2010. Degradation kinetics of hydroxy and hydroxynitro derivatives of benzoic acid by fenton-like and photo-fenton techniques: A comparative study. *Appl. Catal. B.* 98, 171.
- Oliveros, E.; Legrini, O.; Hohl, M.; Müller, T.; Braun, A.M. 1997. Industrial waste water treatment: large scale development of a light-enhanced Fenton reaction. *Chem. Eng. Process.* 36, 397.
- Oller, I.; Malato, S.; Sánchez-Pérez, J.A. 2011. Combination of Advanced Oxidation Processes and biological treatments for wastewater decontamination—A review. *Sci. Total. Environ.* 409, 4141.
- Ortiz de la Plata, G., Alfano, O.M., Cassano, A.E. 2010. Decomposition of 2-chlorophenol employing goethite as Fenton catalyst II: Reaction kinetics of the heterogeneous Fenton and photo-Fenton mechanisms. *Appl. Catal. B.* 95, 14.
- Palominos, R., Mondaca, M.A., Giraldo, A., Peñuela, G., Pérez-Moya, M., Mansilla, H.D. 2009. Photocatalytic oxidation of the antibiotic tetracycline on TiO<sub>2</sub> and ZnO suspensions. *Catal. Today* 144, 100.
- Peirce, J.J., Vesilind, P.A, Weiner, R. *Environmental Pollution and Control*, Fourth Edition Butterworth-Heinemann, USA. 1998. Chapter 3.
- Pérez, M., Torrades, F., Peral, J., Lizama, C., Bravo, C., Casas, S., Freer, J., Mansilla, H.D. 2001. Multivariate approach to photocatalytic degradation of a cellulose bleaching effluent. *Appl. Catal. B.* 33, 89.
- Pérez, M., Torrades, F., Domènech, X., Peral, J. 2002a. Fenton and photo-Fenton oxidation of textile effluents. *Water Res.* 36, 2703.

Pérez, M., Torrades, F., Domènech, X., Peral, J. 2002b. Treatment of bleaching Kraft mill effluents and polychlorinated phenolic compounds with ozonation. *Chem. Technol. Biotechnol.* 77, 891.

Pérez, M., Torrades, F., García-Hortal, J.A., Doménech, X., Peral, J. 2002c. Removal of organic contaminants in paper pulp treatment effluents under Fenton and photo-Fenton conditions. *Appl. Catal. B* 36, 63.

Pérez-Moya, M., Graells, M., del Valle, L.J., Centelles, E., Mansilla, H.D. 2007. Fenton and photo-Fenton degradation of 2-chlorophenol: Multivariate analysis and toxicity monitoring. *Catal. Today* 124, 163.

Pérez-Moya, M. Graells, M., Buenestado, E., Gutiérrez, E., Galindo, J., Mansilla, H.D. 2008. Modelling Approach to Fenton and Photo-Fenton Treatments. *J. Adv. Oxid. Technol.* 11:1, 1.

Pérez-Moya, M., Graells, M., Buenestado, P., Mansilla, H.D. 2010. A comparative study on the empirical modeling of photo-Fenton treatment process performance. *Appl. Catal. B.* 84, 313.

Pérez-Moya, M., Graells, M., Castells, G., Amigó, J., Ortega, E., Buhigas, G., Pérez, L.M., Mansilla, H.D. 2010. Characterization of the degradation performance of the sulfamethazine antibiotic by photo-Fenton process. *Water Res.* 44, 2533.

Pérez-Moya, M., Mansilla, H.D., Graells, M. 2011. A practical parametrical characterization of the Fenton and the photo-Fenton sulfamethazine treatment using semi-empirical modeling. *J. Chem. Technol. Biotechnol.* 86, 826.

Petrovic, M., González, S., Barceló, D. 2003. Analysis and removal of emerging contaminants in wastewater and drinking water. *TRAC-Trend. Anal. Chem.* 22(10), 685.

Pignatello, J.J. 1992. Dark and Photoassisted Fe<sup>3+</sup>-Catalyzed Degradation of Chlorophenoxy Herbicides by Hydrogen Peroxide. *Environ. Sci. Technol.* 26:5, 944.

Pignatello, J.J.; Oliveros, E.; MacKay, A. 2006. Advanced Oxidation Processes for Organic Contaminant Destruction Based on the Fenton Reaction and Related Chemistry. *Crit. Rev. in Environ. Sci. Technol.* 36(1), 1.

Pontes, R.F.F.; Moraes, J.E.F., Machulek Jr., A., Pinto, J.M. 2010. A mechanistic kinetic model for phenol degradation by the Fenton process. *J. Hazard. Mater.* 176, 402.

Pontes, R.F.F., Pinto, J.M. 2011. Optimal synthesis of Fenton reactor networks for phenol degradation. *Chem. Eng. Res. Des.* 89, 706.

Popuri, S.R., Chang, Ch-Y., Xu, J. 2011. A study on different addition approach of Fenton's reagent for DCOD removal from ABS wastewater. *Desalination* 277, 141.

Prieto-Rodríguez, L.; Oller, I.; Zapata, A.; Agüera, A.; Malato, S. 2011. Hydrogen peroxide automatic dosing based on dissolved oxygen concentration during solar photo-Fenton. *Catal. Today* 161, 247.

Reyes, C., Fernandez, J., Freer, J., Mondaca, M.A., Zaror, C., Malato, S. 2006. Degradation and inactivation of tetracycline by TiO<sub>2</sub> photocatalysis. *J. Photochem. Photobiol. A*, 184, 141.

Rios-Enriquez, M., Shahin, N., Durán-de-Bazúa, C., Lang, J., Oliveros, E., Bossmann; S., Braun, A. 2004. Optimization of the heterogeneous Fenton-oxidation of the model pollutant 2,4-xylidine using the optimal experimental design methodology. *Solar Energy* 77, 491.

Rizzo, L., Lofrano, G., Grassi, M., Belgiorno, V. 2008. Pre-treatment of olive mill wastewater by chitosan coagulation and advanced oxidation processes. *Sep. Purif. Technol.* 63, 648.

Rodrigues, A.C., Boroski, M., Shimada, N.S., Garcia, J.C., Nozaki, J., Hioka, N. 2008a. Treatment of paper pulp and paper mill wastewater by coagulation–flocculation followed by heterogeneous photocatalysis. *J. Photochem. Photobiol. A* 194, 1.

Rodrigues, M.A.S., Amado, F.D.R., Xavier, J.L.N., Streit, K.F., Bernardes, A.M., Ferreira, J.Z. 2008b. Application of photoelectrochemical-electrodialysis treatment for the recovery and reuse of water from tannery effluents. *J. Cleaner Prod.* 16, 605.

Rodríguez-Gil, J.L., Catalá, M., González Alonso, S., Romo Maroto, R., Valcárcel, Y., Segura, Y., Molina, R., Melero, J.A., Martínez, F. 2010. Heterogeneous photo-Fenton treatment for the reduction of pharmaceutical contamination in Madrid rivers and ecotoxicological evaluation by a miniaturized fern spores bioassay, *Chemosphere* 80, 381.

Rosal, R., Rodríguez, A., Perdigón-Melón, J.A., Petre, A., García-Calvo, E., Gómez, M.J., Agüera, A., Fernández-Alba, A.R. 2009. Degradation of caffeine and identification of the transformation products generated by ozonation. *Chemosphere* 74, 825.

Rossetti, G.H., Albizzati, E.D., Alfano, O.M. 2002. Decomposition of Formic Acid in a Water Solution Employing the Photo-Fenton Reaction. *Ind. Eng. Chem. Res.* 41, 1436.

Rossetti, G.H., Albizzati, E.D., Alfano, O.M. 2004. Modeling of a flat-plate solar reactor. Degradation of formic acid by the photo-Fenton reaction. *Solar Energy* 77, 461.

Rozas, O., Contreras, D., Moncada, M.A., Pérez-Moya, M., Mansilla, H.D., 2010. Experimental design of Fenton and photo-Fenton reactions for the treatment of ampicillin solutions. *J. Hazard. Mater.* 177, 1025.

San Sebastian Martinez, N., Fernandez, J.F., Segura, X.F., Sanchez Ferrer, A. 2003. Pre-oxidation of an extremely polluted industrial wastewater by the Fenton's reagent. *J. Hazard. Mater.* 101, 315.

Santos-Juanes Jorda, L., Ballesteros Martín, M.M., Ortega Gómez, E., Cabrera Reina, A., Román Sánchez, I.M., Casas López, J.L., Sánchez Pérez, J.A. 2011a. Economic evaluation of the photo-Fenton process. Mineralization level and reaction time: The keys for increasing plant efficiency. *J. Hazard. Mater.* 186, 1924.

Santos-Juanes, L., García Sánchez, J.L., Casas López, J.L., Oller, I., Malato, S., Sánchez Pérez, J.A. 2011b. Dissolved oxygen concentration: A key parameter in monitoring the photo-Fenton process. *Appl. Catal. B* 104, 316.

Shu, H-Y., Hsieh, W-P. 2013. Treatment of dye manufacturing plant effluent using an annular UV/H<sub>2</sub>O<sub>2</sub> reactor with multi-UV lamps. *Sep. Purif. Technol.* 51, 379-386.

Simunovic, M., Kusic, H., Koprivanac, N., Bozic, A.L. 2011. Treatment of simulated industrial wastewater by photo-Fenton process: Part II. The development of mechanistic model. *Chem. Eng. J.* 173, 280.

Stanislaw, L., Monika, S., Renata, Z. 2001. Biodegradation, decolourisation and detoxification of textile wastewater enhanced by advanced oxidation processes. *J Biotechnol* 89, 175.

Stuart, M., Lapworth, D., Crane, E., Hart A. 2012. Review of risk from potential emerging contaminants in UK groundwater. *Sci. Total. Environ.* 416, 1.

Sun, Y.; Pignatello, J.J. 1993. Photochemical Reactions Involved in the Total Mineralization of 2,4-D by Fe<sup>3+</sup>/H<sub>2</sub>O<sub>2</sub>/UV. *Environ. Sci. Technol.* 27:2, 304.

Surmacz-Gorska J. 2001. Degradation of organic compounds in municipal landfill leachate. Lublin: Publishers of Environmental Engineering Committee of Polish Academy of Sciences.

Szabó, L., Tóth, T., Homloka, R., Takács, E., Wojnárovits, L. 2003. Radiolysis of paracetamol in dilute aqueous solution. *Radiat. Phys. Chem.* 66:2, 137.

Szpyrkowicz, L., Juzzolino, C., Kaul, S.N. 2001. A comparative study on oxidation of disperse dyes by electrochemical process, ozone, hypochlorite and Fenton reagent. *Water Res.* 35, 2129.

Teixeira, A.C.S.C., Guardani, R., Nascimento, A.O.C. 2004. Photo-Fenton Remediation of Wastewaters Containing Silicones: Experimental Study and Neural Networks Modeling. *Chem. Eng. Technol.* 27, 800.

Ternes, T.A., Meisenheimer, M., McDowell, D., Sacher, F., Brauch, H.J., Haist-Gulde, B. 2002. Removal of pharmaceuticals during drinking water treatment. *Environ Sci Technol* 36,3855-3863.

Tokumura, M., Tawfeek Znad, H., Kawase, Y. 2006. Modeling of an external light irradiation slurry photoreactor: UV light or sunlight-photoassisted Fenton

discoloration of azo-dye Orange II with natural mineral tourmaline powder. *Chem. Eng. Sci.* 61, 6361.

Tokumura, M., Ohta, A., Znad, H., Kawase, Y. 2006. UV light assisted decolorization of dark brown colored coffee effluent by photo-Fenton reaction. *Water Res.* 40, 3775.

Tokumura, M., Tawfeek, H., Kawase, Y. 2008. Decolorization of dark brown colored coffee effluent by solar photo-Fenton reaction: Effect of solar light dose on decolorization kinetics. *Water Res.* 42, 4665.

Tokumura, M., Morito, R., Hatayama, R., Kawase, Y., 2011. Iron redox cycling in hydroxyl radical generation during the photo-Fenton oxidative degradation: Dynamic change of hydroxyl radical concentration. *Appl. Catal. B* 106, 565.

Torrades, F., Pérez, M., Mansilla, H.D., Peral, J. 2003. Experimental design of Fenton and photo-Fenton reactions for the treatment of cellulose bleaching effluents. *Chemosphere* 53, 1211.

Torrades, F., García-Montaña, J., García-Hortal, J.A., Doménech, X., Peral, J. 2004. Decolorization and mineralization of commercial reactive dyes under solar Light assisted photo-Fenton conditions. *Sol. Energy* 77, 573.

Torrades, F., García-Hortal, J.A., Núñez, L. 2008. Fenton and photo-Fenton oxidation of a model mixture of dyes – overall kinetic analysis. *Color. Technol.* 124, 370.

Trovó, A.G., Paterlini, W.C., Nogueira, R.F.P. 2006. Evaluation of the influences of solution path length and additives concentrations on the solar photo-Fenton degradation of 4-chlorophenol using multivariate analysis. *J. Hazard. Mater. B.* 137, 1577.

Trovó, A.G., Santos Melo, S.A., Nogueira, R.F.P. 2008. Photodegradation of the pharmaceuticals amoxicillin, bezafibrate and paracetamol by the photo-Fenton process—Application to sewage treatment plant effluent. *J. Photochem. Photobio. A* 198, 215.

Trovó, A.G., Silva, T.F.S., Gomes Jr., O., Machado, A.E.H., Borges Neto, W., Muller Jr., P.S., Daniel, D. 2013. Degradation of caffeine by photo-Fenton process: Optimization of treatment conditions using experimental design. *Chemosphere* 90, 170.

Vilhunen, S.; Sillanpää, M. 2010. Recent developments in photochemical and chemical AOPs in water treatment: a mini-review. *Rev. Environ. Sci. Biotechnol.* 9, 323.

Walling, C.; Goosen, A. 1973. Mechanism of the Ferric Ion Catalyzed Decomposition of Hydrogen Peroxide. Effect of Organic Substrates. *J. Am. Chem. Soc.* 95:9, 2987.

- Wammer, K.H., Slattery, M.T., Stemig, A.M, Ditty, J.L. 2011. Tetracycline photolysis in natural waters: Loss of antibacterial activity, *Chemosphere* 85, 1505.
- Wang, C., Yediler, A., Lienert, D., Wang, Z., Kettrup, A. 2003. Ozonation of an azo dye C.I. Remazol Black 5 and toxicological assessment of its oxidation products. *Chemosphere* 52, 1225.
- Wang., S. 2008. A Comparative study of Fenton and Fenton-like reaction kinetics in decolourisation of wastewater. *Dyes Pigments* 76, 714
- Wang, C-T., Chou, W-L., Chung, M-H., Kuo, Y-M. 2010. COD removal from real dyeing wastewater by electro-Fenton technology using an activated carbon fiber cathode. *Desalination* 253, 129.
- Wang, P., He, Y-L., Huang, C-H. 2011. Reactions of tetracycline antibiotics with chlorine dioxide and free chlorine. *Water Res.* 45, 1838.
- Wang, Y., Zhang, H., Zhang, J., Lu, C., Huang, Q., Wu, J., Liu, F. 2011. Degradation of tetracycline in aqueous media by ozonation in an internal loop-lift reactor. *J. Hazard. Mater.* 192, 35.
- Wu, J., Zhang, H., Oturan, N., Wang, Y., Chen, L., Oturan, M.A. 2012. Application of response surface methodology to the removal of the antibiotic tetracycline by electrochemical process using carbon-felt cathode and DSA (Ti/RuO<sub>2</sub>-IrO<sub>2</sub>) anode. *Chemosphere* 87, 614.
- Xing, M., Deng, C., Godefroid, B., Yang, J. 2006. Treatment of pharmaceutical wastewater containing recalcitrant compounds in a Fenton-coagulation process. *J. Environ. Sci.* 18, 459.
- Yamal-Turbay, E., Graells, M., Pérez-Moya, M. 2012. Systematic Assessment of the Influence of Hydrogen Peroxide Dosage on Caffeine Degradation by photo-Fenton Process, *Ind. Eng. Chem. Res.* 51(13), 4770.
- Yang, L., Yu, L.E., Ray, M.B. 2008. Degradation of paracetamol in aqueous solutions by TiO<sub>2</sub> photocatalysis. *Water Res.* 42, 3480.
- Yang, Y., Wang, P., Shi, S., Liu, Y. 2009. Microwave enhanced Fenton-like process for the treatment of high concentration pharmaceutical wastewater. *J. Hazard. Mater.* 168, 238.
- Yuan, F., Hu, C., Hu, X., Wei, D., Chen, Y., Qu, J. 2011. Photodegradation and toxicity changes of antibiotics in UV and UV/H<sub>2</sub>O<sub>2</sub> process. *J. Hazard. Mater.* 185, 1256.
- Zaror, C., Segura, C., Mansilla, H., Modaca, M.A., Gonzalez, P. 2010. Kinetic study of Imidacloprid removal by advanced oxidation based on photo-Fenton process. *Environ. Technol.* 31:13, 1411

Zazo, J. A.; Casas, J. A.; Mohedano, A. F.; Rodríguez, J. J. 2009. Semicontinuous Fenton oxidation of phenol in aqueous solution. A kinetic study. *Water Res.* 43, 4063.

Zhang, G., Ji, S., Xi, B. 2006. Feasibility study of treatment of amoxicillin wastewater with a combination of extraction, Fenton oxidation and reverse osmosis. *Desalination* 196, 32.

Ziylan, A. and Ince N.H. 2011. The occurrence and fate of anti-inflammatory and analgesic pharmaceuticals in sewage and fresh water: Treatability by conventional and non-conventional processes. *J. Hazard. Mater.* 187, 24.





## **Chapter III**

### **Materials and Methods**

This chapter presents a brief description of the experimental methods and mathematical tools used to achieve the objectives of the study. An initial experimental approach was devoted to find a more complete understanding of the process and the variables involved in its performance, while the latter computational approach leads to the formulation and resolution of a model to represent process behavior. The methodologies used to fulfill both approaches are here presented.






### 3.1. Experimental Methods

In this section a description of the methods and tools used to fulfill the objectives of the experimental approach of this research is presented. The pilot plant and its components are described and the analytical methods undertaken are briefly explained.

#### 3.1.1. Pilot plant description

The AOPs pilot plant studied in this research is a flexible and fully monitored installation which has research and educational purposes. Several irradiation sources and configurations are available to study and evaluate different AOPs, namely UV-photolysis, UV/H<sub>2</sub>O<sub>2</sub>, Fenton and photo-Fenton, among others. Table 3.1 presents the description and the photographs of the different photo-reactors available in the pilot plant and Figure 3.1 shows the spectral distribution of each irradiation source. The reactors can work individually or combining the reservoir with one of the photo-reactors in a series arrangement; Figure 3.2 presents a schema of the pilot plant with its possible configurations.

Table 3.1. Photo-reactor and configurations available in the pilot plant under study

Reactor code	Description	Irradiation source	Picture
R1	9 L glass-jacketed tank. It can be operated isothermally. It works as a photo-reactor or as a reservoir	TQ-718 (medium pressure Hg lamp, maximum electrical power 750 W) inside a Pyrex lamp holder with a cooling jacket, placed in the axis of the tank.	
R2	6 L Pyrex photo-reactor	Philips Actinic BL TL-DK 36W/10 1SL, placed in the axis of the reactor	
R3	2 L plastic photo-reactor	PL-L-55W (low pressure Hg lamp) inside a quartz envelope	

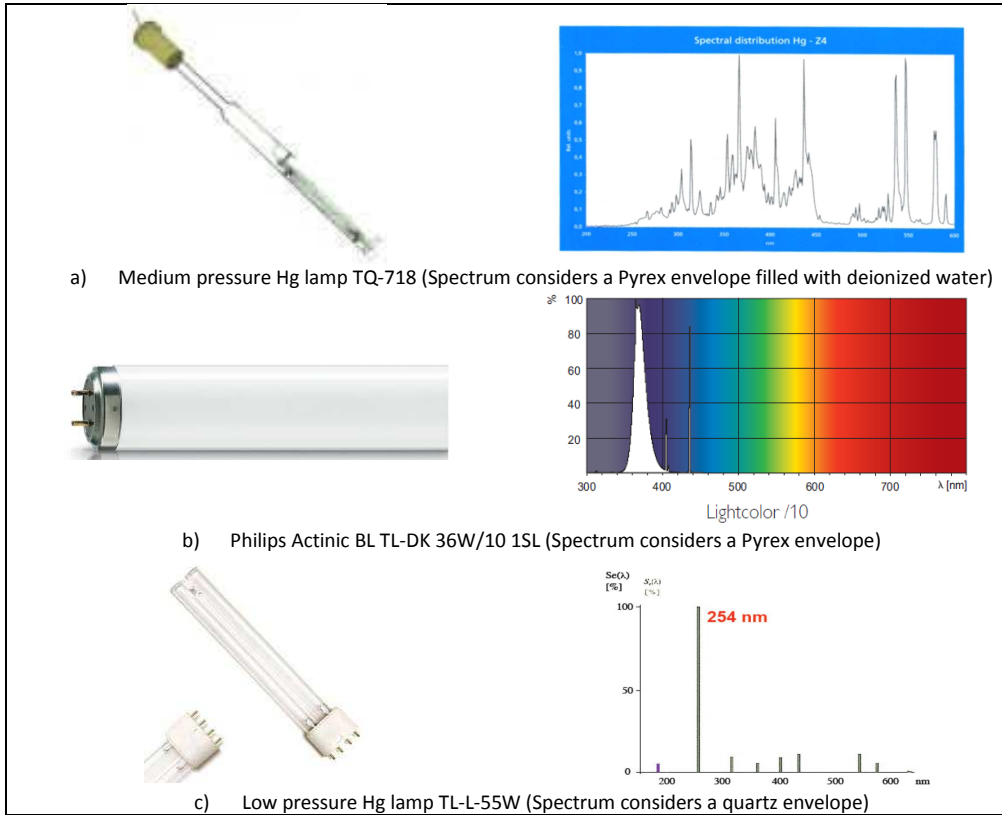


Figure 3.1. Spectral distribution of irradiation sources

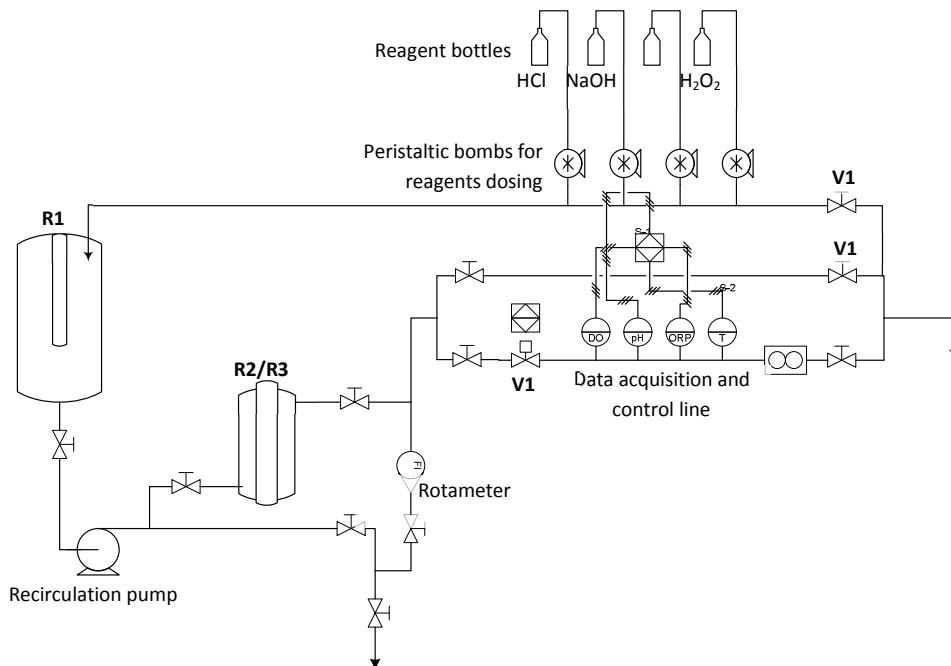


Figure 3.2. Pilot plant schematic representation

With the aim to study the automation and flexibility of the AOPs in the pilot plant, it is equipped with a programmable logic controller (PLC) connected to a Wonderware® InTouch® software for data acquisition and process control. The PLC, externally programmed by its own software, acquires data from in/out modules connected to the pilot plant and manages those data from an OPC server throughout a SCADA. The pump, valves and sensors described in Table 3.2 are connected to the PLC, but can be manually operated as well.

Table 3.2. Units for data acquisition and control in the pilot plant

	Unit	Description	Observation
Pumps	Recirculation pump	Centrifugal pump (Iwaki Magnet Pump, MD-30RZ-220N)	Connected to a variable frequency drive and to the PLC to keep a constant recirculation flow in the whole system
	4 peristaltic pumps for reagent dosing: Pump 1: HCl Pump 2: NaOH Pump 3: available Pump 4: H <sub>2</sub> O <sub>2</sub>	Watson Marlow, OEM 313 VBV 24V	HCL and NaOH are dosed for pH control, undertaken via OPC with a PID programmed in Simulink® or via SCADA with a PID programmed through InTouch® software. H <sub>2</sub> O <sub>2</sub> dosage is programmed through InTouch® software.
Valves	2 electro valves	Hunter PGV-101G-B 1"	Located in the dosing and by-pass lines.
	Proportional electro-valve	mPm, modelo L20-J2	Located in the measuring line, it acts commanded by a PID controller connected to the PLC to maintain measuring line flow in a set point equal to 1 mL/min.
Sensors	pH	Hamilton Polilyte HTVP 120. Conventional sensor in which pH potential is measured against reference	Connected to a Eutech alpha pH 500 indicator. 0-14 pH units
	Conductivity	Sentek 225-85. Two electrodes sensor	Connected to a Eutech CON 500 LCD indicator. 0-10 mS/cm
	Oxidation-reduction potential (ORP)	Hamilton Polilyte RX120	Connected to a Eutech alpha pH 500 indicator. - 2000 to +2000 mV
	Dissolved oxygen (DO)	Hamilton Oxysens. Clark's principle sensor	Connected to a Knick Stratos ECO 2400 indicator. 40 ppb – 40 ppm or 0 – 200%
	Temperature probe	PT-100	Located inside R1 and connected to a Eurotherm 2132i indicator
	Rotameter	Tecfluid 6001/PVC ¾"	Measures flow given by the centrifugal pump. 2 - 15 L/min
	Flowmeter	DIGMESA 04 – 16 L/min, 800 p/L	Located in the data acquisition and control line. Connected to a Eurotherm 2132i indicator. 4 - 16 L/min

### 3.1.2. Analytical methods

Sets of experiments were performed in order to evaluate the efficiency of the processes investigated and the functioning of the pilot plant. Additionally to the on-line measurements, samples were withdrawn at regular time intervals and several off-line variables were also measured in order to study the evolution of the process under different process operational conditions. More specifically, a lumped variables such as the total organic carbon (TOC) and specific concentrations of contaminant and hydrogen peroxide were measured along the studied treatment span. Regarding irradiation, a potassium ferrioxalate actinometry was undertaken to measure incident photo rate.

These analytical methods will be briefly described in the following subsections.

#### 3.1.2.1 Determination of total organic carbon (TOC)

The amount of carbon bound in organic compounds is commonly used as an indirect measurement of the organic substances in a sample and as a non-specific indicator for water and wastewater quality. As it is virtually impossible to identify and follow the generation and decay of all the intermediates formed during the treatment, the evolution of TOC is thought of interest as it is a lumped parameter which concerns all organic compounds in the sample.

A Shimadzu TOC-V<sub>C<sub>SH</sub>/C<sub>SN</sub></sub> analyzer is used in this work for measuring total carbon (TC). In this equipment, the sample is carried through an oxidation catalyst-filled combustion tube heated to 680°C by means of a carrier gas (purified air) at a controlled flow rate; the sample is oxidized to create CO<sub>2</sub>, which is dehumidified and later detected by a non-dispersive infrared detector (NDIR). Similarly, as being inorganic carbon (IC) a combination of carbonate and bicarbonate, an acidified sample is sparged with the carrier gas to convert only the IC in the sample to CO<sub>2</sub>. TOC is then determined by subtracting IC from TC. Figure 3.3 presents a schematic representation of measurement flow in the equipment.

For IC quantification, four linear calibration curves, ranging from 0-20, 0-50, 0-100 and 50-500 mg L<sup>-1</sup> were available, while two calibration curves were established for TC quantification, ranging from 0-50 and 40-200 mg L<sup>-1</sup>.

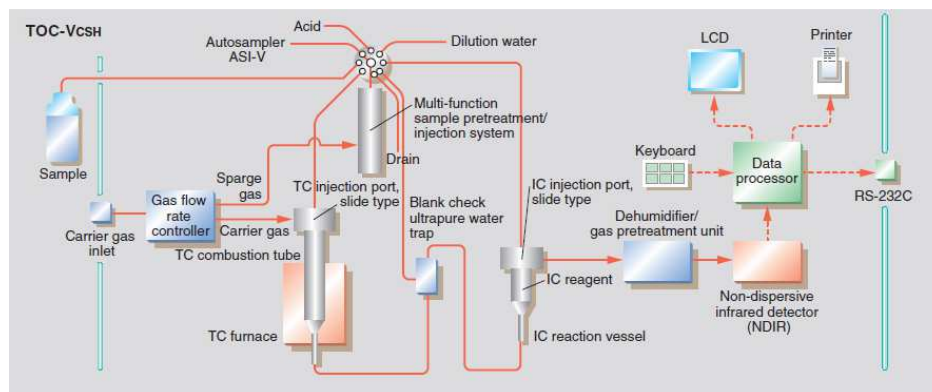


Figure 3.3. Shimadzu TOC-VCSH/CSN analyzer measurement flow diagram

### 3.1.2.2. Determination of contaminant concentration

The measurement the concentration of each specific pollutant was performed by high performance liquid chromatography (HPLC), a quantification technique that involves the separation of the components of a sample when they are forced to flow at high pressure through a packed column (stationary phase) driven by a liquid mixture (mobile phase). Components in the sample are separated one from another by the column than involves various chemical and/or physical interactions between their molecules and the packing particles. These separated components are detected at the exit of the column by an infra-red detector that measures their amount. The quantification is based in calibration curves constructed from solutions with known composition and allows measuring the concentration of the pattern contaminant and therefore its evolution along processing time.

The Agilent® 1200 series HPLC used in this study consists in a modular system equipped with a manual injector, a mobile phase degasser, a quaternary pump, a heating oven and a diode array detector. When the sample is manually injected, it is mixed with the mobile phase and carried out by the quaternary pump throughout the stationary phase for the components to be separated and then they are sent to the detector. The time taken by the compound to travel from the column to the detector is known as retention time and it depends on the pressure, the nature of the stationary phase, the composition of the solvent and the temperature of the column.

The HPLC is connected to a Chem-Station® software (Rev.B.04.06 SP1[647]) where methods can be programmed and data acquisition and processing is performed. Table 3.1 shows the chromatographic conditions used for contaminants studied in this research. HPLC grade reagents and filtered milliQ water were used as mobile phases.

Table 3.3. Chromatographic conditions used for each studied contaminant

Contaminant	Mobile phase	Stationary phase	Temp (°C)	$\lambda$ (nm)	Flow (mL/min)	Retention time (min)
Caffeine	70% water 30% acetonitrile	Agilent Zorbax Eclipse XDB-C18 5 $\mu$ m (4.6x150)mm	25	274	1.5	1.1
Paracetamol	75% water 25% methanol	Akady Ultrabase C-18 5 $\mu$ m (4.6x150)mm	25	243	0.4	9.0
Tetracycline	70% 0.01 M oxalic acid 10% methanol 20% acetonitrile	Agilent Zorbax Eclipse XDB-C18 5 $\mu$ m (4.6x150)mm	30	271	1	2.4
Sulfamethazine	55% water 45% acetonitrile	Agilent Zorbax Eclipse XDB-C18 5 $\mu$ m (4.6x150)mm	25	274	1.5	1.2

### 3.1.2.3 Determination of hydrogen peroxide concentration

The residual concentration of hydrogen peroxide along the treatment span is measured at regular time intervals in order to identify the behavior of this variable and the way it influences the degradation and mineralization of the contaminant at different operational conditions. This variable is commonly measured using a iodometric or permanganate titration, but a spectrophotometric method with titanium sulfate or oxalate and *N,N*-diethyl-*p*-phenylenediamine (DPD) has also been reported. Nevertheless, they present several disadvantages, for instance, iodometric titration is subjected to errors due to volatilization and hydrolysis of I<sub>2</sub> and it is more time-demanding than spectrophotometric determination (Nogueira et al., 2005), permanganate titrations are reliable but cannot be used in Fenton reactions as Fe(II) interferes with the measurement and spectrophotometric determination with DPD involves high costs reagents.

A simple, fast and economic spectrophotometric method was recently proposed by Nogueira et al. (2005) and it consists in the measurement of the absorbance at 450 nm of the peroxovanadium cation (VO<sub>2</sub><sup>+3</sup>) formed when hydrogen peroxide reacts with ammonium metavanadate in acidic medium:



In this reaction, vanadate ion is reduced to peroxovanadium ion and peroxide is reduced to water. An excess of ammonium metavanadate (0.062 M in 0.58 M H<sub>2</sub>SO<sub>4</sub>) is added to ensure total peroxide consumption and, as a result, final concentration of peroxovanadium is equal to initial concentration of hydrogen peroxide; usually, 1 mL aliquot is mixed with 1.1 mL of ammonium metavanadate and then taken to 10 mL.

This method was used in this study and the absorbances at 450 nm were measured by a UV-Vis spectrophotometer Hitachi U-2001 and H<sub>2</sub>O<sub>2</sub> concentration is calculated according the calibration curve showed in Figure 3.4.



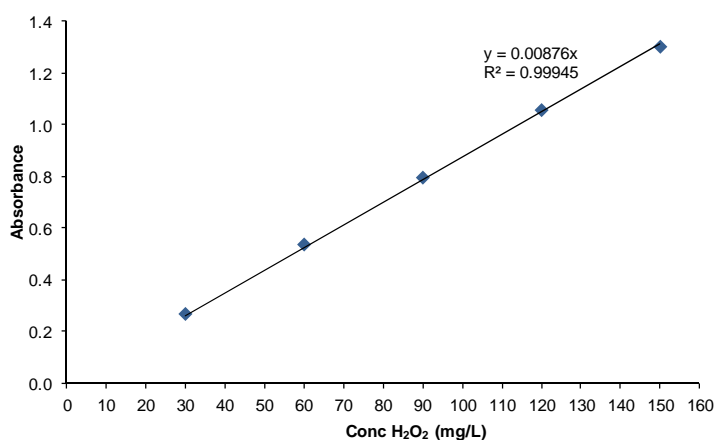


Figure 3.4. Calibration curve used to calculate H<sub>2</sub>O<sub>2</sub> concentration by spectrophotometric technique after reaction with ammonium metavanadate

#### 3.1.2.4. Chemical actinometry

An actinometry is a technique to measure the incident photon rate and, consequently, the quantum yield of a photochemical reaction. The most frequently used method involves chemical actinometry, based on the behavior of a reference substance, namely chemical actinometer, for which the quantum yield is known. The term quantum yield,  $\Phi(\lambda)$ , is defined as the number of reacted molecules divided by the number of absorbed photons of a particular wavelength in the same period of time (Braun et al., 1991).

$$\Phi(\lambda) = \frac{\Delta n}{N_a} \quad (3.2)$$

where  $\Delta n$  is the number of molecules reacted and  $N_a$  is the number of photons absorbed in the system. The expression can be written in differential form:

$$\Phi(\lambda) = \frac{dn/dt}{P_a} \quad (3.3)$$

where  $dn/dt$  is the reaction rate of the photochemical process under consideration and  $P_a$  the number of photons absorbed per unit of time at a stated wavelength of absorbed photonic flux (photos s<sup>-1</sup>)

Kuhn et al. (IUPAC, 2004) define an actinometer as “a chemical system or a physical device by which the number of photons in a beam absorbed into the defined space of a chemical reactor can be determined integrally or per time”. Any substance capable of undergoing a photochemical reaction when it is irradiated and whose quantum yield is known can be used as an actinometer; more specifically, the following requirements must be fulfilled (Braun et al., 1991):

- Quantum yield must be relatively insensitive to changes in wavelength, concentrations, radiation rate and temperature
- Simple and precise photoproducts measurement
- Large molar absorption coefficients ( $\epsilon$ )

The following chemicals are used as actinometers:

- ✓ Potassium ferrioxalate
- ✓ Uranyl oxalate
- ✓ o-Nitrobenzaldehyde
- ✓ Malachite green, crystal violet
- ✓ Chloroacetic acid, 25°C
- ✓ Benzophenone
- ✓ Azobenzene (in methanol)
- ✓ 2-Hexanone
- ✓ Benzophenone/1,3-pentadiene
- ✓ meso-Diphenylhelianthrene
- ✓ Aberchrome 540
- ✓ Aberchrome 999P
- ✓ Reinecke's salt
- ✓ 2,2',4,4'-Tetraisopropylazobenzene

Uranyl oxalate and potassium ferrioxalate are the most used actinometers for the UV and visible domains (Braun et al., 1991). The latter has been reported to be the most practical and economic actinometer and presents the advantage to have an accurately known quantum yield. For these reasons, it was used in this work and it will be explained in detail.

#### **Potassium ferrioxalate actinometry**

This method consists in the reduction of Fe(III) to Fe(II) (Murov, 1973):



Fe(II) produced in the reaction is later quantified spectrophotometrically by measuring the absorbance of the red complex with 1,10-phenanthroline at 510 nm ( $\epsilon = 11100 \text{ L mol}^{-1} \text{ cm}^{-1}$ ). The original ferric ions are not appreciably complexed with the phenanthroline and they do not absorb at 510 nm.



Following the technique proposed by Murov (1973), the actinometer was prepared in the dark by diluting 750 mL of  $\text{Fe}_2(\text{SO}_4)_3$  0.02 M and 750 mL of  $\text{K}_2\text{C}_2\text{O}_4$  1.2 M in 15 L of distilled water. All of the reagents were purchased from Scharlau and were at least of analytical grade. Some other authors suggest synthesizing solid potassium ferrioxalate from  $\text{Fe}^{3+}$  chloride and potassium oxalate (Braun et al., 1991; Montalti et al., 2006).

The total volume of potassium ferrioxalate was placed into the reactor still in the dark. After irradiation starts, 1 mL aliquots were withdrawn at regular time intervals (including  $t=0$ ) and each one of them are mixed in 10 or 100 mL flasks containing 1,10-phenanthroline and an aqueous buffer (sodium acetate in  $\text{H}_2\text{SO}_4$ ) and the mixture is taken up to the volume of the flask. After 1 h stabilization, the absorbances of the samples were measured at 510 nm.

The intensity of the irradiation ( $I$ ) can be calculated by the following expression:

$$I = \frac{V_2 V_3 A_{510nm}}{V_1 d \varepsilon_{510nm} t} \quad (3.6)$$

Where:

$V_1$ : volume of the aliquot (1 mL)

$V_2$ : irradiated volume in the reactor (L)

$V_3$ : volume of the flask used for the complexation with phenanthroline (10 or 100 mL)

$A_{510nm}$ : absorbance of the complex  $\text{Fe}(\text{phen})_3^{2+}$  at 510 nm

$d$ : optical pathlength of the irradiation cell

$\varepsilon_{510nm}$ : molar absorption coefficient of the complex  $\text{Fe}(\text{phen})_3^{2+}$

$\varphi_\lambda$ : quantum yield of Fe(II) production at the used wavelength

$t$ : irradiation time

Plotting the evolution of the absorbance against time, resulting slope is equal to  $A/t$  in eq. (3.6) and  $I$  can be easily obtained. Figure 3.5 presents an example of such plot.

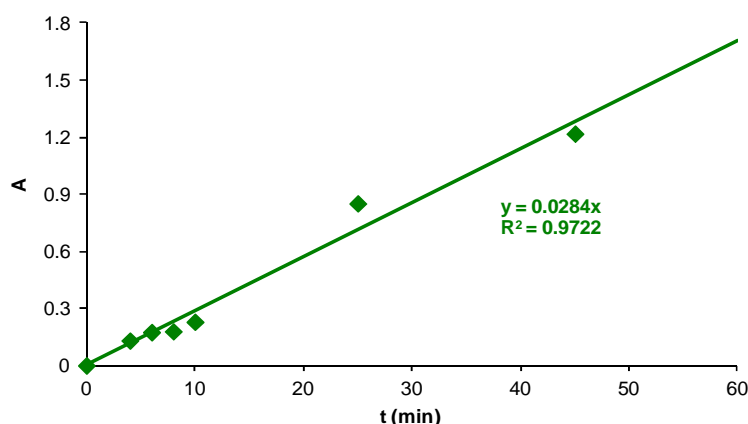


Figure 3.5. Example of a plot of absorbance against time for a potassium ferrioxalate actinometry

## 3.2. Mathematical Tools

Simulations were developed in Matlab<sup>®</sup>, a numerical computing environment and fourth-generation programming language developed by MathWorks<sup>®</sup>. For one hand, it is a programming environment with several pre-built toolboxes and functions which ease the construction of the programming codes and, for the other hand, it offers the possibility of interaction with other software, such as Microsoft<sup>®</sup> Excel<sup>®</sup> or Wonderware<sup>®</sup> InTouch<sup>®</sup>, the control and acquisition software available in the pilot plant under study. For instance, ordinary differential equations (ODEs) are easily solved using one of the available “ODE” functions (*ode45*, *ode152*, *ode23*, *ode113*, among others) and optimization tools as “*fmincon*” or “*fminsearch*” allow solving constrained and unconstrained continuous and discrete problems.

In this study, a semi-empirical model, based on that proposed by Cabrera-Reina et al. (2012) is simulated. Such model comprises nine kinetic expressions and eight ordinary differential equations solved with ODE45 function. In a further stage of the study, Fenton-like reaction was incorporated to the model with its reported kinetic constant, in order to identify its influence on the variables evolution (Küsič et al., 2006).

Furthermore, different reagent dosage strategies were simulated and compared in the search of operational conditions to improve process efficiency and the optimization of the batch recipe is investigated, using *fmincon* as the optimization tool.

### 3.2.1. Optimization tools

The optimization tool “*fmincon*” allows finding minimum of constrained nonlinear multivariable functions. According to MathWorks documentation center (2013),

“*fmincon* attempts to find a constrained minimum of a scalar function of several variables starting at an initial estimate. This is generally referred to as *constrained nonlinear optimization* or *nonlinear programming*”.

In its syntax, *fmincon* involves the following parameters:

```
[x,fval] = fmincon(fun,x0,A,b,Aeq,beq,lb,ub,nonlcon,options)
```

In this case, the tool starts at  $x_0$  and attempts to find a minimizer  $x$  of the function,  $fun$ , subject to the linear inequalities  $A*x \leq b$ .  $lb$  and  $ub$  define lower and upper bounds on the design variables in  $x$ , so that the solution is always in the range  $lb \leq x \leq ub$ .  $Nonlcon$  is the function that computes the nonlinear inequality constraints  $c(x) \leq 0$  and the nonlinear equality constraints  $ceq(x) = 0$ .  $Nonlcon$  accepts a vector  $x$  and returns the two vectors  $c$  and  $ceq$ .  $c$  is a vector that contains the nonlinear inequalities evaluated at  $x$ , and  $ceq$  is a vector that contains the nonlinear equalities evaluated at  $x$ .

### Options

*fmincon* uses a Hessian as an optional input. This Hessian is the second derivatives of the Lagrangian, namely,

$$\nabla_{xx}^2 L(x, \lambda) = \nabla^2 f(x) + \sum \lambda_i \nabla^2 c_i(x) + \sum \lambda_i \nabla^2 ceq_i(x) \quad (3.7)$$

The several *fmincon* algorithms available handle input Hessians in different ways:

- The *active-set* and sequential quadratic programming (*sqp*) algorithms do not accept a user-supplied Hessian. They compute a quasi-Newton approximation to the Hessian of the Lagrangian.
- The *trust-region-reflective* algorithm can accept a user-supplied Hessian as the final output of the objective function. Since this algorithm has only bounds or linear constraints, the Hessian of the Lagrangian is same as the Hessian of the objective function.
- The *interior-point* algorithm (which is used in this work) can accept a user-supplied Hessian as a separately defined function—it is not computed in the objective function.

### 3.3. References

Braun, A.M.; Maurette, M-T.; Oliveros, E. 1991. Photochemical Technology. John Wiley & Sons, England.

Kuhn, H.J.; Braslavsky, S.E.; Schmidt, R. 2004. Chemical Actinometry (IUPAC Technical Report) Pure Appl. Chem. 76(12), 2105–2146.

Kůsič, H., Koprivanac, N., Bozic, A.L., Selanec, I. 2006. Photo-assisted Fenton type processes for the degradation of phenol: A kinetic study. J. Hazard. Mater. 136, 632.

MathWorks® Documentation Center. URL: <http://www.mathworks.es/es/help/optim/ug/fmincon.html>. [Consulted: May 2013]

28

Montalti, M.; Credi, A.; Prodi, L.; Gandolfi, M.T. 2006. Handbook of Photochemistry, third edition. Taylor & Francis Group, United States of America.

Murov, S.L., 1973. Handbook of Photochemistry, Dekker, New York.

Nogueira, R.F.P.; Oliveira, M.C.; Paterlini, W.C. 2005. Simple and fast spectrophotometric determination of H<sub>2</sub>O<sub>2</sub> in photo-Fenton reactions using metavanadate. *Talanta*. 66(1), 86.

## **PART II. EXPERIMENTAL APPROACH**





## **Chapter IV**

### **Characterization of Paracetamol Degradation by Fenton and photo-Fenton processes**

The study of Fenton and photo-Fenton processes was addressed using paracetamol in water solutions as a model pollutant, with the aim to identify the influence of process variables and reagent doses on process behavior. The characterization of the degradation of paracetamol is presented in this chapter.



## 4.1. Introduction

Paracetamol (acetaminophen or 4-amidophenol), from here on PCT, is a widely used analgesic, anti-inflammatory and antipyretic, reported as the most popular non-opioid analgesic sold in Spain in the last years (Martínez Bueno et al., 2012). It has been found in European Sewage Treatment Plants in concentrations around  $6 \mu\text{g L}^{-1}$  (Ternes, 1998) and several studies have demonstrated AOPs capability to degrade paracetamol from different matrixes, as it can be seen in Table 2.6.

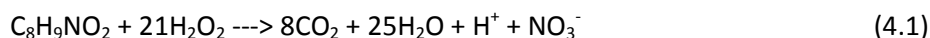
All the mentioned investigations confirmed that UV irradiation above 254 nm does not degrade PCT or mineralize samples, but the presence of hydrogen peroxide or another oxidant leads to total remediation and partial mineralization of the samples. New process control and modeling approaches have been presented, but a more complete understanding of the process will be provided when a model considering photo-enhancement of the process is clarified. As a first step toward this direction, photonic efficiency of PCT degradation via photo-Fenton has to be estimated in order to provide a more complete representation of the process.

## 4.2. Preliminary Assays

### 4.2.1. Selection of the reagent doses

According to the information shown in Table 2.6, a wide range of PCT concentrations have been investigated so far, more specifically, concentrations ranging from  $1 \times 10^{-3}$  to 25 mM have been addressed in the literature. A concentration of  $40 \text{ mg L}^{-1}$  ( $2.65 \times 10^{-4} \text{ M}$ ) was selected in this study, despite being much higher than that found in wastewaters and groundwater (between 0.05 and  $1.9 \text{ mg L}^{-1}$  according to Lapworth et al., 2012). This high concentration allows following the evolution of the contaminant and possible intermediates concentrations along the treatment span and, at the same time, takes into account the detection limit of the available measurement equipment.

Regarding Fe(II) concentration, a maximum level of  $10 \text{ mg L}^{-1}$  was selected, since it is the maximum legal value in wastewaters in Spain (DOGC). A minimum value of half that maximum ( $5 \text{ mg L}^{-1}$ ) was also considered in this study. With regards to  $\text{H}_2\text{O}_2$  concentration, a stoichiometric dose of  $189 \text{ mg L}^{-1}$  was calculated by Eq. 4.1 (considering  $\text{H}_2\text{O}_2$  as the only oxidant in the media) to achieve total mineralization to  $\text{CO}_2$ ,  $\text{H}_2\text{O}$  and inorganic ions. A range between half and four times the stoichiometric dose ( $94.5$  and  $756 \text{ mg L}^{-1}$ , respectively) was selected to study the influence of  $\text{H}_2\text{O}_2$ .



Experiments were carried out using the Pyrex photo-reactor (R2) presented in Table 3.1, equipped with the Actinic BL TL-DK 36W/10 1SL lamp (Fig. 3.1b). According to operative considerations, a total volume of 15 L was used and, in the

search for a convenient degradation rate which permits to follow the concentrations of contaminant and possible intermediates, the lamp was partially covered to achieve an irradiated volume equal to the 10% of the total volume.

#### 4.2.2. Mixing characterization

Once the concentrations of the reagents was established, it was necessary to guarantee perfect mixing conditions at the most extreme set of operational conditions ( $40 \text{ mg L}^{-1}$  PCT,  $10 \text{ mg L}^{-1}$  Fe(II) and  $756 \text{ mg L}^{-1}$   $\text{H}_2\text{O}_2$ ). For that aim, a set of experiments was performed at different recirculation flows, and TOC and  $\text{H}_2\text{O}_2$  concentration were determined. Results are presented in Fig. 4.2 and they show a perfectly agitated system from a recirculation flow of  $7.7 \text{ L min}^{-1}$ . A value of  $12 \text{ L min}^{-1}$  was selected for the subsequent study.

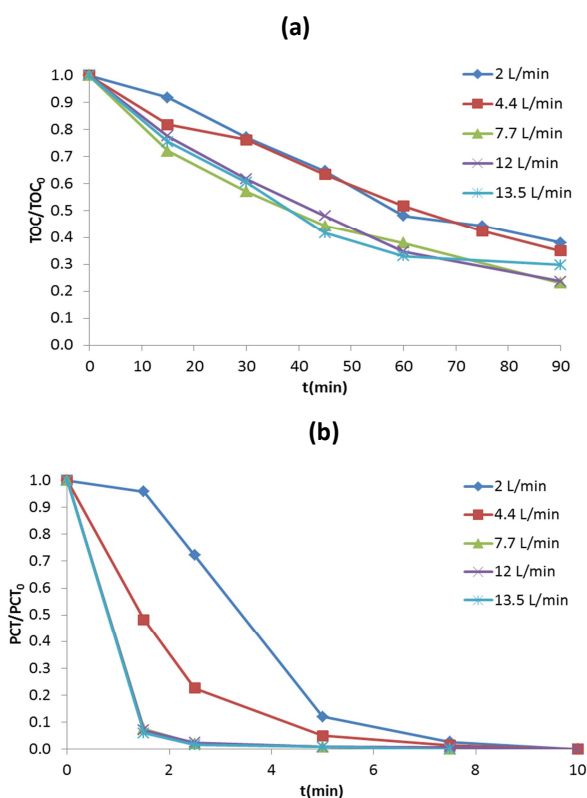


Figure 4.1. Evolution of normalized concentrations at different values of recirculation flow. (a) TOC concentration, (b) PCT concentration

#### 4.2.3. Blank assays

A set of blank assays was performed at the most extreme reagent doses in order to identify the effect of each reagent on the degradation and mineralization of PCT. The three undertaken blank assays correspond to only irradiation, only Fe(II) at a concentration of  $10 \text{ mg L}^{-1}$  and only  $\text{H}_2\text{O}_2$  at a concentration of  $756 \text{ mg L}^{-1}$ . The evolution of mineralization and degradation is presented in Figure 4.3.

The results demonstrate that none of the reagents by themselves achieve any mineralization, but the oxidant power of  $\text{H}_2\text{O}_2$  leads to a reduction in PCT concentration of 18% in 90 minutes treatment. Sole irradiation was not expected to degrade PCT as it does not absorb energy in the range of emission of the lamp. Actually, PCT presents an absorption band below 300 nm, as Figure 4.4 shows.

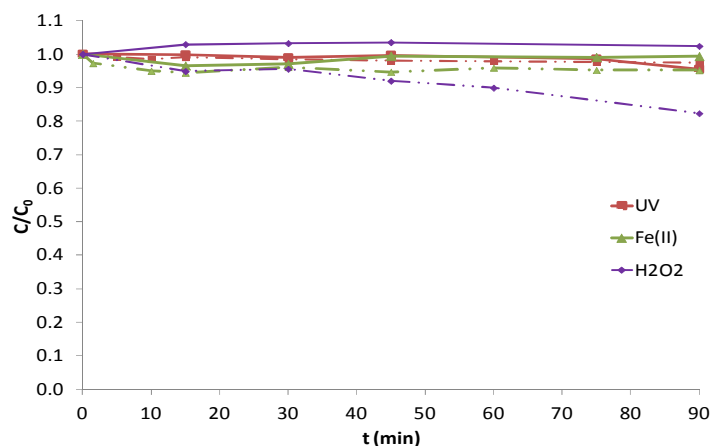


Figure 4.2. Evolution of TOC and PCT concentrations for blank assays. Continuous lines correspond to TOC concentrations.

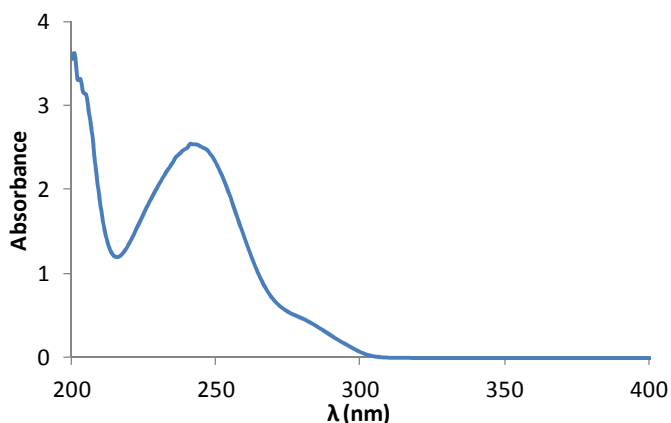


Figure 4.3. Absorption spectrum of a  $40 \text{ mg L}^{-1}$  PCT sample

### 4.3. PCT Degradation and Mineralization Performance

Three factors were considered to characterize the degradation and mineralization of PCT solutions: Fe(II) concentration,  $\text{H}_2\text{O}_2$  concentration and presence/absence of irradiation. The design of experiment presented in Table 4.1 was undertaken. Samples were withdrawn at regular time intervals and TOC,  $\text{H}_2\text{O}_2$  and PCT concentrations were measured. A non-identified intermediate was detected by HPLC and its evolution was also followed along the treatment span.

Table 4.1. Design of experiments for the characterization of PCT degradation

$C^{PCT}$ (mg L <sup>-1</sup> )	$C^{Fe(II)}$ (mg L <sup>-1</sup> )	$C^{H_2O_2}$ (mg L <sup>-1</sup> )	Irradiation	Experiment code
40	5	94.5	ON	PCT_40_5_94.5_ON
			OFF	PCT_40_5_94.5_OFF
		189	ON	PCT_40_5_189_ON
			OFF	PCT_40_5_189_OFF
		378	ON	PCT_40_5_378_ON
			OFF	PCT_40_5_378_OFF
	756	ON	PCT_40_5_756_ON	
		OFF	PCT_40_5_756_OFF	
	10	94.5	ON	PCT_40_10_94.5_ON
			OFF	PCT_40_10_94.5_OFF
		189	ON	PCT_40_10_189_ON
			OFF	PCT_40_10_189_OFF
		378	ON	PCT_40_10_378_ON
			OFF	PCT_40_10_378_OFF
756	ON	PCT_40_10_756_ON		
	OFF	PCT_40_10_756_OFF		

Figures 4.4 and 4.5 shows the results obtained when 5 mg L<sup>-1</sup> and 10 mg L<sup>-1</sup> Fe(II) initial concentrations are added at the beginning of the experiment, respectively. In both case, Fenton and photo-Fenton processes are compared for different initial H<sub>2</sub>O<sub>2</sub> concentrations.

Figures 4.4(a) and (b) demonstrate that, as it was expected, the presence of irradiation remarkably improves mineralization. In the absence of irradiation, mineralization levels of (33±5)% are obtained for both Fe(II) loads, while in the presence of irradiation, a 46% TOC reduction is achieved in the worst case (5 mgL<sup>-1</sup> Fe(II) and 94.5 mg L<sup>-1</sup> H<sub>2</sub>O<sub>2</sub>). The improvement in mineralization with the irradiation ranges between 15 a 40 percentage points for both Fe(II) concentrations and it increases when higher H<sub>2</sub>O<sub>2</sub> concentration are dosed. For the studied range of reagent doses, the best results are obtained for photo-Fenton process when 10 mg L<sup>-1</sup> Fe(II) and 378 mg L<sup>-1</sup> are dosed, achieving 82% mineralization in 90 minutes operation.

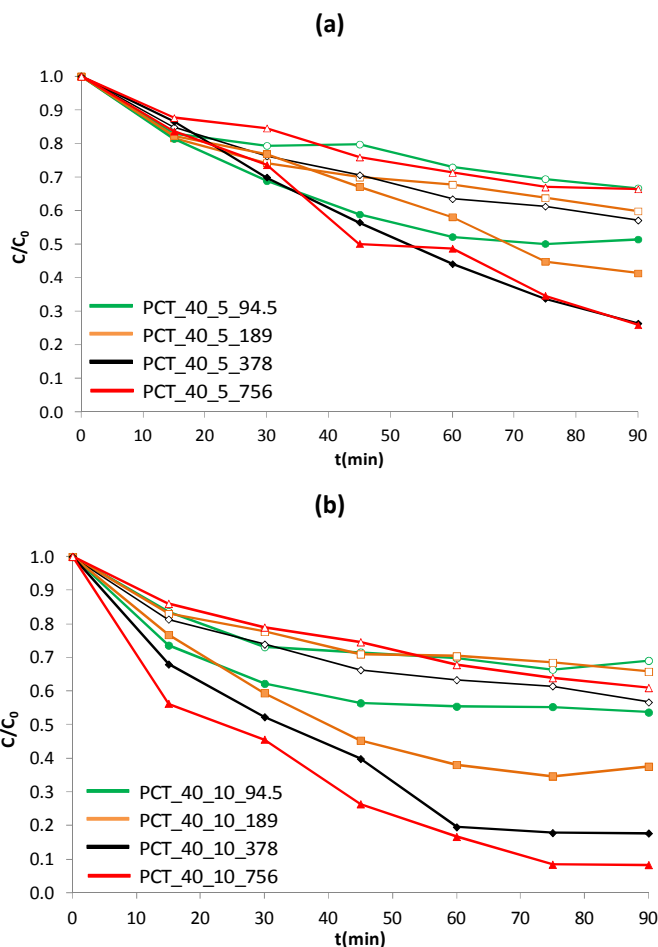


Figure 4.4. Evolution of TOC concentration for Fenton (void symbols) and photo-Fenton (solid symbols) processes **(a)**  $5 \text{ mg L}^{-1} \text{ Fe(II)}$  **(b)**  $10 \text{ mg L}^{-1} \text{ Fe(II)}$

Regarding PCT degradation (Fig. 4.5(a) and (b)), both Fenton and photo-Fenton efficiently degrade PCT in less than 10 min reaction time. Note that doubling the dose of Fe(II) reduces in half the time to achieve total PCT remediation. Additionally, the intermediate observed by HPLC analysis it is also totally eliminated during the same time span. A parallel investigation performed in IMRCP (Toulouse, France) showed that such intermediate might be the product of the hydroxylation of the benzene ring.

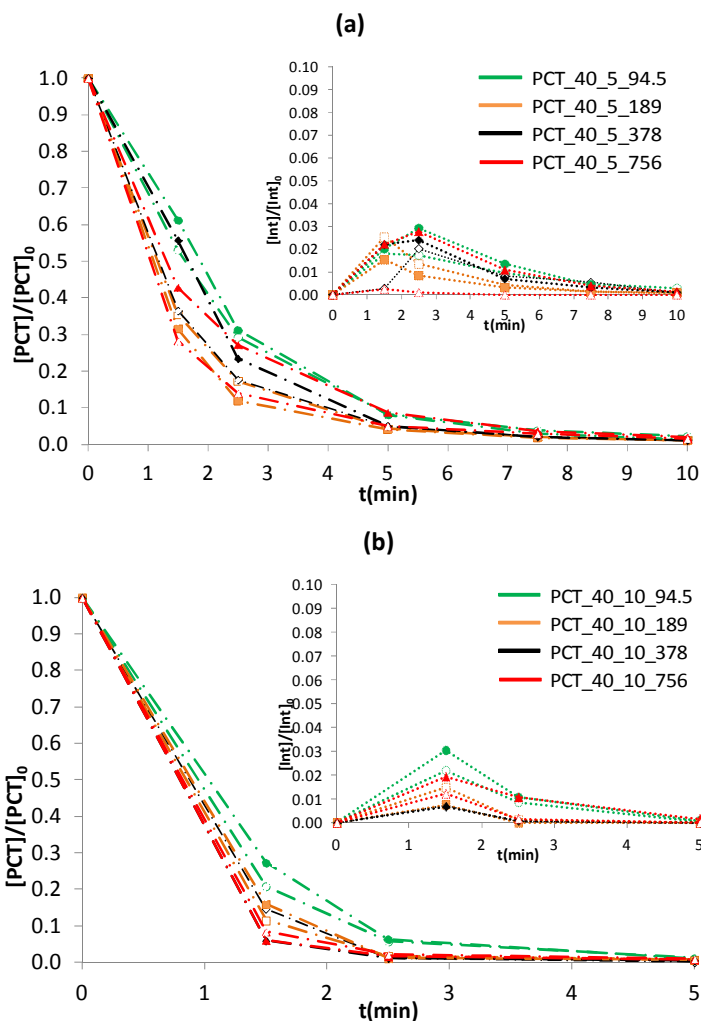


Figure 4.5. Evolution of PCT and intermediate concentrations for Fenton (void symbols) and photo-Fenton (solid symbols) processes. **(a)**  $5\text{mg L}^{-1}\text{ Fe(II)}$  **(b)**  $10\text{mg L}^{-1}\text{ Fe(II)}$

#### 4.4. Photonic Efficiency

One of the terms used to evaluate the efficiency of a photochemical process is the quantum yield, defined as “the number of molecules which react according to this process divided by the numbers of photons absorbed by the system during the same time” (Braun et al., 1991). In the same way that chemical yield of a reaction measures the usage of a given reagent to produce a desired product, the quantum yield measures the usage of photons to produce the desired product in a photochemical reaction. Furthermore, complex phenomenological models, considering the local volumetric rate of photon absorption (LVRPA) require the calculation of such term to provide more applicable and flexible modeling options.



Another term, which is useful for polychromatic radiation and is independent of the geometry of the reactor, is the photonic efficiency or apparent quantum efficiency. It is defined by Benzaquén et al. (2012) as “the ratio of the number of reactant molecules degraded during a given time, to the total number of photons arriving at the reactor wall, during the same period of time”. Mathematically, it can be expressed for a generic reagent “A” as follows:

$$\phi_{app,A} = \frac{[\text{amount of A converted}]}{[\text{amount of photons arriving at the reactor wall}]} \quad (4.2)$$

Applying the previous concept to PCT degradation, photonic efficiency can be calculated as:

$$\phi_{app,PCT} = \frac{(C_{t_0}^{PCT} - C_{t_f}^{PCT}) \cdot V_T}{q_w A_w (t_f - t_0)} \quad (4.3)$$

where  $\phi_{app,PCT}$  is the photonic efficiency of PCT degradation (mol/Einstein),  $C_{t_0}^{PCT}$  and  $C_{t_f}^{PCT}$  are PCT concentrations at initial and final time ( $t_0$  and  $t_f$ ), respectively (mol L<sup>-1</sup>),  $V_T$  the total irradiated volume (L),  $q_w$  the spectral net radiation flux at the reactor wall (Einstein cm<sup>-2</sup>·s<sup>-1</sup>) and  $A_w$  the irradiated area (cm<sup>2</sup>).

In a similar way, in order to evaluate the photonic efficiency of mineralization, the photonic efficiency of mineralization (TOC reduction),  $\phi_{app,TOC}$  can be expressed as:

$$\phi_{app,TOC} = \frac{(C_{t_0}^{TOC} - C_{t_f}^{TOC}) \cdot V_T}{q_w A_w (t_f - t_0)} \quad (4.4)$$

In this study, the influence of the H<sub>2</sub>O<sub>2</sub>/Fe(II) ratio ( $R_{H/Fe}$ ) on photonic efficiency of PCT degradation and mineralization (TOC) was determined at different treatment times, in order to identify the best operational conditions which improve the usage of the irradiation and to open a line towards a more rigorous model of the process. Results are presented in further sub-sections.

#### 4.4.1. Photonic efficiency of PCT degradation ( $\phi_{app,PCT}$ )

Photonic efficiency was calculated at different ratios H<sub>2</sub>O<sub>2</sub>:Fe(II) ( $R_{H/Fe}$ ) and Figure 4.6 presents the results for 10 mg L<sup>-1</sup> Fe(II) initial concentration at different reaction times. A higher photonic efficiency is observed at  $R_{H/Fe} = 37.8$  during the first 2.5 minutes treatment, but it seems to be independent of the ratio after 5 minutes, as it was expected due to the maximum residual PCT in whatever experimental condition after 5 minutes reaction time is 0.4 mg L<sup>-1</sup> (more than 99% degradation).

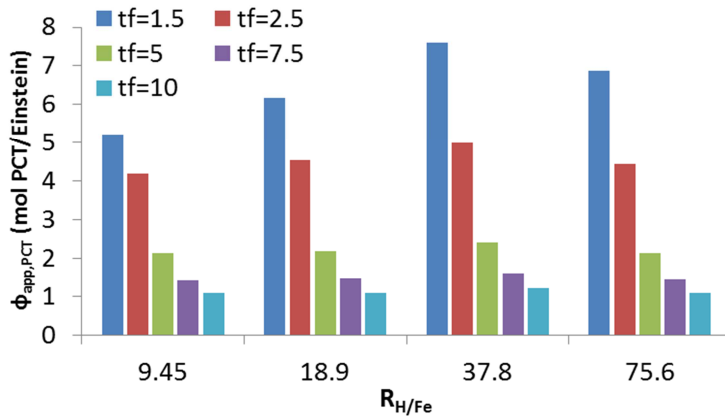


Figure 4.6. Photonic efficiency of PCT degradation for Fe(II) = 10 mg L<sup>-1</sup> and different ratios H<sub>2</sub>O<sub>2</sub>:Fe(II)

Regarding the influence of the Fe(II), Figure 4.7 shows the results obtained for 1.5 minutes treatment and efficiencies are lower when 5 mg L<sup>-1</sup> Fe(II) are supplied instead of 10 mg L<sup>-1</sup>. The best ratio when 5 mg L<sup>-1</sup> Fe(II) is used might be 37.8, but the trend is not sufficiently clear.

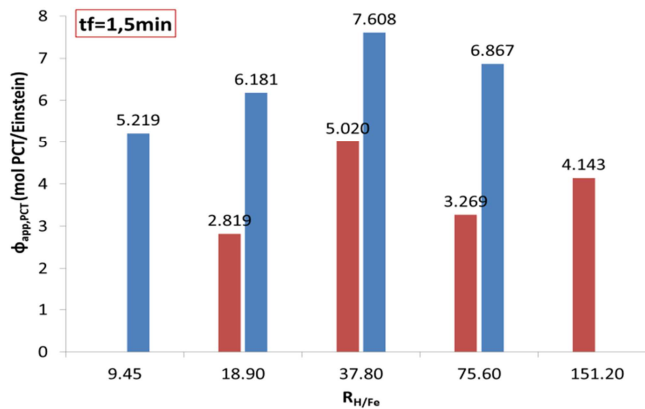


Figure 4.7. Photonic efficiency for PCT degradation at 1.5 min treatment as a function of H<sub>2</sub>O<sub>2</sub>:Fe(II) ratio for two Fe(II) initial concentration (Blue: 10 mg L<sup>-1</sup>. Red: 5 mg L<sup>-1</sup>)

#### 4.4.2. Photonic efficiency of mineralization ( $\phi_{app,TOC}$ )

Photonic efficiencies of mineralization are lower than PCT degradation, as Figure 4.8 demonstrates. This was expected as PCT degradation is much faster than mineralization, which involves the degradation of all the organic matter in the sample.  $\phi_{app,TOC}$  exhibits a similar behavior than  $\phi_{app,PCT}$ , showing a local optimum at R<sub>H/Fe</sub> = 37.8 as well.

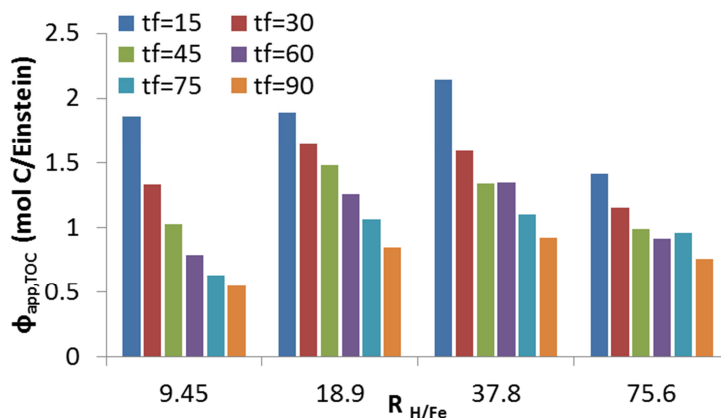


Figure 4.8. Photonic efficiency of mineralization for Fe(II) = 10 mg L<sup>-1</sup> and different ratios H<sub>2</sub>O<sub>2</sub>:Fe(II)

Figure 4.9 shows  $\phi_{app,TOC}$  for the two Fe(II) concentrations studied at 15 minutes treatment and it presents a similar trend than  $\phi_{app,PCT}$  when 10 mg L<sup>-1</sup> Fe(II) are loaded. At 5 mg L<sup>-1</sup> Fe(II) the efficiencies are lower and do not exhibit a clear trend.

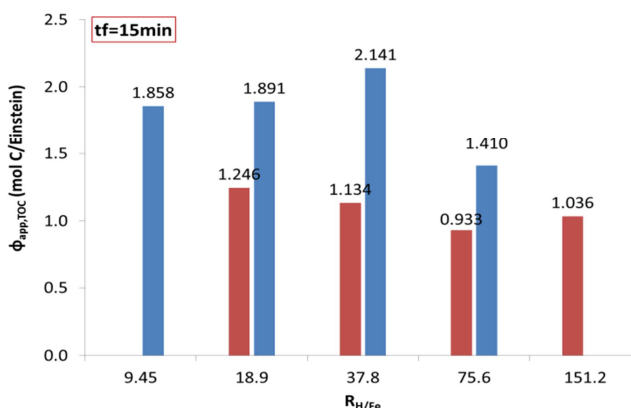


Figure 4.9. Photonic efficiency for mineralization at 15 min treatment as a function of H<sub>2</sub>O<sub>2</sub>:Fe(II) ratio for two Fe(II) initial concentration (Blue: 10 mg L<sup>-1</sup>. Red: 5 mg L<sup>-1</sup>)

Within the tested experimental conditions, higher efficiencies of mineralization are obtained with 10 mg L<sup>-1</sup> Fe(II) and a ratio R<sub>H/Fe</sub> = 37.8. As PCT degradation is achieved during the first 10 min treatment, this parameter combination seems to satisfactorily degrade PCT degradation and mineralizes organic matter with the best usage of reagents and irradiation.

#### 4.5. Conclusions

The presence of irradiation was confirmed to remarkably improve both degradation and mineralization of PCT samples by Fenton process, providing until

40 percentage points more mineralization than thermal Fenton process when 10 mg L<sup>-1</sup> Fe(II) are loaded. It is worth mention, than iron loads inside the legal limit (10 mg·L<sup>-1</sup>) are enough to guaranty even 83% TOC reduction within 90 minutes treatment, while half that dose leads to 74% mineralization.

Regarding Fenton process, its efficiency in mineralizing the organic matter seems to be independent of Fe(II) load when H<sub>2</sub>O<sub>2</sub> dose is over 378 mg L<sup>-1</sup>, but H<sub>2</sub>O<sub>2</sub> load becomes a more important factor in Fenton than in Photo-Fenton process. In all of the cases, Fenton process achieved total PCT degradation in less than 10 minutes operation.

A remarkable improvement of photo-Fenton process efficiency is achieved when applying a convenient Fenton reagent load: 10 mg L<sup>-1</sup> Fe(II) and 378 mg L<sup>-1</sup> H<sub>2</sub>O<sub>2</sub>. Indeed, total degradation in less than 5 minutes operation and 83% mineralization in 90 minutes are possible under these experimental conditions.

As it was expected, photonic efficiency of mineralization and PCT degradation decrease with reaction time and is higher at the higher studied Fe(II) dose. This parameter exhibits a local optimum when H<sub>2</sub>O<sub>2</sub>/Fe(II) ratio of 37.8 for both Fe(II) loads.

This chapter presents a first research to study the influence of process variables on photo-Fenton process behavior. The next chapters are devoted to continue investigating these variables and to propose alternatives lending to improve process performance.

## 4.6. References

- Benzaquén, T.B.; Isla, M.A.; Alfano; O.M. 2012. Quantum efficiencies of the photo-Fenton degradation of atrazine in water. *Water Sci. Technol.* 66, 2209-2216.
- Gernjak, W., Fuerhacker, M., Fernández-Ibañez, P., Blanco, J., Malato, S. 2006. Solar photo-Fenton treatmentdprocess parameters and process control. *Appl. Catal. B* 64 (1–2), 121–130.
- Herney Ramirez, J., Costa, C.A., Madeira, L.M. 2005. Experimental design to optimize the degradation of the synthetic dye Orange II using Fenton's reagent. *Catal. Today* 107–108, 68–76.
- Lapworth, D.J., Baran, N., Stuart, M.E., Ward, R.S. 2012. Emerging organic contaminants in groundwater: A review of sources, fate and occurrence. *Environ. Pollut.* 163, 287-303.
- Martínez Bueno, M.J.; Gomez, M.J.; Herrera, S.; Hernando, M.D.; Agüera, A.; Fernández-Alba, A.R. 2012. Occurrence and persistence of organic emerging contaminants and priority pollutants in five sewage treatment plants of Spain: Two years pilot survey monitoring, *Environ. Pollut.* 164, 267-273.
- Ternes, T.A. 1998. Occurrence of drugs in German sewage treatment plants and rivers, *Water Res.* 32, 3245–3260.

## **Chapter V**

### **Systematic Assessment of a Hydrogen Peroxide dosage on Caffeine Degradation by photo-Fenton Process**

In this chapter, hydrogen peroxide dosage is investigated. A dosage protocol is proposed in order to achieve a more efficient usage of the reagent and the produced hydroxyl radicals. The assessment of the protocol is addressed using coffee samples in water solutions as a model pollutant.



## 5.1. Introduction

One of the most significant factors in photo-Fenton process has been reported to be the Fenton reagent ratio ( $\text{Fe(II)}/\text{H}_2\text{O}_2$ ) (Gulkaya et al., 2006). Lots of works have been devoted to determining experimental conditions enhancing treatment performance (Pignatello et al., 2006). Lately, the use of too high Fenton reaction loads was questioned and efforts have been also steered towards reactant reduction (Klamerth et al., 2010) with regard to legal limits for iron disposal. Most of this research has mainly considered the batch operation mode, but also the use of an initial load to be progressively consumed along the whole reaction span.

Since hydrogen peroxide has been assumed to undergo diverse parallel competitive reactions of uncertain nature (Pignatello et al., 2006), it seems unrealistic to assume that an initial load of hydrogen peroxide will be under control.

Dosage has been recently described as a relevant factor (Ince, 1999); the sequential addition of load portions along the reaction time has been reported to improve mineralization (Chu et al., 2007), and the study of continuous dosage has led to promising results (Zazo et al., 2009; Monteagudo et al., 2009). Very recently, continuous automatic dosage has been investigated and dosing optimization has been foreseen (Prieto-Rodríguez et al., 2011).

These promising results reveal a great opportunity for improving the efficiency of photo-Fenton processes. A flexible operation may be envisaged thanks to new degrees of freedom upon which practical control recipes could be developed. However, dosage has not been addressed in a systematic way towards this end. There is not only the lack of a convenient model, but also a lack of related experimental data. Therefore, this chapter proposes a first step aimed at the experimental characterization of the response of different dosing protocols and the experimental identification of the best dosage tested.

In this chapter, a practical way for parameterizing the dosage is presented and used for planning a set of assays under a Design of Experiments (DOE) scheme. Caffeine is selected for validating this methodological approach to determine the influence of hydrogen peroxide dosage protocol on process efficiency.

Caffeine is almost totally metabolized by the human body. However, rests of beverages containing caffeine are disposed of, and caffeine is detected in low concentrations in sewage treatment plants. Due to its high water solubility and low degradability, caffeine is considered among emerging contaminants (Gómez et al., 2007; Rodríguez-Gil et al., 2010). Additionally, coffee, the most common mixture containing caffeine, harms the environment due to its opacity and its high biological and chemical oxygen demand, causing eutrophication, blocking light, and affecting photosynthesis (Tokumura et al., 2006; Tokumura et al., 2008).

Coffee and caffeine deserve more research in order to find better ways to remediate them from wastewaters.

## 5.2. Preliminary assays and reagent load settings

### 5.2.1. Ferrous salt load

The process performance has been proved to be significantly affected not only by the individual concentrations of Fenton reagents, but also by the hydrogen peroxide-to-iron ratio. The selection of this ratio depends on the nature and concentration of the contaminant (Pignatello et al., 2006).

Herney et al.(2005) reported a wide range of useful load ratios for the Fenton reagents relative to the degradation of different substances (hydrogen peroxide-to-iron weight ratios from 5:1 to 20:1). Other authors present values in the range from 10:1 to 200:126 and even from 100:1 to 1000:1 (Pignatello et al., 2006).

The literature indicates the existence of a limiting iron concentration that guarantees the degradation process (Rossi and Nogueira, 2007), conversely, iron excess decreases the effectiveness of the photo-Fenton (Pérez-Moya et al., 2007) and Fenton processes (Burbano et al., 2008).

The work by Tokumura et al.(2006) reports on photochemical decolorization of coffee effluents by photo-Fenton process, and investigates the effects of light intensity, initial coffee concentration, and iron and H<sub>2</sub>O<sub>2</sub> dose on the color removal of a standard coffee effluent. The initial coffee concentration range was set by Tokumura et al. (2006) between 0 and 446 mg L<sup>-1</sup>, while hydrogen peroxide and iron concentration ranges were set between 0-2400 mg L<sup>-1</sup> and 0-28 mg L<sup>-1</sup>, respectively.

According to the results reported by Tokumura et al.,(2006) coffee concentration for the standard problem sample was set to 300 mg L<sup>-1</sup>, and the corresponding load ranges for iron and hydrogen peroxide used were determined in the subsequent set of assays. The study was conducted in the plastic photo-reactor R3 (Table 3.1), equipped with the irradiation source shown in Figure 3.1c, with iron concentrations between 10 and 40 mg L<sup>-1</sup> and hydrogen peroxide concentration between 1500 and 3000 mg L<sup>-1</sup>, which implies ratios between 75:1 and 107:1; these data confirmed that total caffeine elimination and TOC reductions between 70 and 80 % are possible via photo-Fenton process. Iron doses of 10, 20 and 40 mg L<sup>-1</sup> were investigated and very similar TOC reduction profiles were found for the three cases, which suggested the use of the lowest of these doses. Since reduced iron concentration improves economic and environmental performance of the treatment, the iron load was set to 10 mg L<sup>-1</sup>, which is the legal limit as well (DOGC).

Similar preliminary conclusions were observed for the H<sub>2</sub>O<sub>2</sub> load, and 1500 mg L<sup>-1</sup> proved to be as efficient as 3000 mg L<sup>-1</sup>. However, the decision on the H<sub>2</sub>O<sub>2</sub> load was made after the complementary assays described in section 5.2.3.



### 5.2.2. Blank assays

The next step was to perform a series of blank assays comparing the separate effect of iron, hydrogen peroxide and light (Fig. 5.1). The blank assays demonstrated that the photo-Fenton process is able to eliminate caffeine and degrade organic matter from the standard samples.

All of the samples were prepared in tap water, at a concentration of 300 mg L<sup>-1</sup> of commercial coffee (Nescafe®), equivalent to 17 mg L<sup>-1</sup> caffeine, approximately. Samples were withdrawn at regular time intervals and TOC, hydrogen peroxide and caffeine concentration were measured.

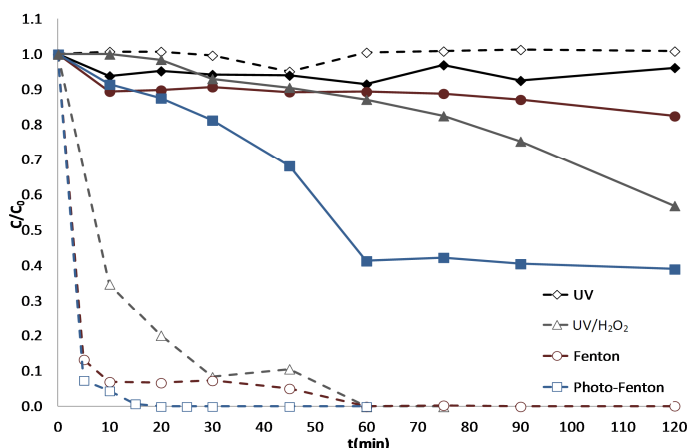


Figure 5.1. Comparative blank assays of the degradation profile of TOC (solid line) and caffeine (dashed line). Standard sample with  $C_{eq,\infty}^{H_2O_2} = 500 \text{ mg L}^{-1}$

These assays lead to further conclusions:

- The sole UV irradiation does not eliminate caffeine, nor reduce TOC.
- The addition of the oxidant (UV/H<sub>2</sub>O<sub>2</sub>) produces both the elimination of the caffeine as well as some TOC reduction (clearly, the organic intermediates formed are only partially degraded).
- Likewise, the Fenton process is not good enough to mineralize all the organic matter, although it degrades caffeine within a similar treatment time.
- The photo-Fenton process not only achieves total caffeine elimination as well, but attains the maximum TOC reduction (around 40%) within the reaction span considered.

### 5.2.3. Stepwise dosage

Chu et al.(2007) investigated the degradation of atrazine by a stepwise Fenton process and showed that Fenton process performance can be significantly improved by splitting the hydrogen peroxide load into several portions dosed

along the process. Therefore, in this final set of preliminary assays, different hydrogen peroxide loads and dosage protocols were compared.

The results obtained (Fig. 5.2) show that the mineralization of the problem samples may be also improved when hydrogen peroxide is dosed at different times and/or quantities along treatment. Furthermore, the same total performance seems to be attainable using reduced hydrogen peroxide loads. In particular, Figure 5.3 shows that using half of the load (9000 mg) may achieve the same degree of mineralization as using the entire load (18000 mg) if conveniently dosed: 3000 at times 0, 45 and 90 minutes.

The hydrogen peroxide data plotted in Figure 5.2 correspond to the equivalent concentration ( $C_{eq,\infty}^{H_2O_2}$ ) that would be obtained by having all the additions at time 0. The concept is formalized next in section 5.2 and should not be mistaken for the actual concentration, which needs to be measured each time. For this case, an equivalent initial concentration of  $750 \text{ mg L}^{-1}$  results from a total amount of 9000 mg ( $3 \times 3000$ ) divided by the total volume of the reactor (12 L).

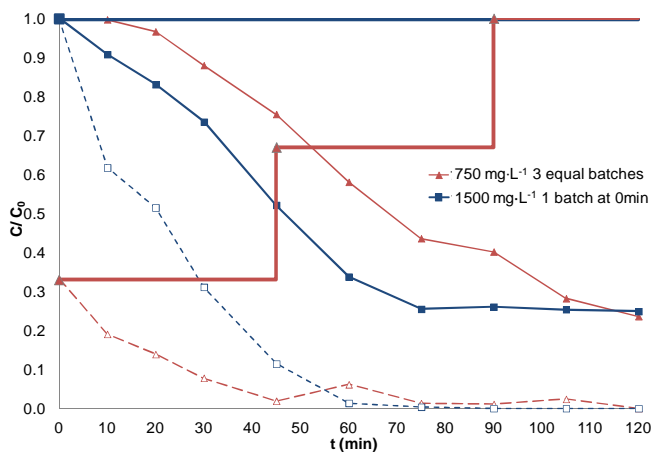


Figure 5.2. Normalized TOC (solid line) and normalized hydrogen peroxide concentration (dashed line) for the standard sample undergoing three stepwise dosage protocols (gray line).  $C_{eq,\infty}^{H_2O_2}$  values are specified in the figure.

Given that, within the 2-hour treatment, up to 75 % TOC reduction may be obtained using 9000 mg ( $750 \text{ mg L}^{-1}$ ), a decision was made to set a lower amount as the fixed value upon which the different dosage options were arranged and assessed. Towards this end, 6000 mg ( $500 \text{ mg L}^{-1}$ ) of hydrogen peroxide was set as a condition allowing a range of performance outcomes wide enough to be of statistical significance.

Up to this point, reagent total loads have been fixed after preliminary assays (caffeine,  $300 \text{ mg L}^{-1}$ ; iron,  $10 \text{ mg L}^{-1}$ ; hydrogen peroxide,  $500 \text{ mg L}^{-1}$ ). Other structural and operational variables are also fixed. Thus, the remaining degrees of freedom are those related to hydrogen peroxide dosage. At this point, the

formalization and parameterization of the hydrogen peroxide dosage is required in order to first determine the governing factors of the process, and next to plan a Design of Experiments (DOE) allowing the identification of the set of operating conditions enhancing process performance.

### 5.3. Experimental Design

Once the loads are fixed (contaminant and reactants), the effect of the way in which one of these fixed amounts is dosed along the time is investigated. The factors governing the dosage need to be first identified and characterized in order to clearly define the problem. The number of factors depends on the degrees of freedom of the dosage protocol adopted: from none, in case the entire load is released at the start, to more degrees of freedom than could be managed in the case a flexible dosing schedule. Furthermore, the option for continuous dosage should be also considered (Zazo et al., 2009).

Thus, a decision is made for such a trade-off and a three-factor hybrid discrete-continuous dosage protocol is proposed. Given the factors, the assays may be planned (DOE) and executed. Finally, the definition of a performance measurement is required to quantitatively discern the most promising options.

#### 5.3.1. Dosage protocol: model and factors

A factor fixed by the previous preliminary study is the total quantity of hydrogen peroxide  $Q^{H_2O_2}$  used for each assay. This amount is related to the equivalent mass concentration of hydrogen peroxide  $Q^{H_2O_2}$ , which is defined as the mass concentration that would be obtained in a reactor of volume  $V_R$  after the dosage of all the volume  $v_D^\infty$  of hydrogen peroxide of a given purity  $P^{H_2O_2}$  (330000 mg L<sup>-1</sup>), provided the absence of reactions (i.e. just considering the dilution effect):

$$C_{eq,\infty}^{H_2O_2} = \frac{v_D^\infty P^{H_2O_2}}{(V_R + v_D^\infty)} = \frac{Q^{H_2O_2}}{(V_R + v_D^\infty)} \cong \frac{Q^{H_2O_2}}{V_R} \quad (5.1)$$

$$v_D^\infty = \frac{Q^{H_2O_2}}{\rho^{H_2O_2}} \quad (5.2)$$

Being this amount fixed (either  $Q^{H_2O_2}$ ,  $Q^{H_2O_2}$  and  $v_D^\infty$ ), the way in which it is dosed is modeled and parameterized in the following way:

$$y(t) = \frac{v_D(t)}{v_D^\infty} = \begin{cases} 0 & \text{if } t < 0 \\ y_0 & \text{if } 0 \leq t < t_{ini} \\ y_0 + \left( \frac{1-y_0}{\Delta t_{add}} \right) (t - t_{ini}) & \text{if } t_{ini} \leq t < t_{ini} + \Delta t_{add} \\ 1 & \text{if } t_{ini} + \Delta t_{add} \leq t < TS \end{cases} \quad (5.3)$$

where  $y(t)$  is the fraction of the total addition that is completed at time  $t$  and  $\Delta t_{add}$  is the time increment corresponding to the dosage duration (min).

Therefore, the proposed dosage protocol consists of an initial release  $y_0$  (kick-off) and a constant inflow  $m=f(y_0, \Delta t_{add})$  during the time interval  $[t_{ini}, t_{ini}+\Delta t_{add})$  and constrained within the treatment span  $TS$ . Figure 5.3 illustrates this dosing procedure and its governing factors.

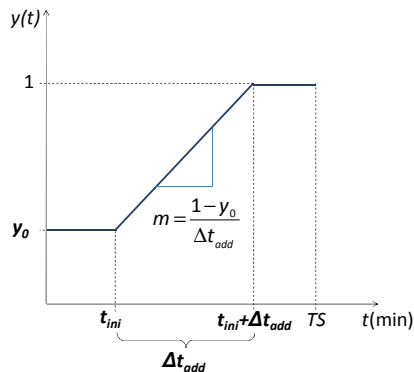


Figure 5.3. Definition of the addition protocol. The three independent parameters ( $y_0$ ,  $t_{ini}$ ,  $\Delta t_{add}$ ) are highlighted.

### 5.3.2. Dosage time interval

The extent of the dosage  $\Delta t_{add}$ , as well as the duration of the entire treatment  $TS$ , are next fixed in order to reduce the space of alternatives. Their values were decided according to the results of the preliminary assays and the additional results given by Figure 5.4 and it illustrates how adding the whole load at the start ( $y_0=1$ ) results less efficient than dosing it continuously. The response obtained from  $y_0=0$  is slower ( $dC/dt$ ), but the progress lasts for longer and further degradation is attained. Regarding TOC reduction, this means that the same load of hydrogen peroxide is used more efficiently when  $y_0=0$ . Namely, part of the load is spent in vain if  $y_0=1$ . Actually, competitive hydroxyl reactions have been indicated as the likely cause of such behavior (Pignatello et al., 2006; Zazo et al., 2009).

Conversely, TOC reduction is slightly affected by the extent of the dosage and no significant difference is found between 60 and 120 minutes assays. Accordingly, the values  $\Delta t_{add}=60$  min and  $TS=120$  min were set on a practical basis. Finally, it is worth noting that Figure 5.5 also confirms the fact that, despite the ways in which hydrogen peroxide is supplied and consumed, its disappearance from the system clearly indicates that no further progress can be expected.

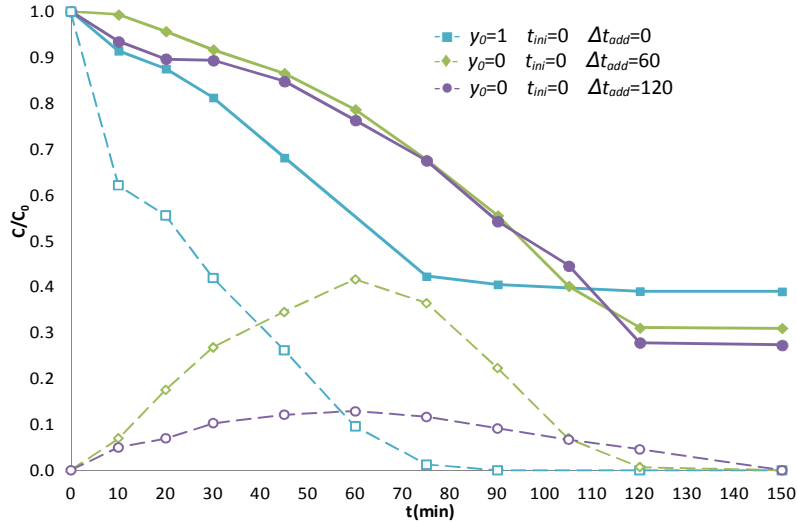


Figure 5.4. Comparison of the effect of different dosage span values:  $\Delta t_{add}$ , and kick-off fractions  $y_0$ . Solid lines denote TOC concentrations ( $\blacksquare, \blacklozenge, \bullet$ ) while dashed lines indicates  $H_2O_2$  concentrations ( $\square, \diamond, \circ$ ).  $C_{eq,\infty}^{H_2O_2} = 500 \text{ mg L}^{-1}$ ;  $C_0^{Fe(II)} = 10 \text{ mg L}^{-1}$ ;  $C_0^{coffee} = 300 \text{ mg L}^{-1}$ .

### 5.3.3. Performance assessment

A quantitative performance index is required (objective function) in order to rank the assays and discriminate the best outcome. This is quite difficult in absolute terms (i.e. economic, environmental, etc.). The achievement of the maximum conversion at the fastest rate ( $\xi^{\max}$  and  $k$ , respectively; Eq. 5.4) was addressed by Pérez-Moya et al. (2011), who suggested a practical multi-objective approach.

$$\frac{dC^{TOC}}{dt} = -k(C_{\infty}^{TOC} - C^{TOC}) \rightarrow \xi = \xi^{\max} e^{-kt} \quad \text{being} \quad \xi^{\max} = 1 - \frac{C_{\infty}^{TOC}}{C_0^{TOC}} \quad (5.4)$$

However, parameters such as  $\xi^{\max}$  and  $k$  are measures of a trend, and are thus obtained as a result of a model and the fitting of this model to the experimental data.

Hence,  $\xi^{\max}$  is not directly measured (neither  $k$ ), but inferred as the extrapolation of a pattern to infinity. This is feasible even with a very much simplified trend model (Eq. 5.6), but it is impracticable without it. A kinetic model of the reactions under variable dosage needs to contemplate equation 5.3, but also the “loss” of hydrogen peroxide, for which a single rate parameter is clearly insufficient. This hints again that further detailed modeling is still required.

On the other hand, the performance of the system may be estimated by a direct outcome attained at a certain time. This option is reasonable for data-based modeling, and measuring the contaminant (or TOC) concentration after a given period has been common practice in the AOP literature.

This research takes the outcome  $\xi$  after the fixed treatment span  $TS$  as the performance indicator. It is also assumed that this is a measure of the maximum conversion  $\xi^{\max}$  attained at infinity, namely:

$$C_{\infty}^{TOC}(\infty) \approx C^{TOC}(TS) \quad (5.5)$$

This seems a reasonable assumption, since hydrogen peroxide confirmed to have been used up in all the cases. Furthermore, steadiness is also corroborated by the fact that the difference between the last consecutive values of caffeine and TOC concentration was below 5% for all the assays.

### 5.3.4. Design of experiments

Once the system and its performance are finally characterized by two factors,

$$\xi^{\max} = f(y_0, t_{ini}) \quad (5.6)$$

a factorial experimental design ( $2^2$ ) was arranged to quantitatively characterize the effect of hydrogen peroxide dosage on the performance of the treatment under the assumptions up to this point stated.

Two levels (low and high) were considered for  $t_{ini}$  and  $y_0$ , which were varied in the ranges 0-30 min and 10-30 %, respectively. Three central points for statistical validity and star points at  $\pm\sqrt{2}$  were also taken into account. The resulting experimental design is shown in Table 5.1.

All of the experiments were replicated for statistical validity. Fe(II) and hydrogen peroxide doses of  $10 \text{ mg L}^{-1}$  and  $500 \text{ mg L}^{-1}$ , respectively, were set as constant for the design of experiments, which correspond to a 50:1 weight ratio.

$$\frac{C_{eq,\infty}^{H_2O_2}}{C_0^{Fe(II)}} = 50 \quad (5.7)$$

Table 5.1. Design of experiment variables levels. The resulting dosing slope is also included.

Codified values	Variables levels		$m = (1 - y_0) / \Delta t_{add}$ ( $\text{min}^{-1}$ )
	$t_{ini}$ (min)	$y_0$ (%)	
1	30.0	30.0	1.167
-1	0.0	10.0	1.500

## 5.4. Results and Discussion

The summary of the results obtained from the complete set of assays performed is given in Table 5.2, regarding the performance attained. Assay R corresponds to the reference experiment (no dosage).

Figure 5.5 shows the evolution of TOC and caffeine concentration for the central experimental conditions ( $y_0=20\%$ ;  $t_{ini}=15 \text{ min}$ ). The average values for the

three assays (E, F, G) repeated twice are represented along with the standard deviation in the error bars. These particular conditions attain total caffeine degradation after 45 minutes and reduce TOC by  $(70.8 \pm 3.5) \%$  within 7S. This performance is comparable to that reported by Tokumura et al. (2006 and 2008), who use higher loads of iron and hydrogen peroxide. Moreover, it is higher than that of the reference assay R obtained with the addition of the entire hydrogen peroxide load at once.

Table 5.2. List of assays carried out: reference (R); design (A to K) and additional (L to N).

	Codified values		Actual values		Results	
	$t_{ini}$	$y_0$	$t_{ini}$ (min)	$y_0$ (%)	$\xi^{max}$	StDev
R	-1	8	0.0	100.0	0.592	0.004
A	-1	-1	0.0	10.0	0.702	0.017
B	1	-1	30.0	10.0	0.650	0.005
C	-1	1	0.0	30.0	0.711	0.018
D	1	1	30.0	30.0	0.720	0.003
E	0	0	15.0	20.0	0.705	0.050
F	0	0	15.0	20.0	0.697	0.037
G	0	0	15.0	20.0	0.721	0.019
H	-1	0	0.0	20.0	0.692	0.059
I	1.414	0	36.2	20.0	0.740	0.035
J	0	-1.414	15.0	5.9	0.674	0.043
K	0	1.414	15.0	34.1	0.715	0.058
L	-1	2	0	0	0.689	0.001
M	-1	3	0	50	0.703	-
N	-1	5	0	70	0.726	0.079

In order to evaluate the influence of investigated factors on  $\xi^{max}$ , a statistical analysis was performed by using a commercial statistics software and results demonstrate that  $y_0$  have a significant and positive effect on response (higher initial percentages lead to higher values of  $\xi^{max}$ ), followed by the interaction between both factors ( $t_{ini} \cdot y_0$ ).

A similar analysis to identify the factors influencing the time needed to totally degrade caffeine proves that this response mostly depends on initial dosing time ( $t_{ini}$ ): the earlier the dosing is started, the faster caffeine is degraded. These facts will be demonstrated and discussed ahead.

In order to help the results discussion from this point on, experiments are named in the figures according to the following nomenclature: "Experiment-code- $y_0$ - $t_{ini}$ ".

Table 5.2 shows the performance improvements ( $\xi^{max}$ ) achieved by all dosage assays. This behavior can be explained because dosage reduces hydroxyl radical concentration during the first stages of the process, minimizes competitive scavenging reactions, and consequently permits a better use of hydroxyl radicals formed along the reaction time (Zazo et al., 2009).

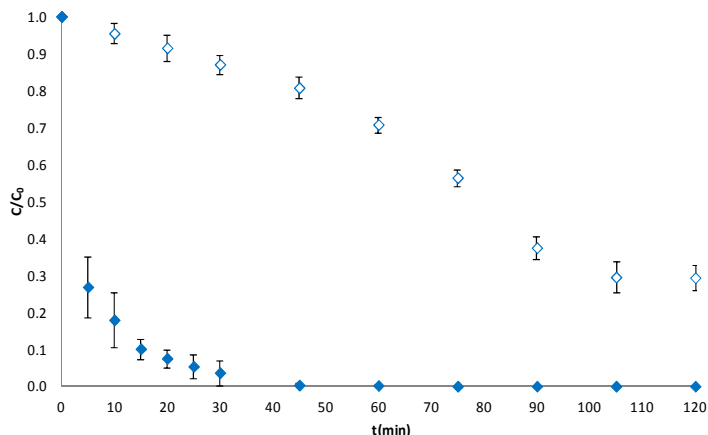


Figure 5.5. TOC and caffeine concentration behavior for the central experiment of the design:  $y_0=20\%$ ;  $t_{ini}=15$  min;  $C_0^{Fe(II)}=10$  mg L<sup>-1</sup>,  $C_{eq,\infty}^{H_2O_2}=500$  mg L<sup>-1</sup>;  $C_0^{coffee}=300$  mg L<sup>-1</sup>. ( $\diamond$ =TOC concentration;  $\blacklozenge$ =caffeine concentration).

Regarding the assays whose dosage starts at  $t_{ini}=15$  min (J, E, F, G, K) TOC reduction is clearly higher than the reference experiment (R). Furthermore, the higher  $y_0$ , the faster caffeine remediation and higher TOC reduction are achieved. In fact, mineralization around 70% is possible instead of 60% observed for the assay R; in particular, for  $y_0=34.1\%$  final mineralization ( $\xi^{max}$ ) increases by 18%.

Assays A and B in Table 5.2 allow to discuss the influence of  $t_{ini}$  for a fixed  $y_0$  value (10%). For this low kick-off (few reagent amount) the highest  $\xi^{max}$  value is achieved when dosage starts earlier ( $t_{ini}=0$  min). Moreover, caffeine is also remediated faster in the A assay.

The interaction between both factors ( $t_{ini} \cdot y_0$ ) is shown in Figure 5.6, as the statistical analysis performed has already revealed. Both factors are clearly related, assays using low  $y_0$  requires also low  $t_{ini}$  in order to obtain high  $\xi^{max}$ . In contrast, for higher kick-off, high  $y_0$ , a better performance is achieved with higher  $t_{ini}$ . However, it is interesting to notice that the influence of  $t_{ini}$  diminishes when higher  $y_0$  is dosed. According to caffeine remediation,  $y_0$  is the most influential factor. Faster performance is obtained for higher kick-off values, specifically, caffeine is totally degraded in 25 minutes when  $y_0=30\%$ .



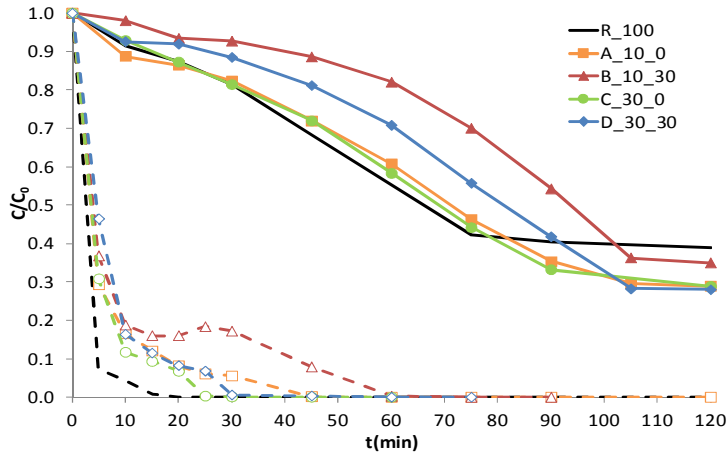


Figure 5.6. TOC and caffeine concentration behavior for different dosage protocols (dashed lines = caffeine concentration).  $C_0^{Fe(II)} = 10 \text{ mg L}^{-1}$ ,  $C_{eq,\infty}^{H_2O_2} = 500 \text{ mg L}^{-1}$ ;

$$C_0^{Coffee} = 300 \text{ mg L}^{-1}$$

Table 5.2 confirms the importance of the hydrogen peroxide dosage, all the assays obtain higher maximum conversion than the reference assay. An improvement of 15 percentage points of  $\xi^{\max}$  is achieved with appropriate dosage protocol, equivalent to 25% global improvement over the reference assay. Thus, the use of the reagent is more efficient and the operation may significantly reduce its cost.

Regarding caffeine, its total remediation is assured during the first minutes of the 120-minute reaction span studied when  $y_0$  is 20% or higher. In contrast, a lower kick off,  $y_0$ , i.e.  $y_0=10\%$  revealed not to be enough to obtain a fast caffeine remediation, requiring reaction times around 45-60 minutes.

Additional experiments were performed in order to evaluate the situation outside the boundaries of the design of experiment. Figure 5.7 shows these results and it is clear that TOC concentration reduction rate is slower when  $y_0=0\%$ , but even in this situation higher mineralization is achieved when comparing with the reference assay. In contrast, a higher kick-off than the ones studied, 30 %, has not revealed better performance related to obtaining high maximum conversion ( $\xi^{\max}$ ).

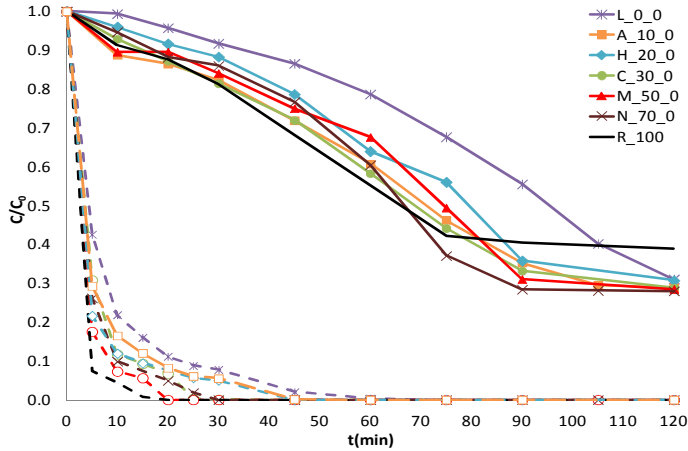


Figure 5.7. TOC and caffeine concentration behavior for different  $y_0$  at  $t_{ini}=0$  min. (dashed lines=caffeine concentration).  $C_0^{Fe(II)}=10 \text{ mg L}^{-1}$ ;  $C_{eq,\infty}^{H_2O_2}=500 \text{ mg L}^{-1}$ ;  $C_0^{Coffee}=300 \text{ mg L}^{-1}$ .

Caffeine is totally degraded in all of the cases, but this goal will be achieved earlier while higher  $y_0$  is provided.

## 5.5. Conclusions

A hybrid discrete-continuous dosage scheme was proposed using two factors ( $y_0$  and  $t_{ini}$ ), which was used in an experimental design ( $2^2$ ) that allowed to obtain the data for quantitatively assessing the influence of Hydrogen Peroxide Dosage on the performance of the photo-Fenton treatment.

With the aim to evaluate the influence of the variables involved in the dosage protocol, the degradation of 12 L samples of commercial coffee ( $300 \text{ mg L}^{-1}$ , approximately  $17 \text{ mg L}^{-1}$  of caffeine) via photo-Fenton treatment ( $C_{eq,\infty}^{H_2O_2}=500 \text{ mg L}^{-1}$ ,  $C_0^{Fe(II)}=10 \text{ mg L}^{-1}$ ) has been addressed. The study has been carried out using iron loads within the legal limit ( $10 \text{ mg L}^{-1}$ ), which is also an advantage in environmental and economic terms.

The quantitative results showed maximum TOC conversions ( $\zeta^{max}$ ) in the range 60-75% obtained with the same reactant loads but different dosage schemes. The best assay increased treatment performance by 15 percentage points (equivalent to 25% global improvement over the reference assay: the addition of the load at once ( $y_0=1$ )). The operating conditions of the assay found were  $y_0=20\%$  and  $t_{ini}=36.1$  min. Additionally, the DOE has also allowed to provide evidence of the cross-effect between the factors of the dosage protocol.

Regarding caffeine degradation, the HPLC monitoring revealed the complete removal of the caffeine in all the cases, far before the end of the treatment span studied. Moreover, caffeine was degraded more efficiently than previously reported (Tokumura et al., 2006) by using lesser amounts of iron and hydrogen

peroxide. Qualitative conclusions may be also withdrawn from the degradation time profiles of the caffeine, specially the trade-off between the size of the kick-off ( $y_0$ ) and the starting of the continuous dosage ( $t_{ini}$ ).

This chapter demonstrates the importance of the hydrogen peroxide dosage and steps into the opportunity of dosage automation and on-line optimization. In the next chapters, the dosage scheme is tested to degrade and mineralize other emerging contaminants in order to confirm its effect on the treatment performance.

## 5.6. References

Burbano, A.A.; Dionysiou, D.D.; Suidan, M.T. 2008. Effect of oxidant-to-substrate ratios on the degradation of MTBE with Fenton reagent. *Water Res.* 42, 3225.

Chu, W.; Chan, K.H.; Kwan, C.Y.; Choi, K.Y. 2007. Degradation of atrazine by modified stepwise-Fenton's processes. *Chemosphere* 67, 755.

DOGC núm. 3894, DECRET 130/2003, de 13/05/2003, (29.5.2003). (URL: <http://www.gencat.cat/diari/3894/03127147.htm>, accessed 10/08/2011)

Gómez, M.J.; Martínez Bueno, M.J.; Lacorte, S.; Fernández-Alba, A.R.; Agüera, A. 2007. Pilot survey monitoring pharmaceuticals and related compounds in a sewage treatment plant located on the Mediterranean coast. *Chemosphere* 66, 993.

Gulkaya, I.; Surucu, A.; Dilek, F. 2006. Importance of  $H_2O_2/Fe^{+2}$  ratio in Fenton's treatment of a carpet dyeing wastewater. *J. Hazard. Mater. B.* 136, 763.

Herney Ramirez, J.; Costa, C.A.; Madeira, L.M. 2005. Experimental design to optimize the degradation of the synthetic dye Orange II using Fenton's reagent. *Catal. Today.* 107-108, 68.

Ince, N.H. 1999. "Critical" effect of hydrogen peroxide in photochemical dye degradation. *Water Res.* 33(4),1080.

Klamerth, N.; Rizzo, L.; Malato, S.; Maldonado, M.I.; Agüera, A.; Fernández-Alba, A.R. 2010. Degradation of emerging contaminants at low concentrations in MWTPs effluents with mild solar photo-Fenton and  $TiO_2$ . *Water Res.* 44(2), 545.

Monteagudo, J.M.; Durán, A.; San Martín, I.; Aguirre, M. 2009. Effect of continuous addition of  $H_2O_2$  and air injection on ferrioxalate-assisted solar photo-Fenton degradation of Orange II. *Appl. Catal. B.* 89, 510.

Pérez-Moya, M.; Graells, M.; del Valle, L.J.; Centelles, E.; Mansilla, H.D. 2007. Fenton and photo-Fenton degradation of 2-chlorophenol: Multivariate analysis and toxicity monitoring. *Catal. Today.* 124(3-4), 163.

Pérez-Moya, M.; Graells, M.; Mansilla, H.D. 2011. A Practical Parametrical Characterization of the Fenton and the Photo-Fenton Sulfamethazine Treatment using Semi-Empirical Modeling. *J. Chem. Technol. Biot.* 86, 826.

Pignatello, J.J.; Oliveros, E.; MacKay, A. 2006. Advanced Oxidation Processes for Organic Contaminant Destruction Based on the Fenton Reaction and Related Chemistry. *Critical Reviews in Environ. Sci. Technol.* 36(1), 1.

Prieto-Rodríguez, L.; Oller, I.; Zapata, A.; Agüera, A.; Malato, S. 2011. Hydrogen peroxide automatic dosing based on dissolved oxygen concentration during solar photo-Fenton. *Catal. Today.* 161, 247.

Rodríguez-Gil, J.; Catalá, M.; González, S.; Romo, R.; Valcárcel, Y.; Segura, Y.; Molina, R.; Melero, J.; Martínez, F. 2010. Heterogeneous photo-Fenton treatment for the reduction of pharmaceutical contamination in Madrid rivers and ecotoxicological evaluation by a miniaturized fern spores bioassay. *Chemosphere* 80, 381.

Rossi, I.; Nogueira, R.F.P. 2007. Degradation of tetracycline by photo-Fenton process—Solar irradiation and matrix effects. *J. Photoch. Photob. A.* 187, 33.

Tokumura, M. ; Ohta, A.; Znad, H.; Kawase, Y. 2006. UV light assisted decolorization of dark brown colored coffee effluent by photo-Fenton reaction. *Water Res.* 40, 3775.

Tokumura, M.; Tawfeek, H.; Kawase, Y. 2008. Decolorization of dark brown colored coffee effluent by solar photo-Fenton reaction: Effect of solar light dose on decolorization kinetics. *Water Res.* 42, 4665.

Zazo, J.A.; Casas, J.A.; Mohedano, A.F.; Rodríguez, J.J. 2009. Semicontinuous Fenton oxidation of phenol in aqueous solution. A kinetic study. *Water Res.* 43, 4063.

## **Chapter VI**

### **Enhanced photo-Fenton Process for Tetracycline Degradation using Efficient Hydrogen Peroxide Dosage Protocol**

The dosage protocol proposed in chapter V is now applied to the degradation of tetracycline, an emerging contaminant, in water solutions. The application of the systematic hydrogen peroxide dosage protocol enhances photo-Fenton process performance, reaching to total degradation and mineralization of the samples.



## 6.1. Introduction

As it was already mentioned in previous sections, the presence of antibiotics in the environment is mainly due to their discharge through excretion whether or not metabolized. As conventional treatments cannot be expected to process antibiotics, they come to appear as contaminants in surface water, groundwater and even in drinking water, developing antibiotic-resistant pathogens, among several other environmental issues (Homem and Santos, 2011; Jiao et al., 2008; Rossi and Nogueira, 2007).

In particular, tetracyclines (TCs) are broad-spectrum antibiotics with activity against gram-positive and gram-negative bacteria. According to Wang et al. (2011) TCs have been detected at concentrations ranging 0.07-1.34  $\mu\text{g L}^{-1}$  in surface water samples. According to Gu and Karthikeyan (2005), a "survey of wastewater treatment plants in Wisconsin, USA, revealed that the compound tetracycline (TC) was the most frequently detected antibiotic, being present in 80% of the wastewater influent and effluent samples." Thus, TC has a significant and common occurrence that deserves special attention.

TC degradation by means of AOPs has also been investigated in the literature. UV has shown to be effective in degrading this contaminant and the presence of  $\text{H}_2\text{O}_2$  has revealed to increase TC degradation and mineralization rates (López-Peñalver, 2010; Kammer et al., 2011; Gómez-Pacheco et al., 2012; Kim and Tanaka, 2009; Yuan et al., 2011). Heterogeneous photocatalysis with  $\text{TiO}_2$  has also been studied, and a lower performance with respect to UV and UV/ $\text{H}_2\text{O}_2$  processes has been reported (Reyes et al., 2006; Maroga Mboula et al., 2012). Electrochemical processes have also shown to be effective for TC degradation (Wu et al., 2012; Jeong et al., 2010). Ozonation (Wang et al., 2011; Wang et al., 2012) has also been examined, as well as the combination of AOPs and conventional treatments (Wang et al., 2012; Yahiaoui et al., 2011).

Surprisingly enough, TC degradation via photo-Fenton process has received scarce attention, although TC is among the components of some wastewaters whose photo-Fenton treatment has been investigated (Rodríguez-Gil et al., 2010). According to Jeong et al. (2010), the research by Rossi and Nogueira (2007), who reported total remediation of 24  $\text{mg L}^{-1}$  TC solutions, is the only work addressing TC degradation using the photo-Fenton process.

The previous chapter proposed a practical parameterization of hydrogen peroxide dosage which led to the improvement of the degradation of coffee solutions by photo-Fenton process. Ortega-Gómez et al. (2012) and Carrá et al. (2012) have used dissolved oxygen monitoring to set up proportional & integral (PI) control of the hydrogen peroxide dosage and improve process performance; this has been applied to the solar photo-Fenton degradation of paracetamol. Regarding the degradation of antibiotics, hydrogen peroxide dosage has been investigated only for Fenton treatments (Ben et al., 2009), and addressing a mixture of sulfonamides and tiamulin fumarate.

To the best of the author's knowledge, no study has been reported on the influence of hydrogen peroxide dosage on the oxidation of TC antibiotic in water solutions via photo-Fenton treatment. Thus, this chapter addresses this issue applying the systematic dosage protocol presented in Chapter V to set a design of experiments and characterize the influence of hydrogen peroxide dosage on the treatment performance. Given a fixed amount of reactants, two objectives will be simultaneously considered in regard to the efficient use of resources: the increase of mineralization and the reduction of processing time. Hence, a set of dosing schemes will be assayed and assessed, and conditions improving process performance will be identified in a practical way.

## 6.2. Results and Discussion

A set of preliminary assays were performed in order to identify the reagent doses to be used and the effect of each one of them on the degradation and mineralization of the contaminant under study. The experiments were performed in the reactor R1 (Table 3.1) with the lamp TQ718 (Figure 3.1a) set at a 30% of its maximum electrical power.

### 6.2.1. Preliminary assays

#### 6.2.1.1. *Reagent doses*

As mentioned in the introduction, the concentrations investigated in previous works concerning TC degradation by means of photolysis and photocatalysis processes ranged between 10 and 300 mg L<sup>-1</sup> (Jiao et al., 2008; Reyes et al., 2006; Gómez-Pacheco et al., 2012; Maroga Mboula et al., 2012), while Rossi et al. (2007) proved that photo-Fenton process can be successfully applied for the degradation of 24 mg L<sup>-1</sup> TC solutions with hydrogen peroxide and ferrous iron initial concentrations ranging from 35 to 680 mg L<sup>-1</sup> and 5.6 and 11 mg L<sup>-1</sup>, respectively. According to this information and taking into account TOC analyzer sensibility, TC concentration was fixed at 40 mg L<sup>-1</sup>, which corresponds to a TOC concentration of 23 mg L<sup>-1</sup> and requires a stoichiometric H<sub>2</sub>O<sub>2</sub> concentration of 150 mg L<sup>-1</sup>.

A 2<sup>2</sup> factorial design of experiments (DOE) with star points was performed to decide Fenton reagent doses. It was important to identify a dose which permits a compromise between degradation and dosage interest. For that aim, Fe<sup>2+</sup> dose was centered at 5 mg L<sup>-1</sup> (10 mg L<sup>-1</sup> is the maximum legal value in effluents in Spanish legislation (DOGC, 2003)), having minimum and maximum values 2 and 8 mg L<sup>-1</sup>, respectively.

Regarding H<sub>2</sub>O<sub>2</sub> load, this ranged between 9% and 90% of the stoichiometric amount given by the TC oxidation just by means of hydrogen peroxide, which is taken as a reference. Sub-stoichiometric hydrogen peroxide loads can be used to ease the identification intermediate species at the early stages of the reaction (Munoz et al., 2012); furthermore, sub-stoichiometric loads can be enough for total TC oxidation since hydrogen peroxide is not the only source of oxygen



(Pignatello et al., 2006; Frontistis et al., 2011). Minimum and maximum values of the  $\text{H}_2\text{O}_2$  load were set at 14.3 and 128.7  $\text{mg L}^{-1}$ , having a center value of 71.5  $\text{mg L}^{-1}$ , which corresponds to a 48% of the stoichiometric amount. Figure 6.2a presents DOE results considering  $\xi^{TS}$  as the system response.

Low iron loads (2  $\text{mg L}^{-1}$ ) provide degradation rates around 55% despite  $\text{H}_2\text{O}_2$  dose (red line). On the contrary, higher iron values (5 or 8  $\text{mg L}^{-1}$ ) noticeably increase response values as  $\text{H}_2\text{O}_2$  doses increase. However, 5  $\text{mg L}^{-1}$  iron loads lead to higher TOC degradation than 8  $\text{mg L}^{-1}$  for equal  $\text{H}_2\text{O}_2$  amounts (lines blue and green). Thus, 5  $\text{mg L}^{-1}$  iron loads offer more efficient use of the hydroxyl radicals generated in the system. According to this, iron dose was set at 5  $\text{mg L}^{-1}$ .

Finally, a hydrogen peroxide dose was set at 71.5  $\text{mg L}^{-1}$  because higher values, when combined with 5  $\text{mg L}^{-1}$  iron doses provide too fast TOC reduction, which complicates the evaluation of the effect of reagent dosage on degradation. In brief, from here on, the following concentrations are used:

- Tetracycline initial concentration = 40  $\text{mg L}^{-1}$
- Hydrogen peroxide equivalent concentration = 71.5  $\text{mg L}^{-1}$
- Iron (II) initial concentration = 5  $\text{mg L}^{-1}$

#### **6.2.1.2. Blank assays**

A set of blank assays was initially performed in order to evaluate the influence of each separate reagent on TOC and TC degradation, which are next presented. Figure 6.2b shows the evolution of TOC,  $\text{H}_2\text{O}_2$  and TC concentrations for UV treatment, UV/ $\text{H}_2\text{O}_2$ , Fenton and photo-Fenton, involving the previously stated reagent doses when applied.

Mineralization by means of UV treatment only reaches 35%, UV/ $\text{H}_2\text{O}_2$  and Fenton allow almost 60%, and the photo-Fenton process may reach 77%. TC is completely degraded in all the cases where  $\text{H}_2\text{O}_2$  is present, being the degradation faster when the ferrous salt is added. On the contrary, only a 40% of TC is degraded by solely using UV irradiation (90 min treatment). Both TC and TOC reduction rates obtained without using  $\text{H}_2\text{O}_2$  are comparatively poor. However, it is important to bear in mind that these rates indicate that, to a non-negligible extent,  $\text{H}_2\text{O}_2$  may not be the sole responsible of the complete oxidation of organic matter.

Once established that the photo-Fenton process is capable of degrading TC and mineralize organic matter,  $\text{H}_2\text{O}_2$  dosage was investigated in order to determine to which extent process efficiency can be improved given the same reagent loads.

## 6.2.2. DOE for dosage characterization

A design of experiments considering the dosage parameters  $y_0$  and  $t_{ini}$  (Eq.5.3) and the response  $\zeta^{TS}$  (Eq. 5.4) was applied; the earliest sample time at which TC is not detected ( $t^{TC}$ ) was also included as a response.

Rigorous optimization is not intended and the study only seeks to illustrate the determination of improved operational conditions. Hence, factorial design is used only as a sensible method for systematically exploring the region of interest and no response surface is fit in order to avoid misleading conclusions (Frontistis et al., 2011). Furthermore, the characterization of the dual response is later presented as a function of a two conflicting objectives (Fig. 6.2).

Table 6.1 lists the levels and results of the planned assays according to a  $2^2$  DOE with start points and three center points for statistical validity; minimum and maximum factors were set at 10 and 30% for  $y_0$  and 0 and 30 minutes for  $t_{ini}$ . Reference experiments were included in the study.

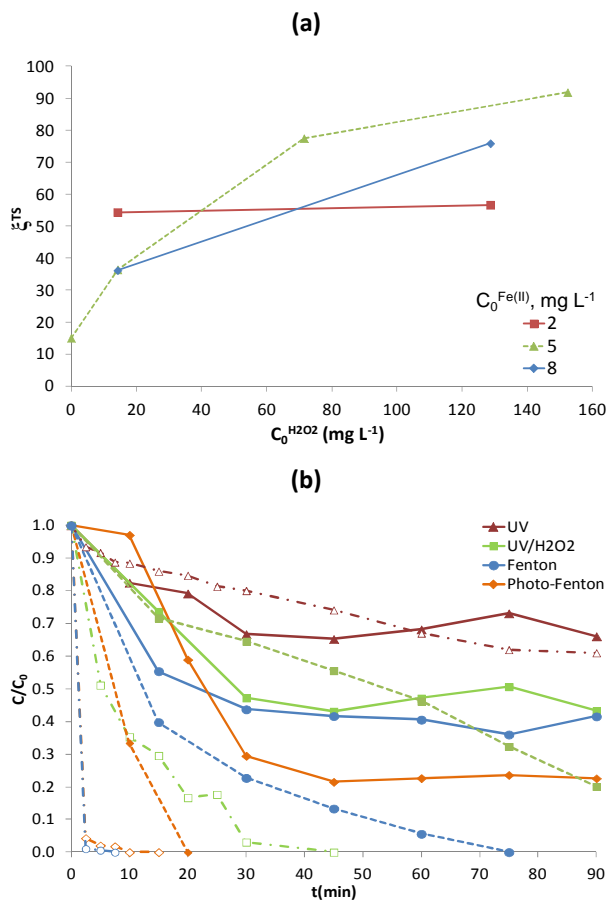


Figure 6.1. **(a)**  $\zeta^{TS}$  obtained for different reagent doses according to the DOE. **(b)** TOC (continuous lines,  $\blacktriangle, \blacksquare, \blacklozenge$ ), TC (--- $\Delta, \square, \diamond$ ---) and H<sub>2</sub>O<sub>2</sub> (dashed lines,  $\blacktriangle, \blacksquare, \blacklozenge$ ) normalized concentration profiles for blank assays.

Table 6.1. Average results of the planned assays: earliest sample time at which TC is not detected ( $t^{TC}$ ) and TC conversion at TS ( $\xi^{TC}$ )

Experiment code	$y_0$ (%)	$t_{ini}$ (min)	$t^{TC}$ (min)	$\xi^{TC}$ (%)
A_10_0	10.0	0.0	5.0	91
B_10_30	10.0	30.0	45.0	77
C_30_0	30.0	0.0	10.0	98
D_30_30	30.0	30.0	7.5	81
Central_20_15	20.0	15.0	10.0	98
H_20_0	20.0	0.0	7.5	83
I_20_36.2	20.0	36.2	10.0	83
J_6_15	6.0	15.0	30.0	80
K_34.1_15	31.4	15.0	5.0	88
L_0_0	0.0	0.0	15.0	91
R_100_0	100	0.0	10.0	77

Figure 6.3a shows the results of the central experiment of the design, which was repeated six times. Average values are presented along with the corresponding standard deviations. Total remediation of the sample is shown to be achieved with these conditions. Regarding TC degradation, it was achieved within 10 minutes treatment. The hydrogen peroxide profile shown in Fig. 5.3a (Central\_20\_15) illustrates that, the concentration drops after the kick off, but it is always maintained below much reduced levels ( $15 \text{ mg L}^{-1}$ ). In the rest of the experiments performed (data not shown) the hydrogen peroxide profiles are below  $13 \text{ mg L}^{-1}$ . These observations confirm that low hydrogen peroxide amounts are sufficient to provide good or even enhanced process response, as well as lower operating costs. Moreover, convenient dosage also decreases treatment time, as shown in Fig. 5.3b and the summary in Fig. 5.4, which similarly affects total process costs.

From this point on, experiments are named according to the following nomenclature: "Experiment-code $_{y_0}t_{ini}$ ". Assay R corresponds to the reference experiment (no dosage protocol).

Figure 6.3b compares the evolution of TOC and TC concentrations for the central assays ( $y_0=20\%$ ;  $t_{ini}=15 \text{ min}$ ), an assay without kick-off (experiment code L,  $y_0=0\%$ ;  $t_{ini}=0 \text{ min}$ ), and the reference assay. The performance obtained is analogous to that obtained by previous studies using caffeine (Yamal-Turabay et al., 2012).

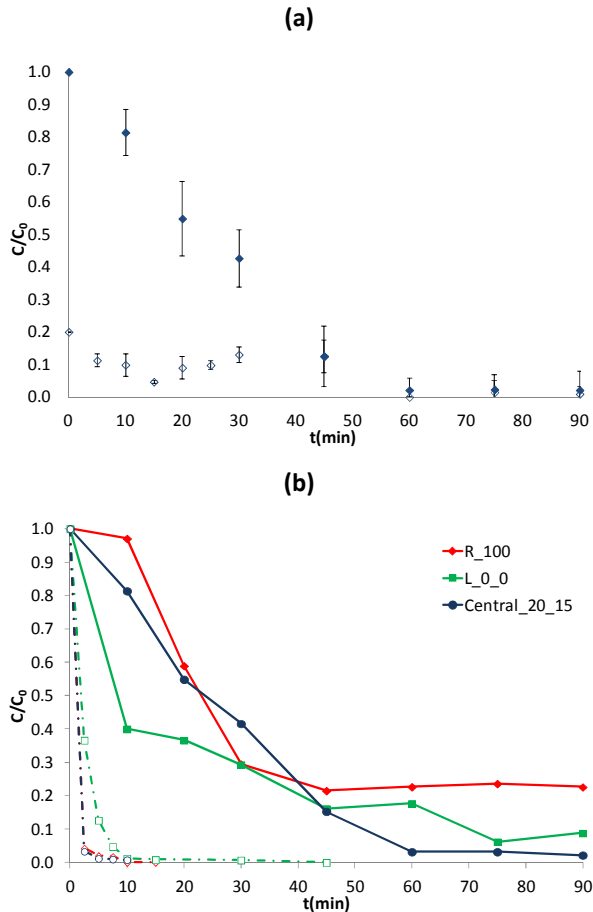


Figure 6.2. **(a)** TOC ( $\blacklozenge$ ) and H<sub>2</sub>O<sub>2</sub> ( $\diamond$ ) normalized concentration profiles for central experiment of the design. **(b)** TOC (solid lines) and TC (dashed lines) normalized concentration profiles for different dosage protocols.

Only 77% mineralization is achieved without dosage. However, the proposed scheme, when conveniently tuned, shows that it is possible to reach up to almost total mineralization (98%), which corresponds to 27 percent points of improvement. According to Prato-Garcia and Buitrón (2012), this may be explained because when the entire reagent dose is added at once, the excess of H<sub>2</sub>O<sub>2</sub> promotes secondary reactions that scavenge hydroxyl radicals and “waste” them. Dosage allows reducing this excess and having a more efficient dedication of hydroxyl radicals to degrading organic matter (Zazo et al., 2009; Gulkaya et al., 2006; Yamal-Turbay et al., 2012).

Regarding TC remediation, table 6.1 shows the earliest sample time ( $t^{TC}$ ) at which TC is not detected and total degradation is assumed. The slowest degradation is observed in experiments B and J, for which  $t^{TC}$  increases up to 45 and 30 minutes respectively, while for the rest of the assays  $t^{TC}$  is below 15 minutes. This behavior can be explained because of the combination of low initial

hydrogen peroxide doses ( $y_0$ ), which is rapidly exhausted and causes the process to stop, and the late dosage ( $t_{ini}$ ), which slows the process down; actually, better performance of experiment J compared to assay B obeys to sooner  $t_{ini}$  despite lower  $y_0$ .

Figure 6.4 shows the relation between conversion at TS,  $\xi^{TS}$ , and the time at which total degradation is assumed,  $t^{TC}$ . This confirms the opportunity to improve the treatment outcome by adjusting the dosage parameters. When the reagent is dosed proportionally without a kick-off (experiment L), an improvement of 18 percent points in TOC reduction is possible, which indicates the reduction of the effect of secondary reactions when  $H_2O_2$  is more efficiently used during the first stages of the process. Furthermore, the adjustment of both variables,  $y_0$  (kick off) and  $t_{ini}$ , allows achieving both objectives simultaneously: maximizing mineralization and minimizing time for degrading TC. That is the case of experiment C:  $y_0=30\%$  suffices to provide a good process response and continuous  $H_2O_2$  dosing from the beginning of the experiment ( $t_{ini}=0$  min) allows a hydroxyl radical concentration which permits a more efficient process (low right corner of the plot).

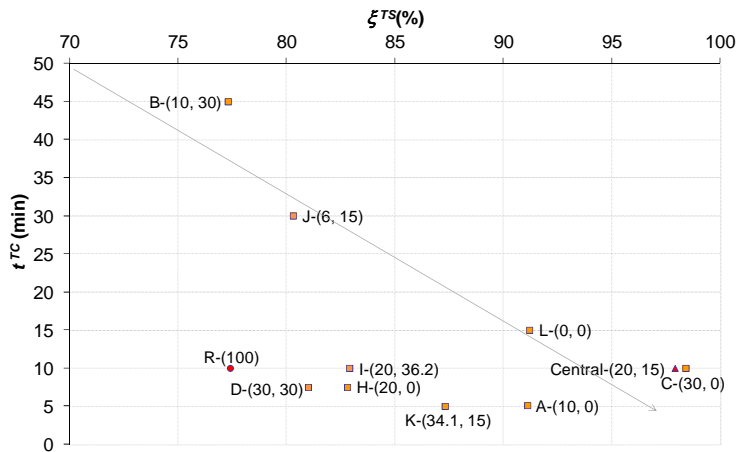


Figure 6.3. Relation between  $t^{TC}$  (to be minimized)  $\xi^{TS}$  (to be maximized)

Alternatively, the proposed treatment could be stopped earlier, before reaching the complete mineralization of the effluent, at a point in which the byproducts are not toxic, in order to reduce the cost of the treatment, as suggested by several authors (Ben et al., 2009; Yahiat et al., 2011). The present study has shown that dosage is able to achieve, given the appropriate tuning, the complete mineralization of the TC solutions, thus guaranteeing that no (toxic) byproducts are present in the effluent, also reducing the cost of the treatment.

Regarding the evident interaction between both factors  $y_0$  and  $t_{ini}$ , these results also indicate the higher significance of the latter. When continuous dosage starts soon, better performance is achieved despite  $y_0$ ; conversely, low  $y_0$  values may require starting dosage at earlier  $t_{ini}$  values. In order to confirm this

hypothesis, further data on the influence of low  $y_0$  values on TC degradation are given in Fig. 6.5. Compared to assay J ( $t_{ini} = 15$  min), the higher  $y_0$  value of new experiment P\_8\_15 (8%) produces no performance changes; however, the lower  $y_0$  value of new experiment Q\_4\_15 (4%) results in the exhaustion of hydrogen peroxide - and therefore of hydroxyl radicals - and the degradation is interrupted until more reagent is dosed after 15 minutes.

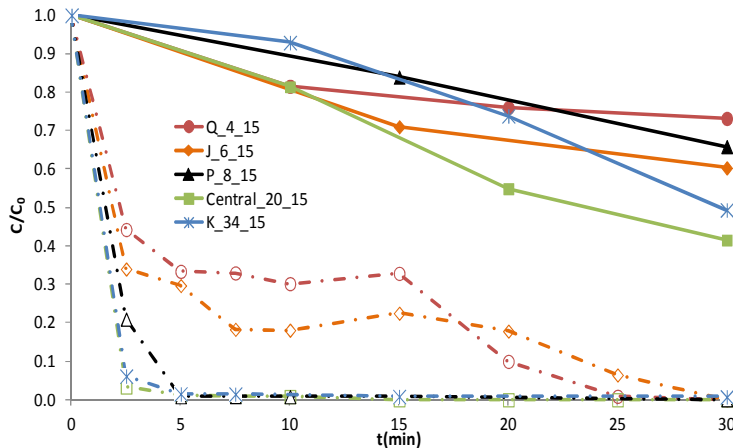


Figure 6.4. TOC (solid lines) and TC (dashed lines) normalized concentration profiles for different  $y_0$  when  $t_{ini}=15$  min.

### 6.3. Conclusions

The oxidation of TC antibiotic in water solutions by means of the photo-Fenton treatment has been investigated in this chapter. The treatment was applied to 12 L of  $40 \text{ mg L}^{-1}$  tetracycline samples with total reagent doses of  $71.5 \text{ mg L}^{-1}$  hydrogen peroxide (48% of stoichiometric dose) and  $5 \text{ mg L}^{-1} \text{ Fe}^{2+}$  (half the legal limit in wastewaters in Spain). These conditions achieved total TC remediation and to produce up to 77% solution mineralization within the reaction span studied.

The systematic parameterization of the dosage led to a DOE for determining the treatment outcome for a given set of assays. Hence, given this fixed  $\text{H}_2\text{O}_2$  load, treatment performance was shown to be able to improve total mineralization (up to 22.6 percent points) when dosage parameters were conveniently adjusted, which confirms the results presented in Chapter V.

The efficient use of hydrogen peroxide, via dosage, has revealed to significantly improve the performance of the treatment of water solutions containing TC by cutting the  $\text{H}_2\text{O}_2$  demand when secondary reactions of hydroxyl radicals scavenging are minimized. The  $\text{H}_2\text{O}_2$  demand can be reduced quite below the stoichiometric value, which suggests the importance of other oxygen sources in the photo-Fenton treatment.

The dosage protocol will be applied for the degradation of a different emerging contaminant in the next chapter, in order to confirm once again its effectiveness and flexibility to improve process performance.

#### 6.4. References

Ben, W.; Qiang, Z.; Pan, X.; Chen, M. 2009. Removal of veterinary antibiotics from sequencing batch reactor (SBR) pretreated swine wastewater by Fenton's reagent, *Water Res.* 43, 4392–4402

DOGC núm. 3894, DECRET 130/2003, de 13/05/2003, (29.5.2003). (URL: <http://www.gencat.cat/diari/3894/03127147.htm>, accessed 10/08/2011)

Frontistis, Z.; Xekoukoulotakis, N.P.; Hapeshi, E.; Venieri, D.; Fatta-Kassinos, D.; Mantzavinos, D. 2011. Fast degradation of estrogen hormones in environmental matrices by photo-Fenton oxidation under simulated solar radiation, *Chem. Eng. J.* 178, 175–182

Gómez-Pacheco, C.V.; Sánchez-Polo, M.; Rivera-Utrilla, J.; López-Peñalver, J.J. 2012. Tetracycline degradation in aqueous phase by ultraviolet radiation, *Chem. Eng. J.* 187, 89-95

Gu, C.; Karthikeyan, K.G. 2005. Interaction of tetracycline with aluminum and iron hydrous oxides, *Environ. Sci. Tech.*, 39:8, 2660–2667

Gulkaya, I.; Surucu, A.; Dilek, F. 2006. Importance of  $H_2O_2/Fe^{2+}$  ratio in Fenton's treatment of a carpet dyeing wastewater, *J. Hazard. Mater. B.* 136, 763-769.

Homem, V.; Santos, L. 2011. Degradation and removal of antibiotics from aqueous matrices. A review, *J. Environ. Manag.* 92, 2304-2347

Jeong, J.; Song, W.; Cooper, W.J.; Jung, J. 2010. Degradation of tetracycline antibiotics: Mechanisms and kinetic studies for advanced oxidation/reduction processes, *Chemosphere* 78, 533–540

Jiao, S.; Zheng, S.; Yin, D.; Wang, L.; Chen, L. 2008 Aqueous photolysis of tetracycline and toxicity of photolytic products to luminescent bacteria, *Chemosphere* 73, 377–382

Kim, I.; Tanaka, H. 2009. Photodegradation characteristics of PPCPs in water with UV treatment, *Environ. Int.* 35, 793–802

López-Peñalver, J.J.; Sánchez-Polo, M.; Gómez-Pacheco, C.V.; Rivera-Utrilla, J. 2010. Photodegradation of tetracyclines in aqueous solution by using UV and UV/ $H_2O_2$  oxidation processes, *J. Chem. Technol. Biotechnol.* DOI 10.1002/jctb.2435

Maroga Mboula, V.; Héquet, V.; Gru, Y.; Colin, R.; Andrès, Y. 2012. Assessment of the efficiency of photocatalysis on tetracycline biodegradation, *J. Hazard. Mater.* 209-210, 355-364

Munoz, M.; de Pedro, Z.M.; Casas, J.A.; Rodriguez, J.J. 2012. Triclosan breakdown by Fenton-like oxidation, *Chem. Eng. J.* 198-199, 275-281

Ortega-Gómez, E.; Moreno Úbeda, J.C.; Álvarez Hervás, J.D.; Casas López, J.L.; Santos-Juanes Jordá, L.; Sánchez Pérez, J.A. 2012. Automatic dosage of hydrogen peroxide in solar photo-Fenton plants: Development of a control strategy for efficiency enhancement, *J. Hazard. Mater.* 237–238, 223–230

Pignatello, J.J.; Oliveros, E.; MacKay, A. 2006. Advanced Oxidation Processes for Organic Contaminant Destruction Based on the Fenton Reaction and Related Chemistry, *Crit. Rev. Environ. Sci. Technol.* 36:1, 1-84

Prato-García, D.; Buitrón, G. 2012. Evaluation of three reagent dosing strategies in a photo-Fenton process for the decolorization of azo dye mixtures, *J. Hazard. Mat.* 217–218, 293–300

Reyes, C.; Fernández, J.; Freer, J.; Mondaca, M.A.; Zaror, C.; Malato, S.; Mansilla, H.D. 2006 Degradation and inactivation of tetracycline by TiO<sub>2</sub> photocatalysis, *J. Photochem. Photobiol. A.* 184, 141–146

Rodríguez-Gil, J.L.; Catalá, M.; González Alonso, S.; Romo Maroto, R.; Valcárcel, Y.; Segura, Y.; Molina, R.; Melero, J.A.; Martínez, F. 2010. Heterogeneous photo-Fenton treatment for the reduction of pharmaceutical contamination in Madrid rivers and ecotoxicological evaluation by a miniaturized fern spores bioassay, *Chemosphere* 80, 381–388

Rossi, I.; Nogueira, R.F.P. 2007. Degradation of tetracycline by photo-Fenton process—Solar irradiation and matrix effects, *J. Photoch. Photob. A.*, 187, 33-39.

Wang, P.; He, Y.L.; Huang, C.H. 2011. Reactions of tetracycline antibiotics with chlorine dioxide and free chlorine, *Water Res.* 45, 1838-1846

Wang, Y.; Zhang, H.; Chen, L.; Wang, S.; Zhang, D. 2012. Ozonation combined with ultrasound for the degradation of tetracycline in a rectangular air-lift reactor, *Sep. Purif. Tech.* 84, 138-146

Wang, Y.; Zhang, H.; Zhang, J.; Lu, C.; Huang, Q.; Wu, J.; Liu, F. 2011. Degradation of tetracycline in aqueous media by ozonation in an internal loop-lift reactor, *J. Hazard. Mater.* 192:1, 35-4

Wu, J.; Zhang, H.; Oturan, N.; Wang, Y.; Chen, L.; Oturan, M.A. 2012. Application of response surface methodology to the removal of the antibiotic tetracycline by electrochemical process using carbon-felt cathode and DSA (Ti/RuO<sub>2</sub>–IrO<sub>2</sub>) anode, *Chemosphere* 87:6, 614-620

Yahiaoui, I.; Aissani-Benissad, F.; Fourcade, F.; Amrane, A. 2013. Removal of tetracycline hydrochloride from water based on direct anodic oxidation (Pb/PbO<sub>2</sub> electrode) coupled to activated sludge culture, *Chem. Eng. J.* 221, 418-425



Yahiat, S.; Fourcade, F.; Brosillon, S.; Amrane, A. 2011. Removal of antibiotics by an integrated process coupling photocatalysis and biological treatment – Case of tetracycline and tylosin, *Int. Biodeter. Biodegr.* 65:7, 997-1003

Yamal-Turbay, E.; Graells, M.; Pérez-Moya, M. 2012. Systematic Assessment of the Influence of Hydrogen Peroxide Dosage on Caffeine Degradation by photo-Fenton Process, *Ind. Eng. Chem. Res.* 51:13, 4770

Yuan, F.; Hu, C.; Hu, X.; Wei, D.; Chen, Y.; Qu, J. 2011. Photodegradation and toxicity changes of antibiotics in UV and UV/H<sub>2</sub>O<sub>2</sub> process, *J. Hazard. Mater.* 185, 1256–1263

Zazo, J.A.; Casas, J.A.; Mohedano, A.F.; Rodríguez, J.J. 2009. Semicontinuous Fenton oxidation of phenol in aqueous solution. A kinetic study, *Water Res.* 43, 4063-4069



## **Chapter VII**

### **Degradation of Sulfamethazine by Means of an Improved photo-Fenton Process Involving a Hydrogen Peroxide Systematic Dosage Protocol**

The degradation of sulfamethazine antibiotic (SMT) in water solutions is addressed in this chapter and the dosage protocol proposed in Chapter V is applied again with outstanding results in improving the degradation and mineralization performances.



## 7.1. Introduction

Sulfamethazine (SMT) or sulfamidine (4-amino-N-(4,6-dimethylpyrimidin-2-yl) benzenesulfonamide) is an antibacterial sulfonamide used in veterinary and human medicine. According to García-Galán et al. (2012), SMT and its metabolites have been detected in waters, from which it is uncertain they can be removed by conventional water treatments. Thus, it is required to search for alternative processes that could ensure mineralization of solutions of this emerging contaminant.

Despite being an emerging contaminant, sulfamethazine (SMT) degradation has been scarcely addressed in the AOPs literature. Specifically, the photo-Fenton treatment was reported by the author to be effective at SMT degradation, but no further work seems to have addressed the opportunities to enhance its efficiency by means of reactants dosage.

This chapter addresses the degradation of SMT in water solutions (12 L of 25 mg L<sup>-1</sup> samples) by means of photo-Fenton process involving the systematic H<sub>2</sub>O<sub>2</sub> dosage protocol proposed in Chapter V. A photo-Fenton process with no dosage using 10 mg L<sup>-1</sup> Fe(II) and 200 mg L<sup>-1</sup> H<sub>2</sub>O<sub>2</sub> initial concentrations led to 86% mineralization after 120 min treatment. Conversely, a conveniently tuned dosage protocol led to total mineralization in less than 75 min treatment. In both cases, total SMT remediation was achieved in less than 10 min. A significant improvement of SMT remediation and solution mineralization is possible by adjusting the dosage of H<sub>2</sub>O<sub>2</sub> in photo-Fenton processes. Results will be discussed in detailed in the next sections.

## 7.2. Results and Discussion

### 7.2.1. Fenton reagents

SMT concentrations and Fenton reagent loads were established according to a previous publication referred on SMT degradation via photo-Fenton (Pérez-Moya et al., 2010). In that work, 1 L of 50 mg L<sup>-1</sup> SMT solutions were used, Fe(II) initial concentrations ranged from 12 to 68 mg L<sup>-1</sup>, and H<sub>2</sub>O<sub>2</sub> concentrations ranged from 176 to 1024 mg L<sup>-1</sup>.

In this part of the investigation, Fe(II) concentration was set at 10 mg L<sup>-1</sup>, the legal limit in liquid effluents permit in Spain (DOGC). As a consequent of this high reduction in the iron tested the amount of contaminant has been fixed to 25 mg L<sup>-1</sup> SMT. Initial H<sub>2</sub>O<sub>2</sub> concentrations was tested at 12, 20, 40, 60, and 200 mg L<sup>-1</sup>, which includes conditions below and above theoretical stoichiometric H<sub>2</sub>O<sub>2</sub> (equal to 140.5 mg L<sup>-1</sup> for 25 mg L<sup>-1</sup> SMT). The experiments were performed in the plastic photo-reactor R3, equipped with the lamp presented in Figure 3.1c.

With the aim to select the most convenient Fenton reagent ratio, for the already fixed iron concentration, 10 mg L<sup>-1</sup>, a set of experiments were conducted

and first order rate constants of TOC degradation ( $k_{TOC}$ ) were estimated and compared to identify the range of most promising (high initial reaction rate)  $H_2O_2$  loads.

Results, presented in Figure 7.1, indicate that a lower dose than  $200 \text{ mg L}^{-1}$  of  $H_2O_2$  at the beginning of the process might improve initial reaction rate, which confirms again the benefit of using  $H_2O_2$  dosage.

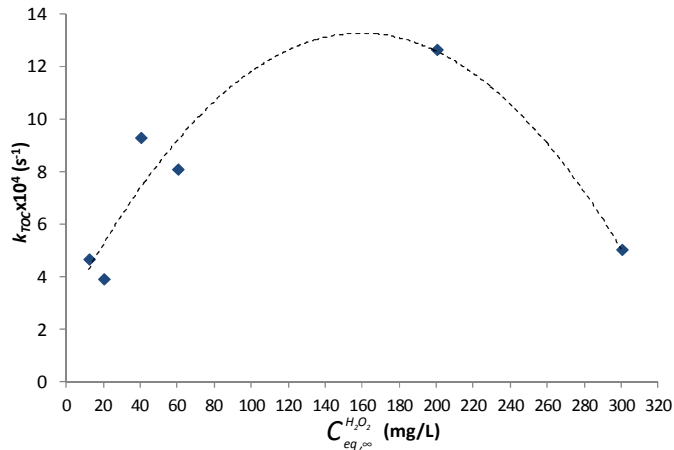


Figure 7.1. First order rate constants for TOC degradation ( $k_{TOC}$ ) versus  $C_{eq,\infty}^{H_2O_2}$  for a  $25 \text{ mg L}^{-1}$  SMT concentration and  $10 \text{ mg L}^{-1}$  iron concentration.

Accordingly, the conditions having produced the highest  $k_{TOC}$  were selected for the subsequent study of the effect of  $H_2O_2$  dosage on the performance of photo-Fenton processes aimed at the mineralization of test samples. Hence:

- SMT initial concentration:  $25 \text{ mg L}^{-1}$
- Fe(II) initial concentration:  $10 \text{ mg L}^{-1}$
- Total  $H_2O_2$  load to be dosed:  $Q^{H_2O_2} = 2400 \text{ mg}$  ( $8.0 \text{ mL}$ ,  $30\% \text{ w/v}$ ), meaning  $C_{eq,\infty}^{H_2O_2} = 200 \text{ mg L}^{-1}$

### 7.2.2. Blank assays

A preliminary set of blank assays was applied to a  $25 \text{ mg L}^{-1}$  SMT sample in tap water in order to characterize the influence of different factors (reagents and irradiation) on the evolution of SMT degradation. Figure 7.2 shows the SMT degradation results, which can be summarized as follows:

- The most efficient reagents are sole  $H_2O_2$  and sole irradiation. A concentration of  $200 \text{ mg L}^{-1}$  of  $H_2O_2$  leads to a 98% SMT degradation. Irradiation alone yields to a 90% SMT degradation, which is in accordance with observations reported elsewhere (Kim and Tanaka, 2009).

- The presence of  $10 \text{ mg L}^{-1}$  Fe(II) degrades only a 13% of the initial SMT and, when combined with irradiation, up to 69% degradation is achieved, which is less than the outcome of UV irradiation alone. This is due to the Fe(II) present in the reaction media, which absorbs part of the photons irradiated, resting efficiency to the photolysis itself of the contaminant when compared to degradation achieved with solely irradiation (Braun et al., 1991; Ferraudi, 1988).
- Regarding mineralization, all blank assays produced no more than 30% TOC reductions (data not shown).

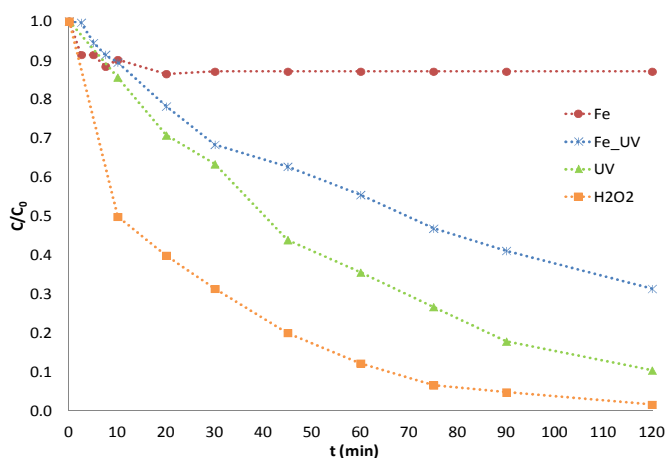


Figure 7.2. Evolution of SMT degradation during blank assays.  $C_0^{SMT} = 25 \text{ mgL}^{-1}$  ;  
 $C_0^{Fe(II)} = 10 \text{ mgL}^{-1}$  ;  $C_0^{H_2O_2} = 200 \text{ mgL}^{-1}$

The blank assays were not efficient to attain SMT mineralization. They confirmed that long reaction times are required to yield a significant increase in SMT degradation (if any). Hence, new assays were proposed for the UV/H<sub>2</sub>O<sub>2</sub>, Fenton and photo-Fenton processes.

### 7.2.3. SMT degradation performance

Three different AOP alternatives were analyzed to compare their performances in terms of TOC reduction (mineralization) and SMT degradation. Figure 7.3 summarizes these results. Regarding SMT, UV/H<sub>2</sub>O<sub>2</sub> requires 30 minutes to remediate 95% of its initial concentration. On the other hand, Fenton and photo-Fenton processes achieve similar performance within only 7.5 min. The three studied AOPs noticeably improve SMT degradation respect to the blank assays discussed in the previous section.

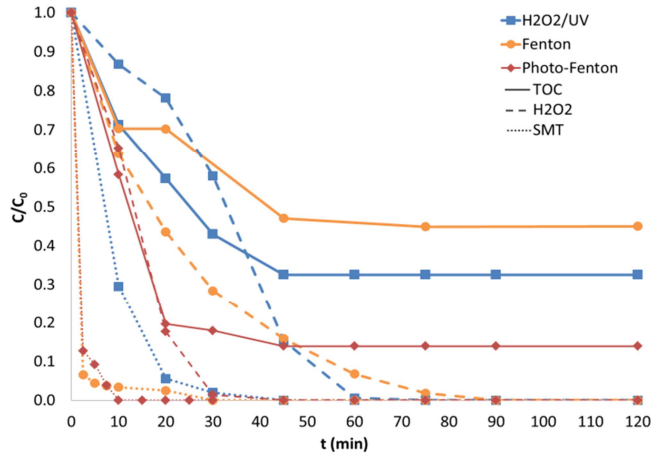


Figure 7.3. TOC, SMT and H<sub>2</sub>O<sub>2</sub> normalized concentration profiles for different AOPs.

$$C_0^{SMT} = 25 \text{ mgL}^{-1}; \quad C_0^{Fe(II)} = 10 \text{ mgL}^{-1}; \quad C_0^{H_2O_2} = 200 \text{ mgL}^{-1}$$

Regarding mineralization, Fenton process reduces 55% of the initial TOC during the first 45 minutes of reaction. No further mineralization is observed even though there still is some residual amount of H<sub>2</sub>O<sub>2</sub>; this agrees with the drop of the cycling rate of Fe(III) into Fe(II) in the absence of irradiation (Pignatello et al., 2006). The UV/H<sub>2</sub>O<sub>2</sub> process stops as H<sub>2</sub>O<sub>2</sub> is exhausted; still, it leads to a higher value of TOC reduction (67%) than that obtained by the Fenton process within the same time span. In the case of the photo-Fenton process, H<sub>2</sub>O<sub>2</sub> exhaustion occurs during the first 30 minutes, when TOC reduction reaches an 86%. This mineralization clearly contrasts with the maximum 30% reached with blank assays.

Once the photo-Fenton process is demonstrated to highly improve SMT remediation and mineralization, next step is to study the effect of H<sub>2</sub>O<sub>2</sub> dosage on the performance of foto-Fenton processes aimed at the mineralization of test samples.

#### 7.2.4. Influence of dosage on process performance

With the aim to characterize the influence of the variables involved in the dosage protocol applied (Yamal-Turbay et al., 2012) on the process performance, the design of experiments (DOE) presented in Table 7.1 was undertaken. Once the duration of the treatment is fixed (120 min), the length of the dosage interval ( $\Delta t_{add}$ ) was decided on the basis of the preliminary assays and set to 60 min in order to limit the alternatives only to a couple of variables of interest. Following the DOE proposed by that work, these variables are:

- $y_0$ : defined as the fraction of the total H<sub>2</sub>O<sub>2</sub> dose released at  $t = 0$  min. The minimum and maximum values of this variable were taken as 10 and 30% (centered in 20%).



- $t_{ini}$ : the time when the rest of the  $H_2O_2$  is started to be continuously added at a constant flow during  $\Delta t_{add}$ . DOE considers 0 and 30 min as minimum and maximum values for this variable, centered in 15 min.

From this point on, experiments are codified as follows:  $code_{y_0}t_{ini}$ , where “code” is a correlative letter.

Table 7.1. Assays carried out according to the DOE.  $C_{eq,\infty}^{H_2O_2} = 200 \text{ mg L}^{-1}$ .

Assay	Codified values		Variables levels	
	$t_{ini}$	$y_0$	$t_{ini}$ (min)	$y_0$ (%)
A_10_0	-1	-1	0	10%
B_10_30	1	-1	30	10%
C_30_0	-1	1	0	30%
D_30_30	1	1	30	30%
Central_20_15	0	0	15	20%
H_20_0	-1	0	0	20%
I_20_36	1.414	0	36	20%
J_6_15	0	-1.414	15	6%
K_34_15	0	1.414	15	34%
L_0_0	-1	-2	0	0%
Ref_100	-1	8	0	100%

Given these two factors, the system response was assessed in two different ways. On the one hand, by the earliest sample time at which SMT is not detected ( $t_{SMT}$ ). This indicator is given by the detection limit of the analytical method (0.5 ppm), which corresponds to more than 95% degradation of the initial SMT concentration. Obviously, the precision in determining this indicator is given by the sample time, which is 2.5 minutes. On the other hand, the system performance is also assessed by the time at which mineralization occurs. The precision of this second indicator is given by the TOC detection limit (1 ppm) and the sample time, which in this case is higher: 10 minutes.

Hence, this study addresses the improvement of the process efficiency. Rigorous optimization cannot and it is not intended. The factorial design employed is just a means for systematically exploring the region of interest and the study only shows how improved operational conditions may be found and identified. Thus, the characterization of the dual response will be later presented as a function of these two objectives that may be conflicting or not (Fig. 7.5).

Two reference assays were carried out: one with a total release of reagent at the initial reaction time,  $t = 0$ , (Ref\_100), and the other one with a continuous inlet of  $H_2O_2$  during the first 60 minutes assay (L\_0\_0). These experiments are compared to the central experiment of the DOE (Central\_20\_15) in Figure 7.4. The

improvement of the process is shown to be clear for both dosage protocols, and total mineralization is achieved in less than 90 min treatment, instead of 86% in 120 minutes when no dosage is applied. This observation conforms to the idea that gradual addition of  $H_2O_2$  reduces the scavenging of hydroxyl radicals (Huston and Pignatello, 1999; Gulkaya et al., 2006; Chu et al., 2007; Zazo et al., 2009; Prato-García et al., 2012; Yamal\_Turbay et al., 2012).

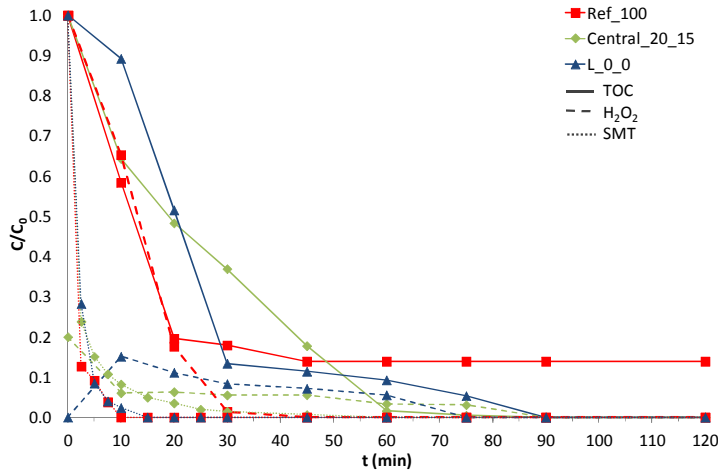


Figure 7.4. TOC, SMT and  $H_2O_2$  normalized concentration profiles for different dosage protocols compared to reference experiment.  $C_0^{SMT} = 25 \text{ mgL}^{-1}$ ;  $C_0^{Fe(II)} = 10 \text{ mgL}^{-1}$ ;  $C_{eq,\infty}^{H_2O_2} = 200 \text{ mgL}^{-1}$

Regarding SMT, elimination in less than 15 minutes was observed in all cases, except the central assay (Central\_20\_15), which needed almost 30 minutes to degrade more than 95% of initial SMT.

As a summary of the DOE results, Figure 7.5 shows the relation between the time necessary to degrade 95% of initial SMT ( $t_{SMT}$ ) and the time to degrade at least 92% of initial TOC ( $t_{TOC}$ ) for all the DOE assays and the two reference ones. Only assay R\_100 does not achieve 92% mineralization within 120 minutes treatment, with 86.1% TOC reduction. In all of the cases where systematic dosage is applied, at least 92% mineralization is achieved. As it was already stated by Yamal-Turbay et al. (2012) both factors,  $y_0$  and  $t_{ini}$ , are related, being the combination of low  $y_0$  with low  $t_{ini}$  the one that leads to a better performance; when a low initial release is provided, it is necessary to start continuous dosage sooner to avoid reagent exhaustion, as may be observed in experiment B\_10\_0 and J\_6\_15.

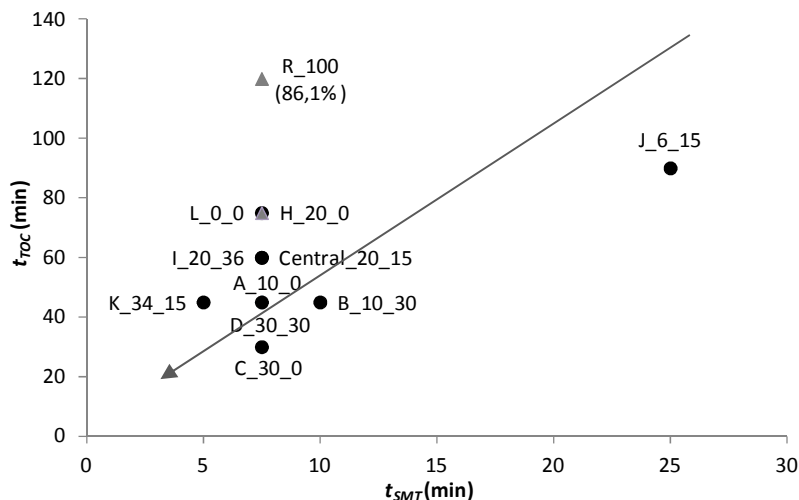


Figure 7.5. Relation between the time necessary to degrade 95% of initial SMT ( $t_{SMT}$ ) and the time necessary to achieve total mineralization ( $t_{TOC}$ ) for all of the DOE and reference assays. Final TOC conversion is indicated in brackets in the case when mineralization (100%) is not achieved (Assay R\_100)

As previously mentioned, the DOE has provided evidence of the cross-effect between the factors of the dosage protocol in Figure 7.6 process performance for different  $y_0$  and  $t_{ini}$  were compared with the aim to visualize this effect. In experiment B\_10\_30, for instance, TOC exhibits a particularly slow behavior after the first 10 minutes of the treatment, when  $H_2O_2$  exhausts and it is evident that process accelerates after reagent continuous dosage starts at 30 minutes. Something similar occurs in experiments D\_30\_30, but  $y_0 = 30\%$  appears to be a sufficient initial dose to keep the process running until continuous dosage starts. Experiment A\_10\_0 exhibits a slower behavior with regard to experiment C\_30\_0 but both of them are faster than B\_10\_30 and D\_30\_30 in degrading TOC due to the presence of  $H_2O_2$  during the first minutes of the treatment.

Nevertheless, 100% mineralization is possible in less than 90 min process for all of the cases when dosage protocol is applied; SMT remediation is remarkably slower when dosage variables are not properly adjusted (e.g. experiment B\_10\_30).

Tuning hydrogen peroxide dosage proved to improve the sample mineralization obtained at the end of the treatment span. Furthermore, SMT mineralization was proved to be achieved within this time if dosage is conveniently adjusted, which is a practical achievement since it results in a significant reduction of the treatment cost.

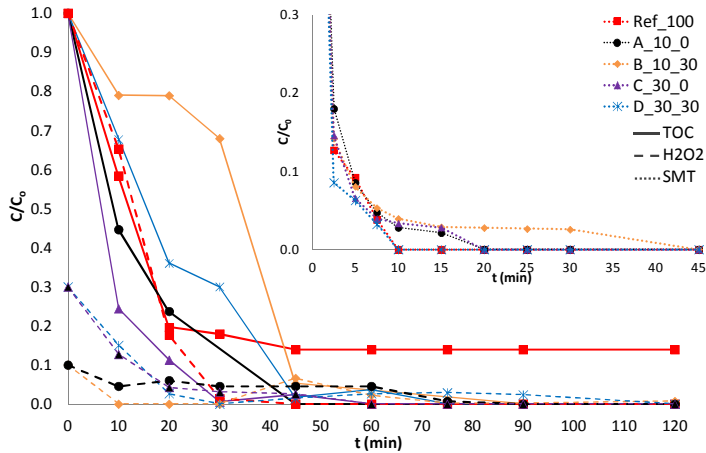


Figure 7.6. TOC, SMT and H<sub>2</sub>O<sub>2</sub> normalized concentration profiles for different  $y_0$  where  $t_{ini} \geq 30$  min.  $C_0^{SMT} = 25 \text{ mgL}^{-1}$ ;  $C_0^{Fe(II)} = 10 \text{ mgL}^{-1}$ ;  $C_{eq,\infty}^{H_2O_2} = 200 \text{ mgL}^{-1}$

Further refinement could be obtained by monitoring biodegradability. As indicated in the literature (Ben et al., 2009; Yahiat et al., 2011) the expensive photo-Fenton process could be derived to conventional processes without achieving total mineralization if biodegradability could be guaranteed. This is a very interesting issue that requires expensive experimentation (toxicity assays) as well as solving the optimization problem posed by the trade-off between the costs associated to the processes engaged. This issue requires further research beyond the scope of this paper.

### 7.3. Conclusions

The photo-Fenton treatment has proved to be effective in totally degrading 12 L of a  $25 \text{ mg L}^{-1}$  SMT sample by using  $10 \text{ mg L}^{-1}$  iron and  $200 \text{ mg L}^{-1}$  H<sub>2</sub>O<sub>2</sub> initial concentrations. However, only 86% mineralization of the sample is achieved when the Fenton reagent is totally supplied at the beginning of the treatment. This represents an improvement of 30 percentage points with respect a previous work (Pérez-Moya et al., 2010) that used larger amounts of reagents (Fe(II): 12 – 68 mg L<sup>-1</sup>, H<sub>2</sub>O<sub>2</sub>: 176 – 1024 mg L<sup>-1</sup>). Next, further enhancement was shown to be possible via H<sub>2</sub>O<sub>2</sub> dosage.

It was again confirmed that an excess of H<sub>2</sub>O<sub>2</sub> during the first stages of the process reduces TOC degradation performance, which can be attributed to the scavenging of hydroxyl radicals.

After that, dosage was investigated by applying the dosage protocol proposed in Chapter V. Hence, the systematic exploration of a set of dosage alternatives led to conditions yielding total mineralization of the problem sample in less than 75 min assay. Total mineralization implies an improvement of 14 percent points compared with the performance obtained without dosage.

Regarding SMT, total degradation is achieved in less than 10 min treatment with the appropriate combination of the dosage protocol variables.

Concerning the tuning of the dosage parameters, the design of experiments reveals again that low  $y_0$  requires low  $t_{ini}$  in order to achieve both aims: fast mineralization and fast degradation. When higher  $y_0$  values are used,  $t_{ini}$  influence on SMT degradation diminishes, but more time is necessary to reach total mineralization. In the next part of this thesis, a model capable to represent this behavior is presented and a first attempt to optimize the process through the tuning of the dosage processes is investigated.

#### 7.4. References

Ben, W.; Qiang, Z.; Pan, X.; Chen M. 2009. Removal of veterinary antibiotics from sequencing batch reactor (SBR) pretreated swine wastewater by Fenton's reagent. *Water Res* 43, 4392–4402.

Braun, A.M.; Maurette, M.T.; Oliveros, E. 1991. Photochemical Technnology, ed by Ollis D, F Serpone. John Wiley & Sons, Inc.

Chu, W.; Chan, K.H.; Kwan, C.Y.; Choi, K.Y. 2007. Degradation of atrazine by modified stepwise-Fenton's processes, *Chemosphere* 67, 755-761.

DOGC núm. 3894, DECRET 130/2003, de 13/05/2003, (29.5.2003). <http://www.gencat.cat/diari/3894/03127147.htm> [accessed Nov 10 2012].

Ferraudi, G 1988. Elements of Inorganic Photochemistry. John Wiley & Sons Inc.

Gao, Y-q.; Gao, N-y.; Deng, Y.; Yang, Y-q.; Ma, Y. 2012. Ultraviolet (UV) light-activated persulfate oxidation of sulfamethazine in water. *Chem Eng J* 195–196, 248–253.

García-Galán, M.J.; Díaz-Cruz, M.S.; Barceló, D 2012. Kinetic studies and characterization of photolytic products of sulfamethazine, sulfapyridine and their acetylated metabolites in water under simulated solar irradiation. *Water Res* 46, 711-722.

Gulkaya, I.; Surucu, A.; Dilek, F. 2006. Importance of  $H_2O_2/Fe^{2+}$  ratio in Fenton's treatment of a carpet dyeing wastewater, *J Hazard Mater B* 136, 763-769.

Huston, P.L.; Pignatello, J.J. 1999. Degradation of selected pesticide active ingredients and commercial formulations in water by the photo-assisted Fenton reaction. *Water Res* 33(5), 1238-1246.

Kim, I.; Tanaka, H. 2009. Photodegradation characteristics of PPCPs in water with UV treatment. *Environ Int* 35, 793–802.

Pérez-Moya, M.; Graells, M.; Castells, G.; Amigó, J.; Ortega, E.; Buhigas, G.; Pérez, L.M.; Mansilla, H.D. 2010. Characterization of the degradation performance of the sulfamethazine antibiotic by photo-Fenton process. *Water Res* 44, 2533-2540.

Pignatello, J.J.; Oliveros, E.; MacKay, A. 2006. Advanced Oxidation Processes for Organic Contaminant Destruction Based on the Fenton Reaction and Related Chemistry, *Crit Rev Environ Sci Technol* 36(1), 1-84.

Prato-Garcia, D.; Buitrón, G. 2012. Evaluation of three reagent dosing strategies in a photo-Fenton process for the decolorization of azo dye mixtures, *J Hazard Mat* 217–218, 293–300.

Yahiat, A.; Fourcade, F.; Brosillon, S.; Amrane, A. 2011. Removal of antibiotics by an integrated process coupling photocatalysis and biological treatment – Case of tetracycline and tylosin. *Int. Biodeter. Biodegr* 65(7), 997-1003.

Yamal-Turbay, E.; Graells, M.; Pérez-Moya, M. 2012. Systematic Assessment of the Influence of Hydrogen Peroxide Dosage on Caffeine Degradation by photo-Fenton Process. *Ind Eng Chem Res* 51(13), 4770-4778.

Zazo, J.A.; Casas, J.A.; Mohedano, A.F.; Rodríguez, J.J., Semicontinuous Fenton oxidation of phenol in aqueous solution. A kinetic study, *Water Res* 43, 4063-4069.

## **PART III. COMPUTATIONAL APPROACH**





## **Chapter VIII**

### **Simulation and Parameter Adjustment**

In this chapter, a model from the literature is applied and modified to represent the behavior of Fenton and photo-Fenton process with the incorporation of the reagent dosage protocol proposed. The kinetic model and the system of differential equations are presented and a set of base cases, including blanks, are simulated. The adjustment of the parameters involved in the model is explored, with satisfactory results.



## 8.1. Model statement

As it was mentioned in section 2.3.2, modeling Fenton and photo-Fenton process has been undertaken from several points of view, from empirical models based on design of experiments, response surface methodology or artificial neural networks through first-principles-based models involving a huge set of chemical reactions and complex irradiation models. Empirical models, despite being simple and easy to understand and apply to real situations, can hardly be extrapolated to different equipment and/or experimental conditions. First-principles-based models, on the contrary, are applicable to most cases, but their use in real or industrial situations is not feasible due to its complexity and the difficulty to elucidate all of the possible intermediates involved in the degradation pathway of the contaminant. The most complex first-principles based models involve the calculation of the local volumetric rate of photon absorption (LVRPA), a term which depends on the geometry of the reactor and the characteristics of the irradiation source (e.g. Rosetti et al., 2002; Farías et al., 2009).

Among the available models, that proposed by Cabrera-Reina et al. (2012) presents an intermediate approach, where a simplified phenomenological model is used to predict the evolution of the involved species concentrations. The authors propose a kinetic model which can be stated as follows:



In this model, Eq. 8.1 and 8.2 are Fenton and photo-Fenton chemical reactions, respectively (including radiation power as a reagent,  $I$ ), Eq. 8.3 and 8.4 correspond to a generic radical (R) and  $H_2O_2$  scavenging reactions, Eq. 8.5 to 8.9 consider a generic degradation pathway for the contaminant and its intermediates to reach mineralization. The model is applied to a generic contaminant M, which produces two partially oxidized dummy intermediates (MX1, MX2) before achieving mineralization through a unique generic radical (R). Hydrogen peroxide ( $H_2O_2$ ) and dissolved oxygen ( $O_2$ ) molar concentrations are also calculated. The

advantage of this model lies in its capability to represent the process behavior throughout lumped easy-to-measure variables, such as TOC, contaminant,  $H_2O_2$  and  $O_2$  concentrations.

In fact, total organic carbon (TOC) concentration is calculated by Cabrera-Reina et al. as the summa of the contaminant and the intermediates concentrations:

$$[TOC] = [M] + [MX1] + [MX2] \quad (8.10)$$

The kinetic expressions of the model are:

$$r_1 = k_1 [Fe(II)] [H_2O_2] \quad (8.11)$$

$$r_2 = k_2 [Fe(III)] [I] \quad (8.12)$$

$$r_3 = k_3 [R] [H_2O_2] \quad (8.13)$$

$$r_4 = k_4 [R] [R] \quad (8.14)$$

$$r_5 = k_5 [M] [R] [O_2] \quad (8.15)$$

$$r_6 = k_6 [M] [R] \quad (8.16)$$

$$r_7 = k_7 [MX1] [R] \quad (8.17)$$

$$r_8 = k_8 [MX1] [R] \quad (8.18)$$

$$r_9 = k_9 [MX2] [R] \quad (8.19)$$

The mass balances on components are written as follows:

$$\frac{d[Fe(II)]}{dt} = -r_1 + r_2 \quad (8.20)$$

$$\frac{d[Fe(III)]}{dt} = r_1 - r_2 \quad (8.21)$$

$$\frac{d[H_2O_2]}{dt} = -r_1 - r_3 \quad (8.22)$$

$$\frac{d[R]}{dt} = -r_1 + r_2 - r_3 - 2r_4 - r_5 - r_6 - r_7 - r_8 - r_9 \quad (8.23)$$

$$\frac{d[M]}{dt} = -r_5 - r_6 \quad (8.24)$$

$$\frac{d[MX1]}{dt} = r_5 + r_6 - r_7 - r_8 \quad (8.25)$$

$$\frac{d[MX2]}{dt} = r_7 - r_9 \quad (8.26)$$

$$\frac{d[O_2]}{dt} = g_1 r_3 + g_2 r_4 - c_1 r_5 + K_L a (O_2^* - O_2) \quad (8.27)$$

Parameters  $g_1$ ,  $g_2$  and  $c_1$  are stoichiometric coefficients related with the oxygen balance,  $K_L a$  is the overall gas-liquid mass transfer coefficient for  $O_2$  ( $2.7 \text{ h}^{-1}$  according to Cabrera-Reina et al, 2012) and  $O_2^*$  is the oxygen dissolved concentration in the equilibrium, assumed to be 0.25 mM.

As the present study aims to model Fenton and photo-Fenton processes behavior, the model by Cabrera-Reina is adopted with some modifications for that purpose. Such a decision is made due to the generic characteristics of the model, which can be easily adapted to any contaminant and irradiation source despite the lack of information about the degradation pathway, reactor geometry or configuration, among other operational conditions.

The first modification implies the inclusion of the number of carbons in the molecule of the contaminant for the calculation of TOC. For instance, to represent paracetamol (PCT =  $C_8H_9NO_2$ ) degradation, and considering the intermediates to be only partially oxidized, TOC will be finally calculated as:

$$[TOC] = 8([M] + [MX1] + [MX2]) \quad (8.10a)$$

The second modification of the model by Cabrera-Reina is the inclusion of the Fenton-like reaction, which considers the cycling of Fe(III) to Fe(II) in the absence of irradiation. Despite the fact that the significance of this reaction seems not to be important when irradiation is present due to its low reaction rate ( $0.01 - 0.02 \text{ M}^{-1}\text{s}^{-1}$  according to Kůsič et al., 2006), it becomes determinant when no irradiation is provided as it implies the continuity of the process when Fe(III) cycles to Fe(II) after the first stages of the process. This reaction can be written as:



An additional kinetic constant ( $k_{10}$ ) is therefore necessary:

$$r_{10} = k_{10} [Fe(III)] [H_2O_2] \quad (8.29)$$

Consequently, mass balances will be:

$$\frac{d[Fe(II)]}{dt} = -r_1 + r_2 + r_{10} \quad (8.20a)$$

$$\frac{d[Fe(III)]}{dt} = r_1 - r_2 - r_{10} \quad (8.21a)$$

$$\frac{d[H_2O_2]}{dt} = -r_1 - r_3 - r_{10} \quad (8.22a)$$

$$\frac{d[R]}{dt} = -r_1 + r_2 - r_3 - 2r_4 - r_5 - r_6 - r_7 - r_8 - r_9 + r_{10} \quad (8.23a)$$

$$\frac{d[M]}{dt} = -r_5 - r_6 \quad (8.24)$$

$$\frac{d[MX1]}{dt} = r_5 + r_6 - r_7 - r_8 \quad (8.25)$$

$$\frac{d[MX2]}{dt} = r_7 - r_9 \quad (8.26)$$

$$\frac{d[O_2]}{dt} = g_1 r_3 + g_2 r_4 - c_1 r_5 + K_L a (O_2^* - O_2) \quad (8.27)$$

The differential-algebraic equation (DAE) system formed by Eq. 8.10, 8.20a to 8.23a and 8.24 to 8.27 is finally used to represent the evolution of the concentrations of Fe(II), Fe(III), H<sub>2</sub>O<sub>2</sub>, O<sub>2</sub>, M, TOC, MX1 and MX2. The model is applied to a set of base cases are simulated in the following section in order to evaluate its feasibility in representing the process evolution under different operational conditions.

### 8.1.1. Simulation of base cases

The simulation in Matlab® of a set of base cases for different contaminants and operational conditions are next presented in order to identify the versatility and applicability of the model to represent Fenton and photo-Fenton processes under different conditions. In all of the cases, the 12 parameters reported by Cabrera-Reina et al., (2012) were used for the simulations, and they are presented in Table 8.1.

Table 8.1. Kinetic constants and stoichiometric coefficients reported by Cabrera-Reina et al. (2012) and used for simulating the base cases

	k <sub>1</sub>	k <sub>2</sub>	k <sub>3</sub>	k <sub>4</sub>	k <sub>5</sub>	k <sub>6</sub>	k <sub>7</sub>	k <sub>8</sub>	k <sub>9</sub>	g <sub>1</sub>	g <sub>2</sub>	c <sub>1</sub>
	mM <sup>-1</sup> h <sup>-1</sup>									Dimensionless		
Adjusted parameters (Cabrera-Reina et al., 2012)	8.81	5.63	75.8	42798	2643	257	2865	271	107	0.75	0.47	0.1

Both Fenton and photo-Fenton processes were simulated for the conditions of all of the base cases. The influence of the Fenton-like reaction in the concentration profiles is evaluated by comparing the results for each case.

A blank base case when no contaminant is present is first simulated in order to evaluate the evolution of Fe(II), Fe(III), H<sub>2</sub>O<sub>2</sub>, R and O<sub>2</sub> concentrations. The results are presented in Fig. 8.1 and they show slight changes in H<sub>2</sub>O<sub>2</sub> and O<sub>2</sub> concentrations when no irradiation is present, but in photo-Fenton process, irradiation allows the cycling of Fe(II) and Fe(III) as well as the production of R by the degradation of H<sub>2</sub>O<sub>2</sub>.

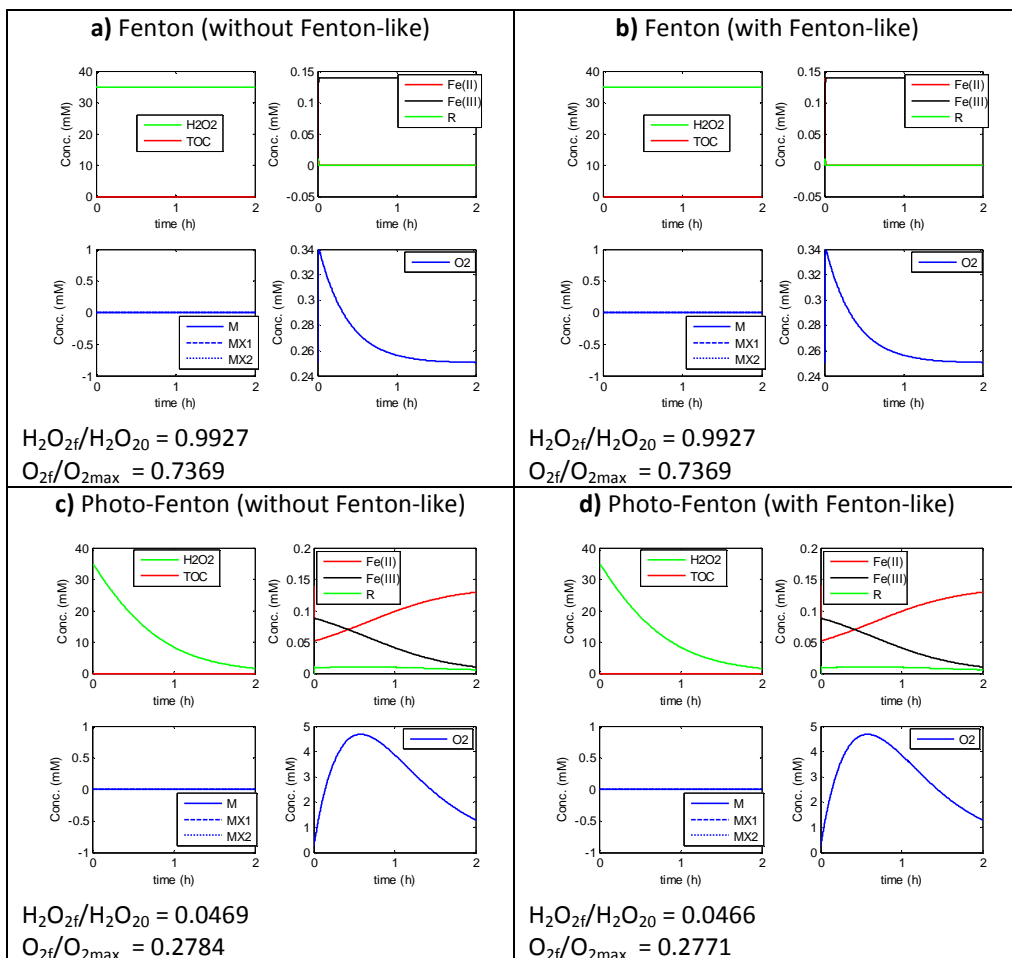


Figure 8.1. Fenton and photo-Fenton process simulation when no organic matter is present

Once it was proved that the model represents the evolution of Fenton and photo-Fenton mechanisms without the presence of organic matter, the base cases including organic matter will be presented, in order to evaluate processes behavior in degrading and mineralizing specific contaminants. Paracetamol (PCT), sulfamethazine (SMT) and tetracycline (TC) are used as model contaminants under different operational conditions of initial reagent concentrations and irradiation.

### Paracetamol (PCT)

Five base cases using PCT as a model contaminant were simulated. Table 8.2 shows the initial concentrations considered for the simulation of each base case, which were taken from those reported by Cabrera-Reina et al. (2012) in their study.

Table 8.2. Initial concentrations considered for the simulation of the PCT base cases.

Species	Initial concentrations (mmol L <sup>-1</sup> )				
	Base case1	Base case2	Base case3	Base case4	Base case5
Fe(II)	0.14	0.35	0.35	0.0001	0.14
Fe(III)	0	0	0	0	0
H <sub>2</sub> O <sub>2</sub>	35.3	35.3	8.83	35.3	0.01
R	0	0	0	0	0
M	1.0413	1.0413	1.0413	1.0413	1.0413
MX1	0	0	0	0	0
MX2	0	0	0	0	0
O <sub>2</sub>	0.25	0.25	0.25	0.25	0.25
I	32	19	19	32	32

Figure 8.2 presents the results of the simulations for base case 1. As it was expected, the incorporation of Fenton-like reaction is more important in Fenton than in photo-Fenton process. When irradiation is supplied, thermal effect becomes almost insignificant as  $k_{10} \ll k_2$ . Estimated behavior of variables in Fenton process is more reliable when Fenton-like reaction is considered, demonstrating some contaminant degradation but minimum TOC reduction as intermediates are generated but not degraded during the time span. From a qualitative point of view, the same behavior has been observed experimentally.



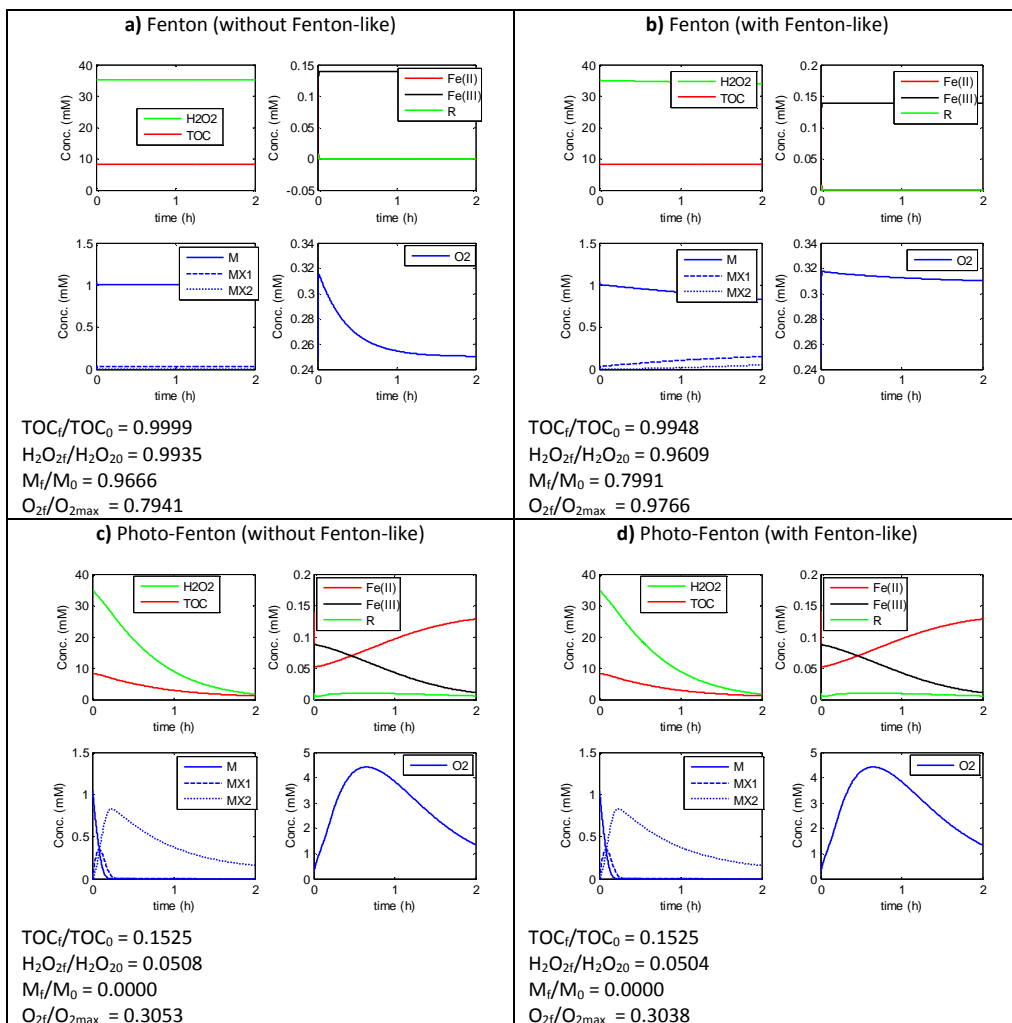


Figure 8.2. Fenton and photo-Fenton process simulation for PCT base case 1

Figure 8.3 shows the results of the simulations of base case 2. In this case, higher Fe(II) dose is supplied at the beginning of the treatment, obtaining a faster contaminant degradation and higher mineralization despite the lower irradiation considered (19 W instead of 32 W in base case 1). As it is expected, mineralization comes to an end when H<sub>2</sub>O<sub>2</sub> is exhausted. Similarly than in the previous case, Fenton-like reaction effect is more important when irradiation is not present.

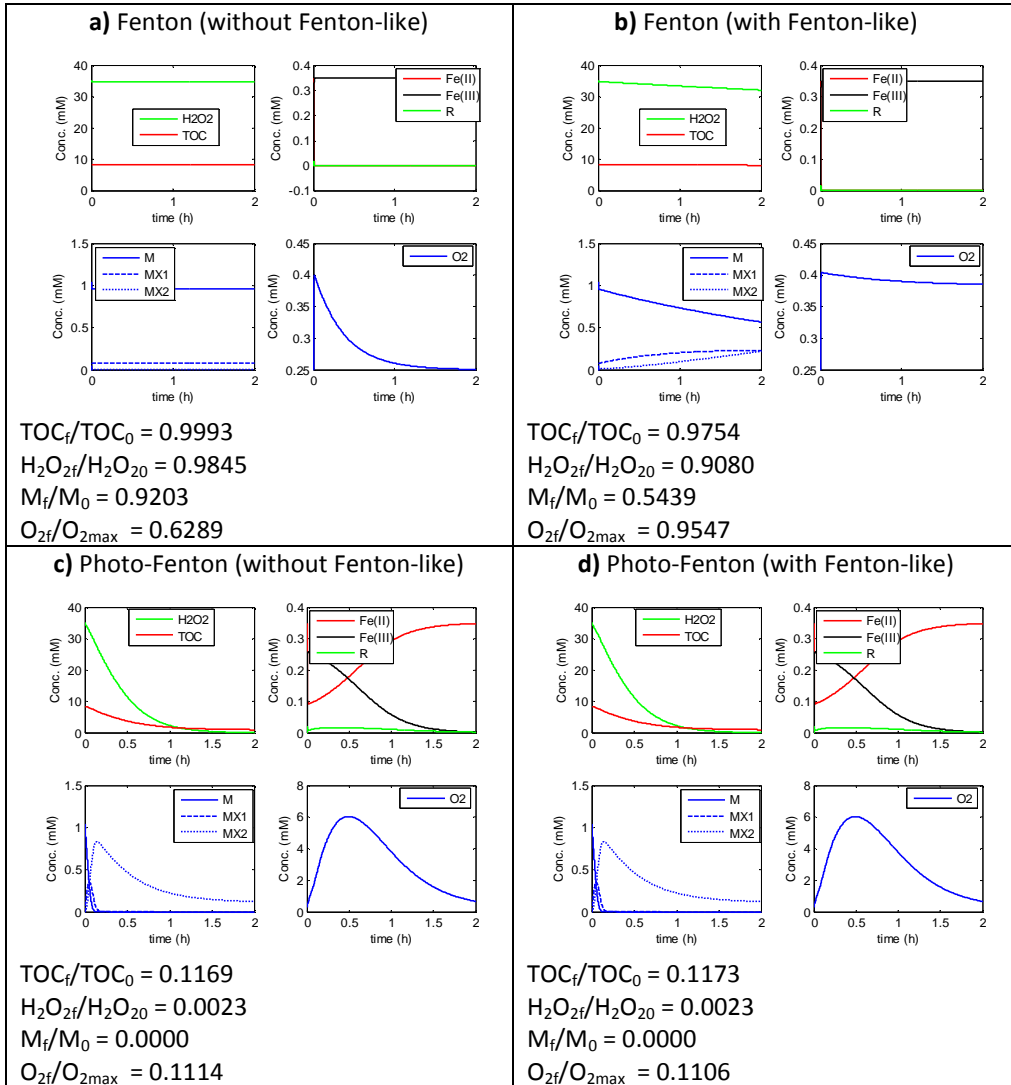


Figure 8.3. Fenton and photo-Fenton process simulation for PCT base case 2

In base case 3 (see Fig. 8.4), the lower H<sub>2</sub>O<sub>2</sub> dose and irradiation, lead to slower degradation and lower mineralization. The evolution of all of the other variables (Fe(II), Fe(III), R, MX1, MX2) is consistent with the model proposed and with observed qualitative behavior.

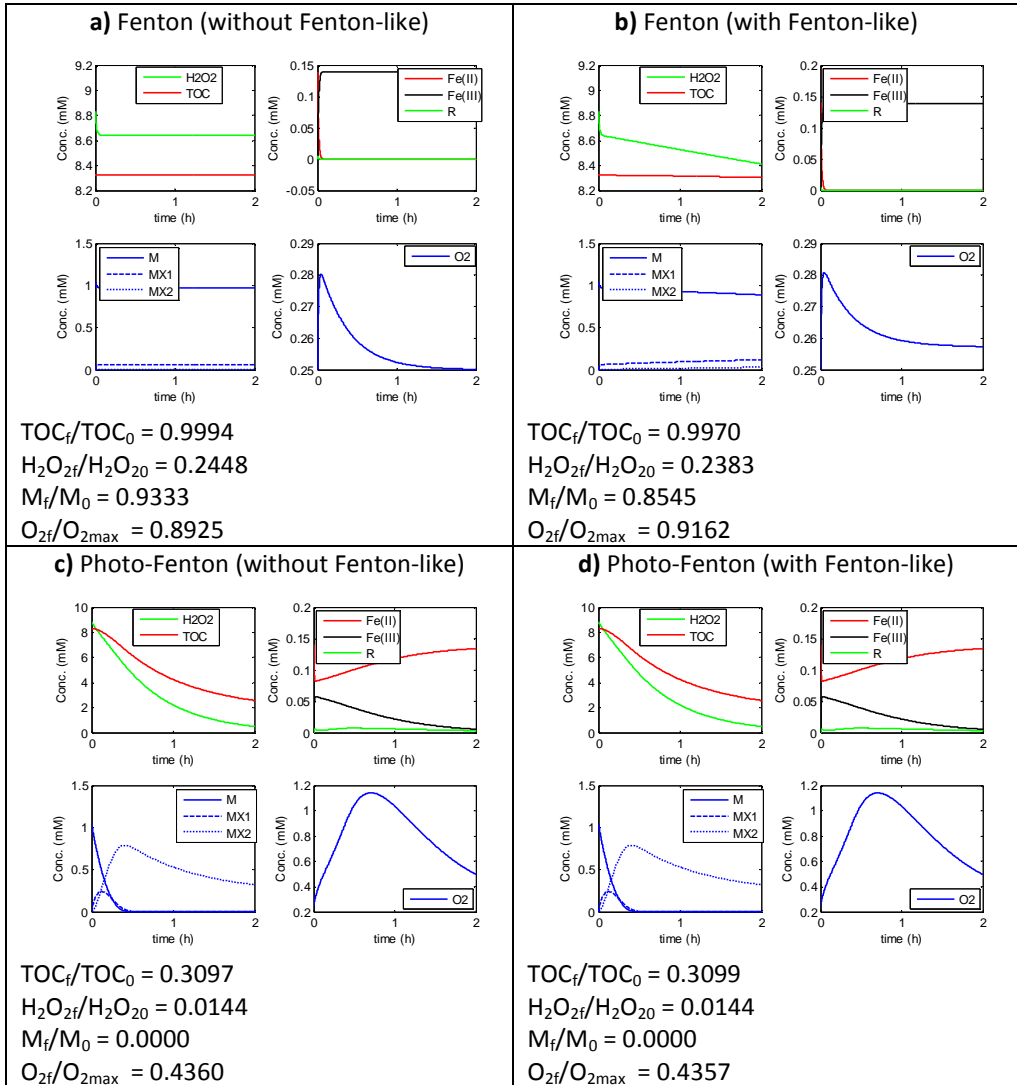


Figure 8.4. Fenton and photo-Fenton process simulation for PCT base case 3

Base case 4, which corresponds to a blank without the addition of H<sub>2</sub>O<sub>2</sub> is presented in Figure 8.5. It is observed that in the absence of H<sub>2</sub>O<sub>2</sub> process does not take place because radicals are not produced. All of the variables behave as expected.

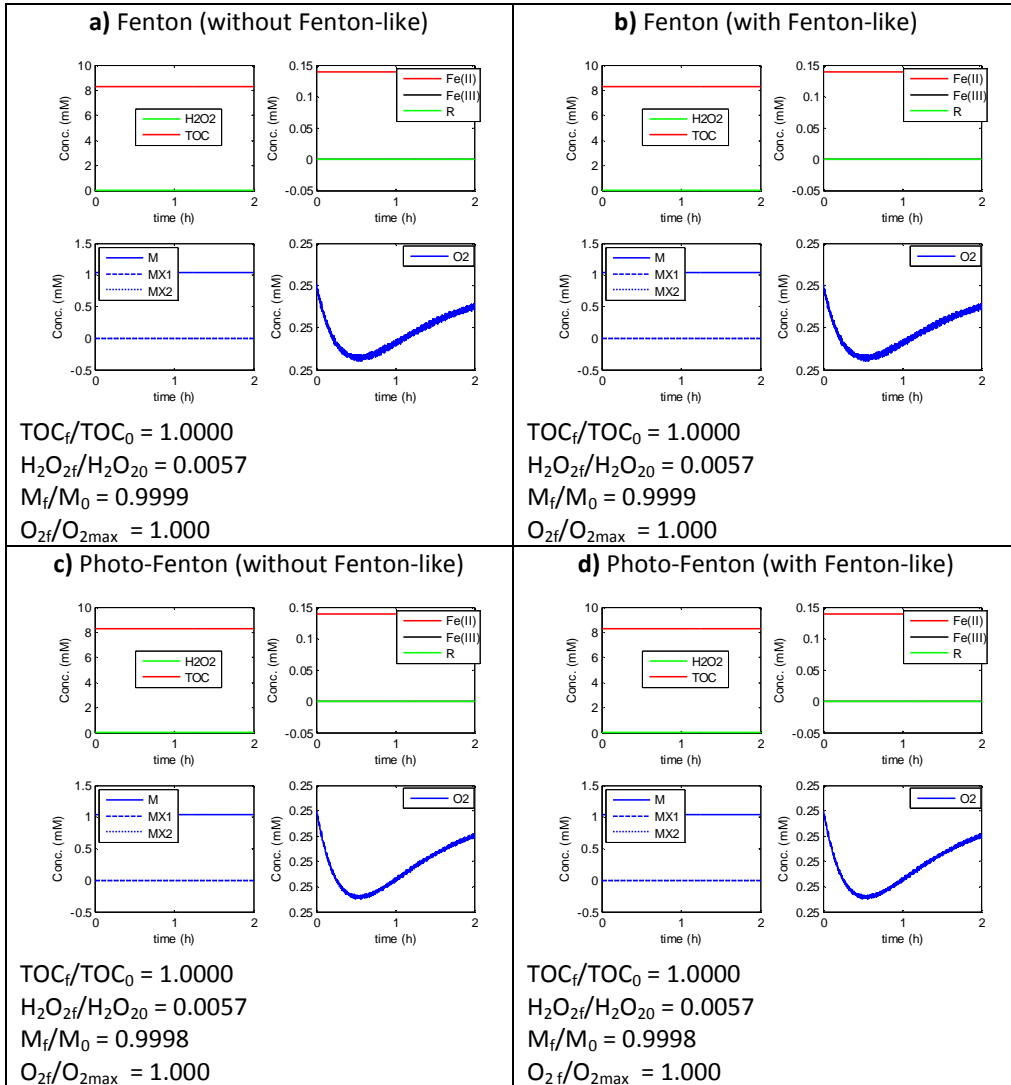


Figure 8.5. Fenton and photo-Fenton process simulation for PCT base case 4

A similar behavior is observed in Figure 8.6 when no Fe(II) is supplied at the beginning of the process (case base 5). In the absence of Fe(II), no radical production is possible and the process does not take place.

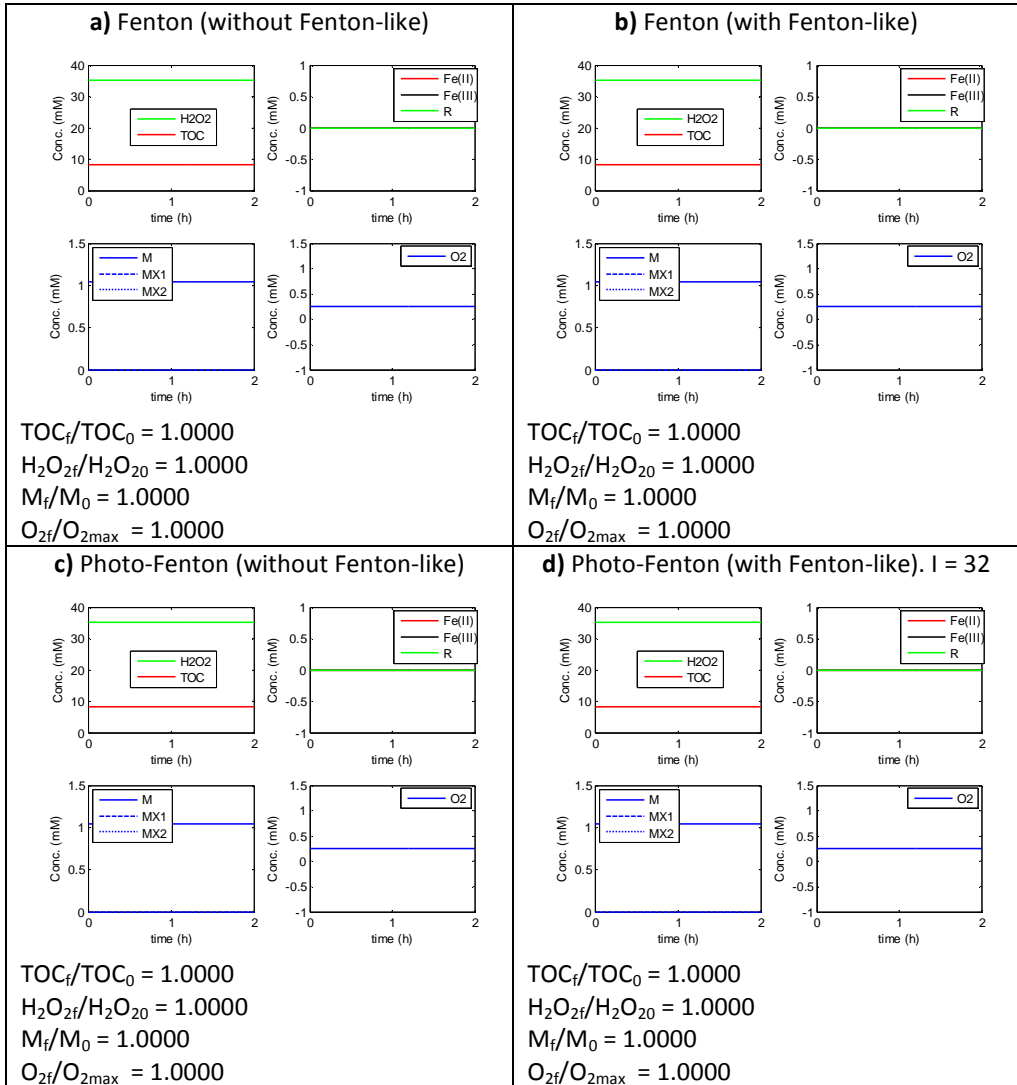


Figure 8.6. Fenton and photo-Fenton process simulation for PCT base case 5

## Sulfamethazine (SMT)

As the molecule of SMT has 12 atoms of carbon ( $C_{12}H_{14}N_4O_2S$ ), Eq. 8.10 will be expressed as follows:

$$[TOC] = 12([M] + [MX1] + [MX2]) \quad (8.10b)$$

The same operational conditions of PCT base case 1 were used to perform this simulation and results are presented in Figure 8.7. The only difference with respect to Figure 8.2 is the initial TOC concentration, but the evolution of the variables follows the same trends and final degradation and mineralization remains without change when compare with PCT base case 1.

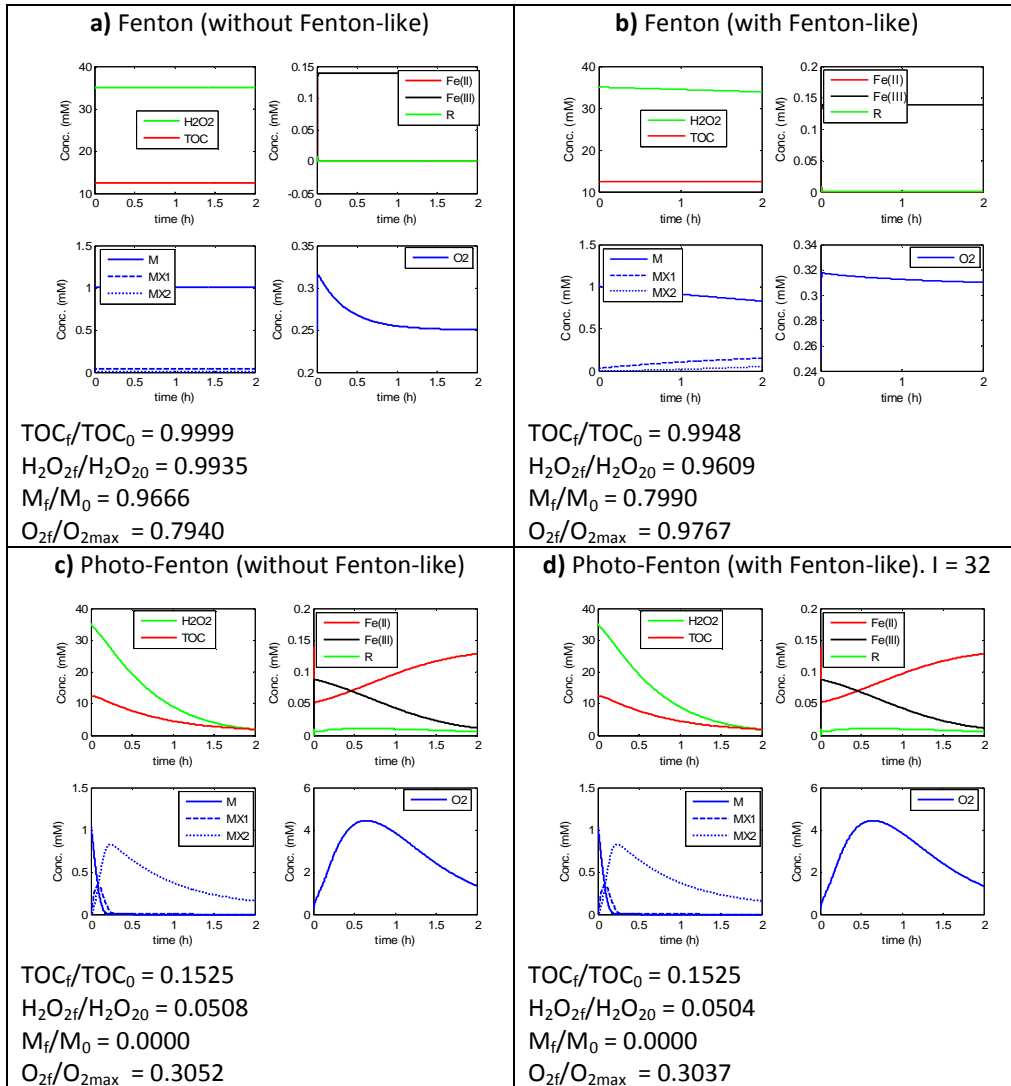


Figure 8.7. Fenton and photo-Fenton process simulation for SMT base case 1

### Tetracycline (TC)

The molecule of TC ( $C_{22}H_{24}N_2O_8$ ) has 22 atoms of carbon and Eq. 8.10 is now written as:

$$[TOC] = 22([M] + [MX1] + [MX2]) \quad (8.10c)$$

Similarly to the previous case of SMT, the same conditions of PCT base case 1 will be considered for the simulation. Figure 8.8 presents the corresponding results and the evolution of the variables is exactly the same, except for the different initial TOC concentration.

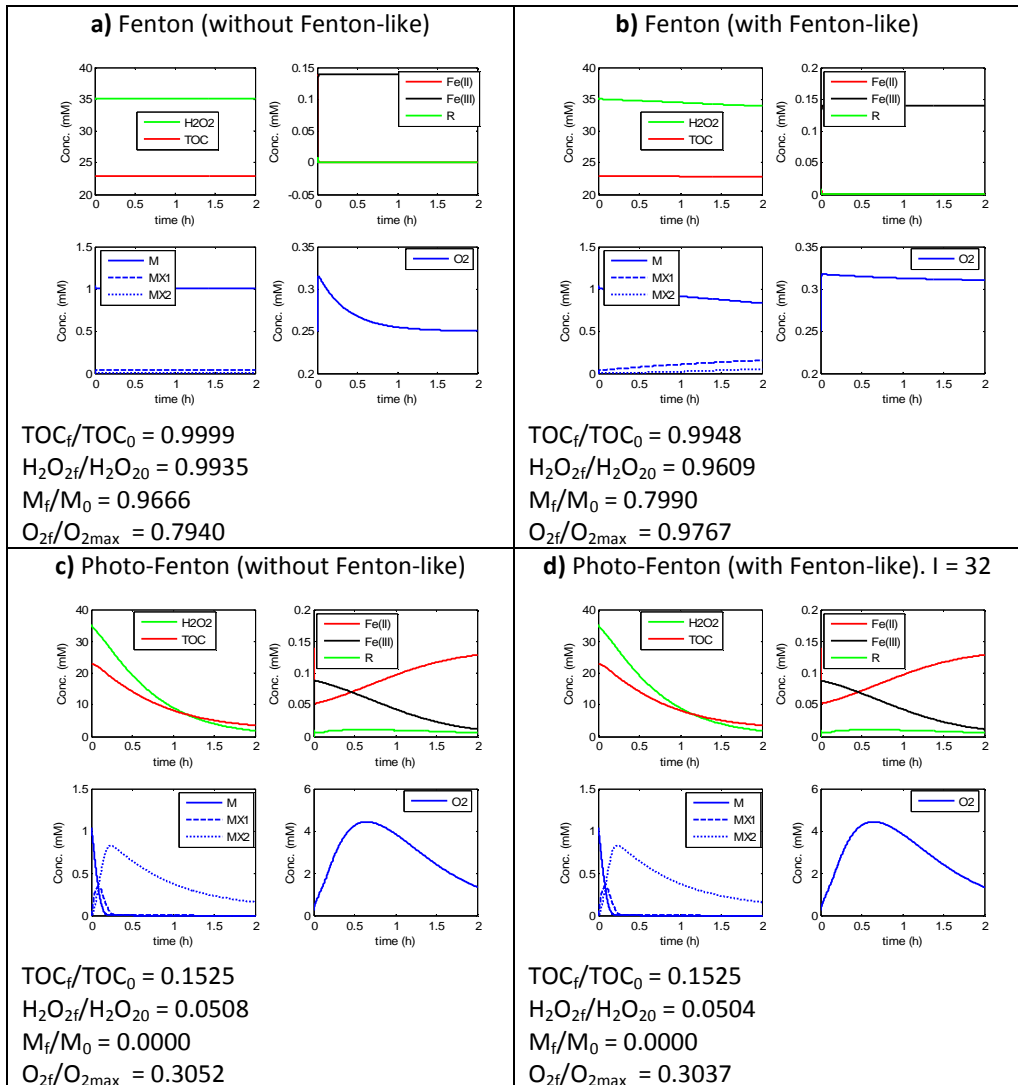


Figure 8.8. Fenton and photo-Fenton process simulation for TC base case 1

Finally, it is possible to predict the evolution of the most important parameters in Fenton and photo-Fenton process, such as the concentrations of

TOC, H<sub>2</sub>O<sub>2</sub>, contaminant and O<sub>2</sub>, which are the variables most commonly measured in facilities at laboratory, pilot or industrial scale. The availability of experimental data would allow the adjustment of the model to each particular case.

## 8.2. Dosage protocol model

As it was already mentioned in previous chapters, the dosage of reagents in Fenton and photo-Fenton processes is commonly addressed in a unique load at the beginning of the treatment. Studies have demonstrated that a high concentration of reagents, specifically of H<sub>2</sub>O<sub>2</sub> at the first stages of the process can lead to a misuse and waste of hydroxyl radicals by favoring their recombination and their reaction with H<sub>2</sub>O<sub>2</sub> (eq. 8.4 and 8.3, respectively). (e.g. Gulkaya et al., 2006; Huston and Pignatello, 1999; Pignatello et al., 2006)

Some of the most recent works have been devoted to identify the benefits of dosing the reagents along the process span, in order to achieve a more efficient degradation and mineralization with lower reagent doses. Some of these works involve batch-wise dosage (e.g. Chu et al., 2007) and some others propose a continuous flow of the reagent (e.g. Zazo et al., 2009). The systematic dosage protocol proposed by Yamal-Turbay et al. (2012) was presented in Chapter IV and its experimental applications are available in Chapters V and VI.

A continuous stepwise flow ( $F_w(t)$ ) can be represented as the summa of  $N$  successive differential inlets of fluid during a dosage time ( $\Delta t_i$ ):

$$F_w(t) = \frac{dv_D(t)}{dt} = \sum_{i=0}^N m_i X_{\Delta t_i}(t) \quad (8.28)$$

where

$$X_{\Delta t_i}(t) = \begin{cases} 0 & \text{if } t \in \Delta T_i \\ 1 & \text{if } t \ni \Delta T_i \end{cases}$$

Being

$$\Delta T_i \cap \Delta T_j = \emptyset \quad \forall_{i \neq j}$$

$$\Delta T_i = (t_i^{ini}, t_i^{fin}] = (t_i^{ini}, t_i^{ini} + t_i^{add}]$$

Hence, if a first inlet of fluid is made at  $t=0$ , namely  $v_D^0$ , the volume dosed at time  $t$  ( $v_D(t)$ ) is:

$$\begin{aligned} v_D(t) &= v_D^0 + \int_0^t F_w(t) dt \\ &= v_D^0 + \sum_{i=0}^N \int_{\min\{t; t_i^{ini}\}}^{\min\{t; t_i^{ini} + t_i^{add}\}} m_i (t_i^{ini} + t_i^{add} - t_i^{ini}) dt \end{aligned} \quad (8.29)$$

Particularly, for  $N=1$ , the volume added by the end of the process ( $v_D^\infty$ ) is:



$$v_D^\infty = v_D^0 + m_i t_i^{add}, \quad v_D(t) = \begin{cases} 0 \\ v_0 \\ v_0 + m_1 \end{cases} \quad (8.30)$$

Considering that the volume dosed ( $v_D^\infty$ ) is much lower than total system volume ( $V_T$ ), a term  $C_{eq,\infty}^{H_2O_2}$  (it would be the initial concentration of the reagent if it was totally added at  $t=0$ ) would be:

$$C_{eq,\infty}^{H_2O_2} = \frac{Q^{H_2O_2}}{(V_T + v_D^\infty)} = \frac{v_D^\infty P}{(V_T + v_D^\infty)} \cong \frac{v_D^\infty P}{V_T} \quad (8.31)$$

Where  $Q^{H_2O_2}$  is the total amount of  $H_2O_2$  to be dosed during the treatment span (mol) and  $P$  is the purity of the  $H_2O_2$  dosed.

Substituting eq. X.30 in eq. X.31:

$$\frac{V_T C_{eq,\infty}^{H_2O_2}}{P} = v_D^0 + m_i t_i^{add} \quad (8.32)$$

$$m_i \cdot t_i^{add} = \frac{V_T C_{eq,\infty}^{H_2O_2}}{P} - v_D^0$$

$$m = \left( \frac{V_T C_{eq,\infty}^{H_2O_2}}{P} - v_D^0 \right) \left( \frac{1}{t^{add}} \right)$$

Being

$$v_D(t) = \begin{cases} v_D^0 & \text{if } t < t^{ini} \\ v_D^0 + m(t - t^{ini}) & \text{if } t^{ini} \leq t < t^{fin} \\ v_D^\infty & \text{if } t \geq t^{fin} \end{cases} \quad (8.33)$$

If  $y(t) = \frac{v_D(t)}{v_D^\infty}$  is a fraction of the total volume of  $H_2O_2$  to be dosed at time  $t$ , eq. X.33 can be written as, and being  $Q^{H_2O_2}$ ,  $C_{eq,\infty}^{H_2O_2}$ ,  $v_D^\infty$  fixed, the way in which  $H_2O_2$  it is dosed along the time is modeled and parameterized as follows:

$$y(t) = \frac{v_D(t)}{v_D^\infty} = \begin{cases} 0 & \text{if } t < 0 \\ y_0 & \text{if } 0 \leq t < t_{ini} \\ y_0 + \left( \frac{1-y_0}{\Delta t_{add}} \right) (t - t_{ini}) & \text{if } t_{ini} \leq t < t_{ini} + \Delta t_{add} \\ 1 & \text{if } t_{ini} + \Delta t_{add} \leq t < TS \end{cases} \quad (8.34)$$

where  $y(t)$  is the fraction of the total addition that is fulfilled at time  $t$  and  $\Delta t_{add}$  is the time increment corresponding to the dosage duration.

Therefore, the proposed dosage protocol consists of an initial release  $y_0$  (kick-off) and a constant inflow  $m = f(y_0, \Delta t_{add})$  during the time interval  $[t_{ini}, t_{ini} + \Delta t_{add})$  and constrained within the treatment span  $TS$ . Figure 5.3 (Chapter V) illustrates this dosing procedure and its governing factors.

This dosage can be modeled as an additional term in the mass balance of  $H_2O_2$ , as follows:

$$\frac{d[H_2O_2]}{dt} = -r_1 - r_3 - r_{10} + v_D(t)/V_R \quad (8.22b)$$

### 8.2.1. Simulation of the dosage protocol

As an example, the dosage protocol is simulated using the conditions corresponding to PCT base case 1 for Fenton and photo-Fenton processes. Two different combinations of dosage parameters are used for this aim:

- a)  $y_0 = 0\%$ ;  $\Delta t_{add} = 1h$ ,  $t_{ini} = 15$  min.
  - b)  $y_0 = 20\%$ ;  $\Delta t_{add} = 1h$ ,  $t_{ini} = 15$  min.
- a) Base case 1 with dosage protocol:  $y_0 = 0\%$ ;  $\Delta t_{add} = 1h$ ,  $t_{ini} = 15$  min

Figure 8.8 shows Fenton process behavior with the dosage protocol is applied. Fenton-like reaction is included in this model. In both cases, no mineralization or degradation occur until  $H_2O_2$  is added to the system. When dosage starts at minute 15,  $H_2O_2$  concentration increases and TOC reduces (slowly when no irradiation is present). The increment of  $H_2O_2$  concentration is constant in Fenton process, but photo-Fenton exhibits a different trend, as  $H_2O_2$  consumes to degrade PCT and its intermediates. In photo-Fenton process, residual TOC is due to the residual concentration of MX2. Fe(II), Fe(III), R and  $O_2$  concentrations evolve as expected.

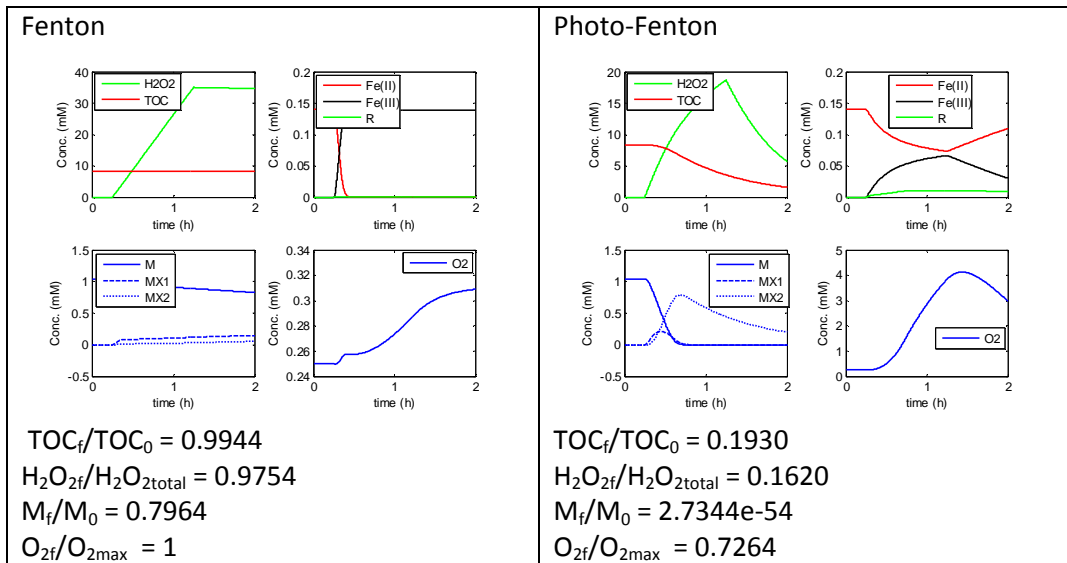


Figure 8.9. Simulation of Fenton and photo-Fenton processes when dosage protocol is applied:  $y_0 = 0\%$ ;  $\Delta t_{add} = 1h$ ,  $t_{ini} = 15$  min.

In contrast with base case 1 when no dosage protocol is applied (Fig. 8.2), the dosage protocol presented in Fig. 8.9 does not improve but worsens the quality of the effluent, achieving 80.7% TOC reduction while no dosage leads to 84.75%

mineralization. A more convenient adjustment of the dosage protocol parameters is necessary in order to obtain better results. Normally, an initial dose of  $\text{H}_2\text{O}_2$  or “kick-off” is needed to the generation of radicals and the initiation of the process. The dosage protocol does not seem to affect contaminant elimination of mineralization by Fenton process behavior.

a) Base case 1 with dosage protocol:  $y_0 = 20\%$ ;  $\Delta t_{add} = 1\text{h}$ ,  $t_{ini} = 15\text{min}$

Figure 8.10 shows the results for this case. As there is no lack of  $\text{H}_2\text{O}_2$  during the first stages of the process, evolution of TOC, M, MX1 and MX2 is similar that base case 1, but the lower  $\text{H}_2\text{O}_2$  concentrations lead to a slower degradation of PCT and its intermediates, but almost 1 percent point TOC reduction improvement is achieved, which confirms the advantage of providing an initial dose of  $\text{H}_2\text{O}_2$ . Fe(II), Fe(III) and  $\text{O}_2$  behave differently from base case 1, conditioned by the lower concentrations of  $\text{H}_2\text{O}_2$ . As in the previous case, neither contaminant remediation nor mineralization by Fenton process seem to be affected by the application of the dosage protocol.

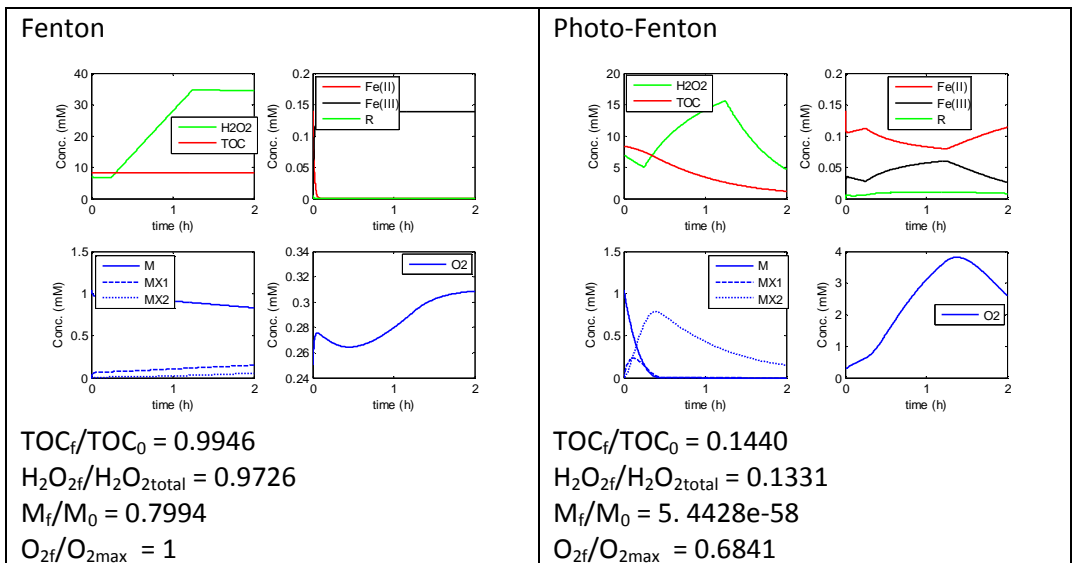


Figure 8.10. Simulation of Fenton and photo-Fenton processes when dosage protocol is applied:  $y_0 = 20\%$ ;  $\Delta t_{add} = 1\text{h}$ ,  $t_{ini} = 15\text{min}$ .

### 8.3. Simulation code

The simulation tool consists in a Matlab® *m*-file which receives information from a Microsoft Excel® worksheet and save the results as *m* files, represents graphically the results and sends some of them to another Excel® worksheet. ODE45 function was used to solve the differential equation system.

The code of the simulation tool is presented next:

```

function [t,y] = model_Fenton_xls(k)
tic
clc
clear all
%% Variables statement
kla = 2.7; %1/h
Osat= 0.25; %mM
tspans = 0:0.001:2;
VT = xlsread('data','Hojal','D15'); %Total volume to be degraded, L
I = xlsread('data','Hojal','D26'); %Light intensity, W
k = xlsread('data','Hojal','D2:D14'); %Kinetic constants, 1/(mM h)
tinimin = xlsread('data','Hojal','D29'); %Time at which continuous dosage
starts, min
tini = tinimin/60; %h
Dtaddmin = xlsread('data','Hojal','D28'); %Total continuous dosage time, min
Dtadd = Dtaddmin/60; %h
pctg0 = xlsread('data','Hojal','D27'); %Initial fraction of total H2O2 dose
H2O20 = xlsread('data','Hojal','D16'); %Equivalent H2O2 concentration, mM
H2O2total = H2O20*VT; %Total H2O2 to be dosed, mol
y0 = xlsread('data','Hojal','D17:D24'); %Initial concentrations, mM
n = xlsread('data','Hojal','D30'); %Number of atoms of carbon in M

%% Solving mass balances
[ts,y]=ode45(@modelfff,tspans,y0);
function dy = modelfff(t,y)
    fe2s = y(1);
    fe3s = y(2);
    H2O2s = y(3);
    Rs = y(4);
    Ms = y(5);
    MX1s = y(6);
    MX2s = y(7);
    O2s = y(8);
    TOCs = n*(Ms + MX1s + MX2s);
    y(:,9) = TOCs(:);
    %mass balances
    r1 = k(1) * fe2s * H2O2s;
    r2 = k(2) * fe3s;
    r3 = k(3) * Rs * H2O2s;
    r4 = k(4) * Rs * Rs;
    r5 = k(5) * Ms * Rs * O2s;
    r6 = k(6) * Ms * Rs;
    r7 = k(7) * MX1s * Rs;
    r8 = k(8) * MX1s * Rs;
    r9 = k(9) * MX2s * Rs;
    r10 = k(13) * fe3s * H2O2s;
    if t<tini
        FH = 0;
    elseif tini<=t && t<tini+Dtadd
        FH = (1-pctg0)* H2O2total/Dtadd;
    elseif t>=(tini + Dtadd)
        FH = 0;
    end
    %differential equations
    dy(1,1) = -r1 + r2 + r10;
    dy(2,1) = r1 - r2 - r10;
    dy(3,1) = -r1 - r3 - r10 + FH/VT;
    dy(4,1) = r1 + r2 - r3 - 2 * r4 - r5 - r6 - r7 - r8 - r9 + r10;
    dy(5,1) = -r5 - r6;
    dy(6,1) = r5 + r6 - r7 - r8;
    dy(7,1) = r7 - r9;
    dy(8,1) = (k(10) * r3) + (k(11) * r4) - (k(12) * r5) + (kla * (Osat-O2s));
end
fe2s = y(:,1);          fe2sN = fe2s/max(fe2s);
fe3s = y(:,2);          fe3sN = fe3s/max(fe3s);

```

```

H2O2s = y(:,3);          H2O2sN = H2O2s*15/H2O2total;
Rs = y(:,4);           RsN = Rs/max(Rs);
Ms = y(:,5);           MsN = Ms/Ms(1);
MX1s = y(:,6);        MX1sN = MX1s/max(MX1s);
MX2s = y(:,7);        MX2sN = MX2s/max(MX2s);
O2s = y(:,8);         O2sN = O2s/max(O2s);
TOCs = n*(Ms + MX1s + MX2s);  TOCsN = TOCs/TOCs(1);
y(:,9) = TOCs(:);
%% Figures construction
figure(2)
subplot(2,2,1);
plot(ts,H2O2s,'-g',ts,TOCs,'-r','linewidth',1.5);
leg = legend('H2O2','TOC'); set (leg,'location','Best');
xlabel('time (h)'); ylabel('Conc. (mM)');
subplot(2,2,2);
plot(ts,fe2s,'-r',ts,fe3s,'-k',ts,Rs,'-g','linewidth',1.5);
leg1 = legend('Fe(II)','Fe(III)','R'); set (leg1,'location','Best');
xlabel('time (h)'); ylabel('Conc. (mM)');
subplot(2,2,3);
plot(ts,Ms,'-b',ts,MX1s,'--b',ts,MX2s,':b','linewidth',1.5);
leg1 = legend('M','MX1','MX2'); set (leg1,'location','Best','fontsize',10);
xlabel('time (h)'); ylabel('Conc. (mM)');
subplot(2,2,4);
plot(ts,O2s,'linewidth',1.5);
leg2 = legend('O2'); set (leg2,'location','Best');
xlabel('time (h)'); ylabel('Conc. (mM)');
%% Saving yexp file (each 0.1hour) and data file (all data)
data = y;
yexp(:,1) = 0:0.1:2; yexp(1,2) = TOCs(1); yexp(1,3) = H2O2s(1);
yexp(1,4) = Ms(1); yexp(1,5) = O2s(1);
for i=1:20;
    j = i*100+1; i = i+1;
    yexp(i,2) = y(j,9); yexp(i,3) = y(j,3);
    yexp(i,4) = y(j,5); yexp(i,5) = y(j,8);
end
save yexp; xlswrite('results1',yexp,'Hojal','B2'); save data;
toc
end

```

## 8.4. Parameter adjustment

With the aim to evaluate the feasibility of the model to represent a real situation, a parameter adjustment was performed using the experimental data obtained from the experiment PCT\_40\_5\_1899\_ON (the design of experiments used for the characterization of PCT degradation was already explained in detail in Chapter IV), which corresponds to the degradation of 15 L of a 40 mg L<sup>-1</sup> (0.2441 mM) PCT sample in the pilot plant, with an initial concentration of 5 mg L<sup>-1</sup> Fe(II) (0.0895 mM) and 189 mg L<sup>-1</sup> H<sub>2</sub>O<sub>2</sub> (5.5588 mM) and a lamp irradiating at 32 W.

The adjustment was performed using off-line data measured at regular time intervals during a 2 h time span. TOC, H<sub>2</sub>O<sub>2</sub> and PCT concentration data were available and were used for that purpose.

Figure 8.11 shows the results, and the obtained coefficients of determination ( $R^2$ ) demonstrate very good approximations of the simulated values (continuous lines) with the experimental data (dots) for the three studied variables. In the case of TOC concentration, it is evident that the model is capable to predict the delay in the TOC response during the first minutes of the treatment, as the partially

oxidized intermediates are still present in the reaction mixture even when the pattern contaminant is totally degraded. It is also important to note that TOC concentration remains constant after the exhaustion of  $\text{H}_2\text{O}_2$ .

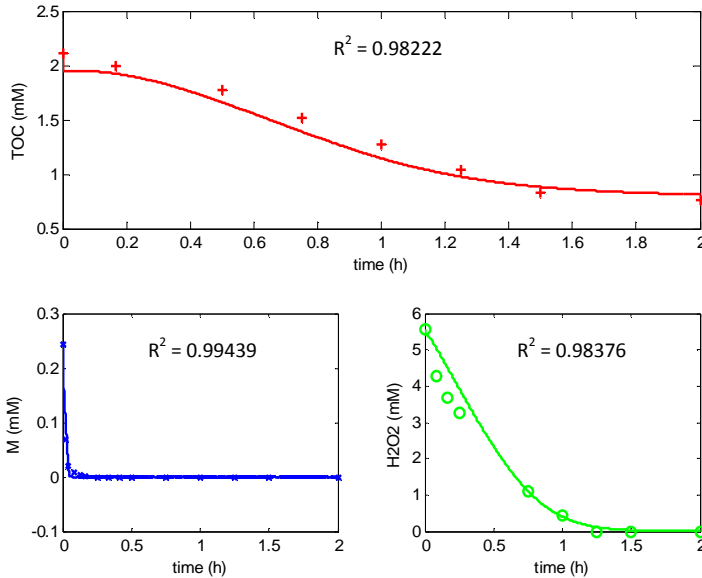


Figure 8.11. Parameter adjustment performed with the available experimental data. Continuous lines: simulated variables. Dots: experimental data

Table 8.3 presents the values of the resulting model parameters obtained with the adjustment.

Table 8.3. Kinetic parameters obtained by adjustment with experimental data

	$k_1$	$k_2$	$k_3$	$k_4$	$k_5$	$k_6$	$k_7$	$k_8$	$k_9$	$g_1$	$g_2$	$C_1$
	$\text{mM}^{-1} \text{h}^{-1}$									Dimensionless		
Value	56.47	33.96	376.8	42799.9	2680.6	307.3	2881.6	0.075	166.7	2316.8	2312.8	295.6

A lot of work is still necessary to obtain an adjusted model for a wide range of operational conditions. A set of kinetic parameters would be obtained for each contaminant at the different reactor configurations/geometry and irradiation sources.

## 8.5. Conclusions

The previously published model by Cabrera Reina et al. (2012) to represent Fenton and photo-Fenton kinetics is applied and modified to simulate the operation of the process and the evolution of the concentration of reagents and products. The original model involves ten kinetic constants and three stoichiometric coefficients and it properly represents the concentration of reagents and products, namely

Fe(II), Fe(III), H<sub>2</sub>O<sub>2</sub>, contaminant (M), two generic intermediates (MX1 and MX2), radicals (R) and dissolved oxygen (O<sub>2</sub>). The dosage protocol proposed in this thesis is also modeled and furtherly incorporated to the simulation.

The simulations show the effect of the parameters of the dosage protocol, which need to be adjusted in order to improve process behavior, otherwise process efficiency can be diminished and the requirement of reagents and therefore, operational costs, can be increased. For that aim, the next chapter investigates the opportunities to optimize operational cost by a most efficient usage of reagents when the dosage parameters are properly tuned.

## 8.6. References

- Cabrera Reina, A., Santos-Juanes, L., García, J.L., Casas, J.L., Sánchez, J.S. 2012. Modelling photo-Fenton process for organic matter mineralization, H<sub>2</sub>O<sub>2</sub> consumption and dissolved oxygen evolution, *Appl. Catal. B.* 119-120, 132.
- Chu, W.; Chan, K.H.; Kwan, C.Y.; Choi, K.Y. 2007. Degradation of atrazine by modified stepwise-Fenton's processes. *Chemosphere* 67, 755.
- Farias, J., Albizzati, E.D., Alfano, O.M. 2009. Kinetic study of the photo-Fenton degradation of formic acid. Combined effects of temperature and iron concentration. *Catal. Today* 144, 117.
- Gulkaya, I.; Surucu, A.; Dilek, F. 2006. Importance of H<sub>2</sub>O<sub>2</sub>/Fe<sup>+2</sup> ratio in Fenton's treatment of a carpet dyeing wastewater. *J. Hazard. Mater. B.* 136, 763.
- Huston, P.L.; Pignatello, J.J. 1999. Degradation of selected pesticide active ingredients and commercial formulations in water by the photo-assisted Fenton reaction. *Water Res* 33(5), 1238-1246.
- Küsič, H., Koprivanac, N., Bozic, A.L., Selanec, I. 2006. Photo-assisted Fenton type processes for the degradation of phenol: A kinetic study. *J. Hazard. Mater.* 136, 632.
- Pignatello, J.J.; Oliveros, E.; MacKay, A. 2006. Advanced Oxidation Processes for Organic Contaminant Destruction Based on the Fenton Reaction and Related Chemistry, *Crit Rev Environ Sci Technol* 36(1), 1-84.
- Rossetti, G.H., Albizzati, E.D., Alfano, O.M. 2002. Decomposition of Formic Acid in a Water Solution Employing the Photo-Fenton Reaction. *Ind. Eng. Chem. Res.* 41, 1436.
- Yamal-Turbay, E.; Graells, M.; Pérez-Moya, M. 2012. Systematic Assessment of the Influence of Hydrogen Peroxide Dosage on Caffeine Degradation by photo-Fenton Process. *Ind Eng Chem Res* 51(13), 4770-4778.
- Zazo, J.A.; Casas, J.A.; Mohedano, A.F.; Rodríguez, J.J. 2009. Semicontinuous Fenton oxidation of phenol in aqueous solution. A kinetic study. *Water Res.* 43, 4063.





## **Chapter IX**

### **Optimization of the Batch Process Recipe**

This chapter explores the opportunities to optimize the processing conditions and the operation time of batch Fenton and photo-Fenton processes. The optimization tools and strategy, as well as the results of the study are next presented.



## 9.1. Introduction

The term mathematical optimization (optimization or mathematical programming) refers to the selection of the best combination of variables from a set of alternatives. In the most general way, an optimization problem consists in maximizing or minimizing a mathematical function subject to a set of constraints. According to Edgar et al. (2001), "optimization is the use of specific methods to determine the most cost-effective and efficient solution to a problem or design for a process".

An optimization problem can be expressed as follows:

$$\begin{array}{ll}
 \underset{x}{\text{minimize}} & f(x) \quad \text{(the objective function)} \\
 \text{subject to} & \\
 h(x) = 0 & \text{(equality constraints)} \\
 g(x) \leq 0 & \text{(inequality constraints)}
 \end{array} \quad \left. \vphantom{\begin{array}{l} \\ \\ \\ \end{array}} \right\} \quad (9.1)$$

where  $x$  is a vector of  $n$  variables,  $h(x)$  is a vector of  $m_1$  equations and  $g(x)$  is a vector of  $m_2$  inequalities, being the total number of constraints ( $m$ ) equal to  $m_1+m_2$ .

$h(x)$  and  $g(x)$  are the mathematical model which represents the phenomenon under study and can be based on physical and chemical laws or be strictly empirical.

The problem of batch process recipe design can be formulated as a dynamic optimization problem as the material balances in the batch reactor compose a differential-algebraic equations (DAE) system which was already described in the previous chapter.

## 9.2. Problem statement

Photo-Fenton process can be used to simply reduce the concentration of a given contaminant from the effluent or to achieve its total mineralization. Depending on the final use to be given to the effluent, the treatment will be stop at different operation time, when the required effluent quality is achieved. Total mineralization of the waste might imply higher operational costs because of longer operational times and higher reagent loads.

Given the quality of the sample to be treated, the required final specifications of the effluent and the operational restrictions of the plant, the minimization of the operational cost will depend on the operation time and the reagent doses to be provided. The parameters concerning the dosage protocol can also be adjusted to minimize reagent consumption and indeed operational cost. The goal of this proposal is to determine the batch process recipe which minimizes the operational cost.

### 9.3. Optimization model

The problem can be formulated as a dynamic optimization model, as the material balances in the reactor (Chapter VIII) involve a differential-algebraic equations (DAE) system. The objective of the optimization is basically to drive the process to a minimum processing cost while fulfilling a set of environmental and technical constraints.

The objective function to be minimized ( $\xi$ ) includes the cost of reagents (Fe(II) and H<sub>2</sub>O<sub>2</sub>) and the cost of the electricity consumed by the lamp and can be written as follows:

$$\begin{aligned}\xi &= \text{Cost}_{\text{Fe}^{2+}} + \text{Cost}_{\text{H}_2\text{O}_2} + \text{Cost}_e = \\ &= p_{\text{Fe(II)}} C_0^{\text{Fe(II)}} V_R + p_{\text{H}_2\text{O}_2} (C_0^{\text{H}_2\text{O}_2} V_R + \int q_{\text{H}_2\text{O}_2} dt) + p_e I A_w t_{\text{end}}\end{aligned}\quad (9.2)$$

where:

$p_{\text{Fe(II)}}$ ,  $p_{\text{H}_2\text{O}_2}$ ,  $p_e$  are the prices for raw materials and electricity, respectively,  
 $C_0^{\text{Fe(II)}}$  and  $C_0^{\text{H}_2\text{O}_2}$  are the initial concentrations of Fe(II) and H<sub>2</sub>O<sub>2</sub>, respectively,  
 $V_R$  is the reaction volume (set at 15 L),

$q_{\text{H}_2\text{O}_2}(t)$  is the input flow of H<sub>2</sub>O<sub>2</sub> along dosage time, when H<sub>2</sub>O<sub>2</sub> is dosed according to the dosage protocol presented in Chapter V,

$I$  is the electrical power of the lamp (set at 36 W),

$A_w$  is the irradiation surface (set at 285.9 cm<sup>2</sup>) and

$t_{\text{end}}$  is the processing time.

It is considered an available and operative plant, so the installation of new equipment elements and investment cost contributions are not included in the objective function (Eq. 9.7).

The problem is subject to the material balance equations described in Chapter VIII (Eq. 8.10, 8.20a to 8.23a and 8.24 to 8.27) and to the required quality of the final effluent which were established as final contaminant and TOC concentrations to be less than a maximum fraction of the initial values:

$$C^{\text{Cont}}(t_{\text{end}}) / C^{\text{Cont}}(t_0) \leq X_{\text{max}}^{\text{Cont}} \quad (9.3)$$

$$C^{\text{TOC}}(t_{\text{end}}) / C^{\text{TOC}}(t_0) \leq X_{\text{max}}^{\text{TOC}} \quad (9.4)$$

The decision variables are the initial concentrations of Fe(II) and H<sub>2</sub>O<sub>2</sub> ( $C_0^{\text{Fe(II)}}$  and  $C_0^{\text{H}_2\text{O}_2}$ , respectively). The boundaries of the decision variables are defined as:

$0 \leq C_0^{\text{Fe(II)}} \leq 0.179 \text{ mmol L}^{-1}$ , which also satisfies the legal iron concentration allowed in effluents (DOGC).

$$0 \leq C_0^{\text{H}_2\text{O}_2} \leq 45 \text{ mmol L}^{-1}.$$

The available processing time ( $t_{end}$ ) is selected beforehand and corresponds to the maximum time horizon in the optimization model. This will be explained in the next sub-section.

Inequalities with process variables, such as the constraints for the final PCT and TOC concentrations (Eq. 9.3 and 9.4), are transformed into penalization terms for the objective function (Eq. 9.7). This strategy is used in the implementations in Matlab, which otherwise require special tool-packages to fulfill these restrictions. Eq.9.3 and 9.4 are transformed into the following quadratic penalty function:

$$Pen_{Cont} = CP (C^{Cont}(t_{end})/C^{Cont}(t_0) - X_{max}^{Cont})^2 \quad (9.5)$$

$$Pen_{TOC} = CP (C^{TOC}(t_{end})/C^{TOC}(t_0) - X_{max}^{TOC})^2 \quad (9.6)$$

where CP is a weighting factor. The objective function is finally written as follows:

$$\xi = p_{Fe(II)} C_0^{Fe(II)} V_R + p_{H_2O_2} (C_0^{H_2O_2} V_R + \int q_{H_2O_2} dt) + p_\epsilon I A_w t_{end} + Pen_{Cont} + Pen_{TOC} \quad (9.7)$$

A base case study considering PCT as a contaminant at an initial concentration of 0.52 mM was undertaken, equivalent to an initial TOC concentration of 4.16 mM, with initial concentrations of reagents ( $H_2O_2$  and Fe(II)) set at 8.82 mM and 0.14 mM, respectively. Table 9.1 presents the data used for the simulation of the base case and the estimated cost of reagents and electricity used for the whole study. Under these conditions and without the application of any optimization, the processing cost for a time horizon of 2 h is  $44.57 \times 10^{-2}$  €.

Table 9.1. Case base definition

Parameter (units)	Value
$C_0^{PCT}$ (mM)	0.52
$C_0^{TOC}$ (mM)	4.16
$C_0^{H_2O_2}$ (mM)	8.82
$C_0^{Fe(II)}$ (mM)	0.14
$p_{Fe(II)}$ (€/mmol)	0.012622
$p_{H_2O_2}$ (€/mmol)	0.003167
$p_\epsilon$ (€/kWh)	0.145578

### 9.3.1. Optimization tools

#### 9.3.1.1. Pareto frontier for cost function $\xi$ versus processing time, $t_{end}$

The processing time  $t_{end}$  only appears in the objective function (Eq. 9.7) related to the electricity cost contribution ( $Cost_\epsilon$ ). However,  $t_{end}$  is a decision variable that indirectly affects  $\xi$  dramatically: an increase of  $t_{end}$  leads to a reduction of reagents consumption and, consequently, a reduction of  $Cost_{Fe^{2+}}$  and  $Cost_{H_2O_2}$ . Therefore, its value will tend to the upper bound in the optimal solution.

In order to elucidate the trade-off between the cost and processing time, the Pareto frontier is first constructed. For that aim, the objective function (Eq. 9.7) is minimized with different upper bounds for the processing time:

$$t_{end}^U \in \{0.7h, \dots, 10h\}.$$

In this step, the initial conditions  $C_0^{Fe(II)}$  and  $C_0^{H2O2}$  are the decision variables and the optimization of dynamic profile along time is not necessary in this case, but only continuous variables in initial time point should be optimized. Then, the optimization problem is solved as a direct-sequential approach in Matlab, with no discretization or characterization of the dosage profile  $q_{H2O2}$ , which is fixed to zero.

The Pareto frontier for the cost function  $\xi$  versus processing time  $t_{end}$  obtained through the process recipe optimization with no dosage is presented in Figure 9.1 for  $X_{max}^{PCT}=0.001$  and  $X_{max}^{TOC}=0.1$ . Table 9.2 presents the general results, including TOC and PCT degradations achieved at  $t_{end}$  ( $X_{t_{end}}^{TOC}$  and  $X_{t_{end}}^{PCT}$ , respectively), time to achieve  $X_{max}^{TOC}$  ( $t_{TOC}$ ) and  $X_{max}^{PCT}$  ( $t_{PCT}$ ) and cost of each reagent and electricity, as well as the corresponding penalizations.

Table 9.2. Optimum operational cost for different time horizons when no dosage protocol is applied

$t_{end}$ (h)	10.00	7.50	5.00	4.00	3.00	2.00	1.50	1.00	0.75	0.70
$C_0^{H2O2}$ (mM)	1.2885	1.3108	1.2936	1.3170	1.3178	1.3757	1.5511	2.4589	5.2388	9.1478
$C_0^{Fe(II)}$ (mM)	0.036	0.047	0.073	0.087	0.117	0.162	0.179	0.179	0.179	0.179
$X_{t_{end}}^{TOC}$ (%)	90.02	90.10	90.05	90.08	90.10	90.08	90.09	90.06	90.08	90.08
$t_{TOC}$ (h)	9.98	7.44	4.98	3.97	2.98	1.99	1.49	1.00	0.75	0.70
$X_{t_{end}}^{PCT}$ (%)	100.00	100.00	100.00	100.00	100.00	100.00	100.00	100.00	99.99	99.99
$t_{PCT}$ (h)	2.34	1.79	1.17	0.96	0.72	0.50	0.39	0.25	0.14	0.10
$\xi \times 10^2$ (€)	6.97	7.18	7.59	7.95	8.51	9.62	10.77	15.10	28.29	47.26
$Cost_{Fe2+} \times 10^2$ (€)	0.69	0.89	1.38	1.65	2.22	3.06	3.39	3.39	3.39	3.39
$Cost_{H2O2} \times 10^2$ (€)	6.12	6.23	6.15	6.26	6.26	6.54	7.37	11.68	24.89	43.46
$Cost_e \times 10^2$ (€)	0.09	0.07	0.05	0.04	0.03	0.02	0.01	0.01	0.01	0.01
Penalization TOC $\times 10^2$ (€)	0.06	0.00	0.02	0.00	0.00	0.00	0.00	0.02	0.01	0.40
Penalization PCT $\times 10^2$ (€)	0.00	0.00	0.00	0.00	0.00	0.00	0.00	0.00	0.00	0.00

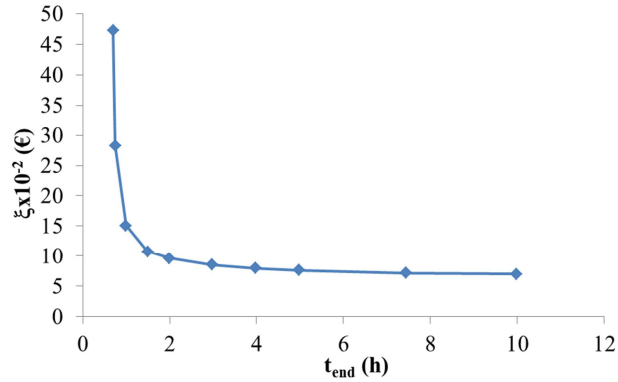


Figure 9.1. Pareto frontier for cost function  $\xi$  versus processing time  $t_{end}$  (no dosage is considered) for  $X_{max}^{TOC} = 0.1$  and  $X_{max}^{PCT} = 0.001$ .

The most critical trade-offs are obtained between 0.7 h and 3h. At lower final times, the TOC elimination of 90% is not achieved. Upper final times do not affect to the reactant consumption, and processing cost tends to  $6.98 \times 10^{-2}$  € per batch. Thus, a processing time of 2 hours is selected, with a treatment cost of  $9.62 \times 10^{-2}$  € per batch. Although the PCT and TOC elimination can be achieved at lower processing times, the interest was set on reducing the cost at the expense of extending the reactor occupation.

### 9.3.1.2. Dosage profile $qH_2O_2$ optimization for a given time horizon.

Once the processing time  $t_{end}$  has been selected, the dynamic profile of  $H_2O_2$  addition rate is optimized, together with  $C_0^{Fe(III)}$  and  $C_0^{H_2O_2}$ . The dosage protocol proposed by Yamal-Turbay et al (2012) is first used.

This dosage protocol was already described in Chapter V (Fig. 5.3) and it consists of an initial load of reagent, and a constant addition of the remaining during a specific time interval (Yamal-Turbay et al., 2012). The addition profile is characterized by the total amount of  $H_2O_2$  ( $Q^{H_2O_2}$ ), the fraction of total reagent that is completed at initial time  $t_0$  ( $y_0$ ), the starting time of the dosage ( $t_{ini}$ ), and the continuous dosage span ( $\Delta t_{add}$ ). The dosage protocol is a particularization of a piece-wise control (PWC) profile with two single step functions: to start and to stop the reagent addition. The dosage protocol results in an optimization problem with continuous time-independent control variables ( $Q^{H_2O_2}$ ,  $y_0$ ,  $t_{ini}$ , and  $\Delta t_{add}$ ) characterizing a dynamic profile, without a discretization of control variables, which is solved by a direct-sequential approach in Matlab.

A 3.3% reduction of the processing cost is obtained, from  $9.62 \times 10^{-2}$  € to  $9.30 \times 10^{-2}$  € per batch, respectively, when optimal solution (without applying the dosage protocol) is improved with the appropriate combination of dosage protocols variables. The improvement related to the base case is given in Table

9.3, along with other key indicators of the process. In addition, the corresponding profiles are presented at Figure 9.2 for each case.

Table 9.3. Key performance indicators (KPIs) in the base case and optimal solutions

KPI	Base case	Optimized base case	Dosage protocol	PWC dosage Profile
Processing cost ( $10^{-2}$ €)	44.57	9.62	9.30	9.13
Processing cost reduction (%)	-	78.4a	79.1a (3.3b)	79.5a (5.1b)
Fe <sup>2+</sup> consumption (mmol)	2.100	2.459	2.425	0.268
H <sub>2</sub> O <sub>2</sub> consumption (mmol)	132.3	20.5	19.6	18.1
Time 99.9% PCT reduction (h)	0.13	0.49	0.64	0.69
Time 90% TOC reduction (h)	0.89	1.99	1.99	2.00
Final PCT elimination (%)	100	100	100	100
Final TOC elimination (%)	99.42	90.1	90.1	90.0

a: respect to base case.  
b: respect to no dosage

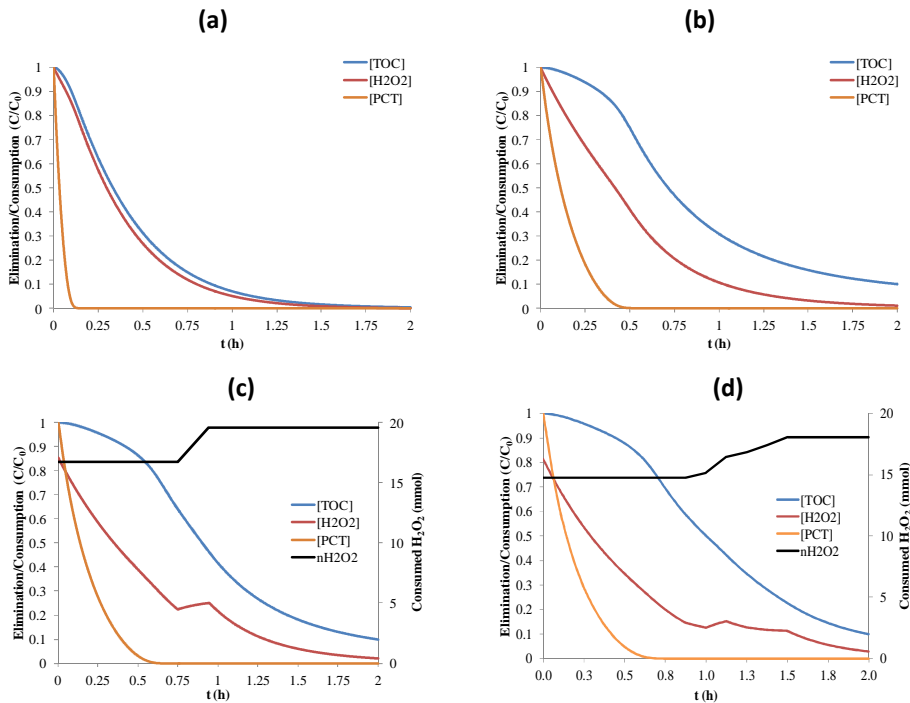


Figure 9.2. Control ( $q_{H_2O_2}$ ) and process (normalized  $C_{TOC}$ ,  $C_{H_2O_2}$  and  $C_{PCT}$ ) variable profiles: **(a)** base case, **(b)** optimal solution with no dosage, **(c)** with dosage protocol, **(d)** with PWC strategy

Another approach was proposed by Moreno-Benito et al. (2013) and it considers the transformation of the problem into a dynamic optimization (DO), where dosage is characterized by the discretization of  $q_{H_2O_2}(t)$  into a finite number of intervals. A direct-simultaneous strategy is used by discretizing the corresponding DAE system and the process and control variables to obtain a non-



linear programming (NLP) model to be optimized. Orthogonal collocation in finite elements (Čižniar et al., 2005) is used in the discretization step. Particularly, sixteen finite elements and three collocation points calculated through shifted Legendre roots are used. The obtained NLP is solved using GAMS/CONOPT. The result of this proposal is presented in Figure 9.2d and it leads to a total processing cost of  $9.13 \times 10^{-2}$  € per batch, which implies an additional cost reduction of 1.8% with respect to dosage protocol.

## 9.4. Conclusions

The model-based recipe optimization to define batch processing strategies ( $\text{H}_2\text{O}_2$  dosage, reagent doses and processing time) is presented as a promising approach for Advanced Oxidation Processes (AOPs).

The batch treatment of a contaminated model solution has been addressed as a case study where operational decisions are crucial to improve the processing and economic performance while fulfilling specific degradation targets.

The results demonstrate that the processing time is a variable of crucial influence over the processing cost (increasing the time from 0.7 to 10 hours may reduce the processing cost by 85%, from  $47.26 \cdot 10^{-2}$  to  $6.97 \cdot 10^{-2}$  € per batch), and this decision variable tends always to its upper bound.

The performance improvement attained through the dynamic optimization of  $\text{H}_2\text{O}_2$  dosage trajectory is quantitatively minor for this case (5.1% regarding the optimal solution without dosage). However, the methods introduced have shown a promising approach to the optimization of AOPs.

Future work must be undertaken for the implementation of the optimal recipes at the pilot plant scale. Hence, the effect of the irradiation source (intensity and wavelength) should be studied as a decision variable, as well as design or retrofit issues such as the equipment configuration and use of serial reactors.

## 9.5. References

Cabrera Reina, A., Santos-Juanes, L., García, J.L., Casas, J.L., Sánchez, J.S. 2012. Modelling photo-Fenton process for organic matter mineralization, hydrogen peroxide consumption and dissolved oxygen evolution, *Appl. Catal. B.* 119-120, 132.

Čižniar, M., Salhi, D., Fikar, M., Latifi, M. 2005, A MATLAB package for orthogonal collocations on finite elements in dynamic optimization, 15th Int. Conf. Process Control, June 7–10, Strbské Pleso, Slovakia.

DOGC núm. 3894, DECRET 130/2003, de 13/05/2003, (29.5.2003). (URL: <http://www.gencat.cat/diari/3894/03127147.htm>, accessed 10/08/2011).

Edgar, T.F., Himmelblau, D.M., Lasdon, L.S. 2001. Optimization of chemical processes. 2<sup>nd</sup> Edition. Mc-Graw Hill.

Moreno-Benito, M., Yamal-Turbay, E., Espuña, A., Pérez-Moya, M., Graells, M. 2013. Optimal recipe design for Paracetamol degradation by advanced oxidation processes (AOPs) in a pilot plant. Computer Aided Chemical Engineer.32, 943-948.

Yamal-Turbay, E., Graells, M., Pérez-Moya, M. 2012, Systematic Assessment of the Influence of Hydrogen Peroxide Dosage on Caffeine Degradation by the Photo-Fenton Process, Ind. Eng. Chem. Res. 51(13), 4770-4778.

## **Chapter X**

### **General Conclusions and Future Work**

This final chapter presents the general conclusions that arise from this investigation as well as some proposals for future works to be undertaken from its results and contributions.



## 10.1. Conclusions

Fenton and especially photo-Fenton processes have been confirmed to be efficient for the degradation and mineralization of pharmaceuticals (paracetamol, caffeine, tetracycline and sulfamethazine were studied in this work), especially when compared with UV irradiation,  $\text{H}_2\text{O}_2$  or  $\text{H}_2\text{O}_2/\text{UV}$  decontamination. However, specific operational conditions such as  $\text{H}_2\text{O}_2/\text{Fe(II)}$  ratio and irradiation source, among others, need to be adjusted according to the nature and concentration of the contaminant. Design of experiments was used to investigate the degradation and mineralization performance of the different pharmaceuticals with the aim to identify the influence of reagents load and dosage on process evolution.

Regarding iron ion concentration, the use of doses below Spanish legal limit ( $10 \text{ mg L}^{-1}$ ) demonstrated to be sufficient to obtain satisfactory results when degrading the studied contaminants at the concentrations of this work, which are at least one thousand times higher than those detected in water sources worldwide. However, those high concentrations are used in this research as a consequence of the detection limits of the available measurement equipment.  $\text{Fe(II)}$  concentration is also related to the absorption of the available photons and, as it was expected, photonic efficiency showed to be higher when higher  $\text{Fe(II)}$  doses are used, which implies a better usage of the energy supplied to the process.

With regard to irradiation and its influence on the remediation of the studied pharmaceuticals, only tetracycline showed to be photodegraded by irradiation at the wavelength used to photoactivate  $\text{Fe(III)}$  in photo-Fenton process. The global tetracycline degradation achieved by photo-Fenton process is assumed to be due to the sum of the effects of the produced hydroxyl radicals and the photolysis. paracetamol, on the contrary, is only affected by the hydroxyl radical and is not photodegraded at wavelengths over 300 nm.

With respect to hydrogen peroxide, in addition to the well-studied load requirements, the dosage of the reagent was deeply investigated to maximize its exploitation in the generation of hydroxyl radicals during photo-Fenton process and, therefore, increase process efficiency. An initial experimental approach was undertaken to identify the influence of the parameters involved in the proposed dosage strategy, leading to a remarkable improvement of the process performance and, furthermore, a model-based approach was later explored.

The proposed strategy consists in a hybrid discrete-continuous systematic hydrogen peroxide dosage protocol, with very satisfactory results. The protocol consists in an initial release of hydrogen peroxide followed by a continuous flow of the reagent during a given time span, starting after a specified initial time. This protocol offers an excellent trade-off between flexibility and controllability, allowing a wide range of dosage possibilities with only three parameters.

The cross effect between two of the studied parameters of the protocol (the initial release of hydrogen peroxide,  $y_0$ , and the time at which the continuous flow starts,  $t_{ini}$ ) was observed and it must be taken into account when the dosage protocol is applied: low  $y_0$  requires low  $t_{ini}$  in order to maintain a convenient hydrogen peroxide concentration and avoid the process to stop. On the contrary, higher  $y_0$  minimizes the effect of  $t_{ini}$ , but low values of the latter may waste the hydroxyl radicals formed during the first stages of the treatment due to an excess of hydrogen peroxide.

The improvement in the process performance achieved by the proposed dosage protocol is a consequence of a more efficient use of the added hydrogen peroxide as well as the produced hydroxyl radicals, throughout the minimization of the undesired reactions of hydroxyl radicals scavenging, even when substoichiometric doses of hydrogen peroxide are used. It was demonstrated that even total mineralization is possible with a convenient combination of operational conditions when the proposed dosage protocol is applied, allowing to maintain an appropriate hydrogen peroxide concentration along the treatment span.

As an additional contribution, the behavior of Fenton and photo-Fenton processes was simulated with the aim to predict the evolution of the concentration of the species involved. The model used for the simulation was selected among a wide range of available approaches, from those absolutely empirical but non-extrapolatable through those first-principles based, widely applicable but difficult to implement. An intermediate approach, first-principles-based involving easy-to-measure lumped parameters was proposed by Cabrera Reina et al. (2012) and was adapted in this thesis with some improvements: one regarding to the calculation of the total organic carbon and another one including the Fenton-like reaction, which was not considered in the original model and involves the cycling of Fe(III) to Fe(II), especially important in the absence of irradiation. The dosage protocol was also incorporated to the model and it allows representing the evolution of the species concentrations during the treatment span.

Finally, a first step towards the optimization of the batch process recipe was proposed by using a cost-based objective function which includes the cost of reagents (Fe(II) and  $H_2O_2$ ) and electricity. The required final levels of degradation and mineralization were taken as constraints and operation time was proven to affect the objective function through electricity cost. These constraints were implemented as penalizations in the objective function.

The optimization of the process recipe leads to a reduction of the processing cost by the adjustment of the reagent doses and hydrogen peroxide dosage protocol. The adjustment of the reagent doses for the case of study provides a cost reduction of 78%, while the dosage of hydrogen peroxide following the protocol proposed in this work and a different piecewise constant dosage strategy lead to 3.3% and 5.1% cost reductions, respectively.

While the dosage protocol strategy offers an easy parameterization of the dosage in a real facility, the piecewise constant dosage could be a useful strategy to implement automatic control alternatives, driving the process to an even more efficient and flexible operation throughout the measurement of on-line variables, but this part of the research is beyond the reach of this thesis and should be undertaken in a future work.

## 10.2. Future Work

As the pilot plant is a fully monitored installation, the following investigative efforts must be taken towards the exploitation of the on-line variables for the automation of the  $H_2O_2$  dosage. Some authors have demonstrated the feasibility of controlling  $H_2O_2$  concentration throughout the online measurement of oxidation-reduction potential, but dissolved oxygen seems to be an alternative to develop such an automatic control. The development of a model to control  $H_2O_2$  concentration through online variables would also allow to investigate and characterize more flexible dosage schemes and to understand its effect on the treatment performance. Actually, piecewise constant dosage scheme would be an interesting option to develop this kind of automatic control.

Another important approach to be undertaken from this research includes the modeling and optimization of the combined photo-Fenton – Sewage Treatment Plant (STP), which can involve a real industrial application: photo-Fenton process can be applied before or after STP, according to the final objective of the treatment. One approach might consider the optimization of the final TOC, DBO or toxicity achieved with photo-Fenton process would lead to feed a more degradable and non-toxic effluent to STPs and a different approach could be the use of photo-Fenton process to refine the quality of the effluent before its final disposal. The optimization of the irradiation source to be used in photo-Fenton stage for every contaminant should be another interesting approach, as different wavelengths have proved to “attack” each contaminant in different ways.

As a consequence of the previous statement, toxicity assays as well as DBO characterization must be performed additionally to the usual measured values (TOC,  $H_2O_2$  and contaminant concentrations).





## **APPENDIXES**



## **Appendix A**

### **Publications**

This section presents a list of the published work in scientific journals and conference and poster presentations made in international congresses as a part of this investigation.



### A.1. Journal publications

**Yamal-Turbay, E.**, Jaén, E., Graells, M., Pérez-Moya, M. 2013. Enhanced photo-Fenton Process for Tetracycline Degradation using Efficient Hydrogen Peroxide Dosage. *Journal of Photochemistry and Photobiology A: Chemistry*. doi:10.1016/j.jphotochem.2013.05.008. Article in press

**Yamal-Turbay, E.**, Graells, M., Pérez-Moya, M. 2012. Systematic Assessment of the Influence of Hydrogen Peroxide Dosage on Caffeine Degradation by the Photo-Fenton Process. *Industrial and Engineering Chemistry Research* 51, 4770–4778

### A.2. Conference proceeding articles

Moreno-Benito, M., **Yamal-Turbay, E.**, Espuña, A., Pérez-Moya, M., Graells, M. 2013. Optimal recipe design for Paracetamol degradation by advanced oxidation processes (AOPs) in a pilot plant. *Computer Aided Chemical Engineering* 32, 943-948.

Monroy, I, **Yamal, E.**, Escudero, G, Pérez-Moya, M, Graells, M. 2012. A novelty detection approach for detecting faulty batches in a photo-Fenton process. *Computer Aided Chemical Engineering* 30, 972-976.

### A.3. Participation in Congresses

Pérez-Moya, M., **Yamal, E.**, Graells, M. Assessing the influence of hydrogen peroxide dosage in the performance of photo-Fenton processes. The 18th International Conference on Advanced Oxidation Technologies for Treatment of Water, Air and Soil (AOTs-18). Jacksonville, Florida, USA. November 11–15 2012.

Pérez-Moya, M., **Yamal, E.**, Graells, M. H<sub>2</sub>O<sub>2</sub> Dosage Evaluation in Photo-Fenton Processes. Second International Conference on Advanced Oxidation Processes (AOP 2012). Society of Environmental Chemistry and Allied Sciences (SECAS). Kottayam, Kerala, India. October 5-11 2012.

Pérez-Moya, M., **Yamal, E.**, Jaén, E., Graells, M. Efficient usage of Hydrogen Peroxide in Tetracycline Degradation via photo-Fenton Process. 7th European Meeting on Solar Chemistry and Photocatalysis: Environmental Applications (SPEA7). Oporto, Portugal. June 2012.

Pérez-Moya, M., **Yamal, E.**, Pérez, L., Mansilla H.D., Graells, M. Efficient Hydrogen Peroxide Usage in Sulfamethazine Remediation via Advanced Oxidation Processes. EcoTechnologies for Wastewater Treatment. EcoSTP. Santiago de Compostela, Spain. June 2012.

Monroy, I., **Yamal, E.**, Escudero, G., Graells M., Pérez-Moya, M. Anomaly detection in a photo-Fenton pilot plant. 12th Mediterranean Congress of Chemical Engineering. Barcelona, Spain. November 15-18 2011.

Pérez-Moya, M., **Yamal, E.**, Jaen, E., Alfano, O.M., Graells, M. On-line inference of hydrogen peroxide concentration: a key parameter towards photo-Fenton and photolysis process enhancement. 12th Mediterranean Congress of Chemical Engineering. Barcelona, Spain. November 15-18 2011.

**Yamal-Turbay, E.**, Graells, M., Pérez-Moya, M. Modelling the influence of hydrogen peroxide dosage on photo-Fenton treatment of caffeine. 8th European Congress of Chemical Engineering & 1st European Congress of Applied Biotechnology. Berlin, Germany. September 25-29 2011.

Pérez-Moya, M., Jaén, E., **Yamal, E.**, Mansilla, H.D., Graells, M. Hydrogen peroxide dosage as influent factor in the tetracycline treatment by photo-Fenton process. Photocatalytic and Advanced Oxidation Technologies for Treatment of Water, Air, Soil and Surfaces. Gdansk, Poland. July 4-8 2011.

**Yamal, E.**, Pérez-Moya, M., Graells, M. Hydrogen peroxide dosage as influent factor in the photo-Fenton and photolysis process. IWA Specialist Conference "Water & Industry 2011". Valladolid, Spain. Mayo 1-4 2011.

**Yamal, E.**, Pérez-Moya, M., Graells, M. Characterization of the degradation performance of Fenton and Photo-Fenton processes under variable hydrogen peroxide dosage. 19th International Congress of Chemical and Process Engineering and 7th European Congress of Chemical Engineering ECCE-7. Prague, Czech Republic. August 28 - September 1 2010.

Pérez-Moya, M., Graells, M., **Yamal, E.**, Mansilla, H.D. Effect of hydrogen peroxide dosage in the photo-Fenton degradation of caffeine. Solar Chemistry and Photocatalysis: Environmental Applications. (SPEA6). Prague, Czech Republic. June 13-16 2010.

## **Appendix B**

### **Application of Fault Diagnosis and Detection to the photo-Fenton Process**

The photo-Fenton pilot plant studied in this thesis work was used as one of the cases study addressed to validate the data processing algorithms developed in Ph.D. Thesis work by Monroy (2011). A novelty approach for detecting faulty batches and novel faults was proposed and the results are briefly presented in this appendix. This work was published by Elsevier in the Computer Aided Chemical Engineering Series (Monroy et al., 2012).





## B.1. Introduction

Fault Diagnosis (FD) in chemical processes based on historic-data models has received increasing attention in the last decade. Many classification algorithms from the Artificial Intelligence (AI) area have been successfully used as diagnosis methods. However, the diagnosis of “novel” faults is a difficulty to overcome and has been barely addressed in this area despite its importance (Burbeck and Nadjm-Tehrani, 2007; Ha An et al., 2011). The detection of faults not learned with the diagnosis methods is called Novelty Detection (ND) or Anomaly Detection (AD) (Patcha and Park, 2007).

This appendix presents an ND approach using Support Vector Machines (SVM) as classification algorithm and it is applied to a fully-monitored photo-Fenton pilot plant, operating batchwise. This approach combines simultaneously a detection or binary classification stage with a diagnosis or multi-class classification stage. In both stages, it is required previously data representation and improvement steps before applying properly the classifier algorithm.

## B.2. Materials and Methods

### B.2.1. Case study

It was considered the use of two of the photo-reactor and irradiation sources described in Chapter III: the plastic photo-reactor R3 (Table 3.1 and Fig. 3.1c) and the Pyrex reservoir (R2) equipped with the TQ718 lamp (Table 3.1 and Fig. 3.1a).

The plant is monitored with an automatic control and a data acquisition system in which eight variables are on-line registered: dissolved oxygen (DO), redox potential (ORP), pH, conductivity, main reactor temperature (T1), on-line temperature (T2), recirculation flow (Q1) and measurement line flow (Q2). Measurements are sampled each second. Recirculation flow is controlled by the pump and the measurement line flow and pH are controlled with PID controllers. The flexible pilot plant could then be configured in several ways affecting volume and irradiation source as indicated in Table B.1. Moreover, different contaminants are also possible to treat with photo-Fenton.

Table B.1. Plant configurations considered in the pilot plant

Class of irradiation	Configuration medium/low P Hg lamp
A	OFF/OFF
B	ON/OFF
C	OFF/ON
D	ON/ON

Furthermore, total organic carbon (TOC) and H<sub>2</sub>O<sub>2</sub> concentrations are off-line measured at different time scales (each 10 or 15 minutes) in photo-Fenton reactions.

### B.2.2. Novelty detection approach

The ND approach consists of two stages: binary and multi-class classification stages. First, both classifiers are set up by constructing and validating the classification models for each registered fault. The detection stage joins the faulty observations in a positive class and nominal data in a negative class. On the contrary, in the diagnosis stage, same training data is just classified according to the corresponding fault, thus leading to as many diagnosis models as faults. Therefore, a novel fault is detected when it is detected (stage 1) and there is a lack of positive diagnosis of all the known faults (stage 2).

In order to apply the ND approach to the photo-Fenton plant, the nominal operating conditions (NOC) are fixed according to Table B.2, as well as the experimental design involving the two factors governing the  $H_2O_2$  dosage:  $t_{ini}$  and  $y_0$ , previously defined in Chapter V (Section 5.3.1).

Table B.2. Variables and parameters values in the photo-Fenton process at NOC

Variable/Parameter	Value / Arrangement	Units
Contaminant ( $CT1$ )	Coffee	-
Irradiation	C	-
Contaminant initial concentration ( $CT1_0$ )	300.0	mg L <sup>-1</sup>
Initial Fe <sup>2+</sup> concentration ( $C_0^{Fe(II)}$ )	10.0	mg L <sup>-1</sup>
Equivalent initial H <sub>2</sub> O <sub>2</sub> concentration ( $C_{eq,\infty}^{H_2O_2}$ )	500.0	mg L <sup>-1</sup>
H <sub>2</sub> O <sub>2</sub> initial dosage time ( $t_{ini}$ )	0 – 36.2	min
H <sub>2</sub> O <sub>2</sub> initial percentage of the total dosage ( $y_0$ )	5.9– 34.1	%
Reactor operation volume ( $V_R$ )	8.0	L
pH	3.0	-
Dosage time ( $\Delta t_{add}$ )	60.0	min
Recirculation flow ( $Q_1$ )	11.3	L min <sup>-1</sup>
Pump work ( $PW$ )	75.0	%
Batch duration ( $TS$ )	120	min

Records from three different situations out of the experimental design and thus of the NOC were available and considered as faults. These three faults are:

- $C_{eq,\infty}^{H_2O_2}$  higher than 500 mg L<sup>-1</sup>, up to 1500 mg L<sup>-1</sup> (fault 1)
- Change of configuration of the irradiation source from C to B (fault 2)
- Different  $H_2O_2$  dosage protocol out of the experimental design (fault 3). Specifically, the  $y_0$  range varies from 70 to 100% and in 0%. For this last case,  $\Delta t_{add}$  is 120 min.

These three faults were used for constructing the detection and diagnosis models required in both stages of the ND approach. Moreover, two different scenarios were considered as novel faults so that the approach could be validated. These novel faults are  $C_0^{Fe(II)}$  higher than 10ppm and configuration A in the irradiation source (lack of irradiation). The performance in both stages of the methodology is measured in terms of the  $F1$  score (Van Rijsbergen, 1979).

### B.3. Results and Discussions

A set of twenty experimental batches under NOC and 10 batches per fault were used for constructing the models due to the lack of more available batches and the time consumed for their generation. The final sampling time considered for the models construction was  $t_s=3$  min and  $TS=120$  min for NOC batches, giving as result 41 observations per batch. In addition, time was included as variable. The total batches (40) were variable-wise unfolded, centered and scaled, and joined in the training set.

A feature extraction step was applied by applying Multiway Principal Component Analysis (MPCA) to the centered and scaled NOC batches, keeping the same number of components than variables (9) and giving as result the projection model. The projection of both NOC and Abnormal Operating Conditions (AOC) batches onto such model produces the scores, used as input of both binary and multi-class classifiers. SVM are applied as classification algorithm.

The training sets are used as validation sets in both classifiers for adjusting parameters. In this way, the polynomial kernel of third order showed the best performance for the binary classifier and a polynomial kernel of fourth order for the multi-class classifier. On the other hand, a test set containing one batch per class is constructed and used for evaluating the performance of both classifiers. Tables B.3 and B.4 show the corresponding results.

Table B.3. Performance of the binary classification stage

Class	F1 score (%)	
	Validation set	Test set
Nominal	100	100
Faulty	100	100

Table B.4. Performance of the multi-class classification stage

Class	F1 score (%)	
	Validation set	Test set
Nominal	100	100
Fault 1	100	100
Fault 2	100	100
Fault 3	100	100
Mean	100	100

The results in Tables B.3 and B.4 show the good performance of both detection and diagnosis stages of the ND approach. In order to assess this system, two batches with two novel faults are tested. These novel faults are:

- $C_0^{Fe(II)}$  higher (40ppm) than the nominal (10ppm) as fault 4
- Lack of irradiation source (configuration A) as fault 5.

The results after applying simultaneously both detection and diagnosis stages are reported in Table B.5. As observed, the whole batch with fault 4 is diagnosed as a novel fault, indicated by its detection as fault by the detection stage and the lack of positive diagnosis of all the known faults (faults 1 to 3). On the contrary,

fault 5 is detected as such but only few observations are diagnosed as novel fault and most of them diagnosed as fault three. This issue points out that the behavior of the on-line variables when there is no irradiation source is similar to their behavior when the H<sub>2</sub>O<sub>2</sub> dosage protocol is different to the protocols included in the experimental design. In general, successful results have been accomplished by applying the proposed ND approach to a Photo-Fenton process in pilot scale.

Table B.5. ND approach validation on two novel faults. Performance in terms of F1(%)

Novel fault	Detection stage		Diagnosis stage			
	NOC	Fault	NOC	Fault 1	Fault 2	Fault 3
Fault 4	-	100	100	-	-	-
Fault 5	-	98.8	7.3	-	-	92.7

## B.4. Conclusions

Novelty Detection approach has been proposed based on the combination of two classification stages: a binary or detection stage and a multi-class or diagnosis stage. The proposed approach has been applied to a Photo-Fenton process in a pilot plant where the contaminant to treat and degrade is coffee. Successful results have been obtained by detecting two novel faults not included in the constructed models.

These results encourage to continue investigating on the use of on-line variables like ORP or DO to monitor and control photo-Fenton processes, as off-line monitoring may be expensive and/or time demanding, actually, off-line chemical analysis of some selected chemical species or lumped parameters such as TOC imply unaffordable delays for operational decision making.

## B.5. References

- Burbeck, K., Nadjm-Tehrani, S. 2007. Adaptive real-time anomaly detection with incremental clustering. Information Security Technical Report 12, 56-67.
- Ha An, S., Heo, G., Heung Chang, S. 2011. Detection of process anomalies using an improved statistical learning framework. Expert Systems with Applications 38, 1356-1363.
- Monroy, I. 2011. An investigation on automatic systems for fault diagnosis in chemical processes. Ph.D Thesis. UPC, BarcelonaTech.
- Monroy, I., Yamal, E., Escudero, G., Pérez-Moya, M., Graells., M. 2012. A novelty detection approach for detecting faulty batches in a photo-Fenton process. Computer Aided Chemical Engineering 20, 972-976.
- Patcha, A., Park, J-M. 2007. An overview of anomaly detection techniques: Existing solutions and latest technological trends. Computer Networks 51, 3448-3470.
- Van Rijsbergen, C.J. 1979. Information retrieval (2<sup>nd</sup> ed.). London: Butterworths

## **Appendix C**

### **Characterization of the photo-oxidation of Tetracycline**

This appendix presents the results obtained during a research stage performed in Laboratoire des Interactions Moléculaires et de la Réactivité Chimique et Photochimique (IMRCP) in Toulouse, France. The UV photo-oxidation of Tetracycline was investigated and the production of singlet oxygen was one of the subjects of interest.



## C.1. Introduction

Chapter VI addressed the degradation of tetracycline (TC) by means of photo-Fenton process and a few comments about the photolysis of this pharmaceutical were mentioned. A more detailed study of the UV-C and UV/H<sub>2</sub>O<sub>2</sub> photolysis of TC are investigated in this chapter and a brief review of these processes is presented first. The State-of-the-Art of the degradation of TC by AOPs is presented in Table 2.5.

Among the available researches concerning TC photolysis, the investigations by Drexel et al. (1990) and Morrison et al. (1991) demonstrate that the photolysis of TC in the absence of O<sub>2</sub> at wavelengths longer than 330 nm (excitation into the low energy absorption band, Fig. C.1) in organic solvents, as well as aqueous solutions at acidic and neutral pH, leads to its conversion to lomitetracycline (LTC) with elimination of dimethylamine. This reaction occurs from a low-lying triplet excited state (T<sub>1</sub>) and is efficiently quenched by oxygen.

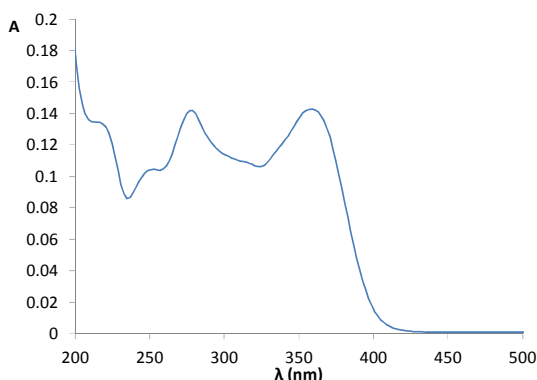
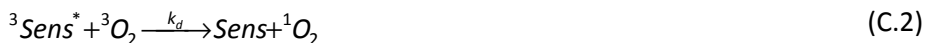


Figure C.1. Tetracycline absorption spectrum in deionized water

An additional primary photochemical reaction is observed when TC is excited at wavelengths shorter than 330 nm (higher energy absorption band, Fig. C.1). In this case, Morrison et al. (1991) propose that TC is converted to de(dimethylamino)tetracycline from an upper triplet excited state (T<sub>2</sub>). At alkaline pH ( $\geq 7.5$ ), formation of anhydrotetracycline (ATC) competes with the above mentioned pathways.

Hasan y Khan (1986) reported the first evidence of the generation of O<sub>2</sub>(<sup>1</sup>Δ<sub>g</sub>) (denoted as <sup>1</sup>O<sub>2</sub> from this point) during TC photolysis. The authors used direct detection of <sup>1</sup>O<sub>2</sub> by its weak phosphorescence in the near-infrared (NIR) and estimated the quantum yield of <sup>1</sup>O<sub>2</sub> production ( $\Phi_A$ ) to be about 0.05 in CCl<sub>4</sub>. Li Anson et al. (1987) and later Miskoski et al. (1998) confirmed, using time-resolved <sup>1</sup>O<sub>2</sub> NIR detection, that TC and some of its derivatives photosensitized <sup>1</sup>O<sub>2</sub> production in aqueous solutions but with quantum yields lower than 0.03 in the most favorable cases (signals at the detection limit of the equipment).

It was also reported that TC, besides being a  $^1\text{O}_2$  sensitizer (Eq. C.1 and C.2), efficiently quenches  $^1\text{O}_2$  (Eq. C.3) and reacts with this species (Eq C.4) to yield poorly characterized oxidation products (Miskoski et al., 1998).



The reaction of TC with  $^1\text{O}_2$  is pH dependent. In alkaline media (pH  $\geq 7.5$ , main results at pH 9), a red species characterized by an absorption band between 500 and 600 nm, was observed by different authors and was attributed to the deamination and oxidation of ring A, yielding a quinone type moiety (Davies et al, 1979, Miskoski et al., 1998).

## C.2. TC photo-oxidation and production of singlet oxygen

### C.2.1. Single oxygen analysis

The analysis and quantification of  $^1\text{O}_2$  were carried out by recording its weak NIR (1270 nm) emission signal upon continuous monochromatic excitation of the sensitizer, as previously described (see *e.g.*, Aminian-Saghafi et al., 1992; Lorente et al., 2003; Cabrerizo et al., 2007). With this system, the evolution of the  $^1\text{O}_2$  signal may be monitored during long periods of time. The signal intensity ( $S_e$ ) is given by:

$$S_e = C P_a \Phi_{\Delta} k_e \tau_{\Delta} \quad (\text{C.5})$$

where

$C$  is a proportionality factor depending on geometric and electronic characteristics of the detection system and on specific parameters of the solvent (refractive index, NIR absorbance),

$P_a = P_0(1-10^{-A})$  is the photon flux absorbed by the sensitizer ( $P_0$  and  $A$  are the incident photon flux and the absorbance of the sensitizer at the wavelength of excitation, respectively),

$\Phi_{\Delta}$  is the quantum yield of  $^1\text{O}_2$  production,

$k_e$  is the rate constant of  $^1\text{O}_2$  emission and

$\tau_{\Delta}$  is the  $^1\text{O}_2$  lifetime in the reaction system.

Quantum yields of  $^1\text{O}_2$  production ( $\Phi_{\Delta}$ ) may be determined by relative measurements of the  $^1\text{O}_2$  luminescence signals, using a reference sensitizer of known  $\Phi_{\Delta}$  ( $\Phi_{\Delta}^R$ ). In this work, 1*H*-Phenalen-1-one (PN) was employed ( $\Phi_{\Delta}^{PN}$  close



to unity in most solvents, Oliveros et al., 1991; Martí et al., 1996). Both TC and PN were irradiated at 367 nm in D<sub>2</sub>O (where the <sup>1</sup>O<sub>2</sub> lifetime is much longer than H<sub>2</sub>O, Wilkinson et al, 1995), using optically matched solutions at the wavelength of irradiation. Under these conditions, the ratio of the <sup>1</sup>O<sub>2</sub> production quantum yields ( $\Phi_{\Delta}^{TC}/\Phi_{\Delta}^{PN}$ ) is equal to:

$$\Phi_{\Delta}^{TC}/\Phi_{\Delta}^{PN} = (S_e^{TC}/S_e^{PN}) (\tau_{\Delta}^{TC}/\tau_{\Delta}^{PN}) \quad (\text{C.6})$$

$$\text{where } \tau_{\Delta}^{TC} = 1/(k_d + k_t^{TC}[\text{TC}]) \quad (\text{C.7})$$

with  $k_d$  (s<sup>-1</sup>) being the pseudo-monomolecular rate constant of <sup>1</sup>O<sub>2</sub> deactivation by the solvent (D<sub>2</sub>O) and  $k_t^{TC}$  (L mol<sup>-1</sup> s<sup>-1</sup>) the bimolecular rate constant of <sup>1</sup>O<sub>2</sub> total quenching by TC ( $k_t^{TC} = k_q^{TC} + k_r^{TC}$ , sum of the rate constants of chemical reactions presented in Eq. C.3 and C.4), and

$$\tau_{\Delta}^{PN} = 1/k_d = \tau_{\Delta,0} \quad (\text{C.8})$$

with  $\tau_{\Delta,0}$ : <sup>1</sup>O<sub>2</sub> lifetime in the absence of quencher, as  $k_t^{PN}[\text{PN}] \ll k_d$ .

The ratio of the <sup>1</sup>O<sub>2</sub> luminescence signals ( $S_e^{TC}/S_e^{PN}$ ) gives an apparent value of  $\Phi_{\Delta}^{TC}$  ( $\Phi_{\Delta,app}^{TC}$ ), not corrected for <sup>1</sup>O<sub>2</sub> quenching by TC itself:

$$\Phi_{\Delta,app}^{TC} = \Phi_{\Delta}^{PN} (S_e^{TC}/S_e^{PN}) \quad (\text{C.9})$$

and

$$\Phi_{\Delta}^{TC} = \Phi_{\Delta,app}^{TC} (1 + \tau_{\Delta,0} k_t^{TC}[\text{TC}]) \quad (\text{C.10})$$

The equipment used to monitor the steady-state <sup>1</sup>O<sub>2</sub> phosphorescence emission at 1279 nm upon continuous monochromatic excitation of a sensitizer was described by Cabrerizo et al. (2007). Singlet oxygen luminescence signals were recorded as a function of irradiation time during a minimum of three minutes. The experimental results were the average of two to three independent series of measurements. Values of  $\tau_{\Delta}$  were determined by time-resolved <sup>1</sup>O<sub>2</sub> phosphorescence measurements, using a laser flash photolysis system and custom-built detectors (aGe photodiode (Judson) or InGaAs photodiode (IR Components)). Measurements were performed at two different concentrations of TC (7.5x10<sup>-5</sup> mol L<sup>-1</sup> and 10<sup>-4</sup> mol L<sup>-1</sup>,  $\epsilon^{TC} = 13600 \pm 100$  L mol<sup>-1</sup>cm<sup>-1</sup> at 367 nm, Anderson et al., 2005).

### C.2.2. Results and discussion

In contrast to PN, the <sup>1</sup>O<sub>2</sub> signals registered upon TC irradiation slowly decreased with time, showing that TC was not stable under these conditions. Therefore, the apparent quantum yields of <sup>1</sup>O<sub>2</sub> production ( $\Phi_{\Delta,app}^{TC}$ ) (Eq. C.9) were calculated using  $S_e^{TC}$  at the beginning of the irradiation time, yielding  $\Phi_{\Delta,app}^{TC}$  values of 0.077 and 0.056 at concentrations of 7.5x10<sup>-5</sup> mol L<sup>-1</sup> and 10<sup>-4</sup> mol L<sup>-1</sup>,

respectively, in agreement with the low values observed by previous authors (Hasan and Khan 1986, Li et al. 1987, Miskoski et al. 1998).

The calculation of  $\Phi_{\Delta}^{TC}$  requires the knowledge of the  $^1\text{O}_2$  lifetime in  $\text{D}_2\text{O}$  ( $62 \pm 3 \mu\text{s}$ ) and of the rate constant of  $^1\text{O}_2$  total quenching by TC ( $k_t^{TC}$ ) (Eq. C.10). Miskoski et al (1998) determined  $k_t^{TC}$  to be  $2.5 \times 10^8 \text{ L mol}^{-1} \text{ s}^{-1}$  in  $\text{D}_2\text{O}$ . From  $\Phi_{\Delta}^{app, TC}$  and  $k_t^{TC}$ , an average value of  $0.16 (\pm 0.02)$  was calculated for  $\Phi_{\Delta}^{TC}$ .

As indicated above, the  $^1\text{O}_2$  signal registered upon TC irradiation slowly decreased with time. This is in agreement with the already reported self-sensitized oxidation of TC under these conditions. Figure C.2 shows the evolution of the absorption spectra of TC solutions in  $\text{D}_2\text{O}$  at two different initial concentrations. The lowest energy absorption band (centered at 359 nm) decreased in intensity and underwent a hypsochromic shift.

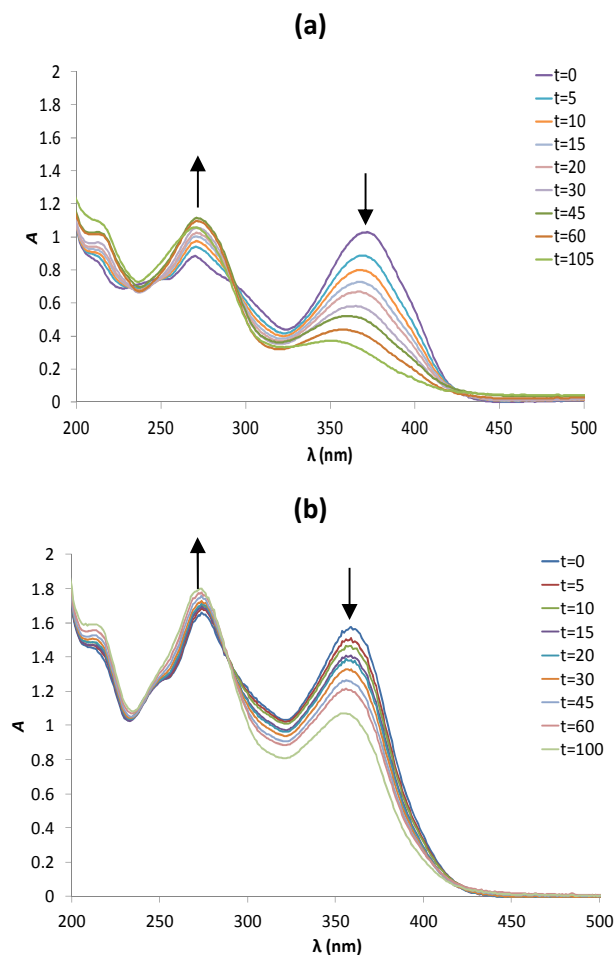


Figure C.2. Absorption spectra evolution during TC irradiation at 367 nm (a)  $7.5 \times 10^{-5} \text{ mol L}^{-1}$  (b)  $1 \times 10^{-4} \text{ mol L}^{-1}$ .

The decrease of the TC concentration in the reaction system implies a decrease of the photon flux absorbed by TC and, therefore, a decrease in the  $^1\text{O}_2$  emission signal would be expected (if TC is the only  $^1\text{O}_2$  sensitizer present in the system, Eq C.5). However, TC is also a  $^1\text{O}_2$  quencher and, combining Eq. C.5 and C.7), the relative value of the  $^1\text{O}_2$  emission signal ( $S_e/S_{e,0}$ ) as a function of irradiation time is given by Eq. C.11, assuming that TC is the only (or dominant) absorbing species at the wavelength of excitation.

$$S_e/S_{e,0} = (\alpha/\alpha_0) \{(1 + \tau_{\Delta,0} k_t^{TC}[\text{TC}]_0)/(1 + \tau_{\Delta,0} k_t^{TC}[\text{TC}])\} \quad (\text{C.11})$$

with  $\alpha = (1-10^{-A})$  and  $\alpha_0 = (1-10^{-A_0})$  are the absorption factors.

During irradiation of TC, the absorption factor decreases but the ratio  $\{(1 + \tau_{\Delta,0} k_t^{TC}[\text{TC}]_0)/(1 + \tau_{\Delta,0} k_t^{TC}[\text{TC}])\}$  increases as  $^1\text{O}_2$  quenching decreases with TC concentration. Simulations of Eq. C.11, assuming that TC is the only  $^1\text{O}_2$  sensitizer and quencher in the solution, show that the  $^1\text{O}_2$  signal should remain practically constant. Plots of  $S_e/S_{e,0}$  and  $\alpha/\alpha_0$  as a function of irradiation time are shown in Figure C.3. for two different TC initial concentrations.

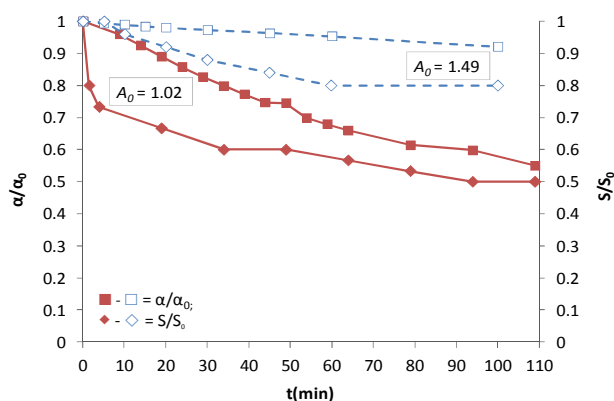


Figure C.3. Evolution of the  $^1\text{O}_2$  signal and the absorption factor during TC irradiation at 367 nm for two different TC initial concentrations: Red lines:  $7.5 \times 10^{-5} \text{ mol L}^{-1}$  (Initial absorption = 1.02); blue lines:  $1 \times 10^{-4} \text{ mol L}^{-1}$  (Initial absorption = 1.49)

In both cases, the  $^1\text{O}_2$  signal decreases more than the absorption factor at 367 nm, which indicates that the products do not produce significant amounts of  $^1\text{O}_2$ , but compete for absorption with TC.

### C.3. Degradation of TC by UV and UV/ $\text{H}_2\text{O}_2$ processes

#### C.3.1. Laboratory reactor description and analytical methods

The 300 mL laboratory batch reactor used in this part of the study (DEMA, Mangels, Bornheim-Roisdorf, Germany, internal radius: 3.6 cm, external radius: 5.5 cm, height: 27 cm) was equipped with a low pressure Hg lamp emitting at 254 nm and positioned in quartz well in the axis of the reactor (electrical power: 5 W, radiant power: 1.2 W, UV-Consulting Peschl, Mainz, Germany). An incident photo

flux of  $4.5 \times 10^{-6}$  Einstein  $s^{-1}$  was reported by uridine (1- $\beta$ -D-ribofuranosyluracil) actinometry (Martignac et al., 2013). The initial concentration of TC was  $9 \times 10^{-5}$  mol  $L^{-1}$ .  $H_2O_2$  initial concentration was varied between  $1.89 \times 10^{-3}$  and  $2.87 \times 10^{-2}$  mol  $L^{-1}$  for determining the optimal  $H_2O_2$  concentration.

TC solutions (pH=3) were continuously bubbled with air or argon and the experiments were performed at a temperature of  $20 \pm 1^\circ C$ . Samples (800  $\mu L$ ) were withdrawn from the reactor at regular intervals and analyzed by UV-Visible spectrophotometry and liquid chromatography coupled with mass spectrometry (LC/MS).

LC-electrospray ionization (ESI) MS/MS analyses were carried out on an instrument consisting of an Agilent 1100 LC (Waters) equipped with UV/visible detector and a Q-trap Applied Biosystem mass spectrometer with an ESI source in positive mode. Data acquisition was handled by the Analyst 1.4.2 software. A Symmetry C18 column (4.6x75mm, 3.5 $\mu m$ , Waters) was used for HPLC analyses with 84% of a 0.1% formic acid aqueous solution as eluent (C) and 16% ACN (eluent D) at a flow rate of 0.4 mL/min. The UV/visible detector was set at 266 nm. The mass spectrometer was operated in a negative/positive ionization mode. The source temperature was set at  $150^\circ C$  and the ionization source at 30 V.

### C.3.2. Results and discussion

UV-C irradiation leads to degrade more than 90% initial TC concentration within 4 h treatment and the contaminant was not detected after 7 h of irradiation (Figure C.4). TC absorption spectrum exhibits an absorption band centered at 278 nm (Fig. C.1), which explains the absorption of energy at 254 nm.

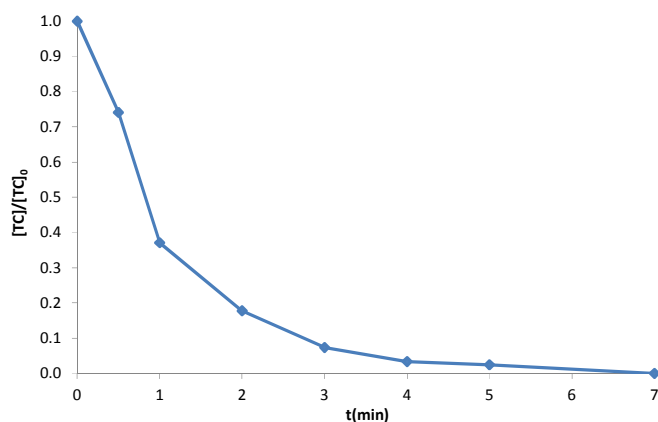


Figure C.4. Evolution of TC normalized concentration during UVC photodegradation

When  $H_2O_2$  is added to the sample and it is irradiated at 254 nm,  $H_2O_2$  absorbs a fraction of the photons irradiated and produces  $HO^\bullet$  which reacts with the substrate, reaching faster degradation. Figure C.5 shows the evolution of the apparent reaction rate ( $k_{app}$ ) as a function of the ratio  $H_2O_2/TC$ . A local maximum is

observed at a ratio between 150 and 212, corresponding to a  $\text{H}_2\text{O}_2$  concentration between  $1.35 \times 10^{-2}$  and  $1.91 \times 10^{-2}$  mM.

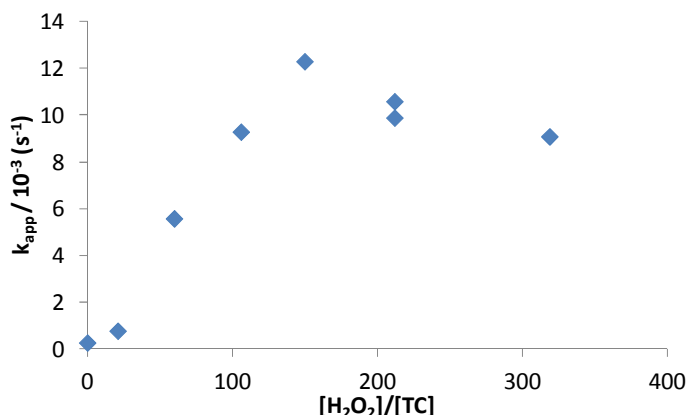


Figure C.5. Evolution of the apparent reaction rate of TC degradation by UV/ $\text{H}_2\text{O}_2$  as a function of the ratio  $\text{H}_2\text{O}_2/\text{TC}$

### Intermediates identification by LC/MS

An effort to identify the possible reaction intermediates producing during  $\text{H}_2\text{O}_2/\text{UV}$  was addressed. After 8 minutes irradiation, several products with  $m/z = 461.15$  were identified, corresponding to the hydroxylation of the TC molecule by the electrophilic addition of  $\text{HO}^\bullet$  to the aromatic ring (Figure C.6). After 30 minutes process, a molecule with  $m/z = 477.15$  (possibly a second hydroxylation:  $\text{C}_{22}\text{H}_{25}\text{N}_2\text{O}_{10}$ ) and another one with  $m/z = 417.16$  were identified. These observations are in agreement with those reported by Wu et al. (2012).

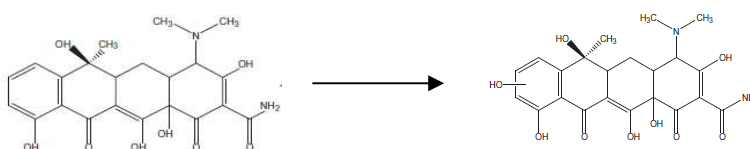


Figure C.6. Possible pathway for the hydroxylation of the TC molecule

Further research must be done in this area if the elucidation of the mechanisms and pathways of TC degradation are required.

## C.4. Conclusions

The UV-C and UV/ $\text{H}_2\text{O}_2$  photolysis of tetracycline in water solutions was addressed at a laboratory scale. UV photolysis of tetracycline can be enhanced by the addition of hydrogen peroxide and an optimum ratio  $\text{H}_2\text{O}_2/\text{TC}$  between 150 and 212 was experimentally obtained for the studied conditions.

The measurement of the phosphorescence emission at 1279 nm upon continuous monochromatic excitation of tetracycline solutions in  $\text{D}_2\text{O}$  demonstrated that tetracycline photolysis produces singlet oxygen with quantum

yields 0.077 and 0.056 at concentrations of  $7.5 \times 10^{-5}$  and  $10^{-4}$  M, respectively. The  $^1\text{O}_2$  signal decreases might indicate that the products do not produce significant amounts of  $^1\text{O}_2$ , but compete for absorption with TC.

Finally, three reaction intermediates formed during UV/ $\text{H}_2\text{O}_2$  were identified by LC/MS, with  $m/z$  equals to 461, 477 and 417. Similar results have been reported previously by We et al., (2012) during  $\text{TiO}_2$  photocatalysis. Further research is required to fully identify these intermediates and to elucidate a complete reaction pathway.

### C.5. References

Aminian-Saghafi, T., Nasini, G., Caronna, T., Braun, A.M., Oliveros, E. 1992. Quantum Yields of Singlet Oxygen Production by Some Natural Quinonoid Fungal Metabolites, *Helv. Chim. Acta* 75, 531-538.

Anderson, C.R., Rupp, H.S., Wu, W-H. 2005. Complexities in tetracycline analysis—chemistry, matrix extraction, cleanup, and liquid chromatography. *J. Chromatogr. A* 1075, 23–32.

Cabrerizo, F.M., Dantola, L., Petroselli, G., Thomas, A.H., Capparelli, A.L., Braun, A.M., Lorente, C., Oliveros, E. 2007. Reactivity of conjugated and unconjugated pterins with singlet oxygen ( $\text{O}_2(^1\Delta_g)$ ): Physical quenching and chemical reaction, *Photochem. Photobiol.* 833, 526-534.

Davies, A.K., McKellar, J.F., Phillips, G.O., Reid, A.G. 1979. Photochemical oxidation of tetracycline in aqueous solution. *J. Chem. Soc., Perkin. Trans. 2*, 369.

Hasan, T., Kahn, A.U. 1986. Phototoxicity of the tetracyclines: Photosensitized emission of singlet delta dioxygen. *Proc. Natl. Acad. Sci. USA* 83, 4604-4606.

Li, A., Chignelland, C.F., Hall, R.D. 1987. Cutaneous phototoxicity of tetracycline antibiotics: generation of free radicals and singlet oxygen during photolysis as measured by spin-trapping and the phosphorescence of singlet molecular oxygen. *Photochem. Photobiol.* 46(3), 379-382.

Lorente, C., Thomas, A.H., Capparelli, A.L., Martinez, C.G., Braun, A.M., Oliveros, E. 2003. Singlet oxygen ( $^1\Delta_g$ ) production by pterin derivatives in aqueous solutions, *Photochem. Photobiol. Sci.* 2, 245-250 and references therein.

Martí, C., Jürgens, O., Cuenca, O., Casals, M., Nonell, S. 1996. Aromatic ketones as standards for singlet molecular oxygen ( $^1\Delta_g$ ) photosensitization. Time-resolved photoacoustics and near-IR emission studies, *J. Photochem. Photobiol., A: Chem.* 97, 11-18 and references therein.

Martignac, M., Oliveros, E., Maurette, M-T., Claparols, C., Benoit-Marquié, F. 2013. Mechanistic pathways of the photolysis of paracetamol in aqueous solution: an example of photo-Fries rearrangement. *Photochem. Photobiol. Sci.* 12, 527.

Miskoski, S., Sánchez, E., Garavano, M., López, M., Soltermann, A.T., Garcia, N.A. 1998. Singlet molecular oxygen-mediated photo-oxidation of tetracyclines: kinetics, mechanism and microbiological implications. *J Photoch Photobio B* 43, 163-171.

Oliveros, E., Murasecco-Suardi, P., Aminian-Saghafi, T., Braun, A.M. 1991. 1H-Phenalen-1-one: photophysical properties and singlet oxygen production, *Helv. Chim. Acta* 74, 79-90.

Wilkinson, F., Helman, H.P., Ross., A.B. 1995. Rate constants for the decay and reaction of the lowest electronically excited singlet state of molecular oxygen in solution. An expanded and revised compilation, *J. Phys. Chem., Ref. Data* 24, 663-934.

Wu, J., Zhang, H., Oturan, N., Wang, Y., Chen, L., Oturan, M.A. 2012. Application of response surface methodology to the removal of the antibiotic tetracycline by electrochemical process using carbon-felt cathode and DSA (Ti/RuO<sub>2</sub>-IrO<sub>2</sub>) anode. *Chemosphere* 87, 614.